School of Advanced Studies

PhD curriculum in chemical sciences

PhD Thesis

SYNTHESIS OF NOVEL ORGANOMETALLIC COMPOUNDS OF GROUPS VIII AND IX AND EVALUATION OF THEIR CATALYTIC AND BIOLOGICAL POTENTIAL

Cycle XXXVI

Scientific-Sector : CHIM/03

PhD candidate

 Dr. Noemi Pagliaricci

Supervisor

Prof. Riccardo Pettinari

2020-2023

Table of contents

PREFACE

Transition metal complexes are a fascinating and essential class of compounds in chemistry. They consist of transition metals, which are elements found in the middle of the periodic table, surrounded by ligands, which are molecules or ions that bind the metal center. Transition metals exhibit different oxidation states and can interact with a large number or type of molecules. Due to the diversity of chemical bonding possible between the metal centre and the different ligands, the advances in these areas have presented unique opportunities and challenges in transition-metal chemistry. In fact, the behaviour of the metal−ligand bond represents a very tuneable aspect for achieving target properties like the interplay between spin, oxidation state, coordination environment and metal-electron configuration. In this way this class of compounds exhibits a wide range of properties which plays crucial roles in various chemical, industrial, and biological processes.[1]

For this reason, the transition metal complexes are attractive targets for the design of a wide range of functional materials with applications in catalysis, supramolecular assemblies, molecular devices and medicinal chemistry. In fact, they have shown important catalytic activities or bioactivities among which anti-inflammatory, antibiotics, anticonvulsant, analgesic, antimicrobial, antiparasitic, antitubercular, anti-HIV, antioxidant and anticancer.[2–7]

According to this, the scope of this doctoral thesis is based on the synthesis of novel coordination compounds containing particular metal and ligands able to provide an intrinsic anti-tumor or catalytic activity. The two research lines are herein described in two different parts:

- **Biologically active compounds**: related to Ru(II) and Os(II) metal centers coordinated with curcumin and bisdemethoxycurcumin derivatives as ligands.

   The curcuminoids (curcumin and bisdemethoxycurcumin) are well-known for their biological potentials which also include the anticancer activity but, unfortunately, their low water solubility and low bioavailability decrease the overall activity. The aim of this part was focused on the strategical modification of the curcuminoids structure (which includes the aryl side chain bioconjugation; reduction of the conjugation's degree and heterocyclization of di-keto functionality) suitable for the improvement of this aspects. Additionally, Ru(II) and Os(II) possess their own anticancer activity. Based on this statements, the scope of this part was to synthesize new complexes and to see the correlation between their chemical structure and the related cytotoxicity.

- **Catalytically active compounds**: referred to Ru(II), Rh(III) and Ir(III) metal centres coordinated with pyrazolone-containing hydrazone ligands.

  The pyrazolone-containing hydrazone compounds are a class of Schiff base molecules acting as polydentate ligands for different metal centres. More precisely, the hydrazine moiety present into the structure, confers a κ-N,O coordinating sphere or, with a pyridine-hydrazine moiety, also a κ-N,N binding mode can be afforded through the nitrogen atom present into the pyridine ring. In both of the coordination typology, the presence of nitrogen atoms makes them suitable as a Lewis base catalytic site.

  Moreover, the Platinum group metals (Lewis acid site) is famous for its huge catalytic applications but no examples of catalysis with Ru(II), Rh(III) and Ir(III) bearing pyrazolone-containing hydrazone are reported in literature. Thus, the novel complexes have been evaluated for their ability to act as bifunctional catalyst toward tandem reactions.

Chapter 1: **Introduction to biological compounds**

1.1 METALS IN MEDICINAL CHEMISTRY

Inorganic compounds have had an enormous impact on medicine,[8-9] in particular in the treatment of cancer. Probably one of the earliest investigations on the anticancer effect of inorganic metal salts and complexes was reported by Collier and Krauss in 1931. In their work, they implanted Ehrlich's mouse carcinoma into white mice and analysed the effect of single-dose subcutaneous administrations of various transition metal compounds on tumour growth (i.e. Cu, Pb, Cr, Mn, Fe, Ni, Co, Ru, Rh and Os). Most of the compounds were inactive, but significant tumour-inhibiting properties were observed for some Pb compounds, $K_2Mn(SO_4)_2$ and $Cs_2[Ru(IV)Cl_6]$ hydrate. They concluded that the biological effect of a metal on the mouse carcinoma was not solely caused by the metal center, but also by the type of ligands and their spatial arrangement.[10]

The first and most important example in this field is represented by the cisplatin (*cis*-dichlorodiammineplatinum II) which was synthesized for the first time by Michel Peyrone in 1845 and for this it was initially known as Peyrone's chloride.[11] Its structure was elucidated in the early 1960s by a team of scientists led by Barnett Rosenberg at Michigan State University and this event has been the major contribution for the establishment of a firm basis of the antiproliferative activity possessed by the coordination chemistry.[12] The discovery of cisplatin's activity was somewhat serendipitous and arose from their research on the effects of electric fields on bacterial cell division.[13] In their experiments, they observed that electric fields could inhibit cell division in Escherichia coli (*E. coli*) bacteria in the presence of, what they later realised to be, the Peyrone's chloride. To investigate this phenomenon, they used platinum electrodes in their setup and noticed that the inhibition of cell division was particularly pronounced when platinum electrodes were used. This led them to investigate whether platinum ions were responsible for the observed effects and, as a consequence of their studies, they recognized the potential significance of this discovery for cancer treatment due to the confirmation of its ability to interfere with cell division. Subsequent research and clinical trials confirmed its effectiveness in treating various types of cancer, and thanks to this, cisplatin became one of the first platinum-based chemotherapy drugs used to combat cancer.

From its discovery, cisplatin was approved as chemotherapeutic agent only in 1979 and nowadays is used in 50–70% of all cancer patients, usually in combination with other drugs, with particularly good activity against testicular, ovarian, oropharyngeal, bronchogenic, cervical and bladder carcinomas, lymphoma, osteosarcoma, melanoma and neuroblastoma. Even though its mechanism of action is still unknow, many studies state that when it reaches

the tumour, cisplatin is taken up into the cells by three possible mechanisms: passive diffusion, copper transporter proteins (e.g. CTR1) and/or organic cation transporters. Once inside the cell, the lower chloride concentration (4–20 mM) results in drug aquation with the loss of one or both the chloride ligands. When aquated, cisplatin can go on to bind to the DNA (acting as main target) at the N7 position of guanine, and to a lesser extent adenine, through the formation of a covalent coordinate bond. After a series of adducts formation, which unwind the helix (between 30 and 60° towards the major groove) of the DNA structure, the distortion generated prevents replication and transcription, which ultimately leads to cellular apoptosis.[14] In addition, cisplatin is also known to bind to RNA and interfere with cellular RNA processing, which may assist in the action of the drug.[15]

Nevertheless, cisplatin it is not without problems, notably it has no selectivity between healthy and tumours cells and exhibits a high general toxicity leading to undesirable side-effects such as nephrotoxicity (reduced kidney function and damage), neurotoxicity (nervous system damage), ototoxicity (hearing loss) and myelosuppression (reduction in bone marrow activity). These severe side effects of cisplatin mean that the dose delivered to patients can be sub-lethal to tumours, particularly ovarian cancers, which means they are then able to develop resistance to further drug treatment. In addition, cisplatin is inactive against many cancer cell lines and metastasis (secondary) cancers.[4] That is why, the challenge of inorganic chemists to develop platinum based anticancer drugs, that are superior to cisplatin, has been met with considerable enthusiasm over the last 30 or so years and literally thousands of compounds have been prepared based on well-conceived ideas to improve the efficacy of the final drug. From these endeavours only two further compounds have entered in the world-wide clinical use, these being carboplatin and oxaliplatin (**Figure 1**) gaining international marketing approval, although three others (nedaplatin, lobaplatin and heptaplatin) are used in the clinic in a limited number of countries and around 10 other platinum drugs are currently undergoing clinical trials.[16] However, still they cannot compete with the efficiency of cisplatin.[17] Since 1999 no new small molecule platinum- based drug has entered clinical trials which is representative of a shift in focus away from that metal.
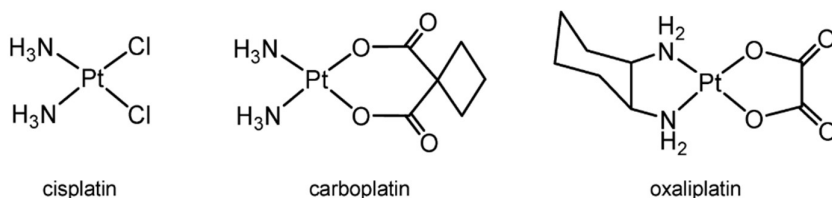
Figure 1 - *Platinum(II) complexes approved worldwide for clinical use in cancer treatment*

In state of this, the quest for alternative drugs to the cisplatin and its derivatives is highly needed and the key for this scope is supposed to be the presence of a metal centre and the intervening years to the Rosenberg's discovery have witnessed a continued expansion of the

periodic table of medicinal elements, with the work mainly devoted to Ru and other metals such as Os, Ir, Re, As and Au.[18]

It is known, in fact, that inorganic elements (metals) play crucial roles in biological and biomedical processes and it is evident that many organic compounds used in medicine do not have a purely organic mode of action: some are activated or bio-transformed by metal ions including metalloenzymes, others have a direct or indirect effect on metal ion metabolism.[19]

The metals in question are not only the 24 or so essential elements, but also for nonessential and even radioactive elements that offers the potential for the design of novel therapeutic and diagnostic agents.

1.1.1 Organometallic Compounds

When the complexes contain an organic ligand and a metal-carbon bond is present, they form a new class of materials named organometallic compounds. These compounds are characterized by the direct coordination of the metal atom to one or more carbon atoms. The nature of metal-carbon bond significantly influences the reactivity and properties of these compounds (e.g. solubility, stability, optical activities etc.). In summary, the M-C bond in organometallic compounds is central to their identity and it governs the electronic, structural, and spectroscopic properties of the referred compound and plays a critical role in their applications, including catalysis, materials science, and organic synthesis. Once again, understanding the nature of the M-C bond is essential for designing and manipulating organometallic complexes for specific purposes. In accordance, in recent years there have been major advances in the design of organometallic compounds for catalysis and therapy: these small molecules can show high specificity for their substrates followed by stereospecific conversions into products or, at the same time, structurally imposed organometallic complexes offer promise as therapeutic agents. Design concepts for such organometallic drugs, however, are still in their infancy; mainly because an understanding of structure–activity relationships (SARs) has not yet reached a level that allows extrapolation to provide general rules. The best candidates usually give high yields, high turn-over numbers (TON) and turn-over frequencies (TOF) and, in the case of enantioselective catalysis, high enantiomeric excesses (ee). In the case of anticancer drugs, for example, an initial measure of efficacy is often the *in vitro* activity towards cancer cells in culture, with potency described by the IC_{50}-value.[20]

Recent reviews and books attest the rapid development of bioorganometallic chemistry (term that was introduced for the first time in 1985 by Gèrard Jaouen) in general based on their potential application as anticancer chemotherapeutics.[21-22] Furthermore, in a *Tutorial Review* from Hartingeer and Dyson[23] many medicinal applications of organometallic therapeutics for

cancer, HIV, malaria and other diseases are reported. Many of these putative drugs are centred on classical organometallic motifs (e.g. metallocenes, metal–arene complexes, metal carbonyl and carbene complexes) where the nature of the metal centre plays a pivotal role. In fact, the essential role of transition metal ions in biological systems is well known [24–26] and the development of metal complexes as pharmaceuticals is due to a prior belief that metal ions are not transported across cell membranes but are incorporated at the formation stage of cells.[27]

To summarize, although treatment with platinum drugs is accompanied by serious side effects, these complexes are considered as ''blockbusters'' in the pharmaceutical industry and in recent years, various approaches were undertaken, e.g. ligand modification, development of polynuclear systems and the use of alternative metals to Pt, to extend the list of treatable tumours.[28] Several classes of organometallic species have also proven to exhibit promising anticancer activity, and selected examples will be showed in the following chapters.

1.1.2 Metallocenes

A metallocene is a type of chemical compound consisting of a transition metal atom sandwiched between two aromatic rings (e.g. cyclopentadienyl anions). These chemicals, due to their unique stability, were the first class of organometallic compounds to be systematically investigated as putative anticancer agents. It is thought, indeed, that the extended π-system plays an important role in the mode of action of these complexes (through electron-transfer or oxidation processes that may happen) beyond their ability to stabilize the metal centre.[29-30] Toward the 1970s Köpf and Köpf-Maier investigated the in vitro antitumour activity of several early transition metal cyclopentadienyl complexes and from these studies *Titanocene* dichloride, $Ti(\eta-C_5H_5)_2Cl_2$, exhibiting a *cis*-chloride motif (similar to cisplatin), showed the best activity.[31] It entered in clinical trials in 1993 prior to attempts to improve its efficacy through rational modifications to the structure, thus, there is considerable potential to develop superior compounds. In fact their *ansa*-titanocenes and, more importantly, benzyl-substituted titanocenes (developed to avoid stereocenters) have been evaluated against a renal cell cancer line (LLC-PK) showing moderate activities. Furthermore, important results have been obtained for oxalato titanocene derivatives for which the in vitro screening is very promising, by leading to higher stability, reduced side-effects and extending the range of treatable tumours.[32-33]

Similarly, iron complexes (Iron(II) sulfates or carboxylates) were the earliest metal compounds to be studied in medicinal chemistry[26] and their organometallic *Ferrocenes* compounds (with their so-called sandwich structure elucidated for the first time by Wilkinson and Fischer in the early 1950s resulted in a Nobel prize) represent the quintessential

organometallic molecule used as precursor for many compounds having biological activity. Many simple *Ferrocene* and *Ferrocinium* compounds have been shown to be cytotoxic. However, the most important class of ferrocene anticancer drugs to emerge are based on a series of elegantly designed estrogen targeting motifs, which instead of being non-tumour specific are selectively active against hormone dependent tumours such as breast cancer. These molecules, developed by Gèrard Jaouen and co-workers, named *Ferrocifens,* present structural modifications lead to more lipophilic compounds (which therefore cross cell membranes more easily) and with a stronger cytotoxic effect. The superior antiproliferative effect of the *Ferrocifens* is believed to be the result of a combination of more than one event, first involving binding of the *Ferrocifen* to the estrogen receptor (ERα) with additional cytotoxicity induced by the ferrocene moiety itself.[34] In contrast to the *Ferrocifens*, the ruthenium analogues behaved as antiestrogens with activity against the hormone-dependent human breast adenocarcinoma MCF7 cells which may be attributed to their differences in biological action.[35]

1.1.3 Half-Sandwich compounds

Half-sandwich compounds are organometallic compounds in which a metal atom is coordinated to one or more arenes and with other type of ligands that complete the coordination sphere. These compounds are known for their distinctive structures and diverse reactivity given by the even more pronounced tunability of the coordinated ligands. In fact, this type of organometallics, have shown promise in various medicinal applications since they can be engineered to interact with biological systems and exhibit diverse properties (including both biological and catalytic ones).[36] This fact is supported by the thousands of thousands of works present in the scientific literature based on this type of compounds that show among the most outstanding antitumor activity. Furthermore, this research group deeply investigated this Ruthenium-Arene complexes and exploited their biological properties obtaining very interesting and promising results.[37–44]

The following chapters and, the whole topic of this doctoral thesis, will turn into the support and confirmation of this statement.

1.2 RUTHENIUM AS ANTICANCER AGENT

Organometallic arene ruthenium complexes have attracted the attention of various scientists, chemists and biologists, owing to their intriguing chemical properties described in the previous chapters. Progress in the chemistry of arene ruthenium complexes stemmed from the discovery of the dinuclear chloride-bridged arene ruthenium complexes [(η^6-arene)Ru(μ-

Cl)Cl]$_2$ occurred in 1967 by Winkhaus and Singer.[45] The facile cleavage of the chloride bridges present in these complexes[46-47] have proved indispensable precursors in organometallic chemistry of Ruthenium and in particular for the synthesis of a range of piano-stool complexes allowing the introduction of a wide range of η^6-arene ligands (benzene = C$_6$H$_6$; toluene = C$_6$H$_5$Me; *p*-cymene = *p*- *i*PrC$_6$H$_4$Me; hexamethylbenzene = C$_6$Me$_6$, etc.) (**Scheme 1**).
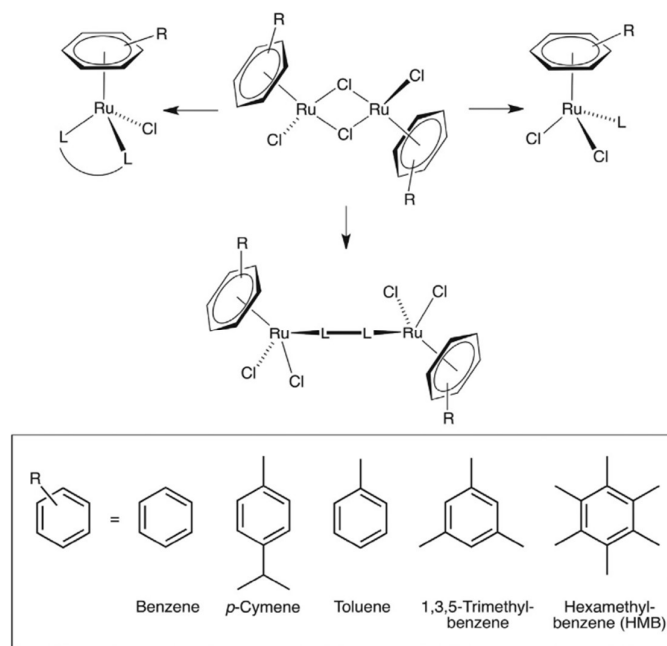
Scheme 1 - *Route for synthesis of different half sandwich piano-stool complexes*

As shown in **Figure 2**, in the half-sandwich Ruthenium-arene complexes the metal centre is in a pseudo-octahedral coordination environment in which three coordination sites are occupied by an aromatic ring bound in a η^6-manner while various ligands can occupy the three other positions. Because of their structural similarity with piano-stools, these types of complexes are also known as half-sandwich piano-stool complexes. Metal–hydrocarbon bonds in arene ruthenium complexes are highly stable under acidic, basic as well as reducing or oxidizing conditions, whereas the other ligands can be easily substituted. According to this, over the last decades, there has been an increase in research activity because of the tremendous demand for high-performance catalysts and non-toxic metallodrugs for practical applications.[48]
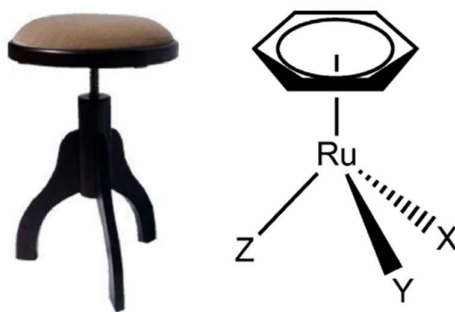
Figure 2 - Piano-stool model for half-sandwich-ruthenium complexes

Applications of arene ruthenium complexes in biology are widely explored because of the lower toxicity, high selectivity and amphiphilic properties provided by hydrophobic arene ligands and hydrophilic metal centres. That is why, arene-ruthenium complexes are the most studied organometallic compounds for possible anticancer activity. The results suggest that ruthenium is one of the most attractive metals in this regard, owing to its accessible redox-states, low toxicity and, more importantly, to the ability to mimic iron binding in biological systems.[47] In fact, as cancer cells over-express transferrin receptors to satisfy their increased demand for iron, ruthenium-based drugs (containing the iron homologue ruthenium) may be delivered more efficiently to cancer cells.[49] [50] In fact, the only non-platinum transition metal compounds currently in clinical trials are two coordination compounds based on ruthenium metal centre.

1.2.1 Ru(III) as anticancer agent

The first report treating the anticancer properties of Ruthenium was in 1976 when Ru(III) compounds as *fac*-Ru(NH$_3$)$_3$Cl$_3$ and *cis*-[RuCl$_2$(NH$_3$)$_4$] were found to induce filamentous growth of *E. coli* at a concentration comparable to that one required for cisplatin to produce similar effects,[51-52] showing anticancer activity as has been reported by Clark in 1980. However, they were too insoluble for pharmacological uses. Since this discovery, there have been several other reports of Ruthenium complexes which exhibit anticancer activity where, most of which, contain Ru in +3 oxidation state and remarkably, in 1986, Keppler et al. reported for the first time innovative water-soluble anionic Ru(III) complexes [i.e., imidazolium trans-bis-imidazoletetrachlororuthenate(III), (ImH)[trans-RuCl$_4$(Im)$_2$] (Im = imidazole)], including one which was later labelled as KP418 (**Figure 3**), having antitumor activity against P388 leukemia and B16 melanoma in BDF1 mice.[53] Notably, also manifested a high efficacy against an autochthonous model of colorectal cancer. The KP418 was the immediate precursor of the less toxic indazole (Ind) analogue, [(Hind)[trans-RuCl$_4$(Ind)$_2$]], known as KP1019 (**Figure 3**), which was later replaced by the more soluble sodium salt Na[trans-RuCl$_4$(Ind)$_2$] (KP1339, **Figure 3**), obtained starting from KP1019 in a two-step metathesis

reaction via the tetramethylammonium salt. These exciting results reported by Keppler on the Ru(III)-azole complexes triggered the development in the early 1990s of another class of structurally related Ru(III)-dmso compounds like X[*trans*-RuCl$_4$(dmso-S)$_2$] (X$^+$ = (dmso)$_2$H$^+$, Na$^+$, NH$_4^+$) prepared for the first time by Mestroni and Alessio.[54]

These compounds and, more importantly, the Na[*trans*-RuCl$_4$(dmso-S)$_2$] turned out to be an excellent precursor for compounds of the general formula Na[*trans*-RuCl$_4$(dmso-S)(L)] (where L = NH$_3$, azole or pyridine), which showed a greater stability in aqueous solution.

X$^+$ = Na$^+$ **NAMI**   X$^+$ = Na$^+$ **KP1339**   **KP418**
X$^+$ = ImH$^+$ **NAMI-A**   X$^+$ = IndH$^+$ **KP1019**
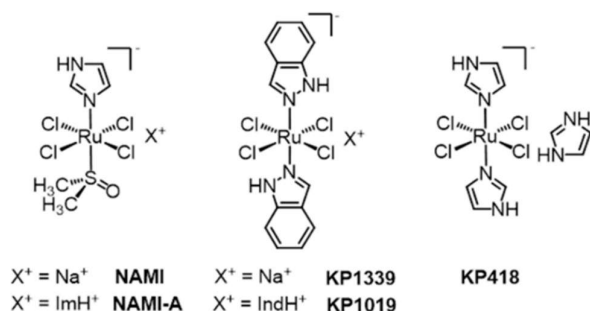
Figure 3 *- Ruthenium(III) derivatives with anticancer activity*

Tests performed by Sava et al. on solid metastasizing tumours in mice shown evidenced that these compounds induced a remarkable reduction of lung metastasis formation. Surprisingly, the antimetastatic effect was more pronounced with low doses given daily than with large doses given with drug-free intervals. Then, the water-soluble imidazole complex Na[*trans*-RuCl$_4$(dmso-S)(Im)] (NAMI, **Figure 3**) was selected for further investigations. NAMI was later replaced by the corresponding imidazolium salt, (ImH)[*trans*-RuCl$_4$(dmso-S)(Im)], called NAMI-A (**Figure 3**), that showed improved preparation, a greater stability in the solid state, and a better analytical profile, while maintaining a good solubility in water. Interestingly, both the KP-type and the NAMI-A-type compounds did not go through the usual pre-screening of in vitro cytotoxicity against cancer cell lines, but were instead investigated immediately on animal models[55-56] and currently the KP1019 it is in Phase I of the Clinical Trials.[57]

There are two significant differences between the two Ruthenium complexes, KP1019 and NAMI-A, and the platinum- based anticancer drugs: the octahedral geometry of the ruthenium complexes *vs*. square-planar geometry of the platinum(II) drugs, and, more importantly, the facility of electron transfer for Ru(II)/Ru(III) couples, while the reduction of Pt(IV) to Pt(II) results in both a change of the coordination number and of the interatomic bond distances. Due to these chemical differences, the mode of antitumor action of ruthenium-based drugs is supposed to differ distinctly from that of platinum compounds. Furthermore, the observed lower toxicity of Ruthenium-based as opposed to platinum-based drugs makes them very attractive for clinical developments. The lower toxicity of Ruthenium(III) complexes might be due, at least in part, to their capacity to act as prodrugs, as generally believed being, transformed *in vivo* or *in situ* into their active species that is the

Ruthenium(II), promoted by a so-called "activation-by-reduction mechanism". In fact, there is a lower oxygen content and more acidic pH in tumours than in normal tissue and so the production of Ru(II) relative to Ru(III) should be favoured.[51]

1.2.2 Ru(II) as anticancer agent

Because Ru(II) may be an active form of Ruthenium, there is now an increased effort into research on the anticancer activity of Ru(II) complexes. Early work on Ruthenium(II) complexes like *cis*-[RuCl$_2$(DMSO)$_4$] and *trans*-[RuCl$_2$(DMSO)$_4$] showed that Ru(II) complexes are potentially interesting in the design of new drugs,[50,58] which soon moved to half-sandwich Ruthenium(II) complexes (**Figure 4**). All complexes of this type contain an η^6-arene occupying three coordination sites, a chelating ligand occupying two positions and a mono-dentate ligand occupying the final site. Depending on the nature of the chelated ligand, these complexes are either neutral or positively charged and the possibility to modify all the different moieties, bound to the metal centre, give the access into a vast library of potential anticancer complexes.
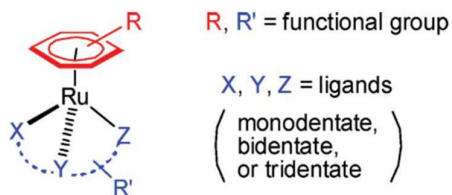
Figure 4 - Coordination environment of half-sandwich arene Ruthenium(II) complexes

The mechanism of cytotoxic action of Ru(II) arenes is thought to involve hydrolysis of the Ru−X bond generating an active Ru−OH$_2$ species (aquation phenomenon). This species will exist over a range of pH values, but above the pH = pK_a value (the pH at which 50% of the species exists as Ru−OH$_2$ and Ru−OH through deprotonation of the H$_2$O ligand) the hydroxo Ru−OH species will predominate, giving a less reactive species (**Scheme 2**). Hydroxide is a less labile ligand than water and hence will not be as easily displaced by biomolecule targets. Thus ideally pKa values of ca. pH >7 for aqua adducts should ensure that the active species predominates at physiological pH (7.2−7.4).[59]
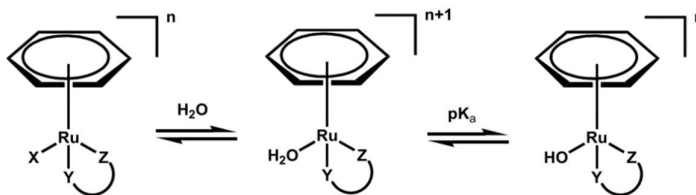
Scheme 2 - Hydrolysis of half-sandwich arene Ruthenium(II) complexes

The primary cellular target for Ru(II) arenes, as for many metal-based drugs, is thought to be DNA and, for this reason, factors affecting DNA binding such as rate and extent of binding and non-covalent interactions such as hydrogen bonding and DNA intercalation become important.[60-61]

Among these Ruthenium(II)-arene compounds two sub-families have been studied in detail (**Figure 5**):

- RAPTA family ([Ru(η^6-arene)(PTA)X_2]; PTA = 1,3,5-triaza-7-phosphaadamantane);
- READ family ([Ru(η^6-arene)(en)Cl]$^+$; en = ethylenediamine).
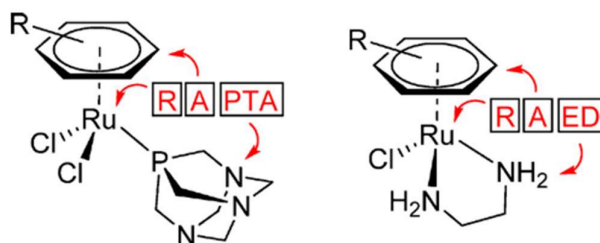
Figure 5 - Generic structures of RAPTA and RAED anticancer agents

The READ family is the first examples of anticancer Ru(II)-arene. It contains chelating σ-donor nitrogen atoms as ligands i.e. [(*p*-cymene)Ru(en)Cl]$^+$, [(*p*-cymene)Ru(en)I]$^+$, [(η^6-biphenyl)Ru(en)Cl]$^+$ and [(η^6-biphenyl)Ru(en-Et)Cl]$^+$, all possessing activity against the A2780 cancer cells with IC$_{50}$ values of between 6–9 μM, comparable to the clinically-used anticancer drug carboplatin (6 μM).

Furthermore complexes containing more hydrophobic arenes such as [(η^6-tetrahydronaphthalene)Ru(en)Cl]$^+$ were even more active, with IC$_{50}$ values equipotent with cisplatin (0.6 μM).[62] In addition, Ruthenium complexes containing mono-dentate ligands such as [(*p*-cymene)Ru(CH$_3$CN)$_2$Cl]$^+$ and [(*p*-cymene)Ru(isonicotinamde)$_2$Cl]$^+$ were inactive towards the same cancer cell line (IC$_{50}$ values >150 μM) indicating that a bidentate chelating ligand is required for cancer cell cytotoxicity together with a more hydrophobic arene ligand and a single ligand exchange centre (e.g. halide).

In contrast, the RAPTA family, is characterized by the presence of an amphiphilic phosphine ligand (PTA) which acts as monodentate neutral ligand that is placed in the coordination site usually occupied by the relatively labile chlorido ligand. PTA is a sterically undemanding ligand relative to other phosphines (with a cone angle of 103°) and may confer a degree of water solubility to the RAPTA complexes depending on the nature of the other co-ligands. This family exhibits a lot of biological properties including the antiviral, antibiotic, antimicrobial[63] and, only later reported, *in vitro* anticancer activity reducing the growth of primary tumours in preclinical models for ovarian and colorectal carcinomas.[64] Particularly,

the RAPTA-C (**Figure 6**, compound **1**) recently showed to also exert a strong anti-angiogenic effect having similarities shared with NAMI-A with a limited direct cytotoxic effects on cancer cells *in vitro* while exhibits important anti-metastatic behaviour *in vivo*.[65] According to this promising result, detailed investigation of RAPTA compounds, as well as model Me-PTA analogues (**Figure 6,** compounds **2** and **4**), has been undertaken, paying particular attention to their aqueous chemistry and *in vitro* cytotoxicity on tumour cells.[66]
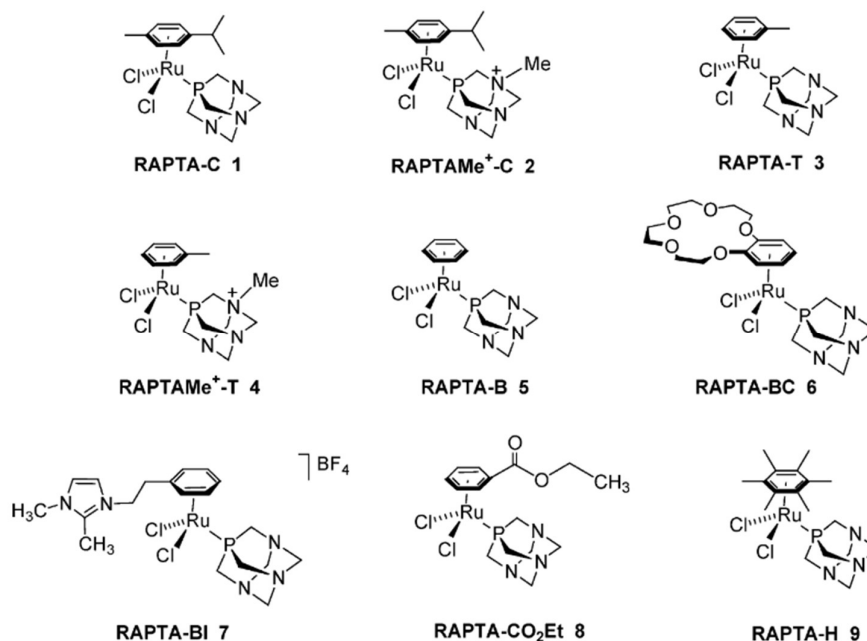
Figure 6 - *Structural variations of the ligands in the RAPTA-like compounds*

According to the reported studies, the antitumoral activity is due to the pH-dependence DNA damage of such family of compounds: the PTA ligand can be protonated at low pH, and the protonated form was considered to be the active agent such that at the pH typical of hypoxic tumour cells, DNA was damaged due to the activity of the protonated aquo compound (see **Scheme 3**), whereas at the pH characteristic of healthy cells, little or no damage was detected.[66]

However, despite showing in general less toxicity than platinum derivatives, ruthenium complexes, like cisplatin and other platinum-based drugs, are not highly selective and are specific to only certain types of cancers. As a consequence, there is still the need to develop even more effective chemotherapeutic agents.
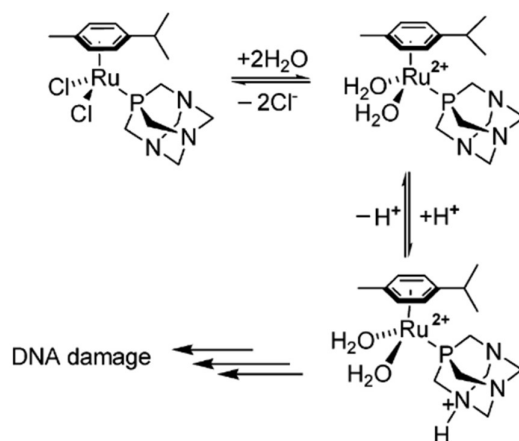
Scheme 3 - Protonation of the RAPTA-C, postulated as being responsible for pH dependant damage to DNA

1.3 OSMIUM AS ANTICANCER AGENT

As result from the previous chapters, is possible to state that elements like Iron and Ruthenium (both belonging to the 8-group of the periodic table) had a huge impact in the metal-based anticancer drug development and, nowadays, is possible to extent this aspect also to the Osmium metal centre because of the close proximity in the periodic table. Studies on bioactive Osmium complexes are still scarce, however, Osmium offers several features distinct from Ruthenium, including the preference for higher oxidation states, slower ligand exchange kinetics, stronger *p*-back-donation from lower oxidation states and markedly stronger spin-orbit coupling. Therefore, osmium complexes are considered interesting alternatives to Ruthenium-based anticancer agents because of their relative inertness and sufficient stability under physiological conditions. Furthermore, depending on the choice of ligand, osmium compounds exhibit diverse modes of action, including redox activation, DNA targeting or inhibition of protein kinases.[67-68] Although the aqueous chemistry of osmium metallodrugs is not completely understood, some trends on physicochemical properties have emerged in comparison to isostructural Ruthenium analogues. A typical feature of Os compounds is the increased inertness towards ligand substitution compared to Ru and therefore it results in reduced or even suppressed hydrolysis of metal–halido bonds. Moreover, upon hydrolysis, the formed Os–aqua species tend to be more acidic than the analogous Ru–aqua species, consequently, if hydrolysis occurs, the Os(II) complexes may be found as unreactive hydroxido species under physiological conditions, while hypoxic and slightly acidic tumour tissues may favor the aqua complexes if the pK_a of the aqua ligand is adjusted accordingly by selection of the ancillary ligands. According to the HSAB principle, Osmium is slightly softer than Ruthenium, which is expected to result in slightly different coordination preferences to biomolecules.[69]

Structural analogues of well-established Ruthenium compounds based on Osmium have been prepared and evaluated for their cytotoxicity, in fact, NAMI-A-analogous of Os(II) and Os(III) complexes have been prepared (**Figure 7**). They showed to be highly resistant toward hydrolysis, even in chloride-free solution, and also appear to have different biological properties. The diverse Os(II)-NAMI-A complexes **2** and **3**, in **Figure 7**, were inactive, while, on the contrary, the Os(III) analogue of NAMI-A, **1** (with more than one dimethyl sulfoxide ligand) displayed significant antiproliferative activity compared with the parent and related compounds.[70]
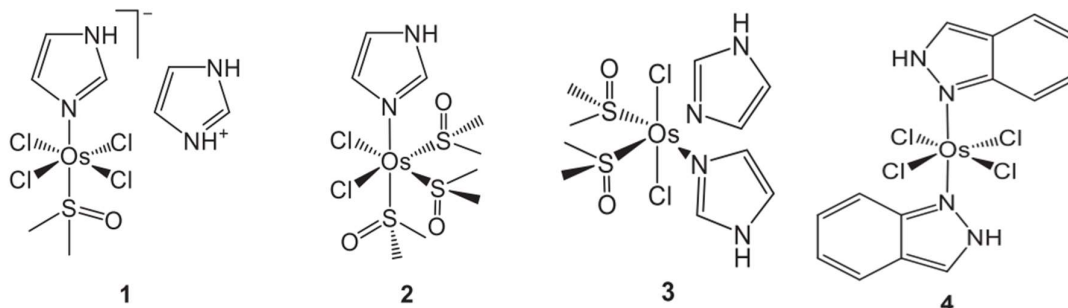
Figure 7 - *Osmium analogues of the Ruthenium-based clinically tested drug candidates NAMI-A*

According to the literature, the pharmacological effect of NAMI-A is attributed to the diverse Ruthenium-hydrolysed species, generated under physiological buffer conditions, that are readily taken up by cells. Therefore, the higher *in vitro* cytotoxicity of inert Osmium analogues was somewhat surprising. This suggests that hydrolysis is not an essential prerequisite for biological activity of this class of compounds.[71] Therefore, Osmium complexes could be used as model compounds for studying the biodistribution of un-hydrolysed NAMI-A and other anticancer-active ruthenium complexes. In a similar way, the Osmium-like KP1019 derivative, **4**, is stable in aqueous solution and demonstrated the same order of cytotoxicity in human cancer cells.[72]

As for Ruthenium, also the studies on Osmium derivatives moved toward their arene-complexes. Sadler and co-workers reported a library of Os(II) complexes of the general formula $[Os(\eta^6\text{-arene})(XY)Z]^+$ (XY = azopyridine derivatives, Z = Cl or I, arene = *p*-cymene or biphenyl) with important anticancer activity against human ovarian, breast, prostate, lung, colon and bladder cancer cell lines and, some of them, demonstrated at least tenfold higher anticancer potency compared with cisplatin against all tested cancer cell lines.[73] However, despite the higher stability of dinuclear Osmium complexes in aqueous solutions, their derivatives having an -O,O instead of an -N,N chelating ligand were about three times less active in vitro than their Ruthenium congeners.[74]

Recent studies on based on arene-Osmium derivatives containing PTA (RAPTA-like compounds) show that these analogues are selective toward tumorigenic cells.[75]

It should be noted that the analysis of different classes of Ruthenium and/or Osmium complexes does not result in a uniform picture. In some cases, the variation of the metal from Ruthenium to Osmium resulted in significantly enhanced cytotoxicity, as in case of NAMI-A analogues, whereas in other cases, the Ruthenium complexes were markedly more active, or the biological properties were independent of the nature of the metal center. Thus, further studies are required to gain comprehensive knowledge of biological processes interfered by Osmium complexes in the body. The interest in biologically active Osmium complexes has been continuously growing and it is believed that several novel Osmium complexes with exciting biological properties will be developed in the future.

1.4 CURCUMIN AND CURCUMINOIDS

Turmeric (also named *Curcuma longa*) is a spice and an important ingredient in curry and gives to the powder its characteristic yellow color. It is a member of the ginger family (*Zingiberaceae*) and it grows in the tropics and subtropics of Asia, especially in India, China, Indonesia, Jamaica, Peru, and Pakistan. *Turmeric* is assigned as rhizomatous and is a monocotyledonous perennial herbaceous plant. It has an intense yellow-colored fleshy root tuber that is very similar, in appearance, to the branched finger-shaped ginger root.(**Figure 8**).[76]

Figure 8 - *Origin of the Turmeric powder*

Turmeric has a wide chemical composition and curcumin (1,7-bis(4-hydroxy-3-methoxyphenyl)-1,6-heptadiene-3,5-dione), also called diferuloylmethane (Curcumin I, **Figure 9**), is the principal component (~70% of the total composition), together with other minor chemicals, known as "curcuminoids" (discovered by Srinivasan in 1952), which are represented by demethoxycurcumin (Curcumin II, ~17%), bisdemethoxycurcumin (Curcumin III, ~3%) and the most recently identified cyclocurcumin (found by Kiuchi et al. in 1993) which is present in traces (all represented in **Figure 9**). Among all the curcuminoids, the curcumin is the most studied since it represents the major component. These pigments are isolated from the rhizome through solvent extraction and subsequent crystallization.
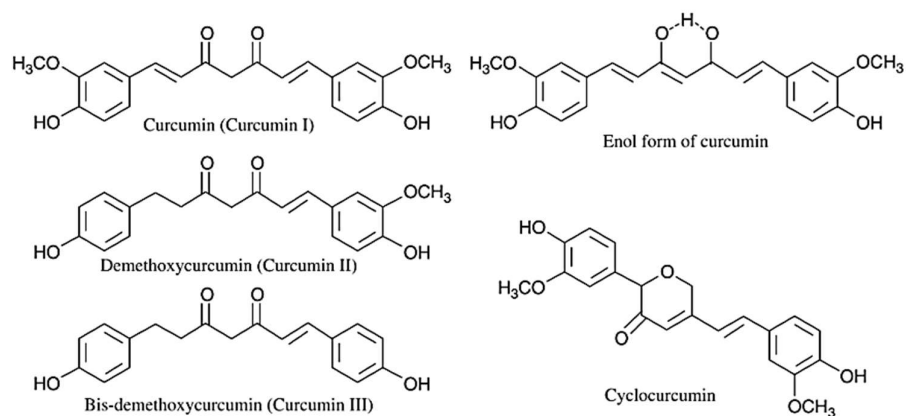
Figure 9 - *Curcuminoids present in the Turmeric*

The main and most important curcuminoids have three chemical entities in their structure (**Figure 11,** *Chapter* 1.4.3):

- The **two aromatic ring** systems containing *p*-hydroxy or *o*-methoxy groups (the only characteristic which differentiate all the curcuminoids between them);
- The seven carbon-linker which connects the two aromatic rings by a consisting of an **α,β-unsaturated** system;
- The **β-diketone moiety** (responsible for the yellow colour) able to exhibit a keto-enol tautomerism, which can exist in different types of conformers depending on the environment (solvents or pH) (**Scheme 4**).
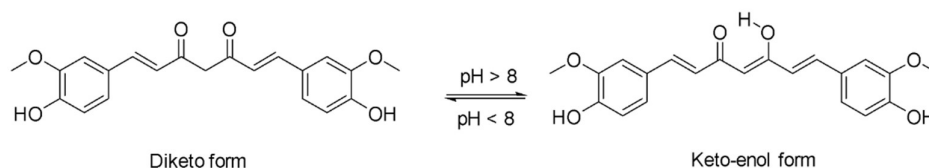
Scheme 4 - *Keto-enol tautomerism in curcumin*

The combination of all these structures leads to a planar, intramolecularly hydrogen-bonded structure in both solution and powder form. In the crystal state it exists in a *cis*-enol configuration, where it is stabilized by resonance assisted hydrogen bonding and the structure consists of three substituted planar groups interconnected through two double bonds. All the curcuminoids are hydrophobic molecules and soluble in most of the non-polar solvents and in moderately polar solvents. Curcumin is non-toxic even at high dosages, to date no toxicity has been found in any animal and human studies and has been classified as 'generally recognized as safe' (GRAS) by the National Cancer Institute.[77]

1.4.1 Biological properties and anticancer activity

Old scriptures described *turmeric* as an essential plant. It is defined as 'Indian saffron' and has been used for more than 4000 years for various purposes such as paint, cosmetic, condiment for food preparation and it is also famous for its use as ancient Indian medicine (*Ayurveda*) as documented by several Indian doctors. Indeed, the use of *turmeric* in medicine has spread to many countries over time.[78] However, the first scientific article on the treatment of biliary disorders with turmeric was published in 1937.[79] Just very few articles (around 73) has been published up to 1990 and only during the past 20 years the number of publications on this topic drastically increased.[80]

Curcumin was first isolated from *turmeric* in 1815, by Vogel and Pelletierand,[81] and identified as diferuloylmethane (curcumin) in 1910. Its biological properties were immediately underlined such as the management of oxidative (it is ten times more antioxidant than vitamin E) and inflammatory conditions, metabolic syndrome, arthritis, anxiety, and hyperlipidemia. It has also immunomodulatory and antiangiogenic effects. Curcumin can suppress symptoms related to diabetes, multiple sclerosis, Alzheimer; it can prevent the heavy metal absorption and hypertension together with many other properties like antibacterial, antiviral, wound healing, anti-cardiovascular, anti-AIDS, anti-gastrointestinal, anti-ischemia, neuroprotective and antidepressant activity. In addition, curcumin showed to target multiple signalling molecules and also demonstrated activity at the cellular level, which has helped to support its multiple health benefit.[82]

In recent years, curcumin's cancer-suppressant characteristic has attracted much attention in cancer research. Curcumin has been used to treat various inflammatory diseases for decades, and its uses in the treatment of leukemia and lymphoma, gastrointestinal, genitourinary, breast, ovarian, squamous (flat) carcinomas of the head and neck, lung cancer, melanoma and neurological cancers have been documented in the past years. It is thought that the main mechanisms of action by which curcumin exhibits its unique anticancer activity include inducing apoptosis and inhibiting proliferation and invasion of tumors by suppressing a variety of cellular signalling pathways. Furthermore, several studies reported curcumin's antitumor activity is capable to target multiple cancer cell lines.[83–85]

Additionally, the good optical and electrical properties of such curcuminoids, due to highly π-electron delocalized system and symmetric structure, make them suitable for applications in photodynamic therapy, biological imaging, three-dimensional optical data storage, optical power limiting and so on. Moreover, the coordination of curcumin into metal complexes exhibits higher quantum yield and larger two-photon absorption (TPA) cross-section in the near infrared (NIR) region compared with the free ligand [86] enhancing its potential application as a biological fluorescent probe.[87]

Although this traditional herbal medicine is considered healthy, the way in which the active principle mediate cancer is still unknown.[88] Anyway, the biological effects are for sure closely related to the peculiar molecular structure. It is indeed demonstrated that curcumin exhibits so great antioxidant and anticancer effects because of its free radical-scavenging properties. Moreover, curcumin's phenolic and enolic functional classes have great antioxidant activity as well. Additionally, other studies have reported that aromatic rings moieties exhibit cytostatic activity.[89]

Most of the research present in literature are focused on curcumin, mainly because it represents the most abundant component inside the *turmeric*, and just very few studies have been focused on the other curcuminoids (demethoxycurcumin and bisdemethoxycurcumin). These latter demonstrated that the curcuminoids exhibit variable anti-inflammatory and anti-proliferative activities,[90] and that, especially the bisdemethoxycurcumin is more stable than curcumin.[91-92] In addition, the degradation of bisdemethoxycurcumin proceeds considerably slower than that of curcumin and demethoxycurcumin. One possible reason for this could be attributable to the absence of the two methoxy groups.

1.4.2 Drawbacks of curcumin

Interestingly, curcumin by itself does not lead in *in vivo* to the associated health benefits due to many disadvantages given by its structure. In spite of all the above mentioned advantages, curcumin's applications are limited due to its low water solubility, which results in poor oral bioavailability, and also low chemical stability, in fact, curcumin will ultimately degrade upon release into physiologic media.[93] Generally, the oral bioavailability of curcumin is low due to a relatively low intestinal (small intestines) absorption and rapid metabolism in the liver, followed by elimination through the gall bladder.[80] Curcumin is, therefore, very poorly absorbed and mainly removed by fecal excretion with minimal elimination in the urine. Another obstacle is the low cellular uptake of curcumin (i.e. low permeability). Due to its hydrophobicity, the curcumin molecule tends to penetrate into the cell membrane and bind to the fatty acyl chains of lipidic membrane through hydrogen binding and hydrophobic interactions, resulting in low availability of curcumin inside the cytoplasm.[84]

The stability of curcumin in aqueous media plays a crucial role in this aspect and has been investigated by Bernabe-Pineda et al. (in 2004) resulting in a pH-dependent way. They showed that the stability of curcumin was improved at high pH values (>11.7) considering the three acidity constants: pKA1 = 8.38 ± 0.04; pKA2 = 9.88 ± 0.02 and pKA3 = 10.51 ± 0.01. Furthermore, Wang et al. examined the degradation kinetics of curcumin under various pH conditions and the stability of curcumin in physiological matrices. They observed that, when curcumin was incubated in 0.1 M phosphate buffer and serum-free medium at pH 7.2 at 37 °C, about 90% decomposed within 30 min. They also tested curcumin stability from pH=3 to

10 and showed that the decomposition of curcumin was pH dependent and occurred faster at neutral to basic conditions.[94] On the other hand, the greatest issue regard the poor bioavailability, which appears to be primarily due to poor absorption, rapid metabolism, and rapid elimination of the molecule.

There are several components that can increase bioavailability for example the assumption together with piperine (that is the major active component of black pepper) and, mainly, when combined in a complex with metal centres, demonstrated to increase bioavailability by 2000%.[95,82] All these aspects will be explored in depth in subsequent chapters.

Anyway, preclinical trials have stated that curcumin concentrations in plasma and target tissues are low because of their high metabolism rates.[96] By now it appears that curcumin has a hydrophobic nature and in the organism it is converted into a more water-soluble form via conjugation reaction. Concentration of curcumin in peripheral veins seems to be small due to its biotransformation, reduction and conjugation with glucuronic acid and sulfate (showed in **Figure 10**) which have been shown to be biologically inactive. The presence of these curcumin conjugates in blood and curcumin in secretions explains the low circulating levels of free curcumin.[97] These drawbacks represent the main obstacle to fully use all the useful properties of this substance, that is why the research, in the last two decades, is moving to try to improve the aspect of bioavailability at a biological level.

curcimin glucuronide

curcimin sulfate
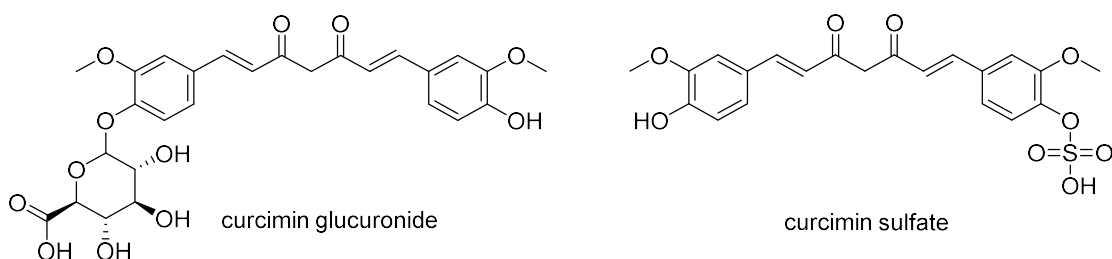
Figure 10 - *Bioconjugate products of curcumin*

1.4.3 Curcumin analogues

To overcome the obstacles reported in the previous chapter and to improve the overall anticancer activity of curcumin, the research is developing several strategies, and one approach is to use different delivery systems to improve curcumin's physiochemical properties and, as a consequence, the anticancer activity. For example, the glucuronidation of curcumin, and hence its phase II metabolism (explained in the following subchapter 1.4.3.1), is inhibited in the presence of piperine and this may increase the bioavailability, however, increasing curcumin bioavailability by inhibiting phase II metabolism should be carefully scrutinized, since many xenobiotics are detoxified through this pathway.

It is widely known that the enhanced permeability and retention effect may improve the accumulation of chemotherapeutic agents at tumor sites. In state of this, liposomes, carbon nanotubes, dendrimers, and micelles have been used as carriers for SN38, doxorubicin, paclitaxel, and cisplatin to improve not only the solubility, but also the drug concentrations in tumors and reduce adverse effects. Although various types of drug delivery systems have been used to enhance the cellular uptake and efficacy of curcumin (i.e. liposomes, nanoparticles, cyclodextrines etc.),[84,98-99] most of these formulations have remained at the proof of concept level and have not been evaluated in clinical trials.

Another approach to deal with the curcumin's drawbacks is its structural modification. To strategically modify the curcumin structure means to change the chemical and physical properties which may increase bioavailability, or enhance stability, and a lot of reported studies confirm also the enhanced selective toxicity towards specific cancer cells.[84] As has been already reported previously, the curcumin has different functional groups in its structure which can be modified to achieve potential benefits (**Figure 11**).
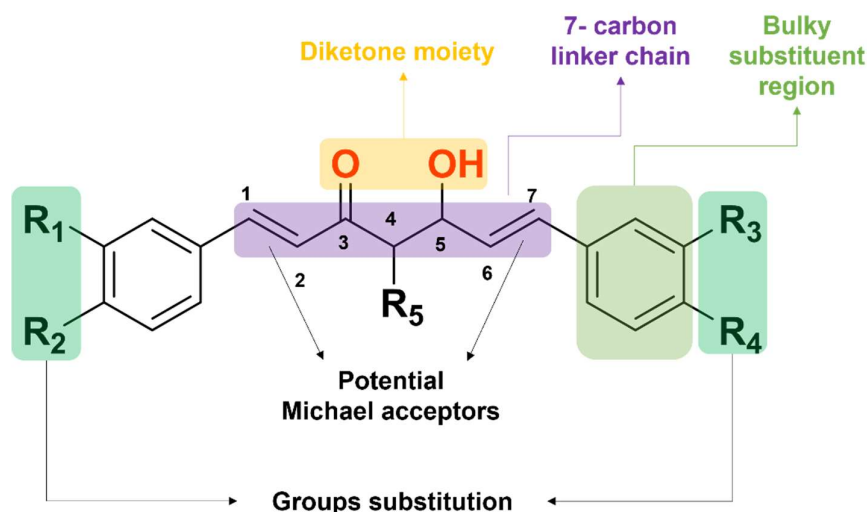
Figure 11 - *Main pharmacophores and potential substitution positions of curcumin's structure*

A structure-activity relationship study (SAR study) of curcumin derivatives underlined that the presence of a coplanar hydrogen donor group and a β-diketone moiety is essential for the antiandrogenic activity for the treatment of prostate cancer.[100] Furthermore, as a result of introducing a methyl group at C4 or both C2 and C6 positions (see **Figure 11**), there is a steric hindrance effect toward metabolizing enzymes that significantly increases the activity in inhibiting endothelial cell proliferation and invasion both *in vitro* and in *vivo*.[100] Moreover, the conjugation reactions, which may occur on the hydroxyl groups attached to the phenyl rings of curcumin, through glycosylation has proven to improve the water solubility and stability, leading to a better therapeutic response.[100] In contrast, a correlation between the

hydrophobic property of the benzyl rings and androgen receptor affinity has been found. In detail, the benzyl rings are also crucial for inhibiting tumor growth, and adding hydrophobic substituents on them, has been linked to the increased antitumor activity of curcumin derivatives.[101] Some of the modified curcuminoids exhibit enhanced anticancer and anti-inflammatory activities compared to curcumin due to the low level of hydrogenation, such as those derivatives produced from the human metabolism: a comparative revealed stronger antioxidant activity for several hydrogenated curcumin derivatives with respect to the original curcumin compound.[101]

This research work deals with this curcuminoids' structural modifications and as follow are reported the main ones that have been considered.

1.4.3.1 Tetrahydrocurcumin: an important metabolite

The metabolism of curcumin in humans produces several less studied products using the main pathways of degradation: reduction and O-conjugation (phase-I and phase-II respectively).[102-103] Particularly, the higher level of conjugation is one of the reasons responsible for the low bioavailability of curcumin. The reduction products are generated in the phase-I of the metabolism where it is involved the hydrogenation of double bonds by which curcumin is converted into tetrahydrocurcumin (THC), hexahydrocurcumin (HHC) and octahydrocurcumin (OHC), by the enzyme *reductase* (**Scheme 5**).[104] The THC represents a major metabolite and was first detected in 1978 by Holder et al.[105] and after that it has been reported to show a wide range of therapeutic properties associated to the parent curcumin molecule such as anti-oxidant, radical-scavenging, anti-metastatic and anti-carcinogenic activities, but unlike curcumin, THC has greater bioavailability.[106-107] There are several reports in which THC showed better pharmacological activities than curcumin like better hepatoprotective effects and antioxidant activities in case of liver injury.[108] Having additional hydrogens, THC is more hydrophilic than curcumin[109] and pharmacokinetic assessments reveal that it is more stable in phosphate buffers at neutral pH and plasma.[110] In fact, the lacks α,β-dienes prevent the formation of Michael adducts with intracellular proteins.
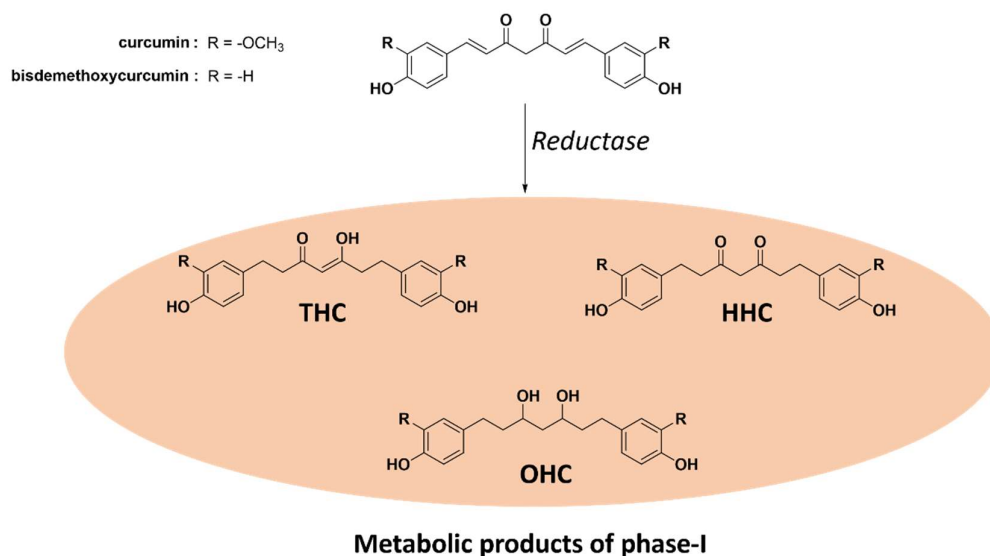
Scheme 5 – *Metabolic reduction of curcumin and bisdemethoxycurcumin*

However, numerous *in vitro* and animal studies have shown that curcumin is more active than THC.[107] Anyway, since the curcumin itself has poor chemical stability, low absorption, and also results in various modification once in the human body, it can be hypothesized that curcumin's degradation products and its metabolites may be responsible for its immense therapeutic effects since it has been observed that the parent compound does not distribute to any specific organs in appreciable levels.[93]

1.4.3.2 Curcumin conjugates

Curcuminoids have different functional groups that can be modified to reach superior or different properties. As occurs for the THC derivative, another alteration of the curcumin structure act to improve its bioavailability is, in fact, the conjugation at the aromatic level. Particularly, the two phenolic groups can act as potential sites for chemical variations and covalent linkage with biomolecules, as occurs for some of their metabolites (transformed into curcumin glucuronide and curcumin sulfate based on enzymatic hydrolysis studies, **Figure 10** of chapter **1.4.2**). The enhanced metabolic stability is due to this fact: masking of phenolic hydroxyl groups and delay in their glucuronide formation during metabolism. Many other curcuminoid conjugates have been synthesized with, for example, fatty acids, folic acid, dipeptides, and hyaluronic acid. Curcumin bioconjugates have shown to enhance cellular uptake of curcumin and possess enhanced antibacterial activity against Gram-positive and Gram-negative bacteria.[111] In detail, a curcumin bioconjugate with palmitoyl chloride did also show to facilitate neuroprotection, preventing oligomeric Aβ40 insult in Alzheimer's disease.[112] In this and many other reports, it has been observed that the bioavailability

improves upon conjugation. The coordination of biomolecules such as peptides, vitamins, sugar, etc. on the drug molecule is known to enhance the internalization of the conjugates selectively into the cancer cells as compared to the normal cells. In addition, attaching sugar molecules to curcumin brings the advantage of increased solubility in the aqueous medium, thus resulting in amplified drug activity.[113] Has been reported that the cellular uptake mechanism of glucose conjugates (**Figure 12**) is related to the ready translocation of the adduct through glucose transporters.[114] Studies on this area are still very few and many other progresses should be done in this new promising field.
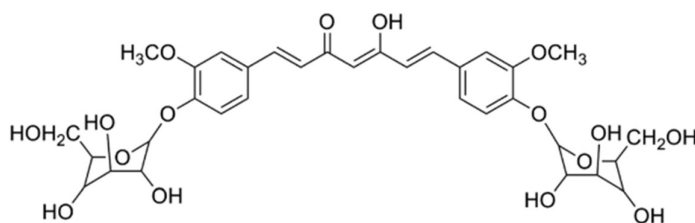
Figure 12 - Curcumin glycosides

The conjugation may occur either in only one or in both phenolic groups generating the monoester and diester derivatives respectively. Monoesters showed better activity than their corresponding diesters since monoesters have both the advantages as a ligand helping in cellular uptake and a free phenolic for binding at active site. The diesters analogues of curcumin, at the same time, showed better anticancer activity than the monoester analogues.[115]

1.4.3.3 Curcumin containing heterocycles

Curcumin can exist in a tautomeric mixture of keto and enol forms in solutions, and the enol form was found to be responsible for the rapid degradation of the curcumin (**Scheme 4** of the chapter **1.4**). In detail, the presence of the methylene group and β-diketone moiety contributes to the instability of curcumin under physiological conditions and that is why the deletion of the β -diketone group may contribute to the enhancement of stability of curcuminoids. The reason depends on the facility with which the α,β-unsaturated ketone, as a Michael acceptor, can form adducts with the –SH groups and generate reactive oxygen species.[115] Structural modifications of curcumin focused on the replacement of the β - diketone group, were proven to be a meaningful approach to discover analogues with enhanced properties and overcame limit like solubility, stability or bioavailability.[116 117 118 119] A few of the structurally modified curcumin analogous have displayed good anti-head and neck cancer activity.[120] Moreover, Chakraborti et al.,[98] found that the stability of curcumin was

improved when the central diketone moiety of the curcumin was replaced by isoxazole and pyrazole groups (**Figure 13**).
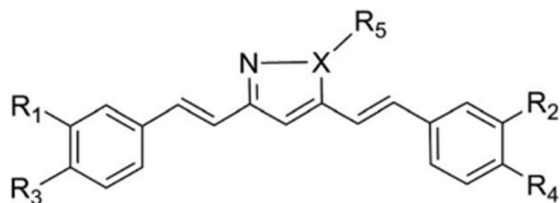
Figure 13 - *General structure of isoxazole (X= O) and pyrazole (X=N) containing curcuminoid compounds*

In fact, the heterocyclic modification at the keto-enol moiety of curcumin has been proven to be an important pharmacophore playing a pivotal role in various biological activities including antioxidant, anti-Alzheimer's and anticancer.[121–123] Most importantly, the pyrazole analogues of curcumin (one example showed in **Figure 14**) demonstrated an increase of the antioxidant power, COX-2 inhibitory activity, antitumor and antimalarial activity as compared to curcumin and, more in detail, showed a broad spectrum cytotoxic activity against KB, A549, CAKI-1, MCF-7, 1A9, HCT-8, SK-MEl-2, U-87-MG, HOS, PC-3, LNCaP, MDA-MB-231, KB-VIN, HepG2, and LNCaP (clone FGC) cell lines. In general, among these heterocycle compounds, pyrazole analogue of curcumin, exhibited the highest activity.
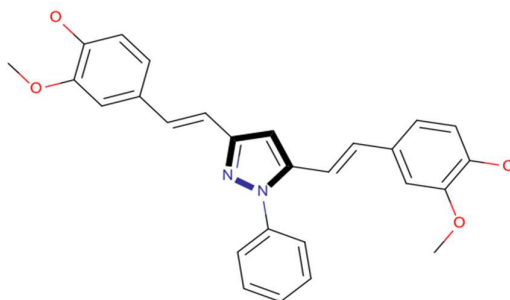
Figure 14 - *CNB001 molecule: an example of pyrazole-containing curcuminoids compound active to cross blood brain barrier*

1.5 ORGANOMETALLIC COMPLEXES OF CURCUMIN

One drawback of the structural modification is that it is difficult to achieve a balance between efficacy and solubility, and in most cases, one has been sacrificed in favour of the other. Most of the structural modifications that improve curcumin efficacy make the molecule more hydrophobic and reduce its solubility. Therefore, more work must be done in this regard to overcome this problem. In recent years, several research groups have focused to explore the applications of curcumin with the aim of improve bioavailability. Nanoparticles, liposomes,

micelles, soy protein isolate, oil body encapsulation and phospholipid complex are being used to enhance the dispersibility and bioactivity of curcumin for clinical trials.[124] A highly promising and innovative approach to deal with the bioavailability issue and to achieve even more diverse potential health benefits is the use of metal curcumin complexes.

As reported in the previous chapters, the metal centre has a fundamental role in terms of improving biological properties, solubility, and stability of the drug, therefore, the coordination of the curcuminoids to a d-block metal centre may deal with the bioavailability issue. There are many studies that report numerous complexes of curcuminoid ligands, with various main groups (d-transition and f-elements),

having selective anticancer activity (including the photo-cytotoxicity), anti-Alzheimer's activity and antioxidative/neuroprotective effects.[125]

Curcumin and the curcuminoids are rare examples of naturally occurring β-diketone ligands. As such, they should be ideally suited to act as chelating ligands toward a variety of metals and to form stable complexes, which may result in synergistic activity between the metal center and the ligand system.

The class of organoruthenium(II) half-sandwich compounds has attracted significant attention in the development of anticancer agents as well as for compounds with other biological activities.[126] That is why, organoruthenium complexes incorporating bioactive ligands such as curcuminoids, could be a key features for the development of new anticancer drugs.

1.5.1 Ruthenium-Arene Complexes of curcumin

The chemistry and potential antitumor activity of Ru(II)−(arene) compounds containing curcumin as a ligand, was only partially explored at the end of last decade.[101,127–129] That is why, more than 10 years ago, my research group decided to investigate this type of coordination compounds.

The first compound of this class that has been synthesized is related to the [(p-cymene)Ru(curc)Cl] (curc = curcumin) (**Scheme 6**) obtained by the interaction of commercial curcumin and the dimer [(p-cymene)RuCl$_2$]$_2$ in stoichiometric ratio 2:1. The reaction was conducted in a methanolic solution in the presence of NaOMe used as deprotonating agent for the enolic form of the curcumin.[130]
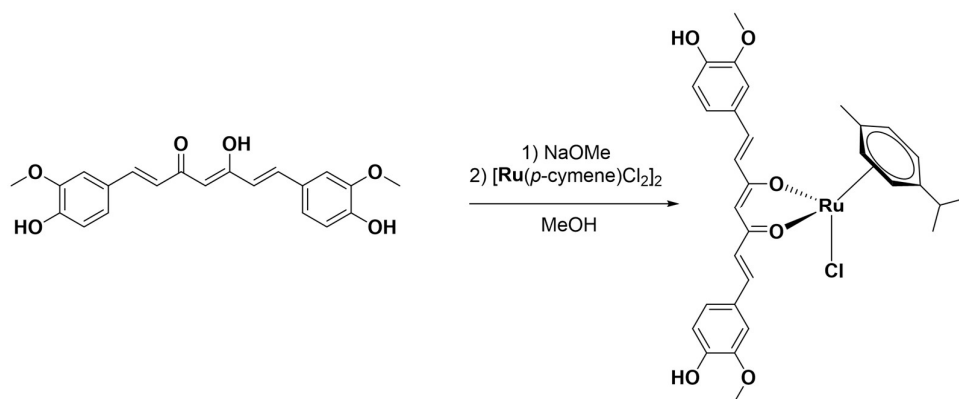
Scheme 6 - *Synthesis of [(p-cymene)Ru(curc)Cl]*

The X-ray diffraction of a single crystal confirms that the metal is bound with the curcumin through the two oxygen donors from the chelating β-diketone moiety. Furthermore, the complex possess the hypothesized piano-stool arrangement containing the *p*-cymene moiety on the axial level and the remaining three positions occupied by the monodentate chloride anion and the curcumin acting as bidentate mono-ionic ligand.

The cytotoxicity of [(*p*-cymene)Ru(curc)Cl][131] have been evaluated and it showed good anticancer activity against the breast adenocarcinoma (MCF7), ovarian carcinoma (A2780), and colon adenocarcinoma (HCT116) cell lines, moreover, the complex is less sensitive to human glioblastoma (U-87) and lung carcinoma (A549), indicating in a sort of way, a selectivity toward the cancerous cell lines. The data were compared with those elicited by cisplatin which resulted a more potent drug. The results, even if not satisfactory, are promising for making suitable chemical modifications to achieve higher biological activity and lower toxicity.

Additionally, [(*p*-cymene)Ru(curc)Cl] has been tested for its anti-aggregating properties toward amyloid 1-40 and 1-42 peptides present in Alzheimer's disease. The modified curcumin was shown to reversibly bind both peptides with moderate affinity and to interfere with the stacking mechanisms of aggregation, therefore it proved that the chemical modification of curcumin enhanced its efficacy, much likely due to a higher hindering effect on amyloid aggregation mechanism.[132]

A following study is focused on the modification of the arene moiety (**Figure 15**) with arene being not only *p*-cymene, but also benzene and hexamethylbenzene.[133]
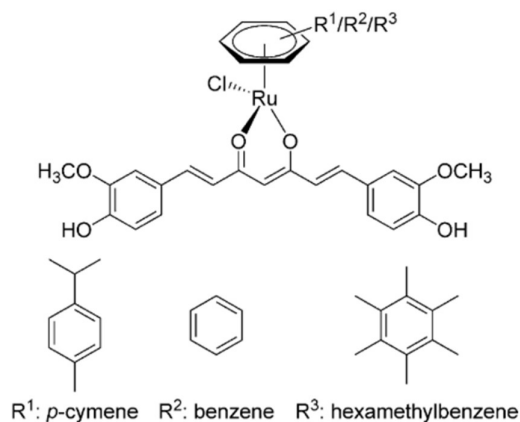
Figure 15 - *Ru-curcumin organometallic compounds bearing different arene structures*

According to the previous studies which report the ability of curcumin to inhibit both isolated and cellular proteasomes, thus contributing to the activation of apoptosis in cancer cells,[134] the ability, for the new complexes, to modulate the proteasome functionality by comparing their efficacies with that of free curcumin has been evaluated. The result states that the nature of the arene influences the interactions and among the derivatives assayed, compound containing the hexamethylbenzene as aromatic group, was able to diminish proteasome activity to a greater extent than free curcumin. Moreover, pro-apoptotic events were observed in HCT116 cells at 4 and 24 h. A further demonstration of the fundamental role imposed by the curcumin as ligand is given by the scientific evidence that a similar concentration of corresponding [(arene)RuCl$_2$]$_2$ dimer did not yield any inhibition of proteasome activity, indicating that curcumin is the molecule responsible for the activity toward the proteasome. The DNA is a potential target for arene–Ru(II) anticancer complexes and this type of compounds showed very high affinity of binding through the Ru-N7 (guanine) coordination.[130] The compound [(hmb)Ru(curc)Cl] was found to be the most effective in inducing DNA fragmentation coherently with its best anti-proteasome activity. This could depend either on the ability of the different complexes to bind in diverse way the DNA or on the lipophilicity of the system. In fact, the same compound which showed the best activity *in vitro* has lower efficacy on cellular proteasomes relative to the isolated enzymes and this, according to the studies, could be attributable to the longer retention time into the cellular membrane given by the higher affinity of Ru(II)-curcumin complexes for hydrophobic solution and environment with respect to the curcumin.

Since the hydrophobic contribution has shown to have a major impact on the anticancer activity, a following study was based on the investigation of *in vitro* antitumor activity of related complexes where the curcumin-like ligands are less polar than the parent compound (**Scheme 7**).[135]
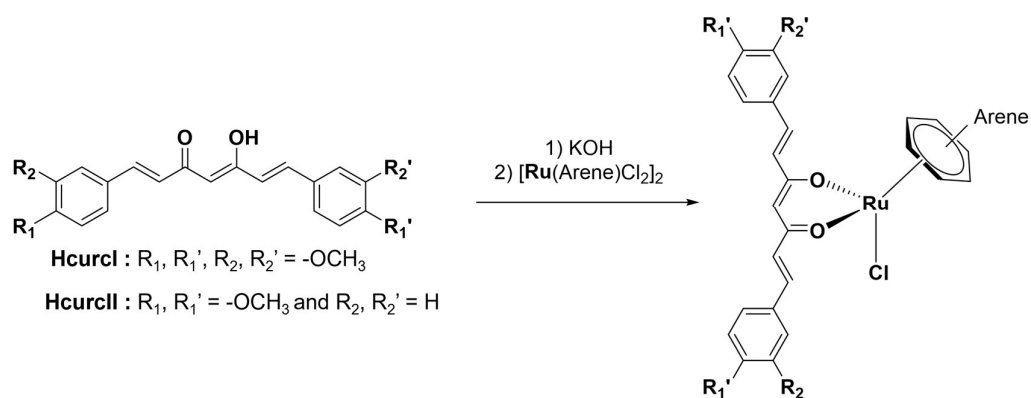
Scheme 7 - *Synthesis of more hydrophobic Ru-curcumin complexes*

In fact, in the curcumin analogues there is a replacement of the -OH groups with an -OCH$_3$ moiety, and the obtained species are HCurcI and HCurcuII (**Scheme 7**). The new Ru complexes represented in **Scheme 7** have an increased antitumor activity, compared to curcumin and its related complexes, toward the same cancerous cell lines (breast MCF7; ovarian A2780; glioblastoma U-87; lung carcinoma A549, and colon-rectal HCT116). In addition, HCurcII is less cytotoxic than curcumin but its related complex [(*p*-cymene)Ru(CurcII)Cl] is twice as active as HCurcII in 3 cell lines. The results obtained from the new arene-Ru curcuminoid species suggest that their increased cytotoxicity on tumor cells is correlated with the increase of curcuminoid lipophilicity. However, the absence of the hydroxyl groups in the curcumin analogues cause a decrease in the antioxidant features which would be non-existent in the related Ru complexes.

According to the great impact had for Ruthenium-Arene-PTA (RAPTA) derivatives in the anticancer treatment, the following research moved to the displacement of chloride anion with the PTA, acting as a neutral hydrophilic phosphine ligand.[136] This was important also to clarify if Ru-Cl bond hydrolysis is fundamental for the complex activity as the Cl− hydrolysis in cisplatin.
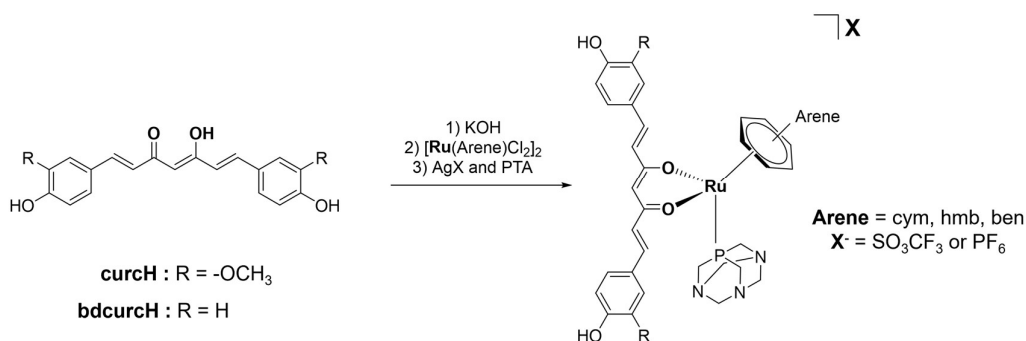
Scheme 8 - *Synthesis of RAPTA-like derivatives of curcumin*

The crucial step for the synthesis of these new RAPTA-like derivatives of curcuminoids is the third one showed in **Scheme 8** that is characterized by a metathesis reaction where the Cl, present as ancillary ligand in the complexes, is removed using a silver salt and replaced by

the PTA leaving the final ionic Ru(II) complex derivatives. This ligand-exchange resulted in a superior cytotoxicity and selectivity index (they are considerably less cytotoxic to nontumorous human embryonic kidney cells, HEK293) in comparison to clinically used cisplatin and this warranted the further development of these complexes. Precisely, these complexes are around 1−2 orders of magnitude more cytotoxic than previous [Ru(*p*-cymene)(curc)Cl] and inhibit the growth of the ovarian cancer cell lines (A2780 and A2780cisR) at lower micromolar concentrations with respect to the RAPTA-C, known in the literature, for which it is essentially inactive.

Moreover, the same RAPTA-type of complexes bearing the bisdemethoxycurcumin (bdcurc) analogue has been synthesized and the cytotoxicity evaluated did not show strong differences in the biological activity. The further increase in polarity possessed by the dicationic species of Ru(II) complexes (**Figure 16**), obtained with the methylated form of PTA (PTA-Me$^+$ having either BF$_4^-$ or I$^-$ as counterion) did not show any enhancement in the antitumoral activity.[137]
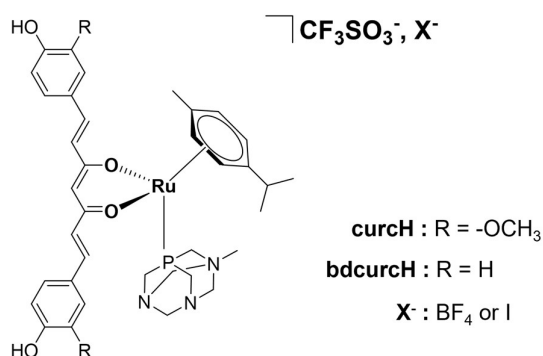
Figure 16 - Ruthenium(II)–arene-curcuminoid dicationic complexes containing PTA-Me as ancillary ligand

PTA-Me complexes display just a modest cytotoxicity and essentially no selectivity, probably due to their higher charge which reduces cellular uptake relative to the monocationic compounds.

Similarly, the same derivatives without the arene structure (**Scheme 9**) showed again just a moderate pharmacological activity which is likely connected to the relatively high stability of the complexes.[138] This underlines the importance of the aromatic feature.
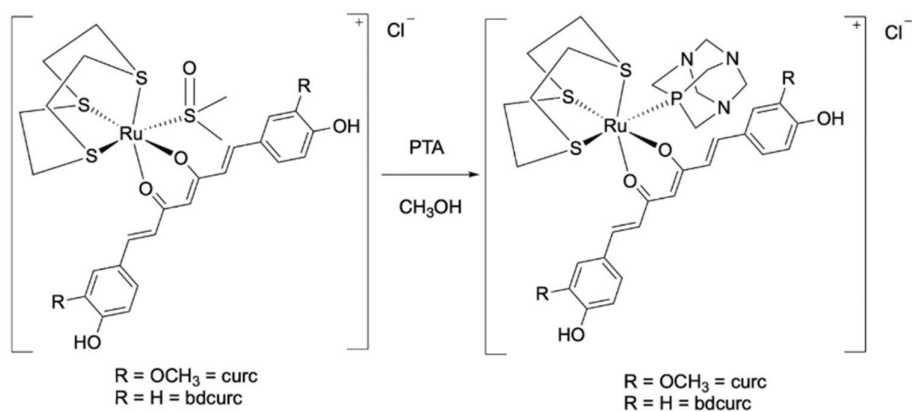
Scheme 9 – *(1,4,7-trithiacyclononane)-Ruthenium(II) complexes of curcumin and bisdemethoxycurcumin*

Additionally, ionic Ru(II) complexes bearing arene rings functionalized with amino or hydroxyl groups and curcuminoids (both curcumin and bisdemethoxycurcumin) as chelating ligands (**Scheme 10**) demonstrated to possess less stability, selectivity and cytotoxicity.[138] Notably, the non-functionalized analogues are considerably more cytotoxic than those with functionalized arene rings indicating that simple (more hydrophobic) arenes are advantageous, with the hydrophobic region potentially facilitating transport across cell membranes.
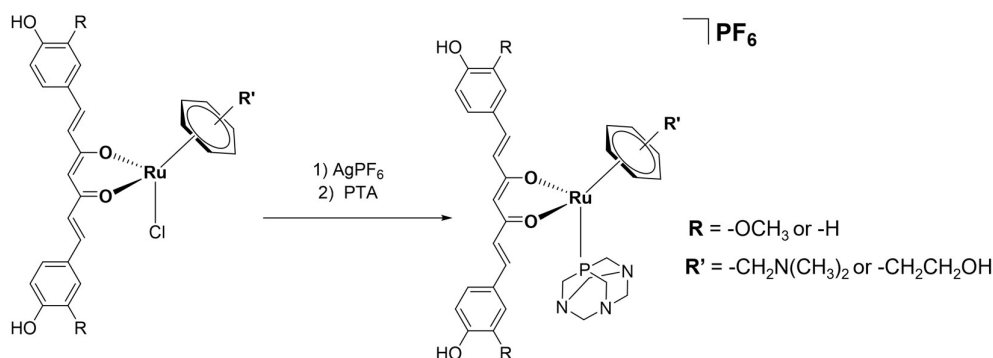
Scheme 10 - *Functionalized η^6-Arene Rings on Ruthenium(II) Curcuminoid Complexes*

The structure-activity relationship studies (SARs) moved then into the investigation of the metal centre varying among Os, Rh and Ir. All of the three metal centres were well known for their anticancer activity, in detail, Rh(I) and Ir(I) compounds with a square-planar geometry similar to that of cisplatin[139-140] and tetranuclear benzoquinonato arene-Osmium complex which was found more active than its Ruthenium analogue toward A2780 and A2780cisR cell lines.[141]

The presented Ir(III) and Rh(III) complexes contain a pentamethylcyclopentadienyl moiety as arene part (**Scheme 11**) and are 20–60 times less active than their corresponding Ruthenium(II) analogues in the ovarian cancer cell lines and, in contrast to the Ru(II), the Ir(III) and Rh(III) complexes containing chloride or PTA co-ligands exhibit similar biological

activities. Since it has been shown that all these compounds are able to release their curcuminoid ligands, under physiological- like conditions, it would suggest that the differences in activity between the pentamethylcyclopentadienyl M(III) (M = Rh/Ir) and arene Ruthenium(II) compounds originate from the different metal fragments, which are known to have different binding preferences for certain biological targets.[142]
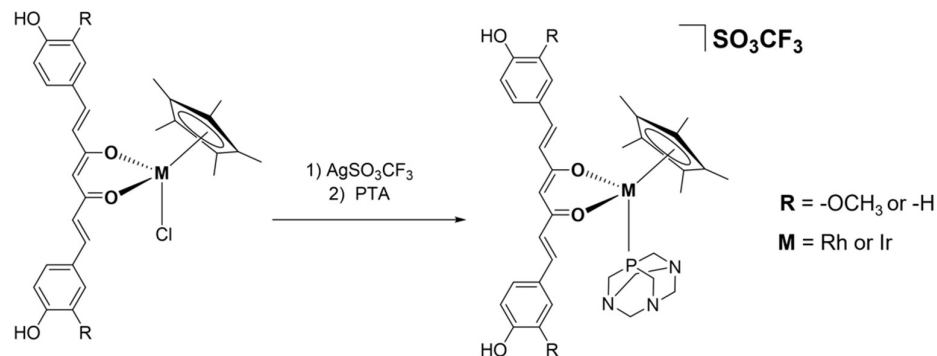
Scheme 11 - *Half-sandwich cyclopentadienyl rhodium(III) and iridium(III) complexes of curcuminoids*

Concerning the Osmium complexes, the cited *p*-cymene-Osmium compounds containing curcumin-based ligands (**Scheme 12**) have been reported for the first-time and studied for their antineoplastic activity.[143] Contrary to what has been said so far, the absence of peripheral methoxy groups in bisdemethoxycurcumin strongly influences the biological activity for these Os(II) complexes being more active with respect to the curcumin analogues.
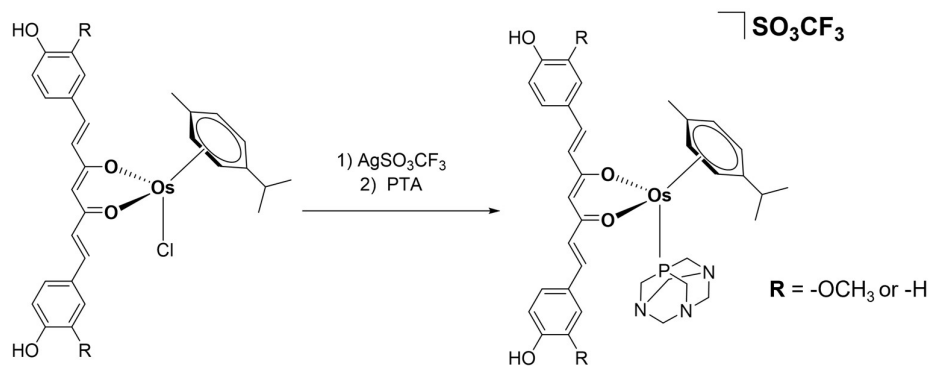
Scheme 12 - *Half-sandwich Os(II) complexes of curcuminoids*

Similarly to Ru(II) analogues the PTA derivatives are more cytotoxic and selective compared to the neutral chlorido compounds, being the Os(II)-PTA with bisdemethoxycurcumin compound only slightly less cytotoxic than its ruthenium analogue.

2.1 Aim of the work

In accordance with what has been said in the introductory chapters, the present work is aimed at an in-depth study of the new class of Ru(II) and Os(II)-(p-cymene) complexes containing curcuminoid-conjugate derivatives. In this research work is reported the synthesis and characterization of new ester-conjugate of curcumin and bisdemethoxycurcumin with the objective to investigate the biological impact of their Ru(II) and Os(II) related compounds. The modified ligands are obtained by nucleophilic substitution reactions between the phenolic groups, present in the curcuminoid structure, and different acyl chlorides having a cyclic, aliphatic, branched, aromatic or heteroaromatic moiety. Thus, the synthesis of the novel curcuminoid ligands is achieved through esterification with cyclopentane-carbonyl chloride, heptanoyl chloride, 2-naphthoyl chloride, 3,3-dimethylbuthyryl chloride and 2-furoyl chloride. The metal complexes have been synthesized using triethylamine as deprotonating agent for the curcuminoids which act as negatively charged bidentate ligands for Ru(II) and Os(II) metal centres obtaining novel half-sandwich M(II)-*p*-cymene complexes with potential anticancer activity thanks to their enhanced bioavailability. Moreover, the cytotoxicity against ovarian carcinoma both cis-platin active and resistant cell lines (AC2780 and AC2780cisR) have been evaluated as well as binding studies toward biological molecules like BSA and DNA.

The palmitic residue promotes the cellular uptake of curcumin and the metal centre influences the kinetic of membrane entry
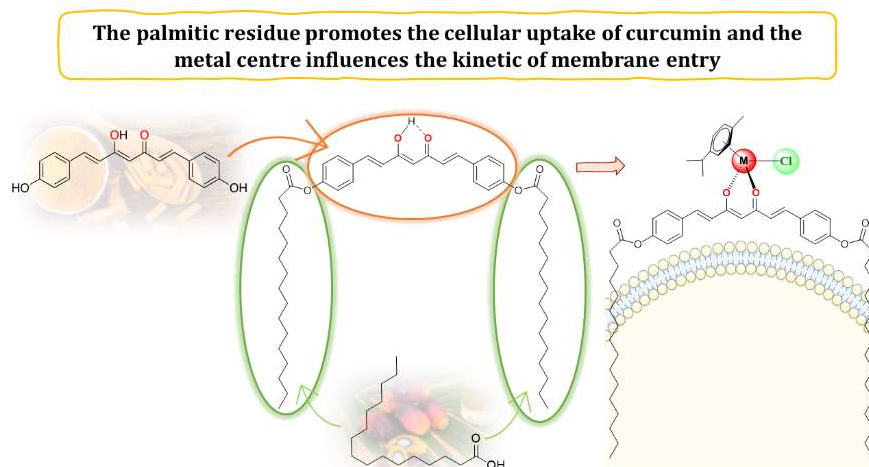
2.1.1 Materials and methods

The dimer [(*p*-cymene)RuCl$_2$]$_2$ was purchased from Aldrich, the [(*p*-cymene)OsCl$_2$]$_2$ was synthesized using literature methods.[144] Curcumin and bisdemethoxycurcumin were purchased from TCI Europe and were used as received. All other materials were obtained from commercial sources and were used as received. IR spectra were recorded from 4000 to 200 cm^{-1} on a PerkinElmer Spectrum 100 FT-IR instrument. ^{1}H, ^{13}C-NMR, ^{31}P-NMR, {^{1}H–^{1}H}-COSY NMR, {^{1}H–^{13}C}-HSQC and {^{1}H–^{13}C}- HMBC spectra were recorded on a 500 Bruker Ascend (500.1 MHz for 1H, 100 MHz for 13C and 202,4 MHz for ^{31}P). Referencing is relative to TMS (^{1}H) and 85% H$_3$PO$_4$ (^{31}P). Positive and negative ion electrospray ionization mass spectra (ESI-MS) were obtained on a Series 1100 MSI detector HP spectrometer using methanol as the mobile phase. Solutions (3 mg mL^{-1}) analysis were prepared using reagent-grade methanol. Masses and intensities were compared to those calculated using IsoPro Isotopic Abundance Simulator, version 2.1.28. Melting points were recorded on an STMP3 Stuart scientific instrument and a capillary apparatus. Samples for microanalysis were dried in vacuo to constant weight (20 °C, ca. 0.1 Torr) and analysed on a Fisons Instruments 1108 CHNS-O elemental analyzer. Uv-stability studies have been conducted with a Varian Caryl spectrometer. Electrical conductivity measurements (ΛM, reported as Ω^{-1} cm^2 mol^{-1}) of acetone solutions of the complexes were recorded using a Crison CDTM 522 conductimeter at room temperature. Binding studies were performed an IAsys + optical biosensor (Affinity Sensors – Cambridge, UK), equipped with carboxylate cuvettes (Neosensors – Crew, UK). Fluorometric assays were performed of a Shimadzu RF-5301PC fluorometer or on a SpectraMax Gemini XPS fluorescence plate reader (Molecular Device, Milan – Italy). HMGR activity assays were performed on an AKTA basic HPLC system.

2.1.2 Cytotoxicity studies

The human ovarian carcinoma cell line and its cisplatin resistant form, A2780 and A2780cis were purchased from the European Collection of Cell Cultures (ECACC, United Kingdom). The human embryonic kidney 293T cell line (HEK293T) was kindly provided by the biological screening facility (EPFL, Switzerland). Fetal bovine serum (FBS) was obtained from (Sigma, Switzerland). RPMI 1640 GlutaMAX and DMEM GlutaMAX media were purchased from Life Technologies. The cells were cultured in RPMI 1640 GlutaMAX supplemented for the ovarian cancer cell lines A2780 and A2780cis and in DMEM GlutaMAX supplemented for HEK293T with 10% heat-inactivated FBS at 37 °C and CO$_2$ (5%). To uphold cisplatin resistance, the A2780cis cell line was routinely treated with cisplatin at a final concentration of 2 μM in the media. MTT (3-(4,5-dimethyl-2-thiazolyl)-2,5-diphenyl-2H-tetra- zolium bromide) assay was used to evaluate the cytotoxicity of the compounds. Stock solutions were prepared in DMSO

and sequentially diluted in cell culture grade water to obtain a con- centration range of 0–1 mM. 10 µL aliquots of these prepared compound solutions were added in triplicates to a 96-well plate to which 90 µL of the cell suspension (approximately 1.4 ×10^4 cells per well) were added (final volume 100 µL/concentrations range 0–100 µM). Cisplatin and RAPTA-C were used as positive (0–100 µM) and negative (0–100 µM) controls, respectively, and the plates were incubated for 72 h. 10 µL of an MTT solution prepared at a concentration of 5 mg mL^{-1} in Dulbecco's phosphate buffered saline (DPBS) was added to the cells, and the plates were incubated for additional 4 h. The culture media was carefully aspirated to preserve the purple formazan crystals that were dissolved in DMSO (100 µL per well). The absorbance of the resulting solutions, which is directly proportional to the number of surviving cells, was measured at 590 nm using SpectroMax M5e microplate reader and the data was analysed with GraphPad Prism software (version 9.3.1). The reported IC$_{50}$ values are based on the means of three or two independent experiments, each com- prising three tests per concentration level.

2.1.3 BSA binding

The interaction between serum albumin and the compounds of interest was explored both fluorometrically, via quenching of BSA tryptophan fluorescence, and according to a biosensor binding assay. First, fluorescence spectra of 10 µM BSA were recorded from 300 nm to 450 nm upon excitation of tryptophan at 295 nm.[145] Titrations were performed by individual additions of 5 in the range 1–10 µM at 37 °C. Next, the binding kinetics of complexes **1**, **2**, **4** and **5** to BSA were further evaluated on an IAsys plus biosensor. BSA sensing surface was prepared pared as previously reported,[130] each complex being independently added at different concentrations in the range 0–2 µM and replicated at different pH values (6.8 and 7.4) at 37 °C. Raw data were globally fitted to both mono- and bi-exponential models, and the validity of each model to fit time courses was assessed by a standard F-test procedure.

2.1.4 Fluorescence anisotropy measurements

The kinetics of transport across cell membranes were explored by monitoring the change in membrane fluidity of Caco-2 cells during the internalization phase of the complexes of interest. Anisotropy measurements were carried out using membrane- anchoring TMA-DPH fluorescent probe (λ_{exc} = 340 nm; λ_{em} = 460 nm) at 37 °C on a RF-5301PC Shimadzu spectrofluorometer under continuous stirring. In detail, 1.5 × 10^5 per mL Caco-2 cells were pre-incubated with 1 µM TMA-DPH, and individually added with 10 µM of **1**–**5** and kept at 37 °C. Fluorescence anisotropy (*r*) was calculated at 10 min intervals for 200 min using the following model:

$$r = \frac{2P}{3 - P}$$

Fluorescence polarization (P) was derived using the equation:

$$P = \frac{I_| - I_\perp}{I_| + I_\perp}$$

with $I_|$ and $I_\perp$ being the fluorescence intensities parallel (0°) and perpendicular (90°) to the excitation beam, respectively. The kinetic rate constants characterizing the main steps of the internalization event (namely, k_{in} and k_{out}) were derived according to a general mono-exponential model:

$$r_{in} = a\left(1 - e^{k_{in}t}\right) + c$$

$$r_{out} = b\left(e^{k_{out}t}\right) + d$$

where r_{in} and r_{out} are the fluorescence anisotropy intervals corresponding to drug entry and exit phases from the membrane, respectively.

2.1.5 DNA binding

The interaction between dsDNA and the compounds of interest (namely **1**, **2**, **4** and **5**) was explored both according to a biosensor binding assay and spectrofluorometrically, by exploiting the ability of the compounds of interest to compete with specific DNA binders. The dsDNA sensing surface was obtained via streptavidin cross-linking as previously described.[130] Briefly, streptavidin protein anchor was covalently blocked *via* NHS-EDC chemistry. Next, a 5′-biotinylated dsDNA probe (sequence: 3′-CCACCCACTACCCTGGTTGGATGC- TAATGT-5) was coupled to surface-blocked the streptavidin. The compounds of interest were independently added to the DNA coated surface at different concentrations, each time following binding kinetics up to equilibrium.[130] Raw data were globally fitted to both mono- and bi-exponential models, and the validity of each model to fit time courses was assessed by a standard F-test procedure. Next, the binding sites on DNA for our complexes were mapped according to specific displacement assays. DNA molecules were independently labelled with DAPI (a minor groove binder) or methyl green (a major groove binder), eventually challenging individual DNA complexes with increasing concentration of the molecule of interest. Specifically, DAPI displacement was monitored from the decrease in the intensity of the emission spectra with increasing

concentrations of the candidate competitors. Reaction mixture contained different concentrations of these molecules (0–100 μM), DNA (20 μM), and DAPI (15 μM) in phosphate buffer (10 mM, pH 7.4). Likewise, methyl green displacement assay was performed by monitoring the absorbance at 630 nm.[130]

2.1.6 DNA docking analysis

The predictive models of all the above-mentioned ligand-DNA complexes were computed by independently docking the crystallographic structure of the ligands onto 3′-CCACCCACTACCCTGGTTGGATGCTAATGT-5′ dsDNA oligo- nucleotide (target oligomer was prepared and energy minimized using Avogadro).[130] Rigid geometric docking and energy refinement was performed using PatchDock[130] and FireDock[130]. As previously reported,[146] **1**, **2**, **4** or **5**, and DNA being uploaded as ligand and receptor, respectively. The images of the best scoring models were rendered with PyMOL (The PyMOL Molecular Graphics System, Version 2.2.3 Schrödinger, LLC).

2.1.7 HAS docking analysis

The molecular models of the complexes between HSA and **1**, **2**, **4** and **5** were obtained by flexible ligand–receptor docking using Autodock 4.2.[147] Ruthenium and osmium atom para-meters used manually set as "atom par Ru 2.96 0.056 12.000- 0.00110 0.0 0.0 0 -1 -1 1 # Non H-bonding", and "atom_par Os 3.12 0.120 12.000 -0.00110 0.0 0.0 0 -1 -1 1 # Non H-bonding", respectively. The 3D structures of the metal complexes were docked onto the crystallographic structure of human serum albumin (PDB entry: 1AO6[148] over a grid box (90 × 90 × 50 Å) embracing the whole protein. Default settings were used throughout. The resulting best scoring models were analyzed using Maestro (Schrödinger Release 2021-2: Maestro, Schrödinger, LLC, New York, NY, USA, 2021) and PyMOL (The PyMOL Molecular Graphics System, Version 2.4 Schrödinger, LLC).

2.1.8 General procedure for synthesis of ligands

HL[1]   ((1E,3Z,6E)-3-hydroxy-5-oxohepta-1,3,6-triene-1,7-diyl)bis(2-methoxy-4,1-phenylene) dipalmitate. Triethylamine (TEA 1.02 mL, 2.43 mmol) was mixed to a solution of curcumin (900 mg, 2.4 mmol) in acetone (27 mL) and then, after 15 minutes, palmitoyl chloride (2.22 mL, 7.33 mmol) was slowly added at 0 °C under N_2 atmosphere. The reaction mixture was stirred at room temperature. Thin layer chromatography (7:3 hexane/ethyl acetate) displayed the disappearance of curcumin and the formation of a faster running yellow spot after 1 hours. At this point the yellow precipitate was extracted from an aqueous

solution with CHCl$_3$ (18 mL x 3 times). At the end, the solution was treated with Na$_2$SO$_4$ and the solvent was evaporated under reduced pressure. The final **HL^1** (**Figure 17**) ligand has been obtained through crystallization in ethanol, precipitating as yellow powder (yield 66%). The ligand is soluble in DMSO, chlorinated solvents, slightly soluble in alcohols and CH$_3$CN and insoluble in H$_2$O, acetone, and n-hexane.

Figure 17 - *Structure of ligand HL^1*

Anal. Calcd. for C$_{53}$H$_{80}$O$_8$: C, 75.32; H, 9.54. Found: C, 75.13; H, 9.62. m.p.: 90-92 °C. IR (cm^{-1}): 2917 vs, 2850 vs v(aliphatic C-H); 1764 s v(-OC=O); 1703 m and 1624 m v(C=O), 1598 m, 1513 s, 1470 s v(C=C).^{1}H-NMR (DMSO-d_6, 293 K): δ 0.84 (t, 6H, C(26-26')H), 1.25 (mbr, 44H, aliphatic chain), 1.38 (m, 4H, C(14-14')H), 1.65 (m, 4H, C(13-13')H), 2.56 (m, 4H, C(12-12')H), 3.84 (s, 6H, OCH_3), 6.21 (s, 2H, C(1)H), 6.98 (d, 2H, C(3-3')H, ^{3}J = 16 Hz), 7.14 (d, 4H, C(9-9')H, ^{3}J = 8.0 Hz), 7.33 (d, 4H, C(10-10')H, ^{3}J = 8.0 Hz), 7.51 (s, 2H, C(6-6')H), 7.65 (d 2H, C(4-4')H, ^{3}J = 16 Hz,). ^{1}H-NMR (CDCl$_3$, 293 K): δ 0.90 (t, 6H, C(26-26')H), 1.28 (mbr, 44H, aliphatic chain), 1.45 (m, 4H, C(14-14')H), 1.65 (m, 4H, C(13-13')H), 2.61 (t, 4H, C(12-12')H), 3.90 (s, 6H, OCH_3), 5.88 (s, 2H, C(1)H), 6.59 (d, 2H, C(3-3')H, ^{3}J = 16 Hz), 7.08 (d, 4H, C(9-9')H, ^{3}J = 8.0 Hz), 7.14 (s, 2H, C(6-6')H), 7.19 (d, 4H, C(10-10')H, ^{3}J = 8.0 Hz), 7.65 (d 2H, C(4-4')H, ^{3}J = 16 Hz,). ^{13}C{^{1}H}-NMR (CDCl$_3$): δ 14.1 [C(26-26')], 22.7 [C(13-13')], 25.0 [C(14-14')], 29.1, 29.3, 29.4, 29.5, .29.6, 29.7, 29.7 [from C(15) to C(25)], 33.2 (*), 34.1 [C(12-12')], 55.9 [-OCH$_3$], 101.7 [C(1)] 111.5 [C(6-6')], 121.1 [C(10-10')], 123.3 [C(9-9')], 124.2 [C(3-3')], 133.9 [C(5-5')], 140.0 [C(4-4')], 141.5 [C(8-8')], 151.5 [C(7-7')], 171.6 [C(11-11')], 183.1 [C(2-2')=O]. ESI-MS (+) CH$_3$CN (m/z [relative intensity, %]): 846 [H$_2$L^1]$^+$.

HL² **((1E,3Z,6E)-3-hydroxy-5-oxohepta-1,3,6-triene-1,7diyl)** **bis(4,1-phenylene)**
dipalmitate. The ligand **HL²** was synthesized as reported for **HL¹** starting from
desmethoxycurcumin. **HL²** was obtained as yellow powder, yield 74% (**Figure 18**). It is
completely soluble in chlorinated solvents and DMF; slightly soluble in acetone, ethers and n-
hexane and insoluble in H_2O, alcohols, DMSO and CH_3CN.
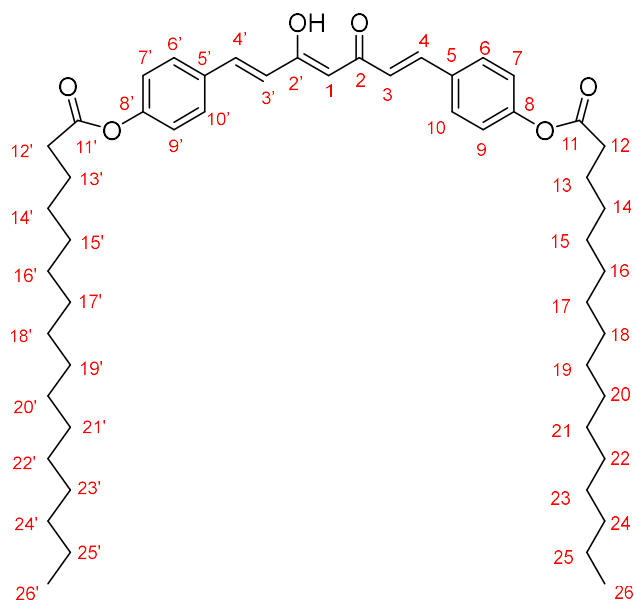
Figure 18 - *Structure of ligand HL²*

Anal. Calcd. For $C_{51}H_{76}O_6$: C, 78.02; H, 9.76. Found: C, 77.74; H, 9.79. m.p. 138-139°C. IR
(cm⁻¹): 2916 vs, 2849 vs v(aliphatic C-H); 1747 s v(-OC=O), 1701 m and 1647 m v(C=O),
1598 m, 1508 m, 1463 m v(C=C).¹H-NMR (CDCl₃, 293 K): δ 0.91 (t, 6H, C(26-26')H), 1.29
(mbr, 44H, aliphatic chain), 1.44 (m, 4H, C(14-14')H), 1.78 (m, 4H, C(13-13')H), 2.59 (t, 4H,
(C(12-12')H), 5.86 (s, 2H, C(1)H), 6.61 (d, 2H, C(3-3')H, ³J = 15.90 Hz), 7.2 (d, 4H, C(9-9')H
and C(7-7')H, ³J = 8.5 Hz), 7.60 (d, 4H, C(10-10')H and C(6-6')H, ³J = 8.5 Hz), 7.67 (d, 2H,
C(4-4')H, ³J = 15.90 Hz). ¹³C{¹H}-NMR (CDCl₃): δ 14.1 [C(26-26')], 22.7 [C(13-13')], 24.8
[C(14-14')], 29.1, 29.3, 29.4, 29.5, 29.6, 29.6, 29.7, 29.7 [from C(15) to C(25)], 31.9 (*), 34.4
[C(12-12')], 101.8 [C(1)], 122.2 [C(9-9) and C(7-7')], 124.1 [C(3-3')], 129.2 [C(10-10') and
C(6-6'), 132.6 [C(5-5')], 139.6 [C(4-4')], 152.1 [C(8-8')], 172.0 [C(11-11')], 183.2 [C(2-2')=O].

HL³ **((1E,6E)-** **3,5-dioxohepta-1,6-diene-1,7-diyl)** **bis** **(2-methoxy-4,1-phenylene)**
dicyclopentanecarboxylate. Triethylamine (TEA 0.34 mL, 2.43 mmol) was mixed to a
solution of curcumin (300 mg, 0.81 mmol) in acetone (9 mL) and then, after 15 minutes,
cyclopentane-carbonyl chloride (0.29 mL, 2.43 mmol) was slowly added at 0 °C under N_2
atmosphere. The reaction mixture was stirred at room temperature. Thin layer
chromatography (7:3 hexane/ethyl acetate) displayed the disappearance of curcumin and the
formation of a faster running yellow spot after 3 hours. At this point the yellow precipitate was

filtered with acetone and then purified by chromatographic column (7:3 hexane/ ethyl acetate). At the end, the solvent was evaporated under reduced pressure. The final **HL³** (**Figure 19**) ligand has been obtained through crystallization in diethyl ether, precipitating as yellow powder (yield 66%). The ligand is soluble in DMSO, chlorinated solvents, slightly soluble in alcohols and CH₃CN and insoluble in H₂O, acetone, and n-hexane.
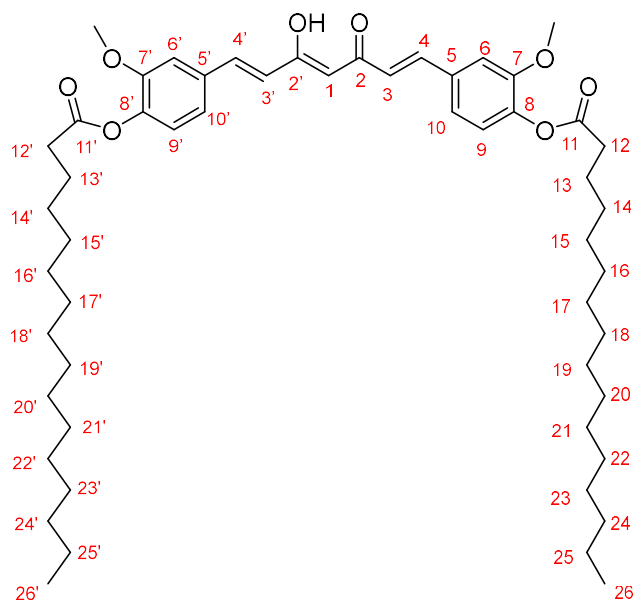

Figure 19 - Structure of ligand HL³

Anal. Calcd for $C_{33}H_{36}O_8$: C, 70.70; H, 6.47. Found: C, 70.02; H, 6.53. m.p.: 149–150°C. IR (cm⁻¹): 2969 wbr, 2871 wbr v(aliphatic C–H); 1753 m, 1746m v(–OC=O), 1622 w v(C=O); 1598 w, 1586 w, 1556 w,1506 m, 1455 w, 1408 w v(C=C); 1371 w, 1296 m, 1247 m, 1156 w, 1116 s, 1027 m, 982 m, 964 m, 890 w, 866 w, 844 m, 774 w, 732 w, 611 w. ¹H-NMR (CDCl₃, 293 K): δ 1.68 m, 181 m [8H, C(14-14')*H* and C(15-15')*H*], 2.05 [m, 8H, C(13-13')*H* and C(16-16')*H*], 3.06 [quint., 2H, C(12-12')*H*], 3.89 [s, 6H,-OC*H₃*], 5.88 [s, 1H, C(1)*H*], 6.59 [d, 2H, C(3–3')*H*, ³J = 16 Hz], 7.07 [d, 2H, C(9-9')*H*, ³J = 8 Hz], 7.14 [s, 2H, C(6-6')*H*], 7.18 [d, 2H, C(10-10')*H*, ³J = 8 Hz], 7.65 [d, 2H, C(4–4')*H*, ³J = 16 Hz]. ¹³C{¹H}-NMR (CDCl₃): δ 25.9 [*C*(14-14') and *C*(15-15')], 30.1 [*C*(13-13') and *C*(16-16')], 43.7 [*C*(12–12')], 56.0 [-OC*H₃*],101.6 [*C*(1)], 111.6 [*C*(6–6')], 121.1 [*C*(10–10')], 123.3 [*C*(9–9')], 124.2 [*C*(3–3')], 133.8 [*C*(5–5')], 140.0 [*C*(4–4')], 141.8 [*C*(8–8')], 151.6 [*C*(7–7')], 174.6 [*C*(11–11')], 183.1 [*C*(2–2')=O]. ESI-MS(-) CH₃OH (m/z [relative intensity, %]): 559 [100] [L³]⁻.

HL⁴ ((1E,6E)-3,5-dioxohepta-1,6-diene-1,7-diyl)bis(4,1-phenylene) dicyclopentane-carboxylate. Triethylamine (TEA 0.41 mL, 2.92 mmol) was mixed to a solution of bisdemethoxycurcumin (300 mg, 0.97 mmol) in acetone (9 mL) and then, after 15 minutes, cyclopentane carbonyl chloride (0.35 mL, 2.92 mmol) was slowly added at 0 °C under N₂ atmosphere. The reaction mixture was stirred at room temperature. Thin layer chromatography (7:3 hexane/ethyl acetate) displayed the disappearance of bisdemethoxycurcumin and the formation of a faster running yellow spot after 4 hours. At this point the yellow precipitate was filtered with acetone and then crystallized by dichloromethane/ ethanol giving **HL⁴** (**Figure 20**) as yellow powder (yield 76%). The ligand is soluble in DMSO and chlorinated solvents, slightly soluble in alcohols and CH₃CN and insoluble in H₂O, acetone, and n-hexane
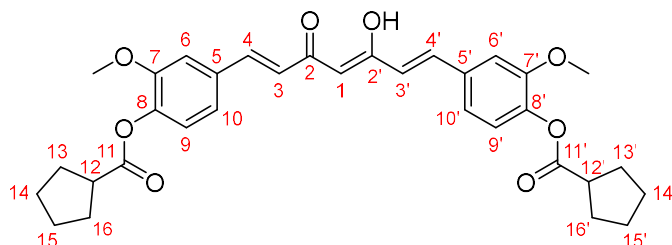
Figure 20 - *Structure of ligand HL^4*

Anal. Calcd for $C_{31}H_{32}O_6$: C, 74.38; H, 6.44. Found: C, 74.44; H, 6.41. m.p.: 218-220°C. IR (cm^{-1}): 2950 m, 2870 m ν(aliphatic C–H); 1743 s ν(–OC=O), 1632 m ν(C=O); 1567 m, 1505 m, 1447 m ν(C=C);1415 m, 1363 m, 1305 m, 1209 s, 1164 s, 1127 s, 1013 m, 967 s, 882 s, 860 s, 726 m, 696 m, 608 m. ^{1}H-NMR (CDCl$_3$, 293 K): δ 1.69 m, 1.81 m [8H, C(14-14')*H* and C(15-15')*H*], 1.99 m, 2.05 [8H, C(13-13')*H* and C(16-16')*H*], 3.02 [quint, 2H, C(12-12')*H*], 5.87 [s, 1H, C(1)*H*], 6.60 [d, 2H, C(3–3')*H*, ^3J = 16 Hz], 7.15 [d, 4H, C(9–9')*H* and C(7–7')*H*, ^3J = 9 Hz], 7.59 [d, 4H, C(10–10')*H* and C(6–6')*H*, ^3J = 9 Hz], 7.67 [d, 2H, C(4–4')*H*, ^3J = 16 Hz], ^{13}C{^{1}H}-NMR (CDCl$_3$): δ 25.9 [*C*(14-14') and *C*(15-15')], 30.1 [*C*(13-13') and *C*(16-16')], 43.9 [*C*(12–12')], 101.9 [*C*(1)], 122.2 [*C*(9–9') and *C*(7–7')], 124.1 [*C*(3–3')], 129.2 [*C*(10–10') and *C*(6–6')], 132.5 [*C*(5–5')], 139.6 [*C*(4–4')], 152.3 [*C*(8–8')], 175.0 [*C*(11–11')], 183.2 [*C*(2–2')=O]. ESI-MS(-) CH$_3$OH (m/z [relative intensity, %]): 499 [100] [L^4]$^-$.

HL^5 ((1E,6E)-3,5-dioxohepta-1,6-diene-1,7-diyl)bis(2-methoxy-4,1-phenylene) diheptanoate. Triethylamine (TEA 0.34 mL, 2.43 mmol) was mixed to a solution of curcumin (300 mg, 0.81 mmol) in acetone (9 mL) and then, after 15 minutes, heptanoyl chloride (0.38 mL, 2,43 mmol) was slowly added at 0°C under N$_2$ atmosphere. The reaction mixture was stirred at room temperature. Thin layer chromatography (7:3 hexane/ethylacetate) displayed the disappearance of curcumin and the formation of a faster running yellow spot after 4 hours. Evaporation of the solvent under reduced pressure provided a yellow solid which was then crystallized by dichloromethane/ethanol giving **HL^5** (**Figure 21**) as yellow powder (yield 74%). The ligand is soluble in DMSO, acetone and chlorinated solvents, slightly soluble in alcohols and CH$_3$CN and insoluble in H$_2$O and n-hexane.
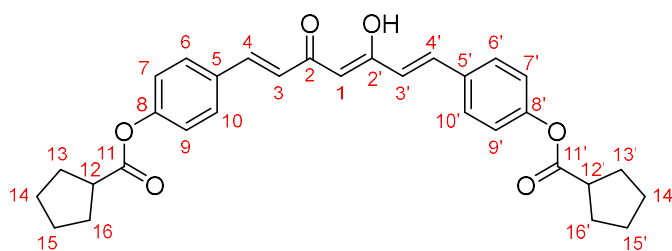

Figure 21 - *Structure of ligand HL^5*

Anal. Calcd for $C_{35}H_{44}O_8$: C, 70.92; H, 7.48. Found: C, 70.76; H, 7.56. m.p.: 105-106°C. IR (cm^{-1}): 2932 m, 2874 w, 2856 w ν(aliphatic C–H); 1766 m ν(–OC=O), 1627m ν(C=O); 1595 m, 1583 m, 1556 m, 1511 s, 1464 m, 1450 m,1410 m ν(C=C); 1380 m, 1300 s, 1255 s, 1233 m, 1204 m, 1162 m, 1132 s, 1118 vs, 1108 vs, 1026 s, 975 s, 940 s, 915 m, 855 s, 824 m, 794 m, 776 m, 723 m, 605 m. ^{1}H-NMR (CDCl$_3$, 293 K): δ 0.94 [t, 6H, C(17-17')*H*], 1.37 [m, 8H, C(16-16')*H* and C(15,15')*H*], 1.46 [m, 4H, C(14-14')*H*], 1.79 [m, 4H, C(13–13')*H*], 2.61 [t, 4H, C(12-12')*H*], 3.90 [s, 6H,-OC*H*$_3$], 5.88 [s, 1H, C(1)*H*], 6.59 [d, 2H, C(3–3')*H*, ^{3}J = 16 Hz], 7.07 [d, 2H, C(9–9')*H*, ^{3}J = 8.0 Hz], 7.14 [s, 2H, C(6–6')*H*], 7.18 [d, 2H, C(10–10')*H*, ^{3}J = 8.0 Hz], 7.64 [d 2H, C(4–4')*H*, ^{3}J = 16 Hz]. ^{13}C{^{1}H}-NMR (CDCl$_3$): δ 14.0 [*C*(17-17')], 22.5 [*C*(15–15')], 25.0 [*C*(13–13')], 28.7 [*C*(14-14')], 31.5 [*C*(16–16')], 34.1 [*C*(12–12')], 55.9 [-O*C*H$_3$], 101.7 [*C*(1)], 111.5 [*C*(6–6')], 121.1 [*C*(10–10')], 123.3 [(*C*(9–9')], 124.2 [*C*(3–3')], 133.9 [*C*(5–5')], 140.0 [*C*(4–4')], 141.5 [*C*(8–8')], 151.5 [*C*(7–7')], 171.6 [*C*(11–11')], 183.1 [*C*(2–2')=O]. ESI-MS(-) CH$_3$OH (m/z [relative intensity, %]): 591 [100] [L^5]$^-$.

HL^6 ((1E,6E)-3,5-dioxohepta-1,6-diene-1,7-diyl)bis(4,1-phenylene)   diheptanoate. Triethylamine (TEA 0.41 mL, 2.92 mmol) was mixed to a solution of bisdemethoxycurcumin (300 mg, 0.97 mmol) in acetone (9 mL) and then, after 15 minutes, heptanoyl chloride (0.45 mL, 2.92 mmol) was slowly added at 0 °C under N$_2$ atmosphere. The reaction mixture was stirred at room temperature. Thin layer chromatography (7:3 hexane/ethyl acetate) displayed the disappearance of bisdemethoxycurcumin and the formation of a faster running yellow spot after 4 hours. Evaporation of the solvent under reduced pressure provided a yellow solid which was then crystallized by dichloromethane/ethanol giving **HL^6** (**Figure 22**) as yellow powder (yield 49%). The ligand is soluble in DMSO, acetone and chlorinated solvents, slightly soluble in alcohols and CH$_3$CN and insoluble in H$_2$O and n-hexane.
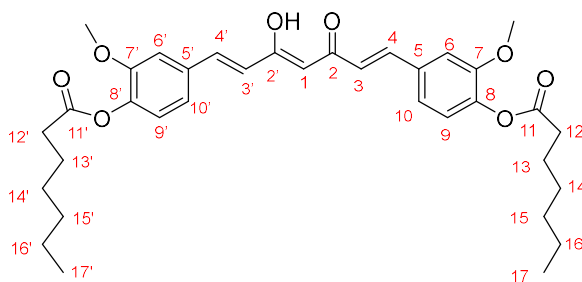

Figure 22 - *Structure of ligand **HL^6***

Anal. Calcd for $C_{33}H_{40}O_6$: C, 74.41; H, 7.57. Found: C, 74.41; H, 7.59. m.p.: 171-172°C.IR (cm^{-1}): 2957 w, 2927 s, 2853 w ν(aliphatic C–H); 1756 s ν(–OC=O), 1627 m ν(C=O); 1586 m, 1556 m, 1506 m, 1465 m, 1414 m ν(C=C); 1379 m, 1344 w, 1320 w, 1283 w, 1213 s, 1165 s, 1133 s, 1105 s, 1036 m, 1014 m, 977 s, 955 s, 922 s, 865 m, 842 vs, 796 m, 779 m, 723 s. ^{1}H-NMR (CDCl$_3$, 293 K): δ 0.94 [t, 6H, C(17-17')*H*], 1.37 [m, 8H, C(16-16')*H* and C(15,15')*H*], 1.45 [m, 4H, C(14-14')*H*], 1.78 [m, 4H, C(13–13')*H*], 2.59 [t, 4H, C(12-12')*H*],

5.86 [s, 1H, C(1)H], 6.60 [d, 2H, C(3–3')H, ^3J = 16 Hz], 7.15 [d, 4H, C(9–9')H and C(7–7')H, ^3J = 9 Hz], 7.59 [d, 4H, C(10–10')H and C(6–6')H, ^3J = 9 Hz], 7.67 [d, 2H, C(4–4')H, ^3J = 16 Hz]. ESI-MS(-) CH$_3$OH (m/z [relative intensity, %]): 531 [100] [L^6]⁻.

HL^7 ((1E,6E)-3,5-dioxohepta-1,6-diene-1,7-diyl)bis(2-methoxy-4,1-phenylene) bis(2-naphthoate). Triethylamine (TEA 0.34 mL, 2.43 mmol) was mixed to a solution of curcumin (300 mg, 0.81 mmol) in acetone (9 mL) and then, after 15 minutes, 2-naphthoyl chloride (463 mg, 2,43 mmol) was slowly added at 0 °C under N$_2$ atmosphere. The reaction mixture was stirred at room temperature. Thin layer chromatography (7:3 hexane/ethyl acetate) displayed the disappearance of curcumin and the formation of a faster running yellow spot after 5 hours. At this point the yellow precipitate was filtered with acetone, crystallized by dichloromethane/methanol (in order to favor the precipitation of the product but not that one of the acyl chloride) and then filtered with ethanol giving **HL^7** (**Figure 23**) as yellow powder (yield 60%). The ligand is soluble in DMSO and chlorinated solvents, slightly soluble in alcohols and CH$_3$CN and insoluble in H$_2$O, acetone and n-hexane.
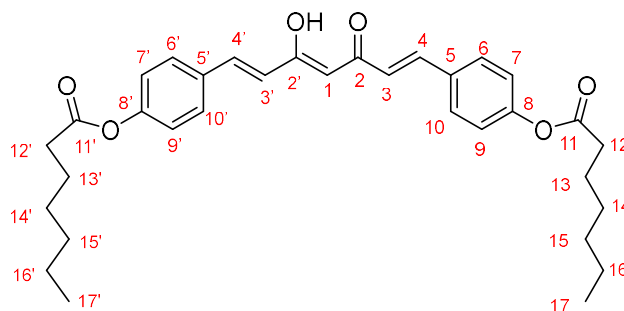

Figure 23 - Structure of ligand **HL^7**

Anal. Calcd for C$_{43}$H$_{32}$O$_8$: C, 76.32; H, 4.77. Found: C, 75.67; H, 4.77. m.p.: 210-211°C. IR (cm^{-1}): 3059 w, 3011 wbr v(aromatic C–H); 1727 s v(–OC=O), 1629 m v(C=O); 1588 m, 1512 m, 1471 m, 1412 m v(C=C); 1356 w, 1320 w, 1302 m, 1283 s, 1253 s, 1228 m, 1212 s, 1194 s, 1126 s, 1061 s, 1032 s, 968 m, 951 m, 908 m, 860 m, 838 m, 821 m, 800 m, 770 s, 759 s, 726 m, 633 w, 600 m. ^{1}H-NMR (CDCl$_3$, 293 K): 3.92 [s, 6H,-OCH_3], 5.94 [s, 1H, C(1)H], 6.65 [d, 2H, C(3–3')H, ^3J = 16 Hz], 7.26 [m, 6H, C(9-9')H, C(6-6')H, C(10-10')H)], 7.61 [t, 2H, C(17–17')H], 7.67 [t, 2H, C(16–16')H], 7.71 [d, 2H, C(4-4')H ^3J = 16 Hz], 7.96 [d, 2H, C(15–15')H, ^3J = 8 Hz], 7.99 [d, 2H, C(18-18')H, ^3J = 8 Hz], 8.04 [d, 2H, C(20-20')H, ^3J = 8 Hz], 8.24 [d, 2H, C(21-21')H, ^3J = 8 Hz], 8.84 [s, 2H, C(13–13')H]. ^{13}C{^{1}H}-NMR (CDCl$_3$): δ 56.0 [-OCH_3], 101.8 [C(1)], 111.7 [C(6–6')], 121.2 [C(10–10')], 123.5 [(C(9–9')], 124.4 [C(3–3')], 125.6 [C(20–20')], 126.4 [C(5–5')], 126.6 [C(17-17')], 127.9 [C(15-15')], 128.4 [C(18–18')], 128.7 [C(16-16')]. 129.5 [C(21-21')], 132.2 [C(13-13')], 132.5 [C(12–12')], 134.1 [C(14-14')], 135.9 [C(19–19')], 140.1 [C(4–4')], 141.8 [C(8–8')], 151.8 [C(7–7')], 164.7 [C(11–11')], 183.2 [C(2–2')=O]. ESI-MS(-) CH$_3$OH (m/z [relative intensity, %]): 675 [100] [L^7]⁻.

HL⁸ **((1E,6E)-3,5-dioxohepta-1,6-diene-1,7-diyl)bis(4,1-phenylene) bis(2-naphthoate).**
Triethylamine (TEA 0.41 mL, 2.92 mmol) was mixed to a solution of bisdemethoxycurcumin (300 mg, 0.97 mmol) in acetone (9 mL) and then, after 15 minutes, 2-naphthoyl chloride (557 mg, 2.92 mmol) was slowly added at 0 °C under N_2 atmosphere. The reaction mixture was stirred at room temperature. Thin layer chromatography (7:3 hexane/ethyl acetate) displayed the disappearance of bisdemethoxycurcumin and the formation of a faster running yellow spot after 3 hours. At this point the yellow precipitate was filtered with acetone and then washed with ethanol under magnetic stirring for 1 hour. Filtration with hot ethanol gave **HL⁸** (**Figure 24**) as yellow powder (yield 81%). The ligand is soluble in DMSO and insoluble in acetone, alcohols, CH_3CN, H_2O, n-hexane and chlorinated solvents.
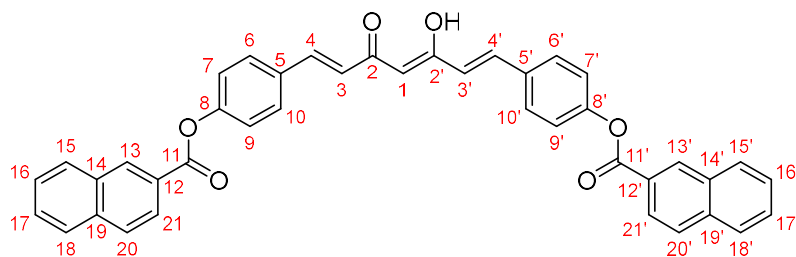
Figure 24 - Structure of ligand HL⁸

Anal. Calcd for $C_{41}H_{28}O_6$: C, 79.86; H, 4.58. Found: C, 79.87; H, 4.56. m.p.: 220-225°C. IR (cm⁻¹): 3056 w v(aromatic C–H); 1736 s v(–OC=O); 1640 m, 1613 m v(C=O); 1595 m, 1572 m, 1505 s, 1461 m, 1415 m v(C=C);1389 w, 1353 m, 1278 s, 1216 s, 1187 s, 1165 s, 1125 s, 1102 s, 1060 s, 1016 m, 972 s, 952 s, 926 m, 893 m, 867 m, 852 m, 811 m, 772 s, 757 s, 726 m, 642 m. ¹H-NMR (DMSO-d_6, 293 K): δ 6.90 [s, 1H, C(1)*H*], 7.31 [d, 2H, C(3-3')*H*, ³J = 8 Hz], 7.45 [d, 2H, C(4-4')*H*, ³J = 8 Hz], 7.63-7.76 [m], 7.81 [d, 4H, C(9-9')*H* and C(7-7')*H*, ³J = 9 Hz], 8.07 [d, 4H, (C(10-10')*H* and C(6-6')*H*, ³J = 9 Hz], 8.11-8.21 [m], 8.85-8.90 [m, 4*H*]. ESI-MS(-) CH_3OH (m/z [relative intensity, %]): 615 [100] [L⁸]⁻.

HL⁹ **((1E,6E)-3,5-dioxohepta-1,6-diene-1,7-diyl)bis(2-methoxy-4,1-phenylene) bis(3,3-dimethylbutanoate).** Triethylamine (TEA 0.34 mL, 2.43 mmol) was mixed to a solution of curcumin (300 mg, 0.81 mmol) in CH_3CN (9 mL) and then, after 15 minutes, 3,3-dimethylbutyryl chloride (0.34 mL, 2,43 mmol) was slowly added at 0 °C under N_2 atmosphere. The reaction mixture was stirred at room temperature. Thin layer chromatography (7:3 hexane/ethyl acetate) displayed the disappearance of curcumin and the formation of a faster running yellow spot after 3 hours. Evaporation of the solvent under reduced pressure provided a yellow solid which was then crystallized by dichloromethane/ethanol giving **HL⁹** (**Figure 25**) as yellow powder (yield 89%). The ligand is soluble in DMSO, CH_3CN and chlorinated solvents, slightly soluble in alcohols and insoluble in H_2O, acetone and n-hexane.
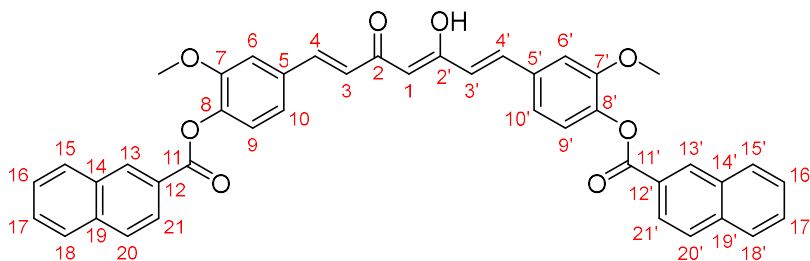
Figure 25 - *Structure of ligand HL⁹*

Anal. Calcd for $C_{33}H_{40}O_8$: C, 70.19; H, 7.14. Found: C, 68.15; H, 7.28. m.p.: 132-135°C. IR (cm^{-1}): 2964 w, 2871 w v(aliphatic C–H); 1748 m v(–OC=O), 1626 m v(C=O); 1598 m, 1586 m, 1506 s, 1464 m, 1418 m v(C=C); 1368 m, 1317 m, 1300 m, 1255 s, 1220 m, 1191 s, 1165 m, 1138 m, 1111 vs, 1033 s, 969 s, 947 m, 926 m, 896 m, 854 m, 842 s, 768 m, 730 m, 627 m, 606 m. ^{1}H-NMR (CDCl$_3$, 293 K): δ 1.18 [s, 18H, C(14-14')*H*, C(15-15')*H* and C(16-16')*H*], 2.50 [s, 4H, C(12-12')*H*], 3.90 [s, 6H,-OC*H₃*], 5.89 [s, 1H, C(1)*H*], 6.59 [d, 2H, C(3-3')*H*, ^{3}J = 16 Hz], 7.07 [d, 2H, C(9-9')*H*, ^{3}J = 8.5 Hz], 7.15 [s, 2H, C(6-6')*H*], 7.18 [d, 2H, C(10–10')*H*, ^{3}J = 8.5 Hz], 7.64 [d, 2H, C(4–4')*H*, ^{3}J = 16 Hz]. ESI-MS(-) CH$_3$OH (m/z [relative intensity, %]): 563 [100] [L⁹]$^-$.

HL¹⁰   ((1E,6E)-3,5-dioxohepta-1,6-diene-1,7-diyl)bis(4,1-phenylene)   bis(3,3-dimethylbutanoate). Triethylamine (TEA 0.41 mL, 2.92 mmol) was mixed to a solution of bisdemethoxycurcumin (300 mg, 0.97 mmol) in acetone (9 mL) and then, after 15 minutes, 3,3-dimethylbutyryl chloride (0.41 mL, 2.92 mmol) was slowly added at 0 °C under N$_2$ atmosphere. The reaction mixture was stirred at room temperature. Thin layer chromatography (7:3 hexane/ethyl acetate) displayed the disappearance of bisdemethoxycurcumin and the formation of a faster running yellow spot after 3 hours. The yellow precipitate was filtered with acetone and then crystallized by dichloromethane/ethanol giving **HL¹⁰** (**Figure 26**) as crystals (yield 50%). The ligand is soluble in DMSO and chlorinated solvents, slightly soluble in alcohols and CH$_3$CN and insoluble in H$_2$O, acetone and n-hexane.

Figure 26 - *Structure of ligand HL¹⁰*

Anal. Calcd for $C_{31}H_{36}O_6$: C, 73.79; H, 7.19. Found: C, 74.19; H, 7.21. m.p.: 202-204 °C. IR (cm^{-1}): 2959 w, 2904 w, 2868 w v(aliphatic C–H); 1754 s v(–OC=O), 1626 m v(C=O); 1595 m, 1580 m, 1535 m, 1506 s, 1469 m, 1415 m v(C=C); 1365 m, 1350 m, 1314 m, 1207 s,

1188 s, 1164 s, 1140 m, 1106 s, 1014 m, 975 s, 956 s, 927 s, 898 s, 838 s, 800 m, 785 m, 727 m, 615 m. ^{1}H-NMR (CDCl$_3$, 293 K): δ 1.17 [s, 18H, C(14-14')*H* C(15-15')*H* and C(16-16')*H*], 2.48 [s, 4H, C(12-12')*H*], 5.87 [s, 1H, C(1)*H*], 6.61 [d, 2H, C(3-3')*H*, ^{3}J = 16 Hz], 7.15 [d, 4H, C(9-9')*H* and C(7–7')*H*, ^{3}J = 9 Hz], 7.59 [d, 4H, C(10–10')*H* and C(6–6')*H*, ^{3}J = 9 Hz], 7.67 [d 2H, C(4–4')*H*, ^{3}J = 16 Hz]. ESI-MS(-) CH$_3$OH (m/z [relative intensity, %]): 504 [100] [L^{10}]$^-$.

HL^{11} ((1E,6E)-3,5-dioxohepta-1,6-diene-1,7-diyl)bis(2-methoxy-4,1-phenylene) bis(furan-2-carboxylate). Triethylamine (TEA 0.23 mL, 1.62 mmol) was mixed to a solution of curcumin (300 mg, 0.81 mmol) in acetone (9 mL) and then, after 15 minutes, 2-furoyl chloride (0.24 mL, 2,43 mmol) was slowly added at 0 °C under N$_2$ atmosphere. The reaction mixture was stirred at room temperature. Thin layer chromatography (7:3 hexane/ethyl acetate) displayed the disappearance of curcumin and the formation of a faster running yellow spot after 3 hours. The yellow precipitate was filtered with acetone and then crystallized by dichloromethane/ethanol giving **HL^{11}** (**Figure 27**) as yellow powder (yield 28%). The ligand is soluble in DMSO, CH$_3$CN and chlorinated solvents, slightly soluble in alcohols and insoluble in H$_2$O, acetone and n-hexane.
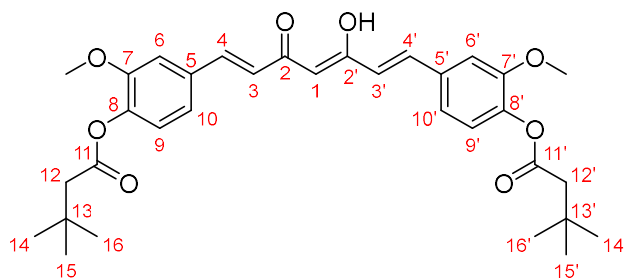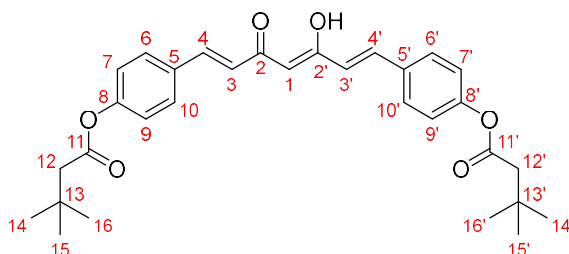

Figure 27 - *Structure of ligand HL^{11}*

Anal. Calcd for C$_{31}$H$_{24}$O$_{10}$: C, 66.90; H, 4.35. Found: C, 64.75; H, 4.17; m.p.: 216-218°C. IR (cm^{-1}): 3154 w, 3134 w, 3116 w 2996 w, 2975 w, 2945 w, 2841 w v(aromatic C–H); 1739 s v(–OC=O), 1627 m, 1601 m v(C=O); 1567 m, 1550 m, 1511 m, 1466 s, 1446 m, 1410 m v(C=C); 1393 m, 1294 s, 1269 m, 1251 m, 1230 m, 1207 m, 1160 s, 1120 s, 1079 s, 1032 s, 1016 s, 968 s, 929 s, 882 m, 851 s, 838 s, 780 s, 748 s, 726 m, 705 m, 654 m, 602 s. ^{1}H-NMR (CDCl$_3$, 293 K): δ 3.90 [s, 6H,-OC*H*$_3$], 5.90 [s, 1H, C(1)*H*], 6.62 [d, 2H, C(3-3')*H*, ^{3}J = 16 Hz], 6.63 [m, 2H, C(14-14')*H*], 7.19 d, 7.21 s, 7.22 d [6H, C(10-10')*H*, C(6-6')*H* and C(9-9')*H*], 7.44 [d, 2H, C(13-13')*H*], 7.67 [d 2H, C(4–4')*H*, ^{3}J = 16 Hz], 7.71 [d, 2H, C(15-15')*H*]. ESI-MS(-) CH$_3$OH (m/z [relative intensity, %]): 555 [100] [L^{11}]$^-$.

HL^{12} ((1E,6E)-3,5-dioxohepta-1,6-diene-1,7-diyl)bis(4,1-phenylene) bis(furan-2-carboxylate). Triethylamine (TEA 0.27 mL, 1.95 mmol) was mixed to a solution of bisdemethoxycurcumin (300 mg, 0.97 mmol) in acetone (9 mL) and then, after 15 minutes, 2-furoyl chloride (0.29 mL, 2.92 mmol) was slowly added at 0 °C under N$_2$ atmosphere. The reaction mixture was stirred at room temperature. Thin layer chromatography (7:3

hexane/ethyl acetate) displayed the disappearance of bisdemethoxycurcumin and the formation of a faster running yellow spot after 3 hours. The yellow precipitate was filtered with acetone and then crystallized by dichloromethane/ethanol giving **HL¹²** (**Figure 28**) as yellow powder (yield 45%). The ligand is soluble in DMSO and chlorinated solvents, slightly soluble in alcohols and CH_3CN and insoluble in H_2O, acetone and n-hexane.
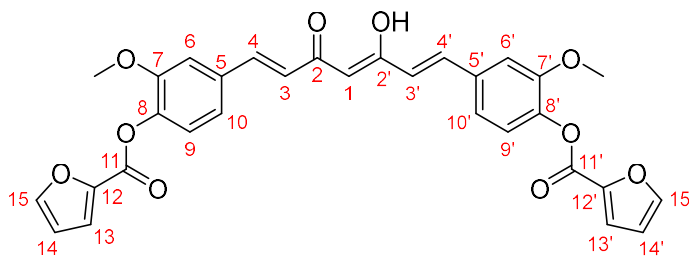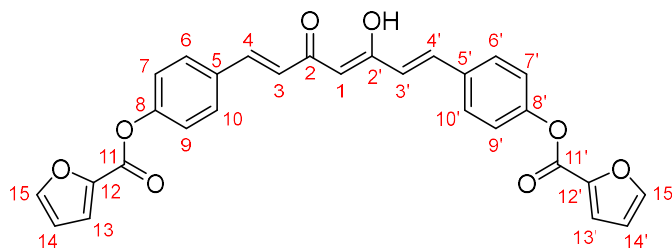

Figure 28 - *Structure of ligand **HL¹²***

Anal. Calcd for $C_{29}H_{20}O_8$: C,70.16; H, 4.06. Found: C,69.99; H, 4.1; m.p.: 210-212°C. IR (cm^{-1}): 3140 w, 3113 w v(aromatic C–H); 1747 m, 1732 s v(–OC=O), 1628 m, 1601 m v(C=O); 1586 m, 1565 m, 1506 s, 1465 s, 1418 m v(C=C); 1393 s, 1321 m, 1296 s, 1234 m, 1213 s, 1172 s, 1133 s, 1070 vs, 1013 s, 964 s, 932 s, 884 s, 847 s, 793 s, 781 s, 747 s, 727 s, 693 m, 651 m. ¹H-NMR (CDCl₃, 293 K): δ 5.88 [s, 1H, C(1)*H*], 6.64 [d, 2H, C(3-3')*H*, ^3J = 16 Hz], 6.64 [m, 2H, C(14-14')*H*], 7.30 [d, 4H, C(9-9')*H* and C(7-7')*H*, ^3J = 9 Hz], 7.43 [d, 2H, C(13-13')*H*], 7.65 [d, 4H, C(6-6')*H* and C(10-10')*H*, ^3J = 9 Hz], 7.70 [d 2H, C(4–4')*H*, ^3J = 16 Hz], 7.72 [d, 2H, C(15-15')*H*]. ESI-MS(-) CH₃OH (m/z [relative intensity, %]): 495 [100] [L¹²]⁻.

2.1.9 General procedure for synthesis of complexes

[**Ru(*p*-cymene)(L¹)Cl**] (**1**). **HL¹** (423 mg, 0.5 mmol) and triethylamine (50 mg, 0.5 mmol) were dissolved in CH_2Cl_2 (10 mL). After 1 h stirring at room temperature, [(*p*-cymene)RuCl₂]₂ (153 mg, 0.25 mmol) was added. The resulting red-orange solution was stirred at reflux for 24 h, after which the solvent volume was reduced, under vacuum, at about 3 ml and then 9 ml of n-hexane has been added. The precipitate formed was filtered off and washed with cold EtOH obtaining a red precipitate (260 mg, 0.23 mmol, yield 52%) which was identified as the pure compound **1** (**Figure 29**). It is completely soluble in DMSO, DMF, acetone and chlorinated solvents; slightly soluble in CH_3CN, ethyl acetate, ethers, alcohols, n-hexane and insoluble in H_2O.

Figure 29 - *Structure of compound 1*

Anal. Calcd. for $C_{63}H_{93}ClO_8Ru$: C, 67.87; H, 8.41. Found: C, 67.36; H, 8.53. mp: 141-143 °C. IR (cm^{-1}): 2916 vs, 2850 vs ν(aliphatic C-H); 1761 s ν(-OC=O, of **L¹**), 1630 m ν(C=O), 1599 w, 1525 vs, 1505 vs ν(C=C); 395 m, 269 s ν(Ru-Cl). ¹H-NMR ($CDCl_3$, 293 K): δ 0.91 (t, 6H, C(26-26')*H*), 1.29 (mbr, 44H, aliphatic chain of **L¹**), 1.41 (d, 6H, -CH(C*H₃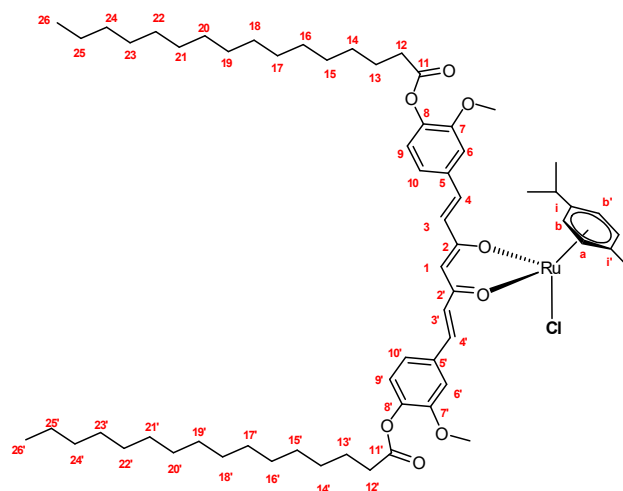*)₂ of *p*-cymene, ^4J = 7 Hz), 1.45 (m, 4H, C(14-14')*H*), 1.79 (m, 4H, C(13-13')*H*), 2.37 (s, 3H, -CH₃ of *p*-cymene), 2.60 (t, 4H, C(12-12')*H*), 3.00 (m, 1H, C*H*(CH₃)₂ of *p*-cymene), 3.88 (s, 6H, -OC*H₃* of **L¹**), 5.52 (s, 1H, C(1)*H* of **L¹**), 5.33 d, 5.60 d (4H, AA′BB′ system, CH₃-C₆*H₄*-CH(CH₃)₂ of *p*-cymene, ^3J = 6 Hz), 6.53 (d, 2H, C(3-3')*H* of curc, $^3J_{trans}$ = 16Hz), 7.03 (d, 2 H, C(9-9')*H* of **L¹**, $^3J_{trans}$= 8 Hz), 7.11 (d, 2H, C(10-10')*H* of **L¹**, ^3J = 8 Hz), 7.10 (sbr, 2H, C(6-6')*H* of **L¹**), 7.58 (d, 2H, C(4-4')H of **L¹**, $^3J_{trans}$ = 16 Hz). ¹³C{¹H}-NMR ($CDCl_3$, 293 K): δ 14.1 [*C*(26-26')], 18.1 (-*CH₃* of *p*-cymene), 22.4, 22.7 (-CH(CH₃)₂ of *p*-cymene), 25.0 [*C*(13-13')], 29.1 [*C*(14-14')], 29.3, 29.4, 29.5, 29.6, 29.7, 29.7 [from *C*(15) to *C*(25) of **L¹**], 30.9 (CH(CH₃)₂ of *p*-cymene), 31.9, 34.1 [*C*(12-12')], 55.9 (-OCH₃ of **L¹**), 79.2 [*C*(a-a')], 83.0 [*C*(b-b')], 97.7 [*C*i'], 99.7 [*C*i], 102.3 [*C*(1)], 111.0 [*C*(6-6')], 120.9 [*C*(10-10')], 123.1 [*C*(9-9')], 127.8 [*C*(3-3')], 134.7 [*C*(5-5')], 138.1 [*C*(4-4')], 140.8 [*C*(8-8')], 151.3 [*C*(7-7')], 171.8 [*C*(11-11')], 178.3 [*C*(2-2')=O]. ESI-MS (+) CH_3CN (m/z [relative intensity, %]): 1079 [100] [Ru(*p*-cymene)(**L¹**)]⁺.

[Ru(*p*-cymene)(L²)Cl] (**2**). **HL²** (392 mg, 0.5 mmol) was dissolved in CH_2Cl_2 (10 mL) and complex **2** was synthesized with a procedure similar to that of compound **1**. The pale-orange powder (355 mg, 0.37 mmol, yield 67%) (**Figure 30**) is completely soluble in DMSO, DMF, CH_3CN; slightly soluble in ethyl acetate, Et_2O, alcohols, acetone, chlorinated solvents and insoluble in H_2O, n-hexane, and petroleum ether.
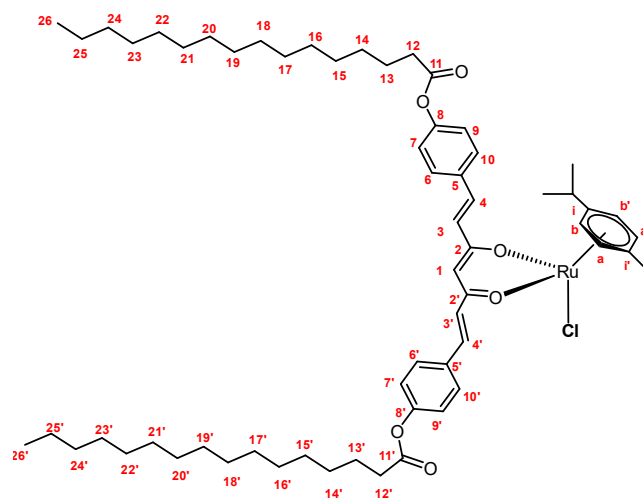
Figure 30 - *Structure of compound 2*

Anal. Calcd. for $C_{61}H_{89}ClO_6Ru$: C, 69.45; H, 8.50. Found: C, 69.08; H, 8.58. mp: 120-123 °C. IR (cm^{-1}): 2916 vs, 2850 vs ν(aliphatic C-H); 1756 s ν(-OC=O, of **L²**), 1631 m ν(C=O), 1541 s, 1520 vs, 1503 s ν(C=C); 270 s ν(Ru-Cl). ^{1}H-NMR (CDCl₃, 293 K): δ 0.91 (t, 6H, C(26-26')*H*), 1.29 (mbr, 44H, aliphatic chain of **L²**), 1.42 (d, 10H, CH(C*H₃*)₂ of *p*-cymene, ^{4}J = 7 Hz, and C(14-14')*H*), 1.78 (m, 4H, C(13-13')*H*), 2.37 (s, 3H, CH₃ of *p*-cymene), 2.58 (t, 4H, C(12-12')*H*), 3.01 (m, 1H, C*H*(CH₃)₂ of *p*-cymene), 5.49 (s, 1H, C(1)*H* of curcumin), 5.33 d, 5.60 d (4H, AA'BB' system, CH₃-C₆*H₄*-CH(CH₃)₂ of *p*-cymene, ^{3}J = 6 Hz), 6.54 (d, 2H, C(3, 3')*H* of **L²**, ^{3}J$_{trans}$ = 16Hz), 7.11 (d, 4 H, C(9-9')*H* and C(7, 7')*H* of **L²**, ^{3}J$_{trans}$ = 9 Hz), 7.54 (d, 4 H, C(10-10')*H* and C(6-6')*H* of **L²**, ^{3}J$_{trans}$ = 9 Hz), 7.60 (d, 2H, C(4-4')H of **L²**, ^{3}J$_{trans}$ = 16 Hz). ^{13}C{^{1}H}-NMR (CDCl₃, 293 K): δ 14.1 [*C*(26-26')], 18.0 [-*C*H₃ of *p*-cymene], 22.4, 22.7 [-CH(*C*H₃)₂ of *p*-cymene], 24.9 [*C*(13-13')], 29.1 [*C*(14-14')], 29.3, 29.4, 29.5, 29.6, 29.7, 29.8 [from *C*(15) to *C*(25)], 30.9 [*C*H(CH₃)₂ of *p*-cymene], 31.9, 34.4 [*C*(12-12')], 79.2 [*C*(a-a')], 83.0 [*C*(b-b')], 97.6 [*C*i'], 99.7 [*C*i], 102.5 [*C*(1)], 122.0 [*C*(9-9') and *C*(7-7')], 127.7 [*C*(3-3')], 128.8 [*C*(10-10') and *C*(6-6')], 133.5 [*C*(5-5')], 137.8 [*C*(4-4')], 151.5 [*C*(8-8')], 172.1 [*C*(11-11')], 178.4 [*C*(2-2')=O]. ESI-MS (+) CH₃CN (m/z [relative intensity, %]): 1019 [5] [Ru(*p*-cymene)(L²)]⁺.

[Os(*p*-cymene)(L¹)Cl] (**3**). **HL¹** (423 mg, 0.5 mmol) and triethylamine (50 mg, 0.5 mmol) were dissolved in CH₂Cl₂ (10 mL). After 1 h stirring at room temperature, [(*p*-cymene)OsCl₂]₂ (150 mg, 0.25 mmol) was added. The resulting red solution was stirred at reflux for 24 h, after which the solvent volume was reduced, under vacuum, at about 3 ml and then 9 ml of n-hexane has been added. The precipitate formed was filtered off and washed with cold EtOH obtaining a red precipitate (339 mg, 0.28 mmol, yield 56%) which was identified as the pure compound **3** (**Figure 31**). It is completely soluble in DMSO, DMF, CH₃CN, acetone, chlorinated solvents, ethyl acetate, Et₂O and n-hexane (at 50°C); slightly soluble in alcohols and insoluble in H₂O.
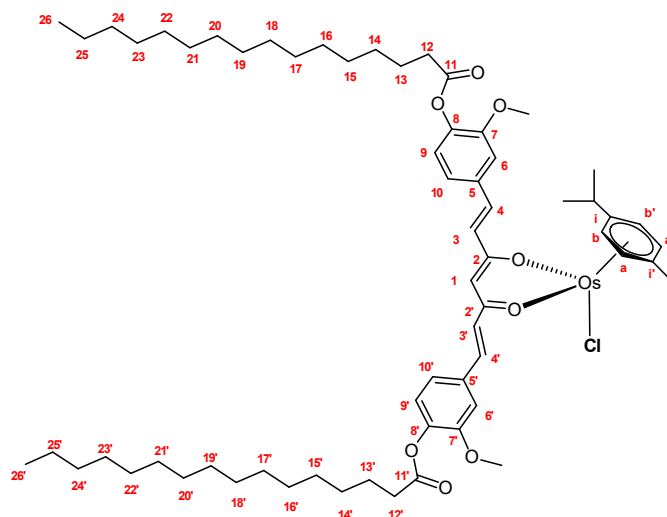
Figure 31 - *Structure of compound 3*

Anal. Calcd. for $C_{63}H_{93}ClO_8Os$: C, 62.84; H, 7.79. Found: C, 62.57; H, 7.80. mp: 102-104 °C. IR (cm^{-1}): 2917 vs, 2849 s v(aliphatic C-H); 1763 s v(-OC=O, of **L¹**), 1630 m v(C=O), 1599 w, 1523 vs, 1505 vs v(C=C); 273 s v(Os-Cl). ¹H-NMR (CDCl₃, 293 K): δ 0.90 (t, 6H, C(26-26')*H*), 1.29 (mbr, 44H, aliphatic chain of **L¹**), 1.37 (d, 6H, -CH(C*H₃*)₂ of *p*-cymene, ^4J = 7 Hz), 1.43 (m, 4H, C(14-14')*H*), 1.78 (m, 4H, C(13-13')*H*), 2.38 (s, 3H, -C*H₃* of *p*-cymene), 2.60 (t, 4H, C(12-12')*H*), 2.83 (m, 1H, C*H*(CH₃)₂ of *p*-cymene), 3.88 (s, 6H, -OC*H₃* of **L¹**), 5.70 (s, 1H, C(1)*H* of **L¹**), 5.83 d, 6.06 d (4H, AA'BB' system, CH₃-C₆H₄-CH(CH₃)₂ of *p*-cymene, ^3J = 6 Hz), 6.51 (d, 2H, C(3-3')*H* of **L¹**, $^3J_{trans}$ = 16Hz), 7.04 (d, 2 H, C(9-9')*H* of **L¹**, $^3J_{trans}$ = 8 Hz), 7.12 (d, 2H, C(10-10')*H*, $^3J_{trans}$ = 8 Hz), 7.11 (sbr, 2H, C(6- 6')*H* of **L¹**), 7.57 (d, 2H, C(4-4')H of **L¹**, $^3J_{trans}$ = 16 Hz). ¹³C{¹H} NMR (CDCl₃, 293 K): δ 14.1 [*C*(26-26')], 18.3 [-*C*H₃ of *p*-cymene], 22.7, 22.8 [-CH(*C*H₃)₂ of *p*-cymene], 25.0 [*C*(13-13')], 29.1 [*C*(14-14')], 29.3, 29.4, 29.5, 29.6, 29.7, 29.8 [from *C*(15) to *C*(25) of **L¹**], 31.5 [*C*H(CH₃)₂ of *p*-cymene], 31.9, 34.1 [*C*(12-12')], 55.9 [-O*C*H₃ of **L¹**], 69.5 [*C*(a-a')], 74.6 [*C*(b-b')], 89.2 [*C*i'], 89.8 [*C*i], 103.7 [*C*1], 111.1 [*C*(6-6')], 120.9 [*C*(10-10')], 123.2 [*C*(9-9')], 127.6 [*C*(3-3')], 134.7 [*C*(5-5')], 138.3 [*C*(4-4')], 140.9 [*C*(8-8')], 151.4 [*C*(7-7')], 171.7 [*C*(11-11')], 177.2 [*C*(2-2')=O]. ESI-MS (+) CH₃CN (m/z [relative intensity, %]): 1170 [100] [Os(*p*-cymene)(L¹)]$^+$.

[Os(*p*-cymene)(L²)Cl] (4). **HL²** (392 mg, 0.5 mmol) was dissolved in CH₂Cl₂ (10 mL) and complex **4** was synthesized with a procedure similar to that of compound **3**. The red powder (314 mg, 0.27 mmol, yield 55%) (**Figure 32**) is completely soluble in DMSO, DMF, CH₃CN, acetone, chlorinated solvents, ethyl acetate, Et₂O and n-hexane; slightly soluble in alcohols and petroleum ether and it is insoluble in H₂O.
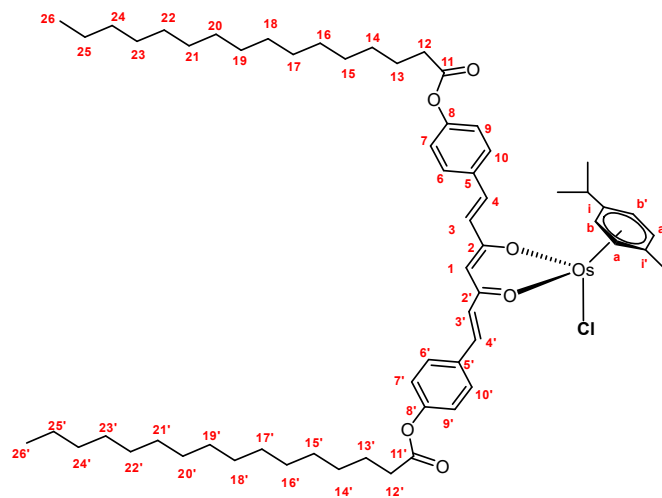
Figure 32 - *Structure of compound 4*

Anal. Calcd. for $C_{61}H_{89}ClO_6Os$: C, 64.04; H, 7.84. Found: C, 64.95; H, 7.84. mp:110-112 °C. IR (cm^{-1}): 2916 vs, 2849 s ν(aliphatic C-H); 1755 , ν(-OC=O, of **L^1**), 1631 m ν(C=O), 1599 w, 1584 w, 1540 s, 1519 vs ν(C=C); 271 s ν(Os-Cl). ^{1}H-NMR (CDCl$_3$, 293 K): δ 0.91 (t, 6H, C(26-26')H), 1.29 (mbr, 44H, aliphatic chain of **L^2**), 1.39 (d, 6H, CH(CH_3)$_2$ of *p*-cymene, ^{4}J = 7 Hz), 1.44 (m, 4H, C(14-14')H), 1.78 (m, 4H, C(13-13')H), 2.37 (s, 3H, CH$_3$ of *p*-cymene), 2.58 (t, 4H, C(12-12')H), 2.84 (m, 1H, CH(CH$_3$)$_2$ of *p*-cymene), 5.67 (s, 1H, C(1)H of curcumin), 5.82 d, 6.06 d (4H, AA′BB′ system, CH$_3$-C$_6H_4$-CH(CH$_3$)$_2$ of *p*-cymene, ^{3}J = 6 Hz), 6.52 (d, 2H, C(3-3')H of **L^2**, ^{3}J$_{trans}$ = 16Hz), 7.11 (d, 4 H, C(9-9')H and C(7-7')H of **L^2**, ^{3}J$_{trans}$ = 9 Hz), 7.54 (d, 4 H, C(10-10')H and C(6-6')H of **L^2**, ^{3}J$_{trans}$ = 9 Hz), 7.59 (d, 2H, C(4-4')H of **L^2**, ^{3}J$_{trans}$ = 16 Hz). ^{13}C{^{1}H}-NMR (CDCl$_3$, 293 K): δ 14.1 [C(26-26')], 18.2 [-CH$_3$ of *p*-cymene], 22.7, 22.8 [-CH(CH$_3$)$_2$ of *p*-cymene], 24.9 [C(13-13')], 29.1 [C(14-14')], 29.3, 29.4, 29.5, 29.6, 29.7, 29.8, 29.9 [from C(15) to C(25)], 31.5 [CH(CH$_3$)$_2$ of *p*-cymene], 31.9, 34.4 [C(12-12')], 69.5 [C(a-a')], 74.6 [C(b-b')], 89.0 [Ci'], 89.7 [Ci], 103.9 [C(1)], 122.0 [C(9-9') and C(7-7')], 127.4 [C(3-3')], 128.8 [C(10-10') and C(6-6')], 133.4 [C(5-5')], 137.9 [C(4-4')], 151.6 [C(8-8')], 172.0 [C(11-11')], 177.3 [C(2-2')=O]. ESI-MS (+) CH$_3$CN (m/z [relative intensity, %]): 1110 [100] [Os(*p*-cymene)(L^2)]$^+$.

[Ru(*p*-cymene)(L^1)(PTA)][SO$_3$CF$_3$] (**5**). Compound **1** (111 mg, 0.1 mmol) was dissolved in CH$_2$Cl$_2$ (10 mL) then the AgSO$_3$CF$_3$ (26 mg, 0.1 mmol) has been added and the final solution was stirred for 1h and filtered to remove the AgCl. PTA (PTA = 1,3,5-triaza-7-phosphaadamantane; 157 mg, 0.1 mmol) was finally added to the filtrate, which was stirred for 24 h at room temperature. Then, the solvent was removed and the crude product recrystallized from a 3/1 mixture of dichloromethane and n-hexane. The red-orange precipitate (73 mg, 0.052 mmol, yield 52%) was identified as the pure compound **5** (**Figure 33**). It is completely soluble in DMSO, DMF, acetone, chlorinated solvents, and ethyl acetate;

slightly soluble in CH$_3$CN, Et$_2$O and alcohols and insoluble in H$_2$O, n-hexane, and petroleum ether.

Figure 33 - *Structure of compound 5*

Anal. Calcd. for C$_{70}$H$_{105}$F$_3$N$_3$O$_{11}$PRuS: C, 60.67; H, 7.64; N, 3.03; Found: C, 59.07; H, 6.70; N, 3.16. mp: 90-92 °C. IR (cm^{-1}): 2922 s, 2853 s v(aliphatic C-H); 1760 m v(-OC=O, of **L^1**), 1625 m v(C=O), 1599 m, 1505 vs v(C=C); 637 s v(Ru-P). ^{1}H-NMR (DMSO-d_6, 293 K): δ 0.86 (t, 6H, C(26-26')*H*), 1.25-1.30 (mbr, 50H, aliphatic chain of **L^1** and CH(C*H$_3$*)$_2$ of *p*-cymene), 1.38 (m, 4H, C(14-14')*H*), 1.64 (m, 4H, C(13-13')*H*), 2.04 (s, 3H, CH$_3$ of *p*-cymene), 2.57 (t, 4H, C(12-12')*H*), 2.67 (m, 1H, C*H*(CH$_3$)$_2$ of *p*-cymene), 3.85 (s, 6H, -OC*H$_3$* of **L^1**), 4.14 (s, 6H, (P-C*H$_2$*-N) of PTA), 4.46 (m, 6H, (N-C*H$_2$*-N) of PTA), 5.94 (s, 1H, C(1)*H* of **L^1**), 6.10 d, 6.16 d (4H, AA'BB' system, CH$_3$-C$_6$H$_4$-CH(CH$_3$)$_2$ of *p*-cymene, ^{3}J = 6 Hz), 6.93 (d, 2H, C(9-9')*H* of **L^1**, ^{3}J = 16 Hz), 7.15 (d, 2H, C(3, 3')*H* of **L^1**, ^{3}J$_{trans}$ = 8 Hz), 7.24 (d, 2H, C(4-4')*H* of **L^1**, ^{3}J$_{trans}$ = 8 Hz), 7.43 [m, 4H, C(10-10')*H* and C(6-6')*H* of **L^1**]. ^{13}C{^{1}H}-NMR (DMSO-d_6, 293 K): δ 14.4 [*C*(26-26')], 16.9 [-*C*H$_3$ of *p*-cymene], 21.0, 22.2 [-*C*H(CH$_3$)$_2$ of *p*-cymene], 24.9 [*C*(13-13')], 28.7 [*C*(14-14')], 29.1, 29.2, 29.3, 29.4, 29.5, 29.6 [from *C*(15) to *C*(25) of **L^1**], 30.5 [-*C*H(CH$_3$)$_2$ of *p*-cymene], 31.8, 33.7 [*C*(12-12')], 50.0, 51.1 [(P-*C*H$_2$-N) of PTA, J= 13 Hz], 56.5 [-O*C*H$_3$ of **L^1**], 72.2, 72.3 [(N-*C*H$_2$-N) of PTA, J= 7 Hz], 88.5 [*C*(b-b')], 90.3 [*C*(a-a')], 96.6 [*C*i'], 104.2 [*C*i], 105.4 [*C*(1)], 111.8 [*C*(6-6')], 122.1 [*C*(4-4')], 123.8 [*C*(3-3')], 127.4 [*C*(9-9')], 134.4 [*C*(5-5')], 139.2 [*C*(10-10')], 141.3 [*C*(8-8')], 151.8 [*C*(7-7')], 171.5 [*C*(11-11')], 180.5 [*C*(2-2')=O].^{31}P-NMR (DMSO-d_6, 298 K): δ −27.09. ESI-MS (+) CH$_3$CN (m/z [relative intensity, %]): 1237 [100] [Ru(*p*-cymene)(L^1)(PTA)]$^+$.

Ru(*p*-cymene)(L^2)(PTA)][SO$_3$CF$_3$] (**6**). Compound **2** (105 mg, 0.1 mmol) was dissolved in CH$_2$Cl$_2$ (10 mL). Complex **6** was synthesized with a procedure similar to that of compound **5**. The dark-red precipitate (74 mg, 0.056 mmol, yield 56 %) (**Figure 34**) is completely soluble in DMSO, DMF, acetone, chlorinated solvents, and ethyl acetate; slightly soluble in CH$_3$CN, Et$_2$O and alcohols and insoluble in H$_2$O, n-hexane and petroleum ether.
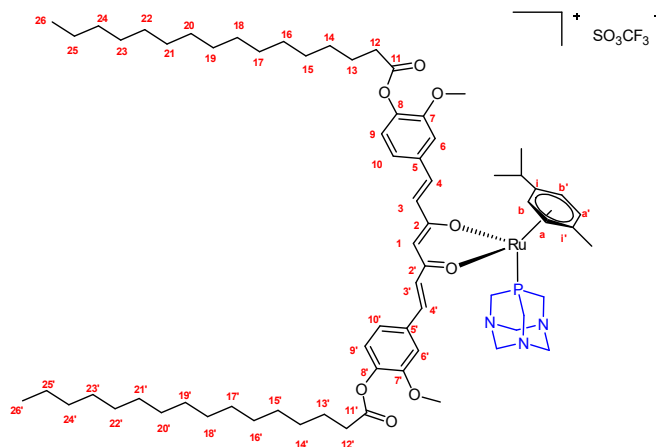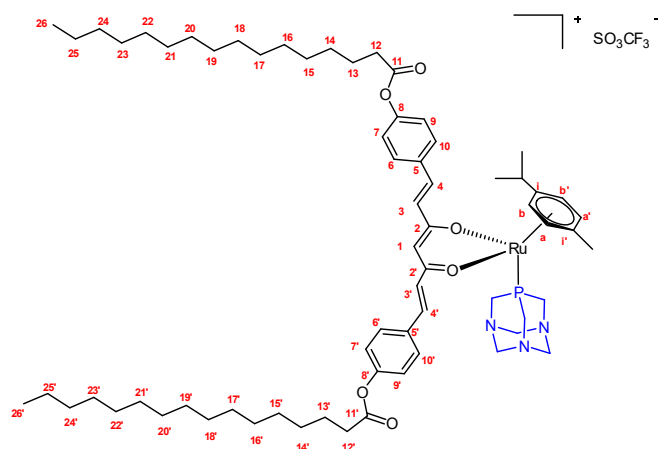
Figure 34 - *Structure of compound 6*

Anal. Calcd. for $C_{68}H_{101}F_3N_3O_9PRuS$: C, 61.61; H, 7.68; N, 3.17. Found: C, 57.22; H, 7.10; N, 3.03. mp: 93-95°C. IR (cm^{-1}): 2922 vs, 2852 s v(aliphatic C-H); 1716 s v(-OC=O, of **L²**), 1623 m v(C=O), 1601 w, 1583 w, 1506 vs v(C=C); 637 s v(Ru-P). ^{1}H-NMR (DMSO-d_6, 293 K): δ 0.86 (t, 6H, C(26-26')H), 1.25-1.30 (mbr, 50H, aliphatic chain of **L²** and CH(CH_3)$_2$ of p-cymene), 1.36 (m, 4H, C(14-14')H), 1.65 (m, 4H, C(13-13')H), 2.03 (s, 3H, CH$_3$ of p-cymene), 2.59 (t, 4H, C(12-12')H), 2.66 (m, 1H, CH(CH$_3$)$_2$ of p-cymene), 4.14 (s, 6H, (P-CH_2-N) of PTA), 4.46 (m, 6H, (N-CH_2-N) of PTA), 5.93 (s, 1H, C(1)H of **L²**), 6.10 d, 6.16 d (4H, AA'BB' system, CH$_3$-C$_6$H$_4$-CH(CH$_3$)$_2$ of p-cymene, ^{3}J = 6 Hz), 6.88 (d, 2H, C(3-3')H of **L²**, ^{3}J$_{trans}$ = 16Hz), 7.20 (d, 4 H, C(9-9')H and C(7-7')H of **L²**, ^{3}J$_{trans}$ = 8 Hz), 7.45 (d, 2H, C(4-4')H of **L²**, ^{3}J$_{trans}$ = 16 Hz), 7.74 (d, 4 H, C(10-10')H and C(6-6')H of **L²**, ^{3}J$_{trans}$ = 8 Hz). ^{13}C{^{1}H}-NMR (DMSO-d_6, 293 K): δ 14.4 [C(26-26')], 16.77 [-CH$_3$ of p-cymene], 22.19, 22.55, [-CH(CH$_3$)$_2$ of p-cymene], 24.75 [C(13-13')], 28.84 [C(14-14')], 29.12, 29.17, 29.3, 29.4, 29.5, 29.5 [from C(15) to C(25) of **L²**], 30.5 [CH(CH$_3$)$_2$ of p-cymene], 31.8 (*), 34.0 [C(12-12')], 50.9, 51.0 [(P-CH$_2$-N) of PTA, J= 13 Hz], 72.1, 72.2 [(N-CH$_2$-N) of PTA, J= 7 Hz], 88.5 [C(b-b')], 90.3 [C(a-a')], 96.5 [Ci'], 104.1 [Ci], 105.3 [C(1)], 123.0 [C(9-9') and C(7-7')], 127.1 [C(3-3')], 129.8 [C(10-10') and C(6-6')], 133.0 [C(5-5')], 138.9 [C(4-4')], 152.2 [C(8-8')], 172.1 [C(11-11')], 180.4 [C(2-2')=O]. ^{31}P-NMR (DMSO-d_6, 298 K): δ −26.93. ESI-MS (+) CH$_3$CN (m/z [relative intensity, %]): 1177 [100] [Ru(p-cymene)(L²)(PTA)]$^+$.

[Os(p-cymene)(L¹)(PTA)][SO₃CF₃] (**7**). Compound **3** (120 mg, 0.1 mmol) was dissolved in CH₂Cl₂ (8 mL) then the AgSO₃CF₃ (26 mg, 0.1 mmol) has been added and the final solution was stirred for 1h and filtered to remove the AgCl. PTA (PTA = 1,3,5-triaza-7-phosphaadamantane; 157 mg, 0.1 mmol) was finally added and the final reaction mixture was stirred for 24 h at room temperature. Then, the solvent was reduced at about 3 ml and the crude product recrystallized from a 3/1 mixture of dichloromethane and n-hexane. The dark-red precipitate (57 mg, 0.039 mmol, yield 39%) was identified as the pure compound **7**

(**Figure 35**). It is completely soluble in DMSO, DMF, CH_3CN, acetone, chlorinated solvents, alcohols, ethyl acetate and Et_2O and it is insoluble in n-hexane, petroleum ether and H_2O.

Figure 35 - *Structure of compound 7*

Anal. Calcd. for $C_{70}H_{105}F_3N_3O_{11}POsS$: C, 57.01; H, 7.18; N, 2.85. Found: C, 56.91; H, 7.13; N, 2.77. mp: 90-92 °C. IR (cm^{-1}): 2922 s, 2853 s v(aliphatic C-H); 1760 m v(-OC=O, of **L^1**), 1624 m v(C=O), 1598 w, 1587 w, 1505 vs v(C=C); 637 s v(Ru-P). ^{1}H-NMR (DMSO-d_6, 293 K): δ 0.86 (t, 6H, C(26-26')H), 1.25-1.38 (mbr, 54H, aliphatic chain of **L^1**, CH(CH_3)$_2$ of p-cymene and C(14-14')H), 1.64 (m, 4H, C(13-13')H), 2.17 (s, 3H, CH$_3$ of p-cymene), 2.57 (t, 4H, C(12-12')H), 2.67 (m, 1H, CH(CH$_3$)$_2$ of p-cymene), 3.85 (s, 6H, -OCH_3 of **L^1**), 4.10 (s, 6H, (P-CH_2-N) of PTA), 4.44 (m, 6H, (N-CH_2-N) of PTA), 6.06 (s, 1H, C(1)H of **L^1**), 6.18 d, 6.26 d (4H, AA'BB' system, CH$_3$-C$_6$H$_4$-CH(CH$_3$)$_2$ of p-cymene, ^{3}J = 6 Hz), 6.90 (d, 2H, C(9-9')H of **L^1**, ^{3}J = 16 Hz), 7.15 (d, 2H, C(3-3')H of **L^1**, ^{3}J$_{trans}$ = 8 Hz), 7.27 (d, 2H, C(4-4')H of curc, ^{3}J$_{trans}$ = 8 Hz), 7.46 [sbr, 2H, C(6-6')H], 7.48 [d, 2H, C(10-10')H of **L^1**, ^{3}J = 16 Hz]. ^{13}C{^{1}H} NMR (DMSO-d_6, 293 K): δ 14.4 [C(26-26')], 16.9 [-CH$_3$ of p-cymene], 22.5, 22.6, [-CH(CH$_3$)$_2$ of p-cymene], 24.9 [C(13-13')], 28.7 [C(14-14')], 29.1, 29.2, 29.3, 29.4, 29.5, 29.5 [from C(15) to C(25) of **L^1**], 30.6 [CH(CH$_3$)$_2$ of p-cymene], 31.8, 33.7 [C(12-12')], 50.1, 50.3 [(P-CH$_2$-N) of PTA, J= 18 Hz], 56.5 [-OCH$_3$ of **L^1**], 72.2, 72.3 [(N-CH$_2$-N) of PTA, J= 7 Hz], 81.4 [C(b-b')], 82.6 [C(a-a')], 88.2 [Ci'], 94.5 [Ci], 106.6 [C(1)], 111.7 [C(6-6')], 122.1 [C(4-4')], 123.9 [C(3-3')], 127.0 [C(9-9')], 134.4 [C(5-5')], 139.2 [C(10-10')], 141.4 [C(8-8')], 151.9 [C(7-7')], 171.4 [C(11-11')], 178.7 [C(2-2')=O]. ^{31}P-NMR (DMSO-d_6, 298 K): δ −65.06. ESI-MS (+) CH_3CN (m/z [relative intensity, %]): 1326 [100] [Os(p-cymene)(L^1)(PTA)]$^+$.

[Os(p-cymene)(L^2)(PTA)][SO$_3$CF$_3$] (**8**). Compound **4** (114 mg, 0.1 mmol) was dissolved in CH_2Cl_2 (8 mL). Complex **8** was synthesized with a procedure similar to that of compound **7**. The dark-red precipitate (57 mg, 0.040 mmol, yield 40%) has been precipitated from the solution by cooling and it was identified as the pure compound **8** (**Figure 36**). It is completely

soluble in DMSO, DMF, CH_3CN, acetone, chlorinated solvents, alcohols, ethyl acetate and Et_2O and it is insoluble in n-hexane, petroleum ether and H_2O.
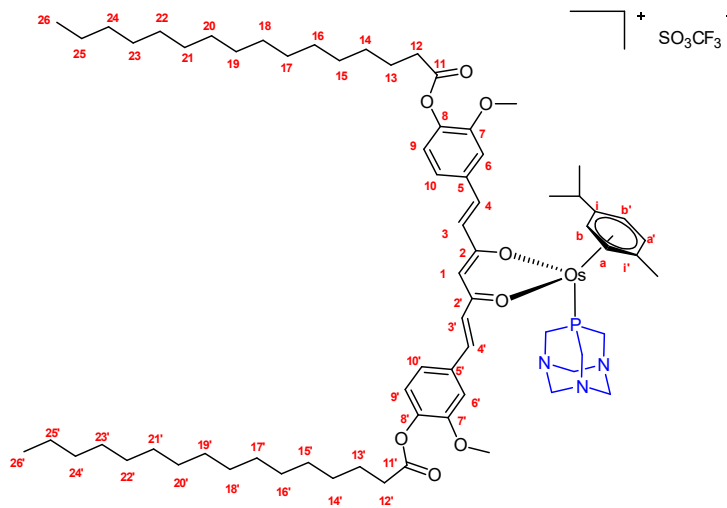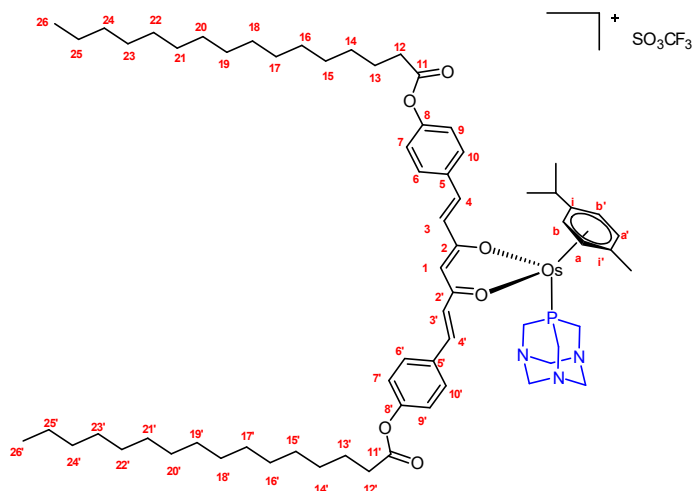

Figure 36 - *Structure of compound 8*

Anal. Calcd. for $C_{68}H_{101}F_3N_3O_9POsS$: C, 57.73; H, 7.20; N, 2.97. Found: C, 57.82; H, 7.18; N, 2.84. mp: 95-97 °C. IR (cm^{-1}): 2922 s, 2852 s v(aliphatic C-H); 1756 m v(-OC=O, of **L¹**), 1622 m v(C=O), 1601 w, 1582 w,1505 vs, 1506 vs v(C=C); 637 s v(Ru-P).¹H-NMR (DMSO-d_6, 293 K): δ 0.86 (t, 6H, C(26-26')H), 1.25 (mbr, 44 H, aliphatic chain of **L²**), 1.32 (d, 6H, CH(CH_3)$_2$ of *p*-cymene, ^4J = 7 Hz), 1.35 (m, 4H, C(14-14')H), 1.65 (m, 4H, C(13-13')H), 2.16 (s, 3H, CH_3 of *p*-cymene), 2.59 (t, 4H, C(12-12')H), 2.67 (m, 1H, CH(CH$_3$)$_2$ of *p*-cymene), 4.09 (s, 6H, (P-CH_2-N) of PTA), 4.43 (m, 6H, (N-CH_2-N) of PTA), 6.05 (s, 1H, C(1)H of **L²**), 6.17 d, 6.26 d (4H, AA'BB' system, CH$_3$-C$_6H_4$-CH(CH$_3$)$_2$ of *p*-cymene, ^3J = 6 Hz), 6.84 (d, 2H, C(3-3')H of **L²**, $^3J_{trans}$ = 16Hz), 7.21 (d, 4 H, C(9-9')H and C(7-7')H of **L²**, $^3J_{trans}$ = 9 Hz), 7.50 (d, 2H, C(4-4')H of **L²**, $^3J_{trans}$ = 16 Hz), 7.76 (d, 4 H, C(10-10')H and C(6, 6')H of **L²**, $^3J_{trans}$ = 9 Hz). ¹³C{¹H}-NMR (DMSO-d_6, 293 K): δ 14.4 [C(26-26')], 16.8 [-CH_3 of *p*-cymene], 22.5, 22.6 [-CH(CH_3)$_2$ of *p*-cymene], 24.7 [C(13-13')], 28.8 [C(14-14')], 29.1, 29.2, 29.3, 29.4, 29.4, 29.5 [from C(15) to C(25) of **L²**], 30.5 [CH(CH$_3$)$_2$ of *p*-cymene], 31.8, 34.0 [C(12-12')], 50.1, 50.3 [(P-CH$_2$-N) of PTA, J= 18 Hz], 72.17, 72.23 [(N-CH$_2$-N) of PTA, J= 8 Hz], 81.6 [C(b-b')], 82.7 [C(a-a')], 88.0 [Ci'], 94.3 [Ci], 106.5 [C(1)], 123.1 [C(9-9') and C(7-7')], 126.7 [C(3-3')], 129.8 [C(10-10') and C(6-6')], 133.1 [C(5-5')], 138.9 [C(4-4')], 152.2 [C(8-8')], 172.0 [C(11-11')], 178.6 [C(2-2')=O]. ³¹P-NMR (DMSO-d_6, 298 K): δ −64.99. ESI-MS (+) CH_3CN (m/z [relative intensity, %]): 1266.6[100] [Os(*p*-cymene)(L²)(PTA)]⁺.

[Ru(*p*-cymene)(L³)(Cl)] (**9**). In a round bottom flask, **HL³** (112 mg, 0.2 mmol) and triethylamine (TEA 28 μL, 0.2 mmol) were dissolved in CH_3CN (5 mL) under magnetic stirring and heating. After 30 minutes, [(p-cymene)RuCl₂]₂ (61 mg, 0.1 mmol) was added at room temperature. The resulting red solution was stirred at reflux for 16 hours. At the end the

solvent was dried under reduced pressure and the obtained oil was precipitated with solvents (CH₂Cl₂/hexane). Then the precipitate was filtered with hexane and washed with cold 2-propanol giving the final complex **9** (**Figure 37**) as a red powder (yield 47%). The complex is soluble in DMSO, CH₃CN and chlorinated solvents; slightly soluble in alcohols and insoluble in H_2O.
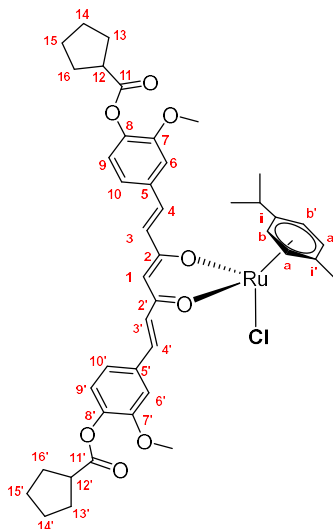

Figure 37 - *Structure of compound* **9**

Anal. Calcd for $C_{43}H_{49}ClO_8Ru$: C, 62.20; H, 5.95. Found: C, 61.09; H, 5.85. m.p.: 165–166 °C. IR (cm⁻¹): 2957 w, 2871 w, 2626 wbr ν(aliphatic C–H); 1755 m ν(–OC=O), 1628 m ν(C=O); 1598 m, 1589 m, 1523 m, 1506 s, 1467 m, 1449 m, 1410 m ν(C=C), 1371 m, 1269 m, 1258 m, 1153 m, 1120 s, 1069 m, 1033 m, 965 m, 860 m, 845 m, 803 m, 770 m, 735 m, 687 m, 666 m, 609 m.¹H-NMR (CDCl₃, 293 K): δ 1.41 [d, 6H, –CH(CH_3)₂ of p-cymene, ⁴J = 7 Hz], 1.68 m, 181 m [8H, C(14-14')*H* and C(15-15')*H*], 2.04 [m, 8H, C(13-13')*H* and C(16-16')H], 2.37 [s, 3H, –CH₃ of p-cymene], 3.00 [sept, 1H, -C*H*(CH₃)₂ of p-cymene], 3.05 [m, 2H, C(12–12')*H*], 3.88 [s, 6H, –OCH_3], 5.33 d, 5.60 d [4H, AA'BB' system, CH₃- C₆H_4-CH(CH₃)₂ of *p*-cymene, ³J = 6 Hz], 5.52 [s, 1H, C(1)*H*], 6.53 [d, 2H, C(3–3')*H* of curc, ³J$_{trans}$ = 16 Hz], 7.03 [d, 2 H, C(9–9')*H*, ³J$_{trans}$ = 8 Hz], 7.10 [s, 2H, C(6–6')*H*], 7.11 [d, 2H, C(10–10')*H*, ³J = 8 Hz], 7.57 [d, 2H, C(4–4')*H*, ³J$_{trans}$ = 16 Hz]. ¹³C{¹H}-NMR (CDCl₃, 293 K): δ 18.1 [–CH₃ of p-cymene], 22.4 (–CH(CH_3)₂ of *p*-cymene), 25.9 [C(13–13')], 30.1 [C(14–14')], 30.9 [-C*H*(CH₃)₂ of *p*-cymene], 43.7 [C(12–12')], 56.0 [–OCH_3] 79.2 [*C*(a–a') of p-cymene], 83.0 [*C*(b–b') of p-cymene], 97.7 [*C*i' of p-cymene], 99.7 [*C*i of p-cymene], 102.2 [*C*(1)], 111.1 [*C*(6–6')], 120.9 [*C*(10–10')], 123.1 [*C*(9–9')], 127.8 [*C*(3–3')], 134.7 [*C*(5–5')], 138.2 [*C*(4–4')], 141.1 [*C*(8–8')], 151.4 [*C*(7–7')], 174.7 [*C*(11–11')], 178.4 [*C*(2–2')=O]. ESI-MS(+) CH₃CN (m/z [relative intensity, %]): 795 [100] [Ru(p-cymene)(L³)]⁺.

[Ru(*p*-cymene)(L⁴)(Cl)] (**10**). In a round bottom flask, **HL⁴** (100 mg, 0.2 mmol) and triethylamine (TEA 28 μL, 0.2 mmol) were dissolved in CH₃CN (5 mL) under magnetic stirring

and heating. After 30 minutes, [(p-cymene)RuCl$_2$]$_2$ (61 mg, 0.1 mmol) was added at room temperature. The resulting red solution was stirred at reflux for 16 hours. At the end the solvent was dried under reduced pressure and the obtained oil was precipitated with solvents (CH$_2$Cl$_2$/hexane). Then the precipitate was filtered with hexane and washed with cold 2-propanol giving the final complex **10** (**Figure 38**) as a red powder (yield 50%). It is soluble in DMSO, CH$_3$CN and chlorinated solvents; slightly soluble in alcohols and insoluble in H$_2$O.

Figure 38 - Structure of compound 10

Anal. Calcd for C$_{41}$H$_{45}$ClO$_6$Ru: C, 63.93; H, 5.89. Found: C, 63.03; H, 5.28. m.p.: 202–205°C. IR (cm^{-1}): 2957 w, 2868 w v(aliphatic C–H); 1748 s v(–OC=O), 1630 m v(C=O); 1598 m, 1517 s, 1506 s, 1455 m, 1405 m v(C=C); 1365 m, 1308 m, 1284 m, 1212 m, 1163 s, 1123 s, 1033 m, 1015 m, 991 m, 969 s, 884 m, 862 m, 803 m, 738 m, 684 m, 645 m. ^{1}H-NMR (CDCl$_3$, 293 K): δ 1.42 [d, 6H, –CH(C*H$_3$*)$_2$ of p-cymene, ^{4}J = 7 Hz], 1.69 m, 1.81m [8H, C(14-14')*H* and C(15-15')*H*], 1.99 m, 2.05m [8H, C(13-13')*H* and C(16-16')*H*], 2.37 [s, 3H, –C*H$_3$* of cymene], 3.02 quint, 3.02 sept [5H, C(12-12')*H* of ligand and -C*H*(CH$_3$)$_2$ of *p*-cymene], 5.33 d, 5.60 d [4H, AA′BB′ system, CH$_3$- C$_6$H$_4$-CH(CH$_3$)$_2$ of p-cymene, ^{3}J = 6 Hz], 5.49 [s, 1H, C(1)*H*], 6.54 [d, 2H, C(3–3')*H*, ^{3}J = 16 Hz], 7.11 [d, 4H, C(9–9')*H* and C(7-7')*H*, ^{3}J = 8.5 Hz], 7.53 [d, 4H, C(6–6')*H* and C(10-10')*H*, ^{3}J = 8.5 Hz], 7.60 [d, 2H, C(4–4')*H*, ^{3}J= 16 Hz]. ESI-MS(+) CH$_3$CN (m/z [relative intensity, %]): 735 [100] [Ru(*p*-cymene)(L^4)]$^+$.

[**Ru(*p*-cymene)(L^5)(Cl)**] (**11**). In a round bottom flask, **HL^5** (118 mg, 0.2 mmol) and triethylamine (TEA 28 µL, 0.2 mmol) were dissolved in CH$_3$CN (5 mL) under magnetic stirring and heating. After 30 minutes, [(*p*-cymene)RuCl$_2$]$_2$ (61 mg, 0.1 mmol) was added at room temperature. The resulting red solution was stirred at reflux for 16 hours. At the end, the solvent was dried under reduced pressure and the obtained oil was precipitated with solvents (CH$_2$Cl$_2$/hexane). Then the precipitate was filtered with hexane and washed with cold 2-

propanol giving the final complex **11** (**Figure 39**) as a red powder (yield 52%). It is soluble in DMSO, CH$_3$CN and chlorinated solvents; slightly soluble in alcohols and insoluble in H$_2$O.
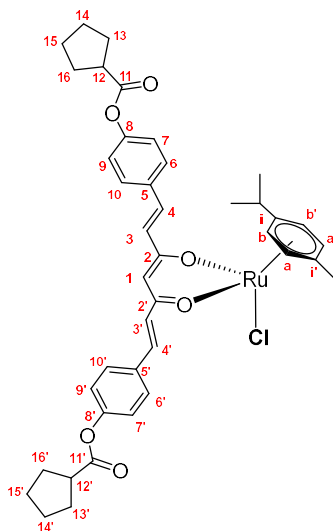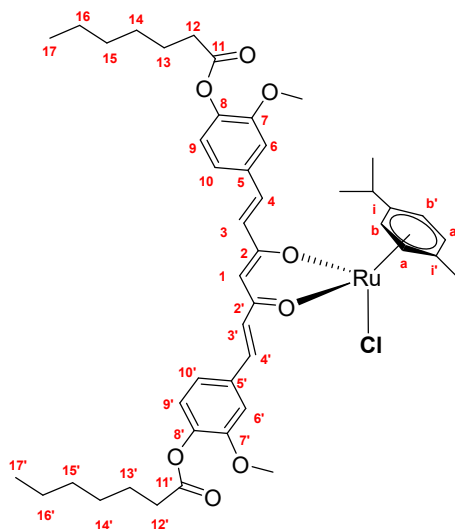

Figure 39 - *Structure of compound **11***

Anal. Calcd for C$_{45}$H$_{57}$ClO$_8$Ru: C, 62.67; H, 6.66. Found: C, 62.31; H, 6.60. m.p.: 152-154 °C. IR (cm^{-1}): 3050 wbr, 2999 wbr, 2956 w, 2930 m, 2857 w v(aliphatic C–H); 1758 s v(–OC=O), 1630 m v(C=O); 1598 w, 1589 w, 1523 vs, 1508 vs, 1466 m, 1460 m, 1450 m, 1412 s v(C=C); 1375 m, 1342 m, 1294 m, 1257 s, 1232 m, 1190 m, 1179 m, 1136 s, 1120 vs, 1103 s, 1060 m, 1037 m, 1025 s, 984 s, 965 s, 954 m, 939 m, 916 m, 885 m, 863 m, 839 m, 826 m, 803 nm, 770 m, 728 m, 683 m, 660 m, 605 m. ^{1}H-NMR (CDCl$_3$, 293 K): δ 0.94 [t, 6H, C(17-17')*H*], 1.37 [m, 8H, C(16-16')*H* and C(15,15')*H*], 1.41 [d, 6H, –CH(C*H$_3$*)$_2$ of *p*-cymene, ^{4}J = 7 Hz],1.46 [m, 4H, C(14-14')*H*], 1.79 [quint., 4H, C(13–13')*H*], 2.37 [s, 3H, –C*H$_3$* of *p*-cymene], 2.61 [t, 4H, C(12-12')*H*], 3.00 [sept, 1H, -C*H*(CH$_3$)$_2$ of *p*-cymene], 3.88 [s, 6H, -OC*H$_3$*], 5.33 d, 5.60 d [4H, AA'BB′ system, CH$_3$- C$_6$H$_4$-CH(CH$_3$)$_2$ of p-cymene, ^{3}J = 6 Hz], 5.53 [s, 1H, C(1)*H*], 6.53 [d, 2H, C(3–3')*H*, ^{3}J = 16 Hz], 7.04 [d, 2H, C(9–9')*H*, ^{3}J = 8.0 Hz], 7.10 [s, 2H, C(6–6')*H*], 7.11 [d, 2H, C(10–10')*H*, ^{3}J = 8.0 Hz], 7.57 [d 2H, C(4–4')*H*, ^{3}J = 16 Hz]. ^{13}C{^{1}H}-NMR (CDCl$_3$): δ 14.0 [*C*(17-17')], 18.1 [–C*H$_3$* of *p*-cymene], 22.4 [-CH(C*H$_3$*)$_2$ of p-cymene], 22.5 [*C*(15-15')], 25.0 [*C*(13–13')], 28.7 [*C*(14–14')], 30.9 [C*H*(CH$_3$)$_2$ of *p*-cymene], 31.5 [*C*(16–16')], 34.1 [*C*(12–12')], 55.9 [-O*C*H$_3$], 79.2 [*C*(a–a') of *p*-cymene], 83.0 [*C*(b–b′) of *p*-cymene], 97.7 [*C*i' of *p*-cymene], 99.7 [*C*i of *p*-cymene], 102.3 [*C*(1)], 111.1 [*C*(6–6')], 120.8 [*C*(10–10')], 123.1 [(*C*(9–9')], 127.8 [*C*(3–3')], 134.8 [*C*(5–5')], 138.1 [*C*(4–4')], 140.8 [*C*(8–8')], 151.4 [*C*(7–7')], 171.7 [*C*(11–11')], 178.4 [*C*(2–2')=O]. ESI-MS(+) CH$_3$CN (m/z [relative intensity, %]): 827 [100] [Ru(*p*-cymene)(L^5)]$^+$.

[**Ru(*p*-cymene)(L^6)(Cl)**] (**12**). In a round bottom flask, **HL^6** (106 mg, 0.2 mmol) and triethylamine (TEA 28 µL, 0.2 mmol) were dissolved in CH$_3$CN (5 mL) under magnetic stirring and heating. After 30 minutes, [(*p*-cymene)RuCl$_2$]$_2$ (61 mg, 0.1 mmol) was added at room

temperature. The resulting red solution was stirred at reflux for 16 hours. At the end, the solvent was dried under reduced pressure and the obtained oil was precipitated with solvents (CH₂Cl₂/hexane). Then the precipitate was filtered with hexane and washed with cold 2-propanol giving the final complex **12** (**Figure 40**) as a red powder (yield 57%). It is soluble in DMSO, CH₃CN and chlorinated solvents; slightly soluble in alcohols and insoluble in H₂O.
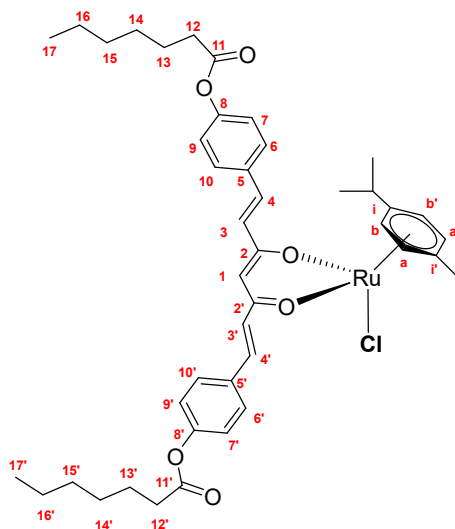

Figure 40 - *Structure of compound 12*

Anal. Calcd for $C_{43}H_{53}ClO_6Ru$: C, 64.37; H, 6.66. Found: C, 65.00; H, 6.83. m.p.: 152-154 °C. IR (cm⁻¹): 3064 w, 3033 w, 2926 w, 2871 w, 2857 w v(aliphatic C–H); 1759 m v(–OC=O), 1635 m v(C=O); 1600 w, 1582 w, 1532 s, 1505 s, 1467 m, 1427 m, 1409 m v(C=C); 1387 m, 1375 m, 1341 w, 1322 w, 1290 w, 1265 w, 1210 m, 1164 s, 1142 s, 1129 s, 1101 vs, 1014 m, 975 m, 944 m, 919 m, 907 m, 866 m, 834 m, 820 m, 806 m, 727 m, 690 w. ¹H-NMR (CDCl₃, 293 K): δ 0.94 [t, 6H, C(17-17')*H*], 1.37 [m, 8H, C(16-16')*H* and C(15,15')*H*], 1.42 [d, 6H, –CH(C*H₃*)₂ of *p*-cymene, ⁴J = 7Hz], 1.45 [m, 4H, C(14–14')*H*], 1.78 [quint., 4H, C(13-13')*H*], 2.36 [s, 3H, -C*H₃* of *p*-cymene], 2.59 [t, 4H, C(12–12')*H*], 3.01 [sept, 1H, –C*H*(CH₃)₂ of *p*-cymene], 5.33 d, 5.60 d [4H, AA'BB' system, CH₃- C₆*H₄*-CH(CH₃)₂ of *p*-cymene, ³J = 6Hz], 5.49 [s, 1H, C(1)*H*], 6.54 [d, 2H, C(3-3')*H*, ³J = 16 Hz], 7.11 [d, 4H, C(9–9')*H* and C(7–7')*H*, ³J = 9 Hz], 7.53 [d, 4H, C(10–10')*H* and C(6–6')*H*, ³J = 9 Hz], 7.60 [d, 2H, C(4–4')*H*, ³J = 16 Hz]. ¹³C{¹H}-NMR (CDCl₃, 293 K): δ 14.0 [*C*(17-17')], 18.0 [–CH₃ of *p*-cymene], 22.4 [–CH(CH₃)₂ of *p*-cymene], 22.5 [*C*(15-15')], 24.9 [*C*(13–13')], 28.8 [*C*(14–14')], 30.9 [-CH(CH₃)₂ of *p*-cymene], 31.4 [*C*(16–16')], 34.4 [s, *C*(12–12')], 79.2 [*C*(a–a') of *p*-cymene], 83.0 [*C*(b–b') of *p*-cymene], 97.6 [*C*i' of *p*-cymene], 99.7 [*C*i of *p*-cymene], 102.5 [*C*(1)], 122.0 [*C*(9–9') and *C*(7–7')], 127.7 [*C*(3–3')], 128.8 [*C*(10–10') and *C*(6–6')], 137.7 [*C*(4–4')], 151.5 [*C*(5-5')], 172.1 [*C*(8–8')], 178.4 [*C*(11–11')], 183.2 [*C*(2–2')=O]. ESI-MS(+) CH₃CN (m/z [relative intensity, %]): 767 [100] [Ru(*p*-cymene)(L⁶)]⁺.

[Ru(*p*-cymene)(L⁷)(Cl)] (**13**). In a round bottom flask, **HL⁷** (135 mg, 0.2 mmol) and triethylamine (TEA 28 µL, 0.2 mmol) were dissolved in CH_3CN (5 mL) under magnetic stirring and heating. After 30 minutes, [(*p*-cymene)RuCl₂]₂ (61 mg, 0.1 mmol) was added at room temperature. The resulting red solution was stirred at reflux for 16 hours The precipitate was filtered off giving the final complex **13** (**Figure 41**) as a red powder (yield 74%). The complex is soluble in DMSO and chlorinated solvents, slightly soluble in CH_3CN and alcohols and insoluble in H_2O.
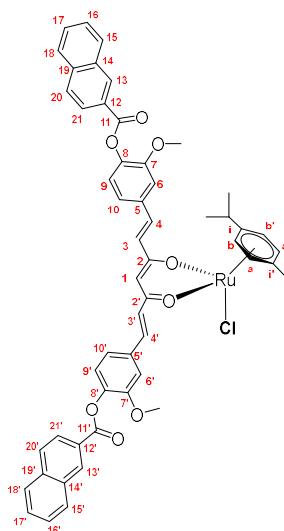

Figure 41 - *Structure of compound 13*

Anal. Calcd for $C_{53}H_{45}ClO_8Ru$: C, 67.26; H, 4.79. Found: C, 66.19; H, 4.81. m.p.: 254-257°C. IR (cm⁻¹): 3073 w, 3056 w, 2956 w, 2867 w, 2844 w, 2354 w, 2327 w, 2317 w v(aromatic C–H); 1728 s v(–OC=O), 1625 w v(C=O); 1599 w, 1584 w, 1528 m, 1512 m, 1505 vs, 1471 m, 1455 m, 1408 s v(C=C), 1386 w, 1372 w, 1354 w, 1284 m, 1261 s, 1223 m, 1188 s, 1171 m, 1154 s, 1123 s, 1074 m, 1066 m, 1057 m, 1028 m, 983 m, 976 m, 952 m, 919 w, 910 w, 892 w, 881 w, 862 m, 841 m, 827 m, 807 w, 775 s, 761 s, 731 m, 715 w, 677 w, 667 w , 635 w. ¹H-NMR (CDCl₃, 293 K): δ 1.44 [d, 6H, –CH(C*H*₃)₂ of *p*-cymene, ⁴J = 7 Hz], 2.40 [s, 3H, –C*H*₃ of *p*-cymene], 3.03 [sept, 1H, -C*H*(CH₃)₂ of *p*-cymene], 3.90 [s, 6H, –OC*H*₃], 5.36 d, 5.63 d [4H, AA′BB′ system, CH₃- C₆*H*₄-CH(CH₃)₂ of *p*-cymene, ³J = 6 Hz], 5.58 [s, 1H, C(1)*H*], 6.60 [d, 2H, C(3–3′)*H*, ³J = 16 Hz], 7.20 [d, 2 H, C(9–9′)*H*, ³J = 8 Hz], 7.21 [s, 2H, C(6–6′)*H*], 7.24 [d, 2H, C(10–10′)*H*, ³J = 8 Hz], 7.61 [t, 2H, C(17–17′)*H*], 7.66 [t, 2H, C(16–16′)*H*], 7.64 [d, 2H, C(4-4′)*H*, ³J = 16 Hz], 7.95 [d, 2H, C(15–15′)*H*, ³J = 8 Hz], 7.98 [d, 2H, C(18-18′)*H*, ³J = 8 Hz], 8.03 [d, 2H, C(20-20′)*H*, ³J = 8 Hz] 8.24 [d, 2H, C(21-21′)*H*, ³J = 8Hz], 8.84 [s, 2H, C(13–13′)*H*]. ¹³C{¹H}-NMR (CDCl₃, 293 K): δ 18.1 [–*C*H₃ of *p*-cymene], 22.5 [–*C*H(CH₃)₂ of *p*-cymene], 30.9 [-*C*H(CH₃)₂ of *p*-cymene], 56.0 [–O*C*H₃], 79.2 [*C*(a–a′) of *p*-cymene], 83.0 [*C*(b–b′) of *p*-cymene], 97.7 [*C*i′ of *p*-cymene], 99.8 [*C*i of *p*-cymene], 102.4 [*C*(1)], 111.2 [*C*(9–9′)], 121.0 [*C*(6-6′)], 123.3 [*C*(10-10′)], 125.6 [*C*(21-21′)], 126.5 *C*(5–5′)], 126.8 [*C*(17-

17')]., 127.8 [C(15–15')], 128.0 [C(3-3')], 128.4 [C18-18')], 128.6 [C(16-16')], 129.5 [C(20-20')], 132.1 [C(13-13')], 132.5 [C(12-12')], 135.0 [C(14-14')], 135.9 [C(19-19')], 138.2 [C(4-4')], 141.1 [C(8–8')], 151.6 [C(7–7')], 164.8 [C(11–11')], 178.4 [C(2–2')=O]. ESI-MS(+) CH_3CN (m/z [relative intensity, %]): 911 [100] [Ru(*p*-cymene)(L^7)]$^+$.

[**Ru(*p*-cymene)(L^8)(Cl)]** (**14**). In a round bottom flask, **HL^8** (123 mg, 0.2 mmol) and triethylamine (TEA 28 µL, 0.2 mmol) were added in CH_3CN (5 mL) and the under magnetic stirring and heating. After 30 minutes, [(*p*-cymene)RuCl$_2$]$_2$ (61 mg, 0.1 mmol) was added at room temperature. The resulting red solution was stirred at reflux for 16 hours The precipitate was filtered off giving the final complex **14** (**Figure 42**) as a red powder (yield 64%). The complex is soluble in DMSO and chlorinated solvents, slightly soluble in CH_3CN and alcohols and insoluble in H_2O.
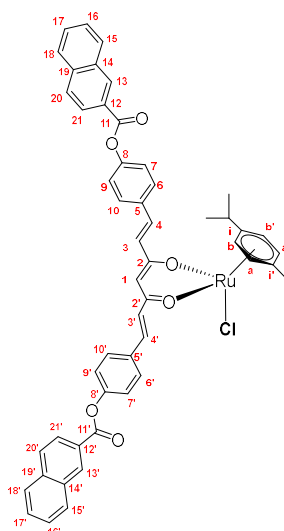

Figure 42 - Structure of compound 14

Anal. Calcd for $C_{51}H_{41}ClO_6Ru$: C, 69.11; H, 4.66. Found: C, 70.91; H, 4.98. m.p.: 193-197°C. IR (cm^{-1}): 3058 w, 3035 w, 3008 w, 2969 w, 2928 w, 2875 w ν(aromatic C–H); 1732 s ν(–OC=O), 1669 w ν(C=O); 1621 w, 1598 w, 1574 w, 1520 m, 1506 m, 1471 w, 1428 w, 1416 w ν(C=C); 1385 w, 1368 w, 1354 w, 1316 w, 1280 m, 1213 m, 1189 s, 1166 s, 1126 m, 1103 m, 1062 s, 1016 w, 997 w, 973 w, 951 m, 912 w, 893 w, 866 m, 849 m, 824 m, 794 w, 773 s, 759 s, 681 w, 638 w. ^{1}H-NMR (DMSO-d_6, 293 K): δ 1.37 [d, 6H, –CH(CH_3)$_2$ of *p*-cymene, ^{4}J = 7Hz], 3.93 [sept, 1H, -CH(CH$_3$)$_2$ of *p*-cymene], 2.33 [s, 3H, –CH_3 of *p*-cymene], 5.50 d, 5.78 d [4H, AA′BB′ system, CH$_3$- C$_6H_4$-CH(CH$_3$)$_2$ of *p*-cymene, ^{3}J = 6 Hz], 5.62 [s, 1H, C(1)H], 6.81 [d, 2H, C(3–3')H, ^{3}J = 16 Hz], 7.44 [d, 4 H, C(9–9')H and C(7-7')H, ^{3}J = 9 Hz], 7.60 [d, 2H, C(4-4')H, ^{3}J = 16 Hz], 7.81 [d, 4H, C(10-10')H and C(6–6')H, ^{3}J = 9Hz], 7.71 m, 8.11 m, 8.89 m [26H, C(13-13')H, C(15-15')H, C(16-16')H, C(17-17')H, C(18-18')H, C(20-20')H and C(21-21')H]. ESI-MS(+) CH_3CN (m/z [relative intensity, %]): 851 [100] [Ru(*p*-cymene)(L^8)]$^+$.

[Ru(*p*-cymene)(L⁹)(Cl)] (**15**). In a round bottom flask, **HL⁹** (113 mg, 0.2 mmol) and triethylamine (TEA 28 µL, 0.2 mmol) were dissolved in CH_3CN (5 mL) under magnetic stirring and heating. After 30 minutes, $[(p\text{-cymene})RuCl_2]_2$ (61 mg, 0.1 mmol) was added at room temperature. The resulting red solution was stirred at reflux for 16 hours. At the end, the solvent was dried under reduced pressure and the obtained oil was precipitated with solvents (CH_2Cl_2/hexane). Then the precipitate was filtered with hexane and washed with cold 2-propanol giving the final complex **15** (**Figure 43**) as a red powder (yield 41%). It is soluble in DMSO, CH_3CN and chlorinated solvents; slightly soluble in alcohols and insoluble in H_2O.
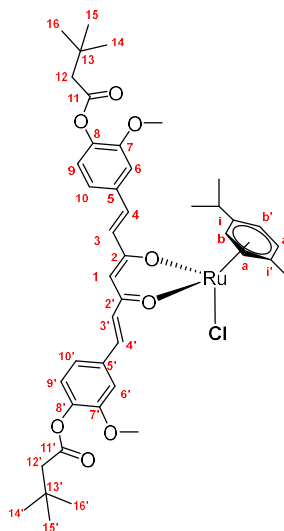

Figure 43 - *Structure of compound 15*

Anal. Calcd for $C_{43}H_{53}ClO_8Ru$: C, 61.90; H, 6.40. Found: C, 61.07; H, 6.35. m.p.: 161-163°C. IR (cm⁻¹): 2955 w, 2909 w, 2868 w ν(aliphatic C–H); 1756 m ν(–OC=O), 1630 m ν(C=O); 1599m, 1586 w, 1525 s, 1505 s, 1469 m, 1417 m ν(C=C), 1366 m, 1350 w, 1317 m, 1296 m, 1258 s, 1220 m, 1185 m, 1154 m, 1107 s, 1029 m, 986 m, 966 m, 947 m, 926 m, 896 w, 865 m, 841 m, 803 m, 726 w, 684 w, 627 w, 606 w. ¹H-NMR ($CDCl_3$, 293 K): δ 1.17 [s, 18H, C(14-14')*H*, C(15-15')*H* and C(16-16')*H*], 1.41 [d, 6H, –CH(C*H₃*)₂ of *p*-cymene, ⁴J = 7 Hz], 2.37 [s, 3H, –C*H₃* of *p*-cymene], 2.49 [s, 4H, C(12-12')*H*], 3.00 [sept, 1H, -C*H*(CH₃)₂ of *p*-cymene], 3.88 [s, 6H, -OC*H₃*], 5.33 d, 5.60 d [4H, AA'BB' system, CH₃- C₆*H₄*-CH(CH₃)₂ of *p*-cymene, ³J = 6Hz], 5.53 [s, 1H, C(1)*H*], 6.53 [d, 2H, C(3–3')*H*, ³J = 16 Hz], 7.03 [d, 2H, C(9–9')*H*, ³J = 8.0 Hz], 7.11 [s, 2H, C(6–6')*H*], 7.12 [d, 2H, C(10–10')*H*, ³J = 8.0 Hz], 7.58 [d 2H, C(4–4')*H*, ³J = 16 Hz]. ¹³C{¹H}-NMR ($CDCl_3$): δ 18.1 [–CH₃ of *p*-cymene], 22.4 [–CH(CH₃)₂ of *p*-cymene], 29.6 [*C*(14–14'), *C*(15-15') and *C*(16-16')], 30.9 [-CH(CH₃)₂ of *p*-cymene], 31.0 [*C*(13–13')], 47.6 [*C*(12–12')], 55.8 [-OCH₃], 79.2 [*C*(a–a') of *p*-cymene], 83.0 [*C*(b–b') of *p*-cymene], 97.6 [*C*i' of *p*-cymene], 99.8 [*C*i of *p*-cymene], 102.2 [*C*(1)], 111.1 [*C*(6–6')], 120.8 [*C*(10–10')], 123.6 [*C*(9–9')], 127.8 [*C*(3–3')], 134.8 [*C*(5–5')], 138.1 [*C*(4–4')], 140.8 [*C*(8–8')],

151.4 [C(7–7')], 170.0 [C(11–11')], 178.4 [C(2–2')=O]. ESI-MS(+) CH$_3$CN (m/z [relative intensity, %]): 799 [100] [Ru(p-cymene)(L^9)]$^+$.

[**Ru(p-cymene)(L^{10})(Cl)**] (**16**). In a round bottom flask, **HL^{10}** (101 mg, 0.2 mmol) and triethylamine (TEA 28 µL, 0.2 mmol) were dissolved in CH$_3$CN (5 mL) under magnetic stirring and heating. After 30 minutes, [(p-cymene)RuCl$_2$]$_2$ (61 mg, 0.1 mmol) was added at room temperature. The resulting red solution was stirred at reflux for 16 hours. At the end, the solvent was dried under reduced pressure and the obtained oil was precipitated with solvents (CH$_2$Cl$_2$/hexane). Then the precipitate was filtered with hexane and washed with cold 2-propanol giving the final complex **16** (**Figure 44**) as a red powder (yield 59%). It is soluble in DMSO, CH$_3$CN and chlorinated solvents; slightly soluble in alcohols and insoluble in H$_2$O.
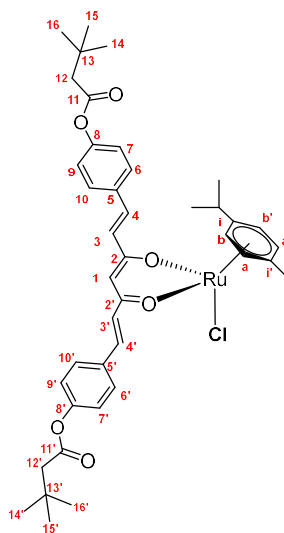

Figure 44 - *Structure of compound 16*

Anal. Calcd for C$_{41}$H$_{49}$ClO$_6$Ru: C, 63.59; H, 6.38. Found: C, 63.72; H, 6.50. m.p.: 225-228°C. IR (cm^{-1}): 2961 w, 2930 w, 2871 w v(aliphatic C–H); 1751 m v(–OC=O), 1635 m v(C=O); 1598 w, 1586 w, 1533 s, 1506 m, 1472 m, 1408 m v(C=C); 1368 m, 1321 m, 1281 w, 1210 m, 1186 s, 1163 s, 1110 s, 1033 m, 1013 m, 976 m, 926 m, 896 m, 875 m, 842 m, 806 w, 723 w, 714 w, 620 m. ^{1}H-NMR (CDCl$_3$, 293 K): δ 1.16 [s, 18H, C(14-14')H, C(15-15')H and C(16-16')H], 1.42 [d, 6H, –CH(CH_3)$_2$ of p-cymene, ^{4}J = 7 Hz], 2.36 [s, 3H, –CH_3 of p-cymene], 2.47 [s, 4H, C(12-12')H], 3.01 [sept, 1H, -CH(CH$_3$)$_2$ of p-cymene], 5.33 d, 5.60 d [4H, AA′BB′ system, CH$_3$- C$_6H_4$-CH(CH$_3$)$_2$ of p-cymene, ^{3}J = 6 Hz], 5.50 [s, 1H, C(1)H], 6.54 [d, 2H, C(3–3')H, ^{3}J = 16 Hz], 7.11 [d, 4H, C(9–9')H and C(7–7')H, ^{3}J = 8.5 Hz], 7.53 [d, 4H, C(10–10')H and C(6–6')H, ^{3}J = 8.5 Hz], 7.60 [d, 2H, C(4–4')H, ^{3}J = 16 Hz]. ^{13}C{^{1}H}-NMR (CDCl$_3$): δ 18.0 [–CH$_3$ of p-cymene], 22.4 [–CH(CH$_3$)$_2$ of p-cymene], 29.7 [C(14–14'), C(15-15') and C(16-16')], 30.9 [-CH(CH$_3$)$_2$ of p-cymene], 31.2 [C(13–13')], 47.9 [C(12–12')], 79.2 [C(a–a') of p-cymene], 83.0 [C(b–b') of p-cymene], 97.6 [Ci′ of p-cymene], 99.7 [Ci of p-cymene], 102.4 [C(1)], 122.0 [C(9–9') and C(7–7')], 127.7 [C(3–3')], 128.8 [C(10–10') and

C(6–6')], 133.5 [*C*(5-5')], 137.7 [*C*(4–4')], 151.4 [*C*(8–8')], 170.5 [*C*(11–11')], 178.4 [*C*(2–2')=O]. ESI-MS(+) CH_3CN (m/z [relative intensity, %]): 739 [100] [Ru(*p*-cymene)(L^{10})]$^+$.

[Ru(*p*-cymene)(L^{11})(Cl)] (**17**). In a round bottom flask, **HL^{11}** (111 mg, 0.2 mmol) and triethylamine (TEA 28 μL, 0.2 mmol) were dissolved in CH_3CN (5 mL) under magnetic stirring and heating. After 30 minutes, [(*p*-cymene)$RuCl_2$]$_2$ (61 mg, 0.1 mmol) was added at room temperature. The resulting red solution was stirred at reflux for 16 hours. At the end, the solvent was dried under reduced pressure and the obtained oil was precipitated with solvents (CH_2Cl_2/hexane). Then the precipitate was filtered with hexane and washed with cold 2-propanol giving the final complex **17** (**Figure 45**) as a red powder (yield 71%). It is soluble in DMSO, CH_3CN and chlorinated solvents; slightly soluble in alcohols and insoluble in H_2O.
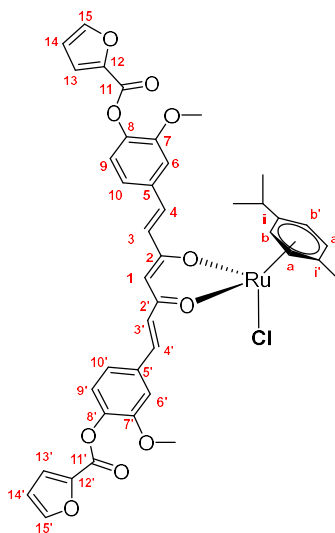

Figure 45 - *Structure of compound* **17**

Anal. Calcd for $C_{41}H_{37}ClO_{10}Ru$: C, 59.60; H, 4.51. Found: C, 59.38; H, 4.69. m.p.: 215-218°C. IR (cm^{-1}): 3145 wbr, 3119 wbr, 2963 w, 2937 w, 2872 w, 2840 w v(aromatic C–H); 1738 s v(–OC=O), 1628 w v(C=O); 1598 w, 1570 w, 1535 m, 1512 vs, 1470 s, 1451 m, 1404 s v(C=C); 1393 s, 1295 s, 1257 s, 1231 m, 1203 m, 1172 s, 1160 s, 1122 s, 1083 s, 1028 m, 1013 s, 994 m, 971 m, 928 m, 884 m, 847 m, 802 m, 766 s, 751 s, 734 m, 685 w, 611 m. ^{1}H-NMR (CDCl$_3$, 293 K): δ 1.42 [d, 6H, –CH(C*H*$_3$)$_2$ of *p*-cymene, ^{4}J = 7 Hz], 2.38 [s, 3H, –C*H*$_3$ of *p*-cymene], 3.01 [sept, 1H, -C*H*(CH$_3$)$_2$ of *p*-cymene], 3.89 [s, 6H, -OC*H*$_3$], 5.34 d, 5.61 d [4H, AA′BB′ system, CH$_3$- C$_6$*H*$_4$-CH(CH$_3$)$_2$ of *p*-cymene, ^{3}J = 6 Hz], 5.54 [s, 1H, C(1)*H*], 6.57 [d, 2H, C(3–3')*H*, ^{3}J = 16 Hz], 6.63 [d, 2H, C(14-14')*H*, ^{3}J = 8.0 Hz], 7.15, 7.16, 7.18 [m, 6H, C(10–10')*H*, C(6-6')*H*, C(9-9')*H*], 7.43 [d, 2H, C(13–13')*H*, ^{3}J = 8.0 Hz], 7.61 [d 2H, C(4–4')*H*, ^{3}J = 16 Hz], 7.71 [s, 2H, C(15-15')*H*]. ^{13}C{^{1}H}-NMR (CDCl$_3$): δ 18.1 [–CH$_3$ of *p*-cymene], 22.4 [–CH(CH$_3$)$_2$ of *p*-cymene], 30.9 [-CH(CH$_3$)$_2$ of *p*-cymene], 56.0 [-OCH$_3$], 79.2 [*C*(a–a') of *p*-cymene], 83.0 [*C*(b–b') of *p*-cymene], 97.7 [*C*i' of *p*-cymene], 99.8 [*C*i of *p*-cymene], 102.4 [*C*(1)], 111.2 [*C*(9–9')], 112.2[*C*(14–14')], 119.6 [*C*(13–13')], 120.9 [*C*(10–10')], 123.2 [*C*(6–

6')], 128.1 [C(3–3')], 135.2 [C(5–5')], 138.0 [C(4–4')], 140.0 [C(8-8')], 143.8 [C(12–12')], 147.1 [C(15–15')], 151.5 [C(7–7')], 156.2 [C(11-11')], 178.4 [C(2–2')=O]. ESI-MS(+) CH$_3$CN (m/z [relative intensity, %]): 791 [100] [Ru(p-cymene)(L^{11})]$^+$.

[**Ru(p-cymene)(L^{12})(Cl)**] (**18**). In a round bottom flask, **HL^{12}** (99 mg, 0.2 mmol) and triethylamine (TEA 28 µL, 0.2 mmol) were dissolved in CH$_3$CN (5 mL) under magnetic stirring and heating. After 30 minutes, [(p-cymene)RuCl$_2$]$_2$ (61 mg, 0.1 mmol) was added at room temperature. The resulting red solution was stirred at reflux for 16 hours The precipitate was filtered giving the final complex **18** (**Figure 46**) as a red powder (yield 74%). The complex is soluble in DMSO and chlorinated solvents, slightly soluble in CH$_3$CN and alcohols and insoluble in H$_2$O.
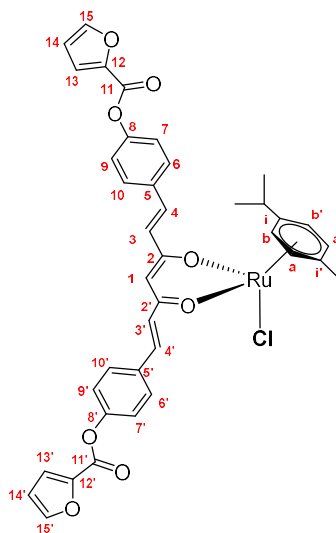

Figure 46 - *Structure of compound 18*

Anal. Calcd for C$_{39}$H$_{33}$ClO$_8$Ru: C, 61.14; H, 4.34. Found: C, 61.34; H, 4.41. m.p.: 267-269°C. IR (cm^{-1}): 3141 w, 3128 w, 3112 w, 3037 w, 2923 w, 2866 w ν(aromatic C–H); 1732 m ν(–OC=O), 1627 m ν(C=O); 1599 w, 1568 w, 1541 m, 1509 s, 1467 s, 1401 s ν(C=C); 1330 w, 1319 w, 1295 s, 1231 m, 1204 s, 1172 s, 1159 s, 1090 s, 1010 m, 998 m, 990 m, 977 m, 969 m, 948 m, 928 m, 883 m, 869 m, 853 m, 825 m, 805 m, 796 ,m, 768m, 751 m, 734 m, 685 m, 610 m. ^{1}H-NMR (CDCl$_3$, 293 K): δ 1.43 [d, 6H, –CH(CH_3)$_2$ of p-cymene, ^{4}J = 7 Hz], 2.38 [s, 3H, –CH_3 of p-cymene], 3.02 [sept, 1H, -CH(CH$_3$)$_2$ of p-cymene], 5.34 d, 5.61 d [4H, AA'BB' system, CH$_3$- C$_6$$H_4$-CH(CH$_3$)$_2$ of p-cymene, ^{3}J = 6 Hz], 5.51 [s, 1H, C(1)H], 6.58 [d, 2H, C(3–3')H, ^{3}J = 16 Hz], 6.63 [m, 2H, C(14-14')H], 7.26 [d, 4H, C(9–9')H and C(7–7')H, ^{3}J = 9 Hz], 7.42 [d, 2H, C(13–13')H], 7.59 [d, 4H, (d, 4H, C(10–10')H and C(6–6')H, ^{3}J = 9 Hz], 7.63 [d, 2H, C(4-4')H, ^{3}J = 16 Hz], 7.72 [s, 2H, C(15-15')H]. ^{13}C{^{1}H}-NMR (CDCl$_3$): δ 18.0 [–CH$_3$ of p-cymene], 22.4 [–CH(CH_3)$_2$ of p-cymene], 30.9 [-CH(CH$_3$)$_2$ of p-cymene], 79.2 [C(a–a') of p-cymene], 83.1 [C(b–b') of p-cymene], 97.6 [Ci' of p-cymene], 99.7 [Ci of p-cymene], 102.6 [C(1)], 112.3 [C(14–14')], 119.7 [C(13–13')], 122.0 [C(9–9') and C(7–7')], 127.9 [C(3–3')],

128.9 [C(10–10′) and C(6–6′)], 133,8 [C(5-5′)], 137.7 [C(4–4′)], 143.9 [C(12-12′)], 147.3 [C(15–15′)], 150.9 [C(8-8′)], 156.2 [C(11-11′)], 178.4 [C(2–2′)=O]. ESI-MS(+) CH$_3$CN (m/z [relative intensity, %]): 731 [100] [Ru(p-cymene)(L^{12})]$^+$.

2.2 RESULTS AND DISCUSSION

2.2.1 Synthesis and characterization of ligands

The bioconjugate curcumin ligands, **HL¹-HL¹²**, were synthesized as reported in **Scheme 13** at room temperature and under inert atmosphere (N$_2$ flux), starting from the commercially available curcumin (for **HL¹**, **HL³**, **HL⁵**, **HL⁷**, **HL⁹** and **HL¹¹** ligands) and bisdemethoxycurcumin (for **HL²**, **HL⁴**, **HL⁶**, **HL⁸**, **HL¹⁰** and **HL¹²** ligands). In brief, curcumin or bisdemethoxycurcumin were dissolved in the reaction solvent which, in most of the case, was acetone. However, the use of acetone as solvent in the reaction between curcumin and 3,3-dimethylbutyryl chloride did not give the desired product **HL⁹** and, as a consequence, this reaction was carried out by using another polar aprotic solvent such as CH$_3$CN. The following step was characterized by the addition of triethylamine (TEA), in order to provide a basic environment required for the deprotonation of the two phenolic -OH groups in the aromatic moieties. The change in color from yellow to red confirms this process. The presence of a Lewis base instead of a Brønsted one was necessary to avoid secondary and unwanted reactions which did not allow the reaction to proceed. The esterification reaction has been carried out in the presence of relative acyl chloride which has been added dropwise at 0 °C to counteract the exothermic reaction due to its very high reactivity. The solution immediately turned yellow and the formation of a precipitate has been observed after few minutes. Both the base (TEA) and the acyl chloride have been used in excess with respect to the curcuminoids (3:1) and not in stoichiometric quantity (2:1) in order to favor the formation of the diesterified product. Anyway, in the case of the synthesis of **HL¹¹** and **HL¹²** ligands the stoichiometric quantity of triethylamine was necessary, since by using an excess of it did not allow to obtain the desired product leading secondary reactions take place like the formation of amide between the amine and the heteroaromatic acyl chloride (2-furoyl chloride). At the end, in order to purify the desired product from the reactants, the crystallization has proved to be an excellent alternative to this procedure avoiding the common use of chromatographic separation as it avoids the loss of the product in the column and allows less waste of solvent.
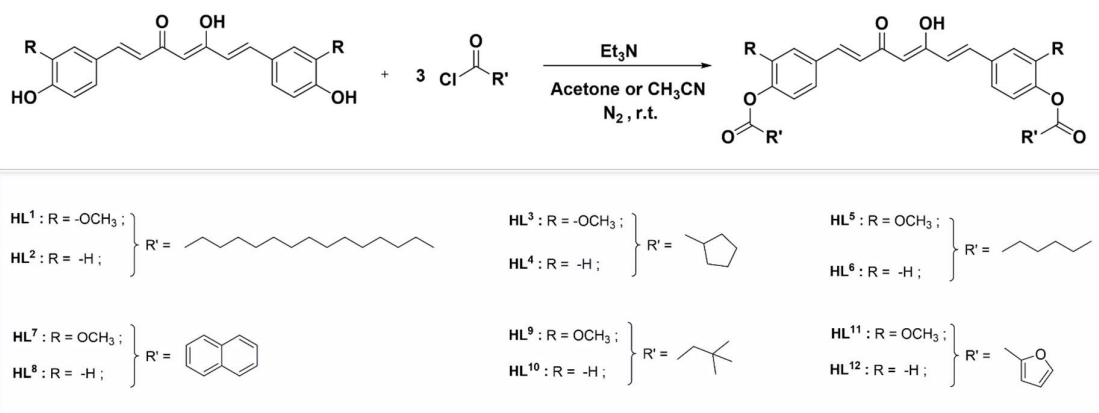
Scheme 13 - *Synthetic procedure for the ligands HL¹-HL¹²*

The so obtained compounds **HL^1-HL^{12}** are air-stable and soluble in most of the organic solvents, but not in water. The elemental analyses and ESI-MS spectrometry have confirmed the expected structures of the ligands, showing a very good purity of the products, which is also confirmed by the narrow melting points. The molecular structures of these ligands have been confirmed by the presence of the molecular peaks at m/z [M-1], attributable to the deprotonated [L^n]$^-$ (n = 1-12) species.

The IR spectra of the ligands have been carried out on solid samples and from which it was possible to infer some confirmation of the occurred esterification. First of all, from the disappearance of the broad absorption above 3000 cm^{-1} attributable to the stretching of the O-H bonds, originally present in the starting curcuminoids and, additionally, a new strong absorption is observed at around 1740 cm^{-1}, attributable to the stretching of the added -OC=O group (an example in **Figure 47**). Moreover, the spectra have shown all the expected absorption bands: weak or medium absorptions in the range 2970-2870 cm^{-1} due to the C-H bonds followed by that relative to the stretching of the –C=O at around 1622 cm^{-1} and, at the end, a medium absorption in the range 1598 and 1408 cm^{-1} resulting from the C=C double bonds.
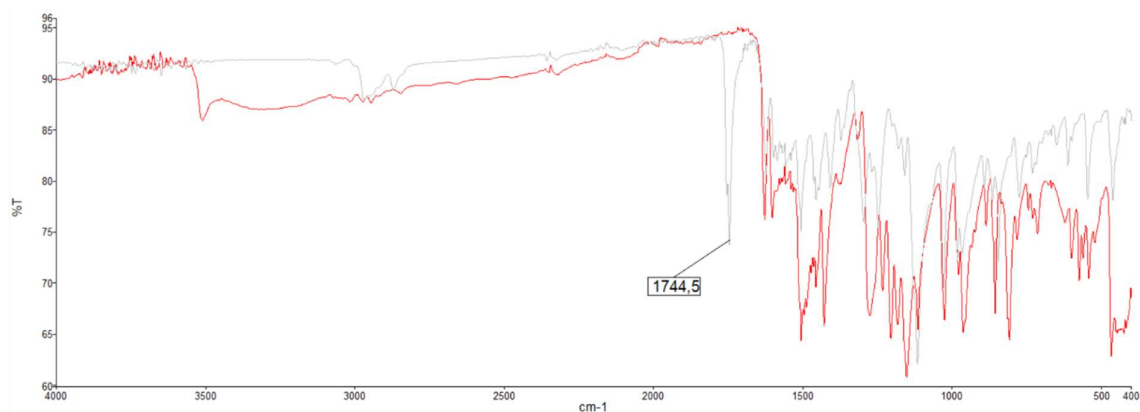

Figure 47 - *Comparison between the IR spectra of **HL^3** ligand (grey line) and the curcumin parent compound (red line)*

All the ^{1}H-NMR spectra have been recorded in CDCl$_3$ solution except for the compounds **1** and **2** for which DMSO-d_6 has been used. They have shown a single set of resonances for the two acyl substituents, indicating both the chemical and magnetic equivalence of the diesterified products. This confirmed that the symmetry of the starting molecules is maintained in the final products. The same analogues of the esterified products of curcumin and bisdemethoxycurcumin between them, show a similarity in the NMR spectra and this reflects the structural similarity of the couple ligands. The difference lies in the presence of the methoxy group for curcumin derivatives that generates a singlet at about 3.8 ppm and, three more other signals, attributable to the protons of the tri-substituted aromatic rings. On the other hand, the absence of the methoxy group in the bisdemethoxycurcumin derivatives, generates a di-substituted aromatic ring in *para* position, resulting in the presence of two

doublets in the aromatic region of the spectrum. In both cases, the keto-enol tautomerism is confirmed by the presence of a singlet at about 5.8 ppm attributable to 1-C*H*, that integrates just a single proton. In addition to the signals occurring at higher frequencies, due to the conjugated system of the curcuminoid structure, the aliphatic protons belonging to the acyl moiety of the diesterified products **HL¹**, **HL²**, **HL³**, **HL⁴**, **HL⁵**, **HL⁶**, **HL⁹**, **HL¹⁰**, are detectable as multiplets in the region of upfield (¹H-NMR examples of compounds **HL⁴** and **HL⁵** in **Figure 48a and 48b** respectively).
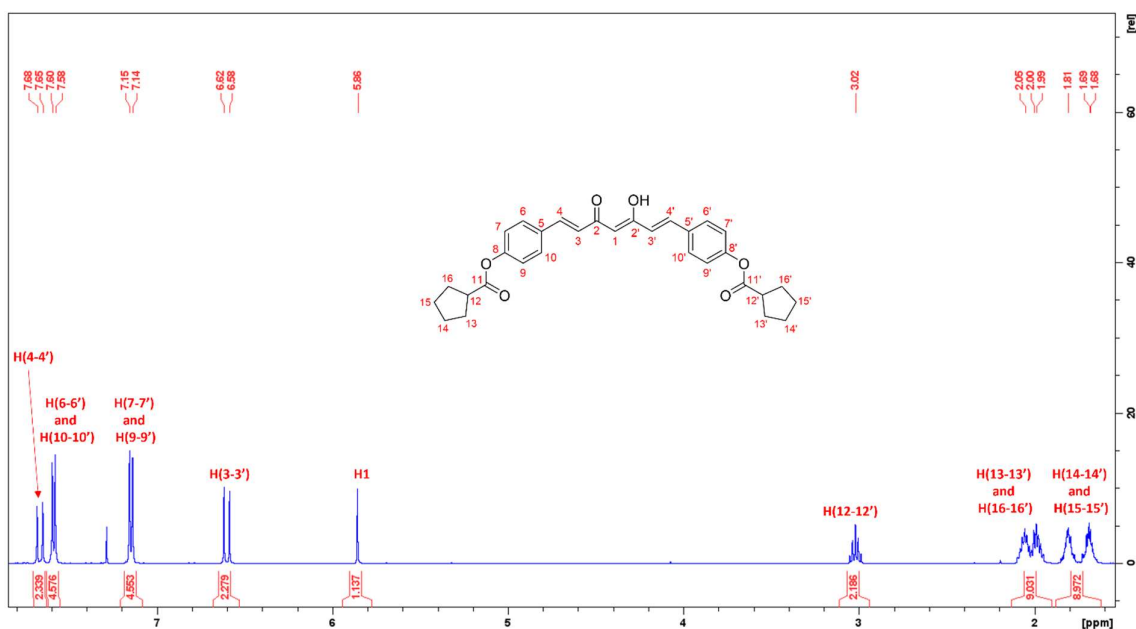

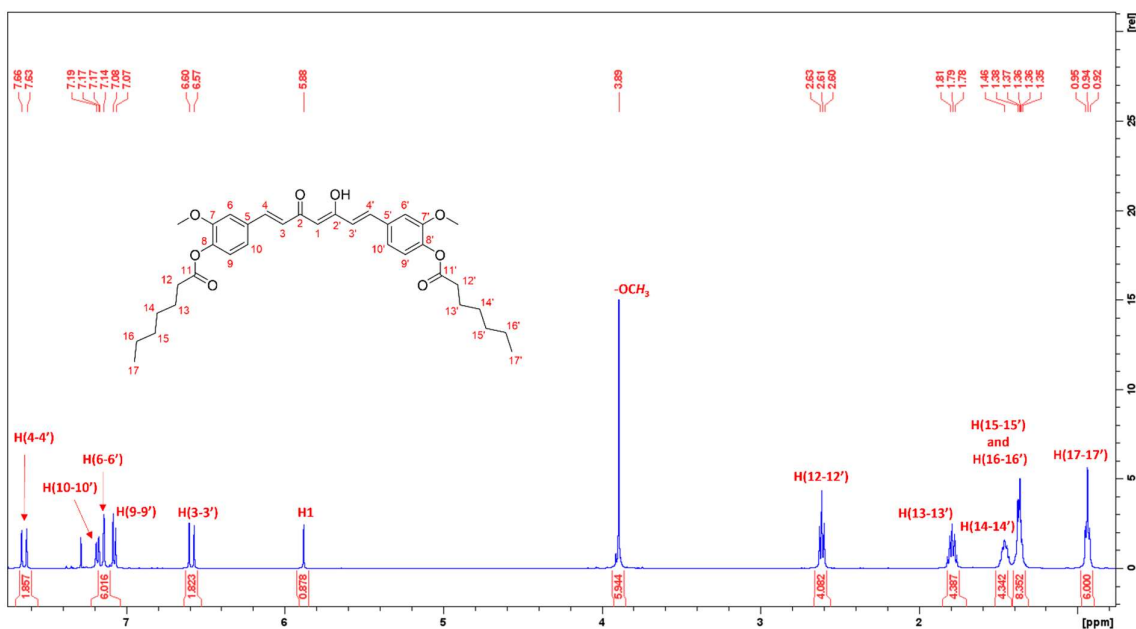***Figure 48a -*** *¹H-NMR spectrum of ligand **HL⁴** recorded in CDCl₃*

Figure 48b – *¹H-NMR spectrum of ligand **HL⁵** recorded in CDCl₃*

Among these aliphatic signals, the more deshielded protons are those bound to 12/12'-C*H* since they are closer to the ester group. In the case of **HL⁷**, **HL⁸**, **HL¹¹** and **HL¹²**, the aromatic region of the spectrum, where the curcumin signals fall, is more complex due to the presence of additional aromatic protons due to the acyl substituent (¹H-NMR example of compound **HL¹¹** showed in **Figure 49**). ¹H-NMR spectra were assigned based on the ¹³C-NMR, and one-bond and long-range couplings from {¹H −¹H}-COSY, {¹H −¹³C}-HSQC, and {¹H −¹³C}-HMBC experiments.
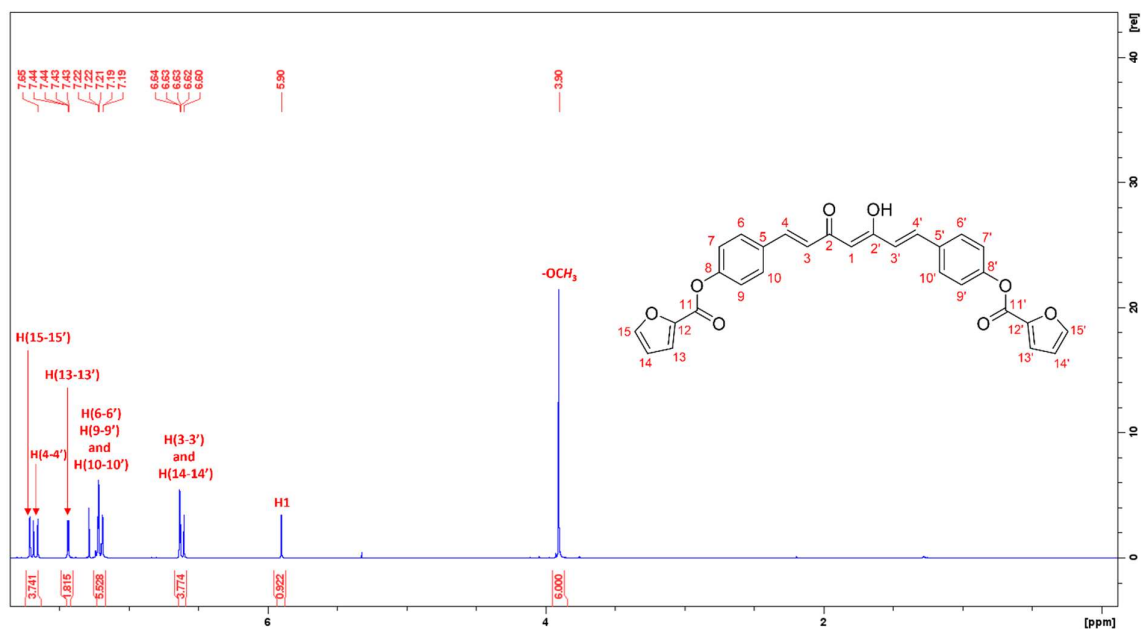

Figure 49 - *¹H-NMR spectrum of ligand* **HL¹¹** *recorded in CDCl₃*

2.2.2 Synthesis and characterization of the complexes

All the complexes have been synthesized in good yields. The compounds **9-18** were obtained by dissolving the respective, previously reported, curcuminoid ligands in a CH_3CN solution under magnetic stirring and heating to favour the solubilization of the starting material. For complexes **1-4** the use of an even more apolar solvent, like CH_2Cl_2, was necessary since the very high hydrophobicity of palmitoyl residue. Then, the triethylamine has been added in stoichiometric quantity to the solution to provide a basic environment required for the deprotonation of the enolic form belonging to the curcuminoid structure. In this way the coordination of the ligands to the metal centre is further facilitated. No change in color were observed in this case. After 30 minutes, the dimer [(p-cymene)MCl₂]₂ (where M = Ru except for complexes **3** and **4** for which M = Os) has been added and the resulting solutions have been stirred at reflux for 16 or 24 hours (**Scheme 14**). The time required for complexes **1-4** was a bit longer. The resulting clear solutions have been dried at reduced pressure and the complexes have been precipitated with solvents (using a mixture of CH_2Cl_2

/ Hexane) and washed with 2-propanol (or EtOH for compounds **1-4**) in order to remove the residue of triethylammonium chloride salt formed during the reaction. These final steps were not necessary for compounds **13** and **14**, for which, after 16 hours under reflux the formation of a red precipitate was observed, thus the corresponding products were isolated by filtration.
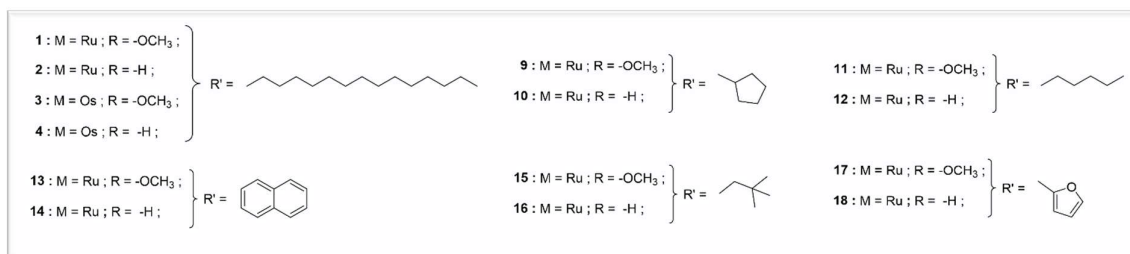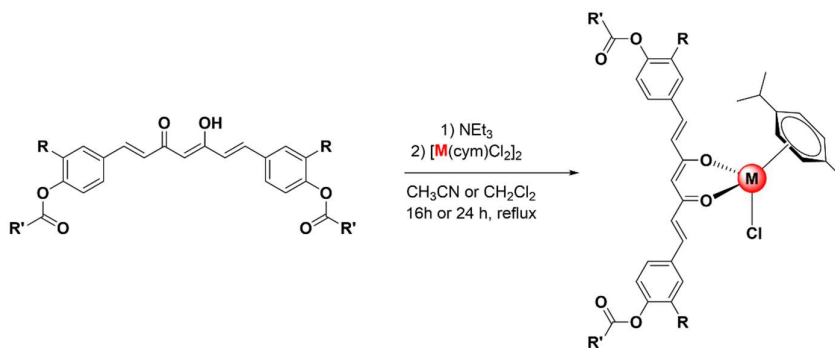
Scheme 14 - *Synthetic procedure for compounds 1-4 and 9-18*

The so obtained compounds **1-4** and **9-18** are air-stable and soluble in most of the organic solvents, but not in water. The elemental analyses and ESI-MS spectrometry have confirmed the expected structures, showing a very good purity of the products, which is also confirmed by the narrow melting points. The molecular structures have been confirmed by the presence of the molecular peaks at m/z [M-35], attributable to the hydrolysis of M-Cl bond.

The IR spectra have been carried out on solid samples. They have shown all the expected absorption bands and in particular the typical $v(C=O)$ vibrations relative to the complexes are shifted at lower wavenumbers compared to the corresponding free ligands due to coordination through both the carbonyl arms toward the metal. The occurred coordination could be inferred also to the sharper peaks' structure (**Figure 50**). Furthermore, in the far-IR region, strong absorptions at around 270 cm^{-1} may be assigned to $v(M–Cl)$.
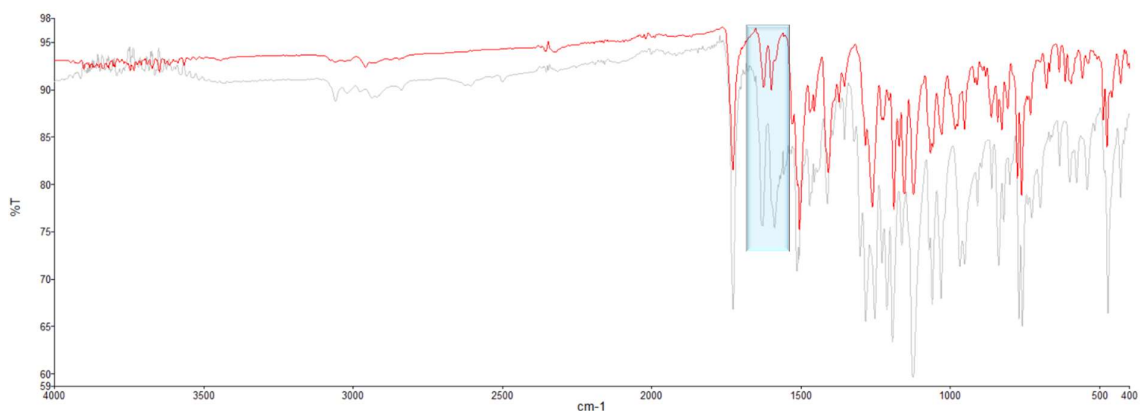
Figure 50 - *Comparison between the IR spectra of* **HL⁷** *ligand (grey line) and the relative complex* **13** *(red line)*

All the ¹H-NMR spectra of the complexes have been recorded in $CDCl_3$ solution except for compounds **13** and **14** for which has been used DMSO-d_6. The same analogues of curcumin and bisdemethoxycurcumin, between them, show a similarity of the NMR spectra. The only difference lies in the presence of the methoxy group (for curcumin derivatives) that generates a singlet at about 3.8 ppm and the signals coming from the different substituted aromatic rings (an example of complexes bearing the same curcumin and bisdemethoxycurcumin derivative in **Figure 51**).
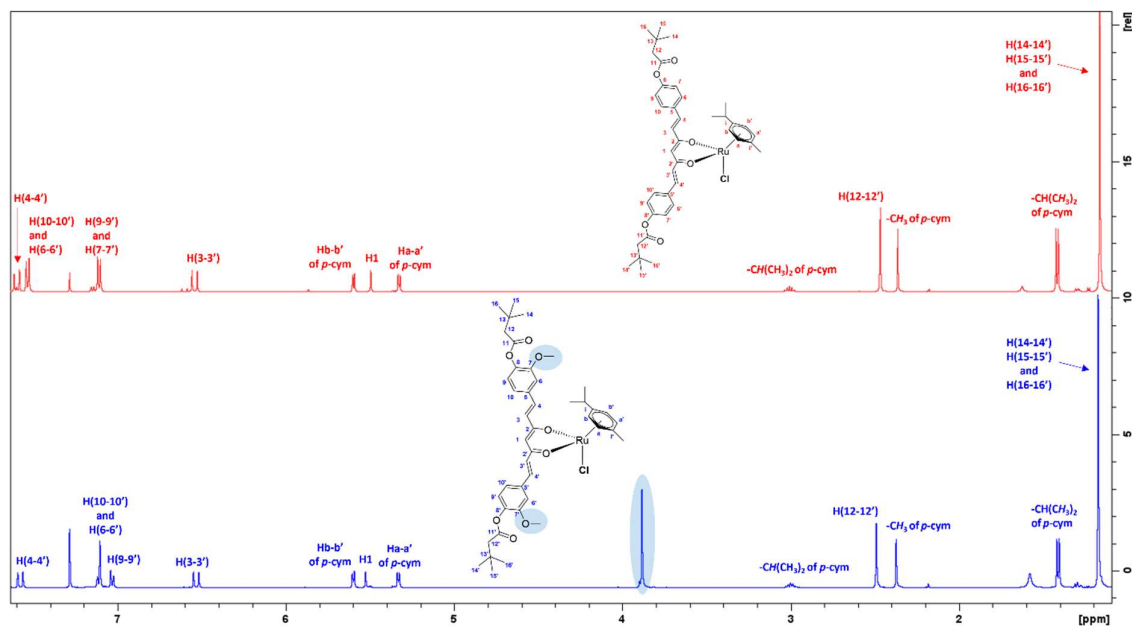

Figure 51 - *Comparison between the* ¹H-NMR *spectra recorded in* $CDCl_3$ *of compound* **15** *(blue line) and* **16** *(red line)*

In the spectra all the set of signals related to the ligands' protons far from the coordination environment, are just a little bit shifted compared to the signals of the free ligands. Thus, the most shifted and representative signals of the occurred complexation are: that one of the

proton in *alpha* position (1-C*H*), found at weaker fields as consequence of the coordination to the metal centre through the carbonyl groups; and the 3-C*H* and 3'-C*H* protons, being in the immediate proximity of the coordination sphere.

The 1-C*H* proton signal is always found at around 5.5 ppm and appears between the two doublets arising from the aromatic protons of the *p*-cymene system (Ha-a' and Hb-b'). Furthermore, additional signals coming from the arene system appear in the aliphatic region of the spectrum and result in a singlet (due to the isolated -CH$_3$) and a septet plus a doublet due to the -CH(CH$_3$)$_2$ group (a representative example in **Figure 52**).
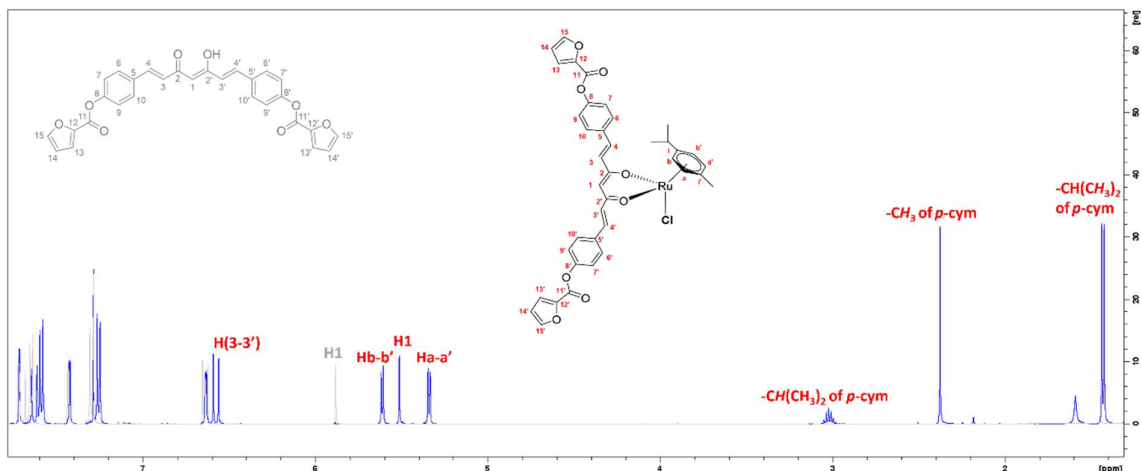

Figure 52 - *Comparison between the ¹H-NMR spectra recorded in CDCl₃ of compound **18** (blu line) and its relative ligand **HL¹²** (grey line)*

The ¹H- and ¹³C-NMR spectra were assigned based on the one-bond and long-range couplings, from {¹H–¹H}-COSY, {¹H–¹³C}-HSQC, and {¹H–¹³C}-HMBC experiments (examples of bidimensional analysis of compound **1** are showed in **Figures 53a, 53b and 53c**).
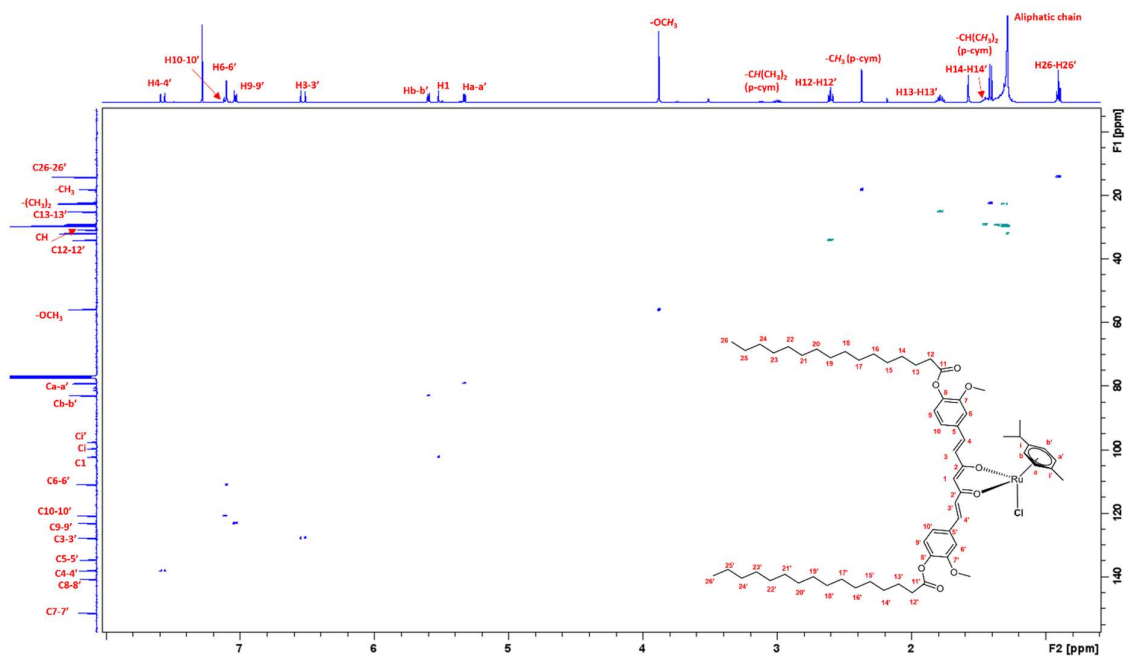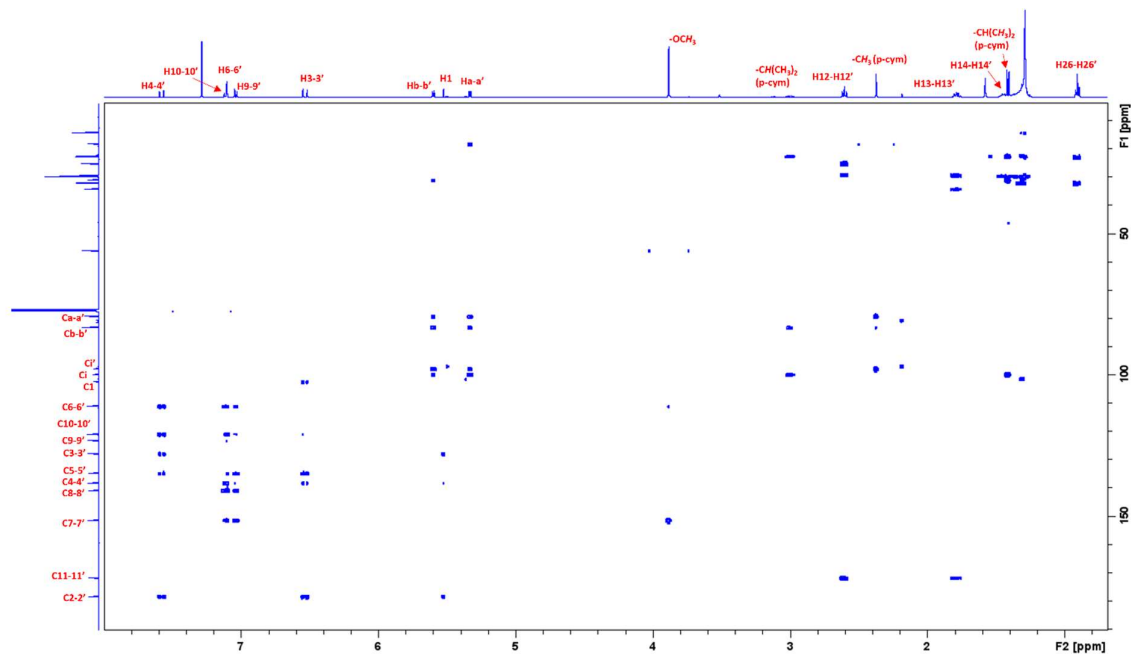
Figure 53a - *{ ¹H-¹³C}-HSQC NMR of **1** in CDCl₃*
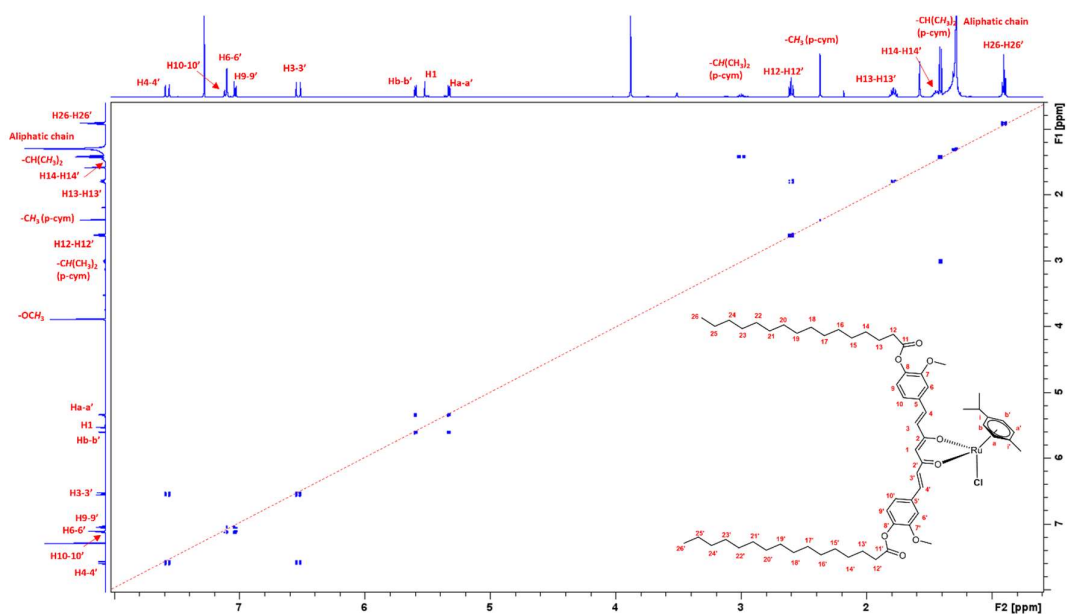

Figure 53b –*{ ¹H-¹³C}-HMBC NMR of **1** in CDCl₃*

Figure 53c – { ^1H-^1H}-COSY NMR of **1** in CDCl₃

Similarly, to the compounds **1** and **2**, which are ruthenium complexes of **HL¹** and **HL²** ligands respectively, also osmium derivatives **3** and **4** of the same ligands have been synthesized. They present the same ^{1}H-NMR patterns except for the signals coming from the arene part (*p*-cymene moiety) which are more deshielded for the osmium analogues. A less pronounced shifting, can be also seen for the proton of the ligand 1-C*H* in *alpha* position and for the septet of the -C*H*(CH₃)₂ group. Any particular difference was found for the doublet of -CH(C*H₃*)₂ and for the singlet of -C*H₃* (**Figure 54**).
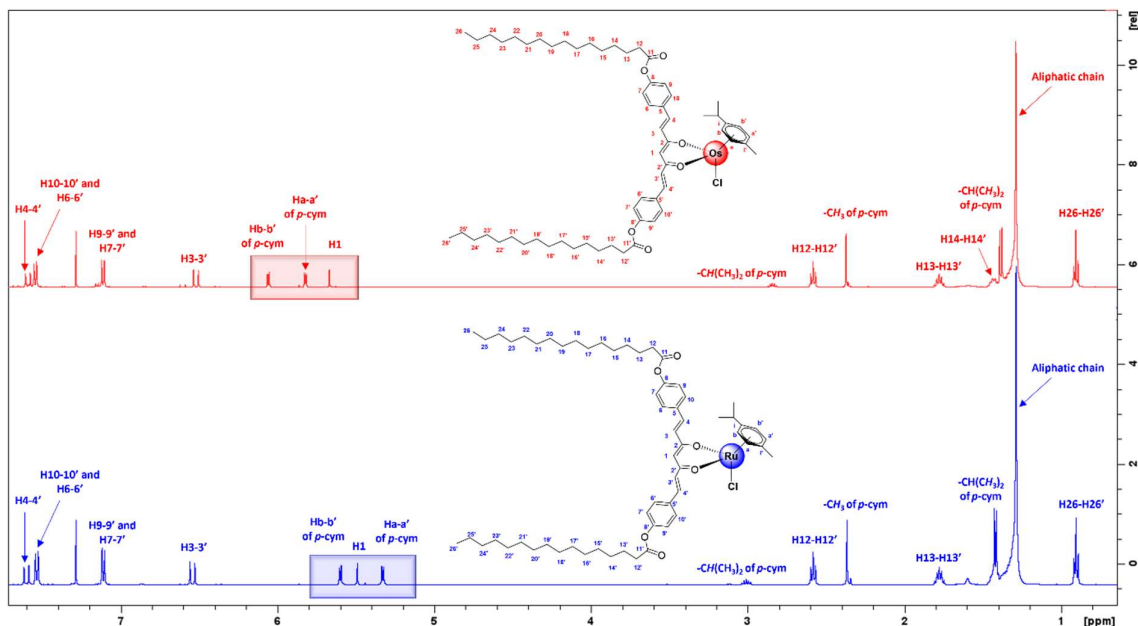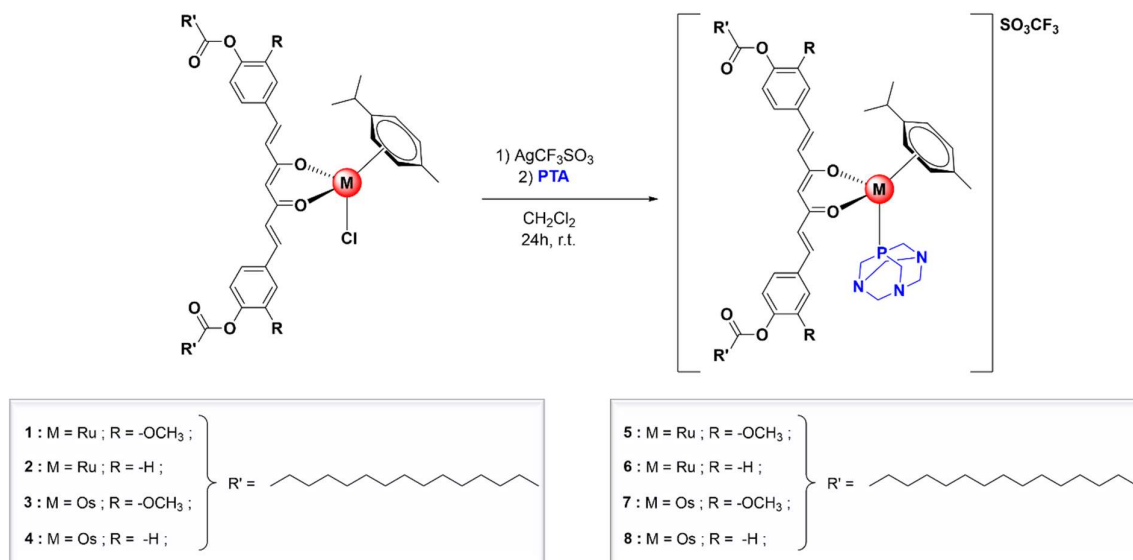

Figure 54 - *Comparison between the ^{1}H-NMR spectra recorded in CDCl₃ of compounds containing the Ruthenium, **2** (blue line) and Osmium, **4** (red line) analogues of **HL²** ligand*

Additionally, the RAPTA-like compounds **5-8** have been synthesized in good yields starting from **1-4** (**Scheme 15**). The parent complexes **1-4** have been initially solubilized in CH_2Cl_2 and the hydrolysis of M-Cl ligand was promoted by the addition of the silver salt $AgSO_3CF_3$ that gave the precipitation of AgCl, leaving in solution the $[(p\text{-cymene})M(L^n) - SO_3CF_3]$ species (where n= 1-2 and M = Ru or Os). The reaction was stirred at room temperature for 1 hour and then the solution was filtered to remove the AgCl salt. PTA (1,3,5-triaza-7-phosphaadamantane) was finally added to the filtrate and then the solution was stirred for other 24 h at room temperature to obtain the ionic derivatives **5-8** having the triflate species $(SO_3CF_3^-)$ as counterion in the outer-sphere of coordination. The products have been precipitated from a 3/1 mixture of dichloromethane and *n*-hexane.

1 : M = Ru ; R = -OCH$_3$;
2 : M = Ru ; R = -H ;
3 : M = Os ; R = -OCH$_3$;
4 : M = Os ; R = -H ;

5 : M = Ru ; R = -OCH$_3$;
6 : M = Ru ; R = -H ;
7 : M = Os ; R = -OCH$_3$;
8 : M = Os ; R = -H ;

Scheme 15 - *Synthetic procedure for compounds* ***5-8***

Again, the obtained compounds are air-stable and soluble in most organic solvents, but not in water.

The elemental analyses and ESI-MS spectrometry have confirmed the expected structures, showing a very good purity of the products, which is also confirmed by the narrow melting points. The molecular structures of these complexes have been underlined by the presence, in the mass spectrum, of the molecular peaks attributable to the remotion of the $SO_3CF_3^-$ counterion from the complexes. Furthermore, the conductance values in acetone confirm the existence of 1:1 electrolyte species for **5–8** and are consistent with the conductance values of their neutral derivatives **1-4**. It has been observed that he bisdemethoxycurcumin-like derivatives **6** and **8** have a lower dissociation than their curcumin-like analogues **5** and **7**. The substitution of chloride by PTA and the formation of the ionic compounds were confirmed by the absence of the ν(M–Cl) absorption band in the IR spectra. Moreover, a

characteristic absorption pattern in the region 1000–1200 cm^{-1}, indicative of a non-coordinated SO$_3$CF$_3^-$ anion, is observed. The ^{31}P-NMR resonances in DMSO-d_6 attributable to the PTA ligand are observed at lower field compared to that of uncoordinated PTA, thus confirming the binding to the metal center.

Moreover, the ^{1}H-NMR spectra show the additional peaks due to the presence of PTA ligand which generates a singlet around 4.10 ppm (NCH_2P) and a multiplet at about 4.46 (NCH_2N) (**Figure 55**).
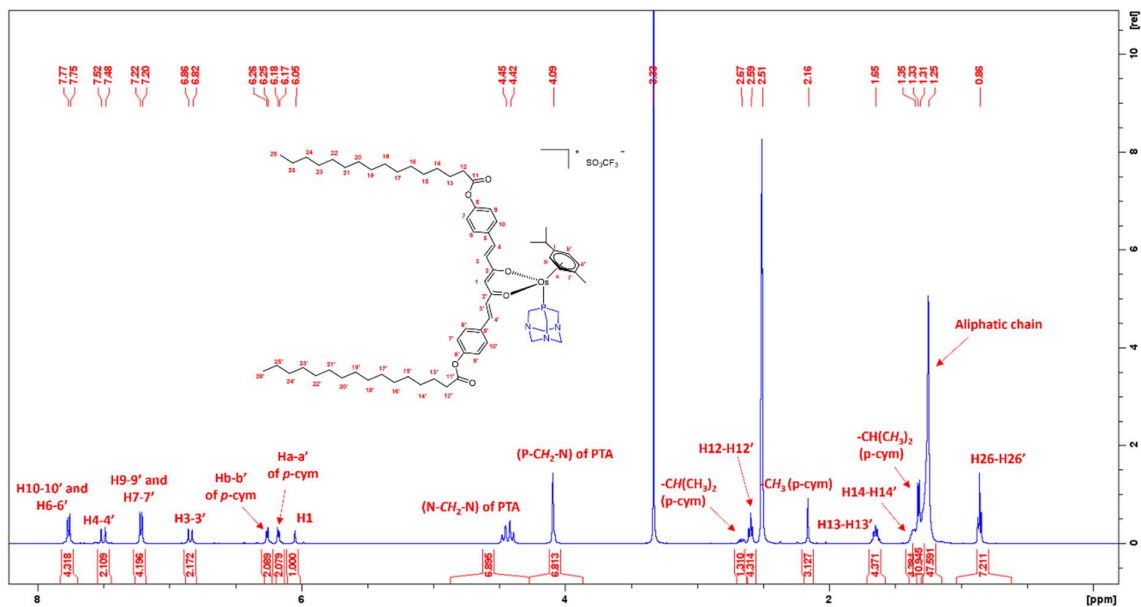

Figure 55 - ^{1}H-NMRspectrum of **8** recorded in DMSO

2.2.3 Stability studies

To investigate the stability of **5**–**8** a series of ^{31}P-NMR spectra were recorded in DMSO-d^6 solution over time. The δ values of the characteristic peaks for phosphorous in all the spectra remained unchanged over 3 days, indicating that the complexes are stable in DMSO. The ^{1}H-NMR spectra of the same complexes confirm their stability although a slight release of curcumin ligand is observed after 6 days for complexes **5** and **6**, underling the greater inertness and stability of the osmium complexes **7** and **8** compared to ruthenium (see **Figures 56a, 56b** and **56c**).

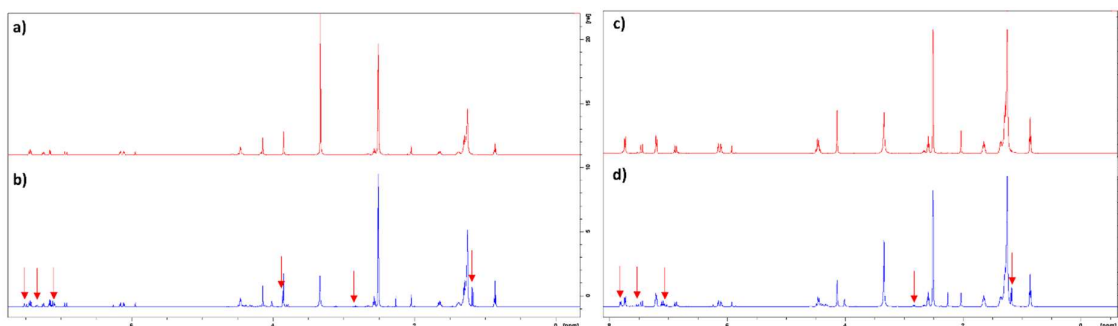**Figure 56a -** ^{1}H-NMR in DMSO-d^6 of **5** at t=0 (**a**) and t=6 days (**b**) and of **6** at t=0 (**c**) and t=6 days (**d**)
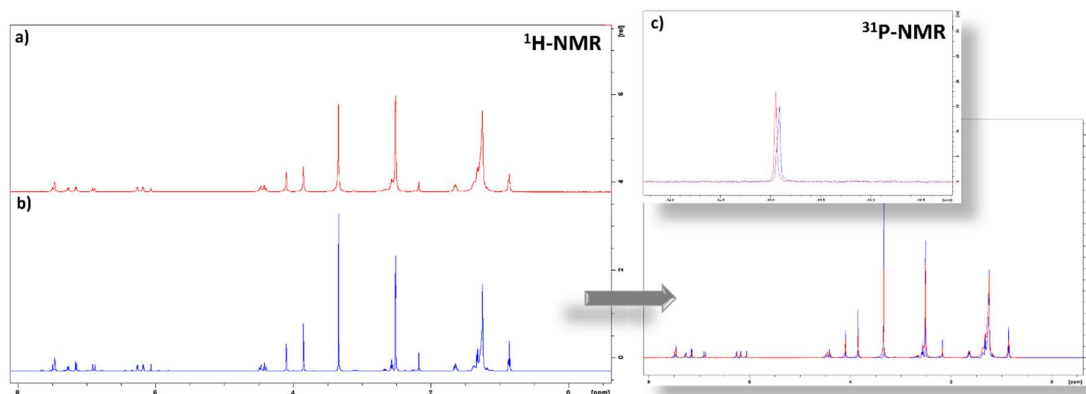

Figure 56b – ^{1}H-NMR of **7** in DMSO-d^6 at t=0 (**a**) and t=6 days (**b**) and the ^{31}P-NMR recorded after 6 days (**c**)
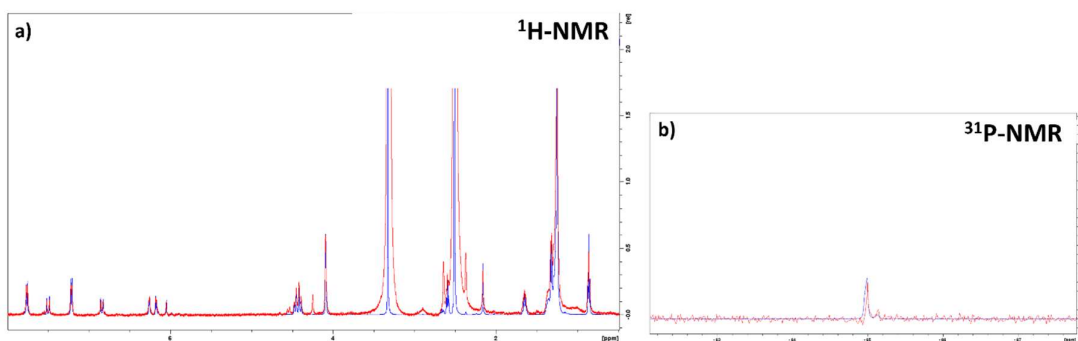
Figure 56c – *¹H-NMR of **8** in DMSO-d⁶ after 6 days (**a**) and the ³¹P-NMR recorded after 6 days (**b**)*

Furthermore, the stability of the neutral derivative **1** in DMSO solution was confirmed using UV-vis spectroscopy. The spectrum remained unchanged for a period of 72 h, displaying an absorption band at about 400 nm (**Figure 57a**). In order to investigate the stability profile under physiologically relevant conditions, phosphate- buffered solutions (PBS, pH = 7.4) of **1**, **3** and **5** were monitored over time using UV-Visible spectroscopy. The complexes were initially dissolved in DMSO (0.7 mg L^{-1}, 0.16 mg L^{-1} and 97.5 mg L^{-1} respectively) and then diluted to 5% DMSO with PBS. The absorbance spectra were collected after 0, 4, 18, 24, 48 and 72 h (**Figure 57b, 57c and 57d**).
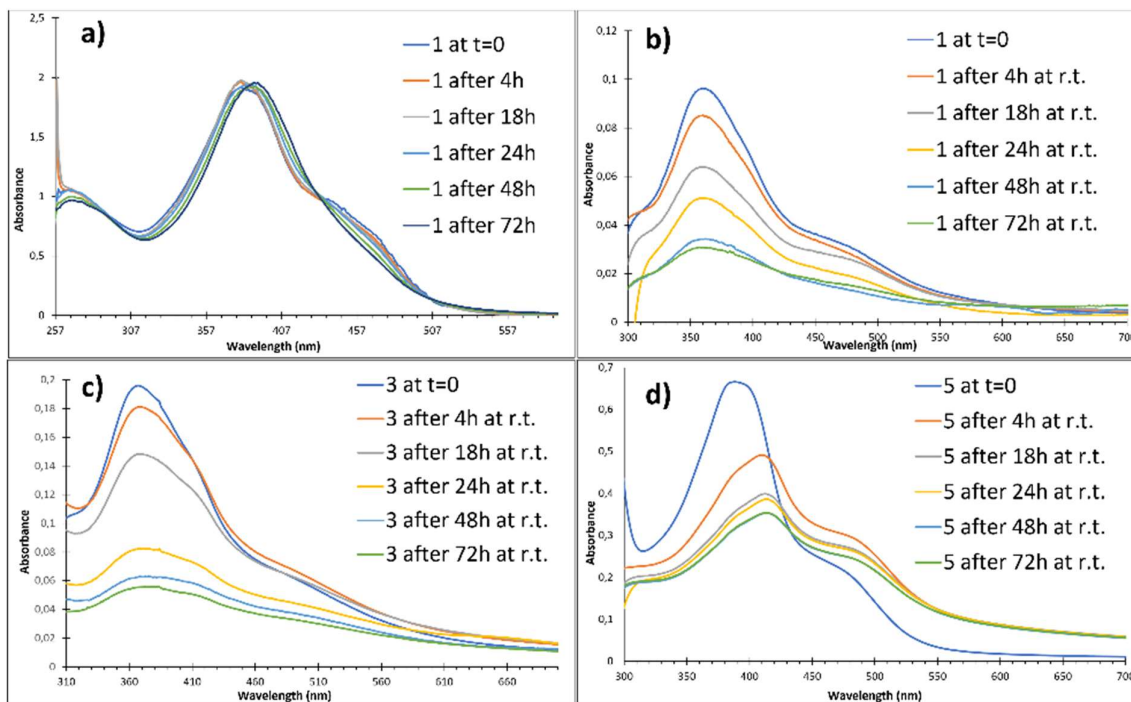
Figure 57 - *UV-visible spectra of **1** in DMSO solution (**a**) and of **1** (**b**), **3** (**c**) and **5** (**d**) in 5% DMSO-PBS solution at room temperature within 72 hours*

This time, the absorption energy of the complexes in 5% DMSO-PBS decreases over time, which may be attributed to precipitation, observable by clouding of the solution, probably due to the very long lipophilic chain of the palmitoyl residue. For **1** and **3** the exchange of the

chloride ligand with a solvent molecule occurs immediately and λ_{max} remains unchanged within 72 h. In contrast, complex **5** containing PTA shows a slight decrease in the wavelength of the maximum absorption energy which might be caused by the replacement of $SO_3CF_3^-$ counterion with an anion present in the buffer solution. In fact, the intermolecular contacts between the anionic species with the complexes may affect the electronic structure and the structural arrangement, as previously reported by others.[149] All the complexes showed transitions in the range 350–400 nm assignable to MLCT (metal–ligand charge transfer) from the filled 4d orbitals of Ru(II) to the empty π* ligand orbitals ($4d^6$ Ru → π*). For complex **5** the substitution of the counterion hypothesized above is consistent with the stability studies in solution carried out using ^{31}P-NMR spectroscopy in which the phosphorus signal remains unchanged over 72 hours. The osmium complex **4** showed greater stability than the analogous ruthenium derivative **1**.

2.2.4 Cytotoxicity studies

The cytotoxicity of the compounds **1-8** was determined on the human ovarian carcinoma cell line (A2780) and its cisplatin resistant form (A780cis) as well as non-tumorigenic human embryonic kidney (HEK293T) cells over an incubation period of 72 h using the MTT assay. The resulting IC_{50} values of the compounds are presented in **Table 1** together with the values for cisplatin and Rapta-C used as positive and negative controls, respectively. Complexes **2** and **4** display the highest cytotoxicity to the

A2780 cells, with IC_{50} values of 0.5 ± 0.2 and 0.4 ± 0.1 µM, respectively, combined with excellent selectivity profiles, with a selectivity index > 100 (IC50 >50 µM in the HEK293T cell line). Compared to cisplatin, used as a positive control, **2** and **4** are more cytotoxic to the A2780 cells and are more selective, but do not effectively overcome acquired resistance due to cisplatin. Complexes **1** and **3** are the least cytotoxic to the A2780 cells with IC_{50} values of 43 ± 5 µM and 49 ± 6 µM, respectively. Previous studies on ruthenium complexes with curcumin and bisdemethoxycurcumin ligands indicated that the ionic PTA derivatives tend to be more effective. Here, however, the neutral Ru and Os complexes are superior to the ionic PTA derivatives.

The higher cytotoxicity observed for **2** and **4** compared to previously reported compounds may be attributed to the presence of long aliphatic chains in the ligands that presumably favour uptake. Overall, the best results are observed for bisdemethoxycurcumin derivatives, regardless of their neutral or charged nature. SAR data revealed that bisdemethoxycurcumin complexes are generally more active and selective than the analogous curcumin-containing complexes.

Compound	A2780	A2780cis	HEK293T
HL[1]	4.2 ± 4.9	6.8 ± 3.0	>50
HL[2]	n.a *	n.a *	n.a *
1	43 ± 5.0	>50	>50
2	0.5 ± 0.2	6.3 ± 7.7	>50
3	49 ± 6.0	>50	>50
4	0.4 ± 0.1	>50	>50
5	6.1 ± 1.7	11.2 ± 0.6	24 ± 80
6	11.8 ± 2.6	14.4 ± 5.7	21 ± 19
7	10.3 ± 2.9	14.9 ± 2.6	21 ± 10
8	3.7 ± 2.2	2.3 ± 0.4	3.7 ± 0.8
Cisplatin	1.1 ± 0.5	7.7 ± 0.9	3.4 ± 1.7
Rapta-C	>100	>100	>100

Values not reproducible due to low solubility

Table 1 - *IC$_{50}$ values of p-curcH and p-bdcurcH, **1–8**, cisplatin and RAPTA-C on the human ovarian carcinoma (A2780), its cisplatin resistant form (A2780cis), and human embryonic kidney (HEK293T) cell lines. IC$_{50}$ values (μM) are given as the mean obtained from triplicate values for poorly soluble compounds or 3 independent experiments ± standard deviation*

2.2.5 Binding with BSA

The interaction between serum proteins and drugs is of fundamental pharmacological importance since human serum albumin (HSA) is a major plasma protein with an established role in drug transport. The binding drug-serum albumin is known to occur mainly through the formation of non-covalent interactions at specific binding sites. Previous crystallographic studies reported that a wide variety of drugs and small molecule toxins targeted the deep cleft between domains I and III of HSA. A similar binding mode was predicted in the case of complexes **1**, **2**, **4** and **5**. In particular, the structural analysis with Maestro R.2021-2 showed that the complexes were stabilized by hydrophobic interactions with residues Pro-113, Leu-115, Val-116, Pro-147, Tyr-148, Tyr-150, Ala-191, and by short-range polar interactions with residues Arg-114, Arg-117, Lys- 190, Lys-432, Lys-436 (**Figure 58**).
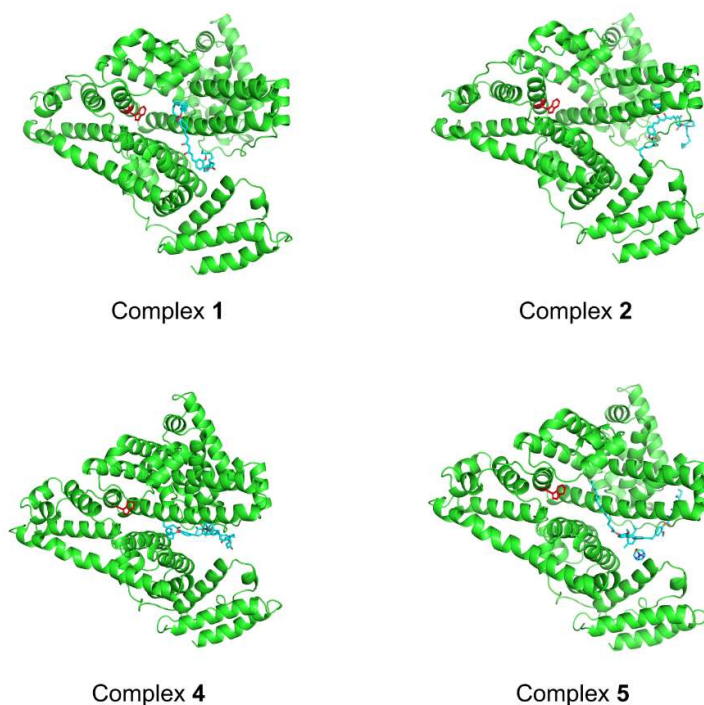
Figure 58 - Comparison of the computed binding modes of complexes 1, 2, 4 and 5 to crystallographic structure of HSA. Trp residue responsible for the intrinsic fluorescence of HSA is rendered as red stick

Given the high structural homology, bovine serum albumin (BSA) was used instead of HSA, in experimental binding studies of selected complexes (**1**, **2**, **4** and **5**) using a fluorometric quenching assay.26 Upon excitation of tryptophan residue at 295 nm, fluorescence emission spectra were recorded in the range 340–600 nm after addition of the complexes. All compounds quenched the intrinsic fluorescence of BSA, although to different extents, based on different affinities for BSA and the distance between the fluorophore and the binding site. The biosensor analyses reported a reversible interaction, characterized by a moderate affinity in the micromolar range, with low values of both association and dissociation kinetic constants. These values indicate the slow formation of kinetically stable interactions between BSA and metal complexes **1**, **2**, **4** and **5**, consistent with the results obtained with the docking analyses. Notably, our results showed pH-dependent affinities (**Table 2**), that decreases with pH.

Compound	pH	k_{ass} (M^{-1}s^{-1})	k_{diss} (s-1)	K_D (mM)
1	7.4	4350 ± 760	0.007 ± 0.002	1.6 ± 0.7
	6.8	3125 ± 342	0.025 ± 0.009	7.9 ± 1.4
2	7.4	2654 ± 784	0.007 ± 0.004	2.6 ± 0.9
	6.8	2765 ± 433	0.054 ± 0.013	19.5 ± 4.4
4	7.4	3534 ± 218	0.010 ± 0.001	2.8 ± 1.2
	6.8	3876 ± 782	0.081 ± 0.034	20.9 ± 5.5
5	7.4	2350 ± 540	0.008 ± 0.003	3.4 ± 1.3
	6.8	3210 ± 667	0.036 ± 0.05	11.2 ± 1.6

Table 2 - *Comparison of kinetic and equilibrium parameters of complexes **1, 2, 4** and **5** binding to BSA under different pH conditions.*

This behaviour is in line with the formation of stable protein-complexes that favour the transport in the blood (at pH = 7.3–7.5) and the promotion of the drug release at tumour sites, which are characterized by lower values of pH (6.0–7.0). This decrease in binding affinity at a lower pH value, is probably the cause of the ability of albumins to undergo a reversible conformational transition with changes in pH. Specifically, a significant loss of alpha helices, and the consequent increase in protein volume, causes a relaxation of the 3D BSA structure, which supports the release of the metal-complexes given a less favourable accommodation in the pocket.

2.2.6 Cell membrane permeability

The ability of the complexes to cross cell membrane was evaluated by monitoring the changes in cell membrane fluidity using trimethylammonium diphenylhexatriene (TMA-DPH) as a fluorescent probe. Most evidently, different behaviour was observed between the less polar (**1**, **2**, **4**) and ionic (**5**) complexes, which is in line with their observed cytotoxicity. Specifically, complexes **2** and **4** could easily cross cell membrane by passive transfer according to a three-stage drug internalization process (stage 1: membrane entry; stage 2: per- maintenance in membrane; stage 3: release from membrane) in approx. 150 min. The nature of the metal centre induces significant quantitative differences only in the kinetics of membrane entry (see **Figures 59a** and **59b**) with the membrane entry of the Ru complex (**2**) being faster than the Os counterpart (**4**).
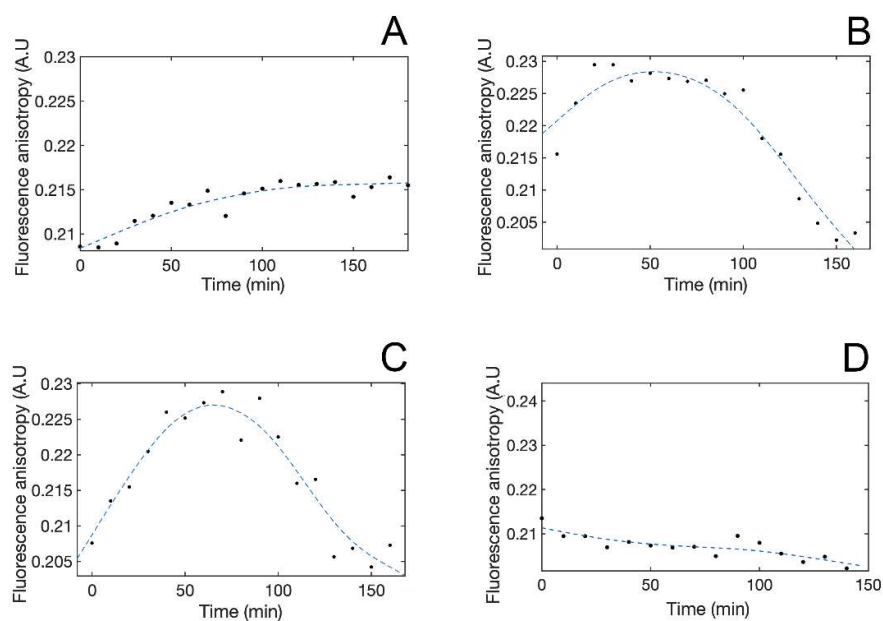
Figure 59a *- Comparative changes in emission anisotropy with time observed upon cell membrane passage of **1** (Panel A), **2** (Panel B), **3** (Panel C) and **4** (Panel D)*
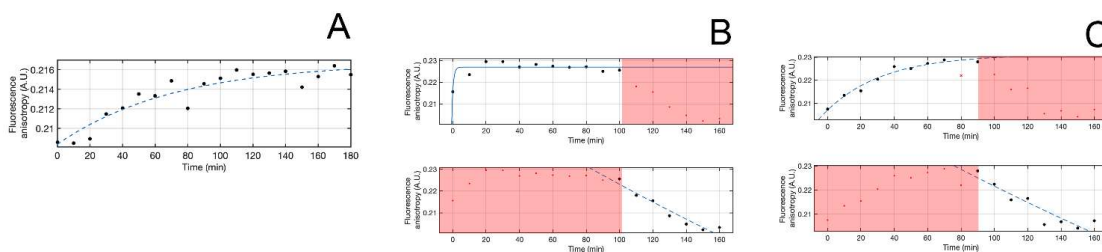

Figure 59b *– Detailed kinetic analyses of individual membrane entry/release stages of complex **1** (Panel A), complex **2** (Panel B) and complex **4** (Panel C)*

On the other hand, complex **1** could still penetrate the cell membrane although with lower efficacy than **2** and **4**, and it was retained longer in the membrane, presumably due to its higher hydrophobicity, before being released. Conversely, in a comparable time frame (180 min) no significant changes in membrane fluidity were observed upon incubation of TMA-DPH labelled cells with complex **5**, the polar/ionic nature of the complex hindering its passage across cell membranes.

2.2.7 Binding with the DNA

The interactions of a representative selection of the complexes, i.e. **1**, **2**, **4** and **5**, with DNA were determined using a biosensor-based approach, with a dsDNA probe acting as the "molecular bait" for the molecules of interest. All complexes reversibly bind DNA without any apparent difference observed between the two curcuminoid ligands (**HL^1** and **HL^2**). In

contrast, the nature of the metal centre significantly affected the recognition event and in turn its affinity for DNA. The ruthenium derivatives (**1**, **2** and **5**) have a higher rate of adduct formation (higher values of k_{ass}) and higher stability for the binding with DNA (lower dissociation rates, k_{diss}, and lower KD values) compared to the osmium derivative (**4**), which is consistent with the cytotoxicity studies conducted (**Table 3**).

Compound	k_{ass} $(M^{-1}s^{-1})$	k_{diss} (s^{-1})	K_D (μM)
1	550000±37000	0.0076±0.0045	0.0138±0.00825
2	400000±90000	0.0088±0.016	0.022±0.0091
4	110000±20000	0.0103±0.027	0.1024±0.0211
5	416000±120000	0.013±0.009	0.0308±0.0241

Table 3 - *Kinetic and equilibrium parameters for the interaction between complexes 1, 2, 4 and 5 and surface blocked DNA*

Although the nature of ligands does not affect the interaction with the DNA, it has shown, through competitive binding experiments, to provide evidence for a different binding mode to the biological target. These experimental results were also rationalized by molecular docking models, which showed a peculiar "hug-anchoring" mode for **1** and **5**, in which the complexes wrap the ds-DNA helix and shield two contiguous major and minor grooves. The complexes containing the **HL²** ligands, i.e. **2** and **4**, showed selectivity toward the major groove of DNA (**Figure 60**) as the absence of the methoxy group results in less steric hindrance.
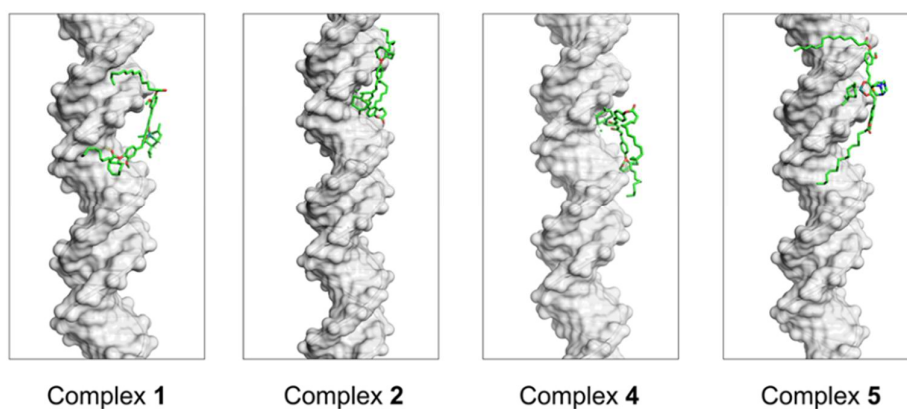

Complex **1**   Complex **2**   Complex **4**   Complex **5**

Figure 60 - *Comparative visualization of the best scoring complexes formed upon docking 1, 2, 4 and 5 onto dsDNA. Metal complexes and DNA are rendered as green sticks and grey solid surface, respectively.*

3.1 Aim of the work

Coherently to the previous research work, this section is based on the synthesis and biological evaluation of novel half-sandwich Ruthenium(II) complexes bearing human metabolites of the curcuminoids. The reduced form of curcumin and bisdemethoxycurcumin (**HL¹³** and **HL¹⁴** respectively), in fact, possess a very interesting biological properties and, most importantly, enhanced solubility and stability under physiological conditions. The new Ru(II)-arene complexes [arene = p-cymene (cym), hexamethylbenzene (hmb) and benzene (benz)] containing **HL¹³** and **HL¹⁴** were completely characterized by NMR spectroscopy and ESI mass spectrometry, and the crystal structures of three complexes were determined by X-ray diffraction analysis. Compared to curcuminoids, these metabolites lose their conjugated double bonds system responsible for their planarity, showing unique *closed* conformation crystal structure. Both *closed* and *open* conformations have been theoretically analysed and rationalized using density functional theory (DFT). Furthermore, the cytotoxicity of the complexes was evaluated in vitro against human ovarian carcinoma cells (A2780 and A2780cisR), human breast adenocarcinoma cells (MCF-7 and MCF-7CR), as well as against non-tumorous Human Embryonic Kidney cells (HEK293), and nontumorigenic human breast (MCF-10A) cells and compared to the free ligand, cisplatin, and RAPTA-C.
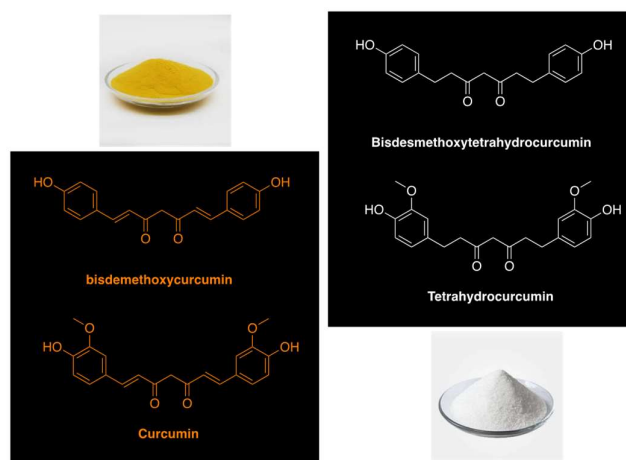
3.1.1 Materials and methods

The dimer [(*p*-cymene)RuCl$_2$]$_2$ was purchased from Aldrich while curcumin and bisdemethoxycurcumin were purchased from TCI Europe and were used as received. The samples for microanalyses were dried in vacuo to constant weight (35 °C, ca. 0.1 Torr). Elemental analyses (C, H, N) were performed in-house with a Fisons Instruments 1108 CHNS-O Elemental Analyser. IR spectra were recorded on a Perkin-Elmer Frontier FT-IR instrument. ^{1}H and ^{13}C NMR spectra were recorded on a 500 Bruker Ascend (500 MHz for ^{1}H, 125 MHz for ^{13}C) instrument operating at room temperature relative to TMS. Positive ion electrospray mass spectra were obtained on a Series 1100 MSI detector HP spectrometer, using acetonitrile as solvent for all complexes 1-5. Solutions (3 mg/mL) for electrospray ionization mass spectrometry (ESI-MS) were prepared using reagent-grade methanol. Masses and intensities were compared to those calculated using IsoPro Isotopic Abundance Simulator, version 2.1.28. Melting points were recorded on a STMP3 Stuart scientific instrument and on a capillary apparatus. Samples for microanalysis were dried in vacuo to constant weight (20°C, ca. 0.1 Torr) and analyzed on a Fisons Instruments 1108 CHNS-O elemental analyzer. Uv-stability studies have been conducted with a Varian Caryl spectrometer.

3.1.2 Cytotoxicity studies

The human ovarian cancer cell line A2780 and its cisplatin resistant form A2780cisR were purchased from the European Collection of Cell Cultures (ECACC, United Kingdom). The Human Embryonic Kidney 293T cell line, HEK293T, was kindly provided by the BSF facility in EPFL. The media DMEM GlutaMAX and RPMI 1640 GlutaMAX were purchased from Life Technologies. The fetal bovine serum (FBS) was obtained from Sigma. A2780 and A2780cis cells were cultured in RPMI 1640 GlutaMAX, and HEK293T cells in DMEM GlutaMAX media containing 10% heat inactivated FBS at 37 °C and 5% CO2. To maintain resistance, the A2780cis cell line was routinely treated with cisplatin (2 µM) in the media. MCF-7 cells were grown in MEM supplemented with 10% FBS, 1% sodium pyruvate, antibiotic, and antimycotic; MCF-10A cells were cultured in a DMEM/F12 Ham's mixture supplemented with 5% equine serum, 20 ng/mL EGF, 10 µg/ mL insulin, 0.5 mg/mL hydrocortisone, antibiotics, and antimycotics. MCF-7CR cells were grown in minimum essential medium (MEM), 10% FBS supplemented with cisplatin 0.1 mg/mL, sodium pyruvate, antibiotics, and antimycotics. All these chemicals were cell culture grade and were obtained from Merck-Sigma. The cytotoxicity was determined using the MTT (3-(4,5-dimethyl-2-thiazolyl)-2,5-diphenyl2H-tetrazolium bromide) assay. The compounds were dissolved in DMSO and the resulting

stock solutions were sequentially diluted in cell culture grade water to obtain a concentration range of 0–1 mM. 10 µL aliquots of these solutions were added in triplicates to a flat-bottomed 96-well plate. Subsequently, the cells were seeded in these plates as a suspension in the appropriate medium for each cell line (90 µL aliquots and approximately 1.4×10^4 cells/well), and the plates were incubated for 72 h. Cisplatin and RAPTA-C were used as positive and negative controls (0–100 µM), respectively. 10 µL of an MTT solution (5 mg/mL in Dulbecco's phosphate buffered saline) were added in each well, and the plates were incubated for 4 h at 37 °C. The medium was then carefully aspirated to conserve the purple formazan crystals, that were subsequently dissolved in 100 µL of DMSO/well. The absorbance of the resulting solutions, directly proportional to the number of surviving cells, was quantified at 590 nm using a SpectroMax M5e multimode microplate reader (using SoftMax Pro software, version 6.2.2). The data was analyzed with GraphPad Prism software (version 9.3.1). The percentage of surviving cells was calculated from the absorbance of wells corresponding to the untreated control cells (100%), and cell treated with 10 µM of gambogic acid (0%). The reported IC_{50} values are based on the means from three independent experiments, each comprising three tests per concentration level.

3.1.3 Computational details

The electronic structure and geometries of the **HL^{13}** and **HL^{14}** proligands and their corresponding anions were calculated using density functional theory at the B3LYP level with the 6-311G* basis set. Similarly, ruthenium complexes **19-24** (*closed* and *open* conformations) and the related complexes **19'-2a'** were also calculated using DFT at the B3LYP level. The Ru ion was described with the LANL2DZ basis set, while the 6-31G* basis set was used for the other atoms. Molecular geometries of 20-22 were optimized starting from the crystallographic coordinates. Frequency calculations were carried out at the same level of theory to identify all of the stationary points as minima (zero imaginary frequencies). DFT calculations were performed using the Gaussian 09 suite of programs. The computed IR spectra were scaled by a factor of 0.96.

3.1.4 X-ray crystallography

Suitable crystals of were selected and mounted on an XtaLAB Synergy R, a DW system, and a HyPix-Arc 150 diffractometer, where intensities were collected at 140 K using Cu Kα radiation. The datasets were reduced and corrected for absorption using *CrysAlis*[Pro].[150] The structure was solved with the ShelXT[151] solution program using dual methods and by using

Olex2 1.5 as the graphical interface.[152] All non-hydrogen atoms were refined anisotropically using full-matrix least-squares based on $|F|^2$. Hydrogen atoms were placed at calculated positions using the 'riding' model. The CCDC numbers 2266740, 2266741 and 2266742 contain the crystallographic data for compounds **20-22**, respectively. These data can be obtained free of charge via www.ccdc.cam.ac.uk/data_request/cif.

3.1.5 DNA binding

The kinetics of binding of **HL^{13}** and **HL^{14}** and complexes **19-24** to DNA was initially evaluated using a biosensor-based assay. Upon equilibration of the carboxylate surface of the sensor with PBS buffer (10 mM Na_2HPO_4, 2.7 mM KCl, 138 mM NaCl, pH = 7.4), a 5′-biotinylated dsDNA oligomer (3′-CCACCCACTACCCTGGTTGGATGCTAATGT-5′) was blocked via streptavidin crosslinking as previously reported.[146] Next, each molecule was independently added to the DNA-coated surface at different concentrations in the range of 0.6−6 µM, each time following binding kinetics up to equilibrium. Dissociation and regeneration steps were performed with fresh PBS buffer. The biosensor chamber was thermostatted at 37 °C throughout.

The mapping of the binding sites on DNA was performed according to independent competitive binding assays in solution [42] using DAPI (a minor groove binder) and Methyl Green (a major groove binder). Briefly, the DAPI displacement assay was performed by monitoring the changes in the emission spectra (400−650 nm) of solutions containing different concentrations of the compounds of interest in the range of 0−200 µM, DNA (20 µM), and DAPI (15 µM) in phosphate buffer (10 mM, pH 7.4) at room temperature after excitation at 338 nm on a Gemini XPS fluorescence microplate reader. Analogously, the changes in the absorbance at 630 nm of the preformed DNA−Methyl Green complex (obtained after 24 h of incubation at 37 °C in 50 mM Tris-HCl buffer, pH 7.5, containing 7.5 mM $MgSO_4$) were monitored after additional 24 h upon addition of different the molecules of interest with a Bio-Tek Visible plate reader.

3.1.6 DNA docking analysis

The binding modes for all the complexes of interest to DNA were obtained by independently docking the crystallographic structure of each molecule onto the 3D modelled 3'-CCACCCACTACCCTGGTTGGATGCTAATGT-5' dsDNA oligonucleotide (Avogadro[153] according to flexible ligand-receptor docking using Autodock 4 with a grid box placed all around the target DNA molecule. Ruthenium atom parameters used were "atom par Ru 2.96

0.056 12.000 -0.00110 0.0 0.0 0 -1 -1 1 # Non H-bonding".[154] All other settings were kept to default values. The best scoring complexes and images were rendered with PyMOL (The PyMOL Molecular Graphics System, Version 2.4.2 Schrödinger, LLC).

3.1.7 Immunometric quantification of p62/SQSTM1

The intracellular levels of p62/SQSTM1 were quantitated by western blotting upon treatment of MCF7 cells with 5 μM of complex **1** and parent curcuminoid ligand. The proper amount of cell lysates (15 μg of total proteins) was separated by electrophoresis on 12% SDS-PAGE and electroblotted onto PVDF membranes Millipore (Milan, Italy). After incubation with primary antibodies, the immunoblot detections were carried out with the Enhanced ChemiLuminescence Western Blotting analysis system (Amersham-Pharmacia-Biotech). The gels were always loaded with molecular weight protein markers in the range of 6.5−205 kDa, and glyceraldehyde-3-phosphate dehydrogenase (GAPDH) was used as a control for equal protein loading. Western blot results were analyzed using ImageJ software.[155]

3.1.8 General procedure for synthesis of ligands

HL^{13} (1,7-bis(4-hydroxy-3-methoxyphenyl)heptane-3,5-dione). Curcumin (500 mg, 1.4 mmol) and Pd/BaSO$_4$ (50 mg) were dissolved in CH$_3$OH (25 mL). After 10 h agitation under a H$_2$ atmosphere (2 atm) the reaction mixture was filtered and the remaining oil purified using column chromatography (cyclohexane: ethylacetate, 60:40) to obtain the ligand **HL^{13}** (**Figure 61**), as white powder, yield 78%. It is completely soluble in CH$_3$OH, CH$_3$CN, DMSO and CH$_3$Cl and insoluble in H$_2$O and hexane. Anal. Calcd. for C$_{21}$H$_{24}$O$_6$: C, 67.73; H, 6.50. Found: C, 67.94; H, 6.78. m.p. 87-90 °C. IR (cm^{-1}): 3407 mbr ν(-OH); 3064 w, 3023 w, 3004 w, 2961 w, 2933 m, 2844 w ν(aliphatic C-H); 1702 w, 1601 mbr ν(-C=O); 1450 m, 1429 m. ^{1}H-NMR (CDCl$_3$, 293 K): δ 2.55 (t, 4H, C(3-3')H), 2.85 (t, 4H, C(4-4')H), 3.86 (s, 6H, -OCH_3), 5.43 (s, 1H, C(1)H), 5.51 (sbr, 2H, O-H), 6.69 (m, 4H, C(6-6')H and C(10-10')H), 6.85 (d, 2H, C(9-9')H). ^{13}C{^{1}H}-NMR (CDCl$_3$, 293 K): δ 31.3 [C(4-4')], 40.4 [C(3-3')], 55.9 [-OCH_3], 99.8 [C(1)], 111.0 [C(6-6')], 114.4 [C(9-9')], 120.8 [C(10-10')], 132.6 [C(5-5')], 144.0 [C(7-7')], 146.4 [C(8-8')], 193.2 [C(2-2')]. ESI-MS (-) CH$_3$CN (m/z [relative intensity, %]): 371 [100] [(**L^{13}**)]$^-$.
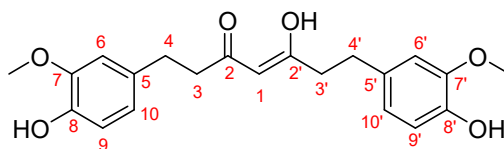

Figure 61 - *Structure of ligand **HL$^{13}***

HL^{14} (1,7-bis(4-hydroxyphenyl)heptane-3,5-dione). The ligand **HL^{14}** was synthesized as reported for **HL^{13}** starting from bisdemethoxycurcumin (500 mg, 1.6 mmol). The ligand (**Figure 62**) was obtained as white powder, yield 60%. It is completely soluble in CH_3OH, CH_3CN, DMSO and CH_3Cl and insoluble in H_2O and hexane. Anal. Calcd. For $C_{19}H_{20}O_4$: C, 73.06; H, 6.45. Found: C, 72.52; H, 6.53. m.p. 105-107 °C. IR (cm^{-1}): 3270 mbr ν(-OH); 3024 w, 2963 sh, 2930 w, 2859 w ν(aliphatic C-H); 1072 w; 1629 sh, 1614 m, 1602 m ν(-C=O); 1514 vs, 1462 m. ^{1}H-NMR (CD$_3$CN, 293 K): δ 2.56 (t, 4H, C(3-3')H), 2.81 (t, 4H, C(4-4')H), 5.60 (s, 1H, C(1)H), 6.73 (m, 4H, C(7-7')H), 7.05 (m, 4H, C(6-6')H). ^{13}C{^{1}H}-NMR (CD$_3$CN, 293 K): δ 30.3 [C(4-4')], 39.7 [C(3-3')], 99.5 [C(1)], 115.1 [C(7-7')], 129.3 [C(6-6')], 155.2 [C(8-8')] 193.7 [C(5-5')], 204.3 [C(2-2')]. ESI-MS (-) CH$_3$CN (m/z [relative intensity, %]): 311 [100] [(**L^{14}**)]$^-$.
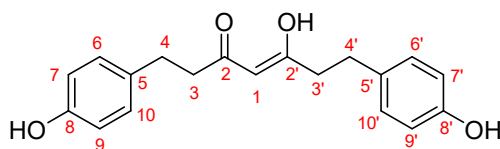

Figure 62 - Structure of ligand HL^{14}

3.1.9 General procedure for synthesis of complexes

[Ru(*p*-cymene)(L^{13})Cl] (19). **HL^{13}** (74 mg, 0.2 mmol) and KOH (11 mg, 0.2 mmol) were dissolved in CH$_3$OH (5 mL). After 1 h stirring at room temperature, [Ru(*p*-cymene)Cl$_2$]$_2$ (61 mg, 0.1 mmol) was added. The resulting solution was stirred at room temperature for 6 h, after which the solvent was removed under vacuum. The KCl salt was precipitated in a CH$_2$Cl$_2$ solution and **19** crystallized by adding n-hexane. The yellow precipitate (**Figure 63**, yield 93%) was filtered and characterized. It is completely soluble in CH$_3$OH, CH$_3$CN, DMSO and CH$_3$Cl, it is partly soluble in H$_2$O and insoluble in hexane.
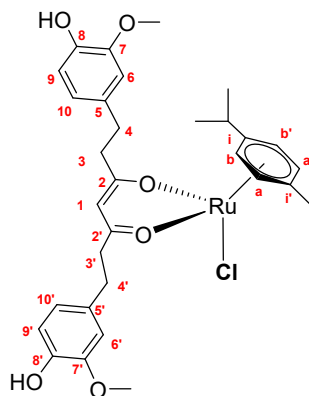

Figure 63 - Structure of compound 19

Anal. Calcd. for $C_{31}H_{37}ClO_6Ru$: C, 57.98; H, 5.81. Found: C, 56.63; H, 5.67. mp: 135-138 °C. IR (cm^{-1}): IR (cm^{-1}): 3401 mbr v(-OH); 3068 w, 2967 w, 2919 w, 2850 w v(aliphatic C-H); 1557 m v(-C=O); 1514 m; 287 v(Ru-Cl). ^{1}H-NMR (CDCl$_3$, 293 K): δ 1.31 (d, 6H, -CH(CH_3)$_2$ of p-cymene, ^{3}J = 7 Hz), 2.22 (s, 3H, -CH_3 of p-cymene), 2.51 (t, 4H, C3-3'H)), 2.84 (m, 5H, C(4-4')H and CH(CH$_3$)$_2$ of p-cymene), 3.90 (s, 6H, -OCH_3), 5.15 (s, 1H, C(1)H),5.13 d, 5.38 d (4H, AA′BB′ system, CH$_3$-C$_6$$H_4$-CH(CH$_3$)$_2$ of p-cymene, ^{3}J = 6 Hz), 5.51 (sbr, 2H, -OH), 6.69 (d, 2H, C(10-10')H, ^{3}J$_{trans}$ = 8 Hz), 6.74 (s, 2H, (C-6-6')H), 6.85 (d, 2H, C(9-9')H, ^{3}J$_{trans}$ = 8 Hz).^{13}C{^{1}H}-NMR (CDCl$_3$, 293 K): δ 17.8 [-CH$_3$ of p-cymene], 22.3 [-CH(CH$_3$)$_2$ of p-cymene], 30.7 [CH(CH$_3$)$_2$ of p-cymene], 32.5 [C(4-4')], 42.4 [C(3-3')], 56.0 [-OCH$_3$], 70.8 [C(b-b')], 82.8 [C(a-a')], 97.3 [Ci'], 98.0 [C(1)], 99.4 [Ci], 111.2 [C(6-6')], 114.1 [C(9-9')], 120.8 [C(10-10')], 133.5 [C(5-5')], 143.8 [C(8-8')], 146.4 [C(7-7')], 188.5 [C(2-2')=O]. ESI-MS (+) CH$_3$CN (m/z [relative intensity, %]): 607 [100] [Ru(p-cymene)(L^{13})]$^+$.

[Ru(hmb)(L^{13})Cl] (**20**). **HL^{13}** (74 mg, 0.2 mmol) and KOH (11 mg, 0.2 mmol) were dissolved in CH$_3$OH (5 mL). After 1 h stirring at room temperature, [Ru(hmb)Cl$_2$]$_2$ (67 mg, 0.1 mmol) was added. The resulting solution was stirred at room temperature for 6 h, after which the solvent was removed under vacuum. The KCl salt was precipitated in a CH$_2$Cl$_2$ solution and **20** crystallized by adding n-hexane. The yellow precipitate (**Figure 64**, yield 60%) was filtered and characterized. It is completely soluble in in CH$_3$OH, CH$_3$CN, DMSO and CH$_3$Cl, it is partly soluble in H$_2$O and insoluble in hexane.
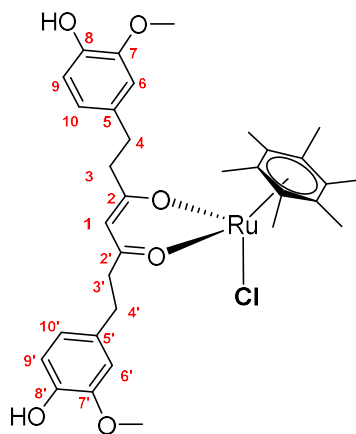

Figure 64 - *Structure of compound 20*

Anal. Calcd. for $C_{33}H_{41}ClO_6Ru$: C, 59.14; H, 6.17. Found: C, 59.04; H,.6.29. mp: 217-219 °C. IR (cm^{-1}): 3278 mbr v(-OH); 3004 w, 2960 w, 2931 w, 2856 w v(aliphatic C-H); 1599 w; 1569 vs v(-C=O); 1513 sbr; 295 v(Ru-Cl). ^{1}H-NMR (CDCl$_3$, 293 K): δ 2.06 (s, 18H, -(CH_3)$_6$ of hmb), 2.50 (m, 4H, C(3-3')H)), 2.79 m, 2.98 m, (4H, C(4-4')H), 3.90 (s, 6H, -OCH_3), 5.10 (s, 1H, C(1)H), 5.49 (sbr, 2H, O-H), 6.70 (d, 2H, C(10-10')H, ^{3}J$_{trans}$ = 8 Hz), 6.74 (s, 2H, (C-6-6')H), 6.84 (d, 2H, C(9-9')H, ^{3}J$_{trans}$ = 8 Hz).^{13}C{^{1}H}-NMR (CDCl$_3$, 293 K): δ 15.0 [-(CH$_3$)$_6$ of hmb], 32.5 [C(4-4')], 42.6 [C(3-3')], 56.1 [-OCH$_3$], 89.9 [C_6 of hmb], 97.6 [C(1)], 111.1 [C(6-6')],

114.1 [C(9-9')], 120.8 [C(10-10'), 133.5 [C(5-5')], 143.8 [C(8-8')], 146.4 [C(7-7')], 188.1 [C(2-2')=O]. ESI-MS (+) CH$_3$CN (m/z [relative intensity, %]): 635 [100] [Ru(hmb)(L^{13})]$^+$.

[Ru(benz)(L^{13})Cl] (**21**). **HL^{13}** (74 mg, 0.2 mmol) and KOH (11 mg, 0.2 mmol) were dissolved in CH$_3$OH (5 mL). After 1 h stirring at room temperature, [Ru(benz)Cl$_2$]$_2$ (50 mg, 0.1 mmol) was added. The resulting solution was stirred at room temperature for 6 h, after which the solvent was removed under vacuum. The KCl salt was precipitated in a CH$_2$Cl$_2$ solution and **21** crystallized by adding n-hexane. The red precipitate (**Figure 65**, yield 34%) was filtered and characterized. It is completely soluble in in CH$_3$OH, CH$_3$CN, DMSO and CH$_3$Cl, it is partly soluble in H$_2$O and insoluble in hexane.
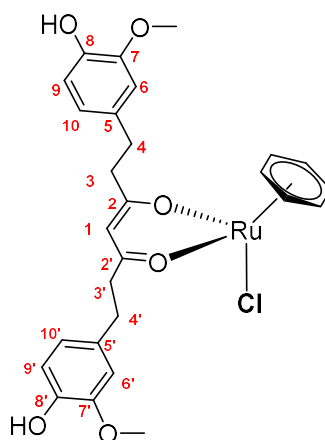

Figure 65 - Structure of compound *21*

Anal. Calcd. for C$_{27}$H$_{29}$ClO$_6$Ru: C, 55.34; H, 4.99. Found: C, 55.34; H, 4.99. mp: 101-104 °C. IR (cm^{-1}): 3414 mbr v(-OH); 3071 w, 2963 w, 2934 w, 2845 v(aliphatic C-H); 1614 sh, 1601 w; 1563 m, 1558 m v(-C=O); 1514 sbr, 1506 s; 266 v(Ru-Cl). ^{1}H-NMR (CDCl$_3$, 293 K): 2.53 (t, 4H, C(3-3')H)), 2.85 (m, 4H, C(4-4')H), 3.90 (s, 6H, -OCH_3), 5.17 (s, 1H, C(1)H), 5.32 (sbr, 2H, O-H), 5.50 (s, 6H, C$_6$$H_6$ of benz), 6.69 (d, 2H, C(10-10')H, ^{3}J$_{trans}$ = 8 Hz), 6.75 (s, 2H, (C-6-6')H), 6.85 (d, 2H, C(9-9')H, ^{3}J$_{trans}$ = 8 Hz).^{13}C{^{1}H}-NMR (CDCl$_3$, 293 K): δ 32.7 [C(4-4')], 42.4 [C(3-3')], 56.1 [-OCH$_3$], 82.3 [C_6H$_6$ of benz], 98.2 [C(1)], 111.3 [C(6-6')], 114.0 [C(9-9')], 120.9 [C(10-10'), 133.4 [C(5-5')], 143.9 [C(8-8')], 146.3 [C(7-7')], 188.8 [C(2-2')=O]. ESI-MS (+) CH$_3$CN (m/z [relative intensity, %]): 551 [100] [Ru(benz)(L^{13})]$^+$.

[Ru(p-cymene)(L^{14})Cl] (**22**). **HL^{14}** (62 mg, 0.2 mmol) and KOH (11 mg, 0.2 mmol) were dissolved in CH$_3$OH (5 mL). After 1 h stirring at room temperature, [Ru(p-cymene)Cl$_2$]$_2$ (61 mg, 0.1 mmol) was added. The resulting solution was stirred at room temperature for 6 h, after which the solvent was removed under vacuum. The KCl salt was precipitated in a CH$_2$Cl$_2$ solution and **22** crystallized by adding n-hexane. The yellow precipitate (**Figure 66,** yield 70%) was filtered and characterized. It is completely soluble in in CH$_3$OH, CH$_3$CN, DMSO and CH$_3$Cl, it is partly soluble in H$_2$O and insoluble in hexane.
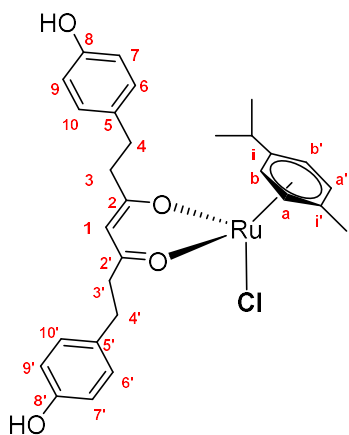
Figure 66 - *Structure of compound 22*

Anal. Calcd. for $C_{29}H_{33}ClO_4Ru$: C,59.84; H, 5.71. Found: C, 60.06; H, 5.59. mp: 195-197 °C. IR (cm^{-1}): 3406 mbr ν(-OH); 3069 w, 2963 m, 2923 m, 2875 w, 2856 w ν(aliphatic C-H); 1613 m ν(-C=O); 1592 m, 1564 vs; 294 ν(Ru-Cl). ^{1}H-NMR (CD$_3$CN, 293 K): δ 1.26 (d, 6H, CH(C*H*$_3$)$_2$ of *p*-cymene, ^{3}J = 7 Hz), 2.10 (s, 3H, -C*H*$_3$ of *p*-cymene), 2.41 (m, 4H, C(3-3')*H*), 2.70 (m, 1H, C*H*(CH$_3$)$_2$ of *p*-cymene), 2.81 (m, 4H, C(4-4')*H*), 5.10 d, 5.34 d (4H, AA'BB' system, CH$_3$-C$_6$*H*$_4$-CH(CH$_3$)$_2$ of *p*-cymene, ^{3}J = 6 Hz), 5.17 (s, 1H, C(1)*H*), 6.77 (d, 4H, C(7, 7')*H*, ^{3}J$_{trans}$ = 8 Hz), 6.89 (sbr, 2H, O-*H*), 7.07 (d, 4H, C(6-6')*H*, ^{3}J$_{trans}$ = 8 Hz). ^{13}C{^{1}H}-NMR (CD$_3$CN, 293 K): δ 16.9 [-*C*H$_3$ of *p*-cymene], 21.4 [-CH(*C*H$_3$)$_2$ of *p*-cymene], 30.4 [*C*H(CH$_3$)$_2$ of *p*-cymene], 31.5 [*C*(4-4')], 42.0 [*C*(3-3')], 78.9 [*C*(b-b')], 82.5 [*C*(a-a')], 96.7 [*C*i'], 97.6 [*C*(1)], 99.2 [*C*i], 115.0 [*C*(7-7')], 129.4 [*C*(6-6')], 132.7 [*C*(5-5')], 155.1 [*C*(8-8')], 188.2 [*C*(2-2')=O]. ESI-MS (+) CH$_3$CN (m/z [relative intensity, %]): 547 [100] [Ru(*p*-cymene)(L^{14})]$^+$.

[Ru(hmb)(L^{14})Cl] (**23**)**. HL^{14}** (62 mg, 0.2 mmol) and KOH (11 mg, 0.2 mmol) were dissolved in CH$_3$OH (5 mL). After 1 h stirring at room temperature, [Ru(hmb)Cl$_2$]$_2$ (67 mg, 0.1 mmol) was added. The resulting solution was stirred at room temperature for 6 h, after which the solvent was removed under vacuum. The KCl salt was precipitated in a CH$_2$Cl$_2$ solution and **23** crystallized by adding n-hexane. The orange precipitate (**Figure 67,** yield 33%) was filtered and characterized. It is completely soluble in in CH$_3$OH, CH$_3$CN, DMSO and CH$_3$Cl, it is partly soluble in H$_2$O and insoluble in hexane.
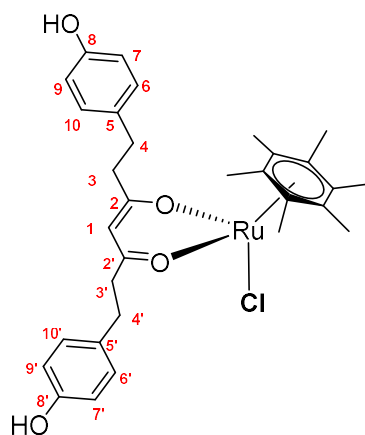
Figure 67 - *Structure of compound* **23**

Anal. Calcd. for $C_{31}H_{37}ClO_4Ru$: C, 61.02; H, 6.11. Found: C, 60.74; H, 6.20. mp: 230-232 °C. IR (cm^{-1}): 3296 mbr ν(-OH); 3012 w, 2955 w, 2923 w, 2857 w ν(aliphatic C-H); 1614 m ν(-C=O); 1574 sbr; 228 ν(Ru-Cl). ^{1}H-NMR (CD$_3$CN, 293 K): δ 1.98 (s, 18H, -(C*H*$_3$)$_6$ of hmb), 2.36 m, 2.44 m, 2.56 m (4H, C(3-3')*H*)), 2.82 (4H, C(4-4')*H*), 5.14 (s, 1H, C(1)*H*), 6.75 (d, 4H, C(7-7')*H*, $^3J_{trans}$ = 8 Hz), 7.03 (m, 4H, (C-6-6')*H*). ^{13}C{^{1}H}-NMR (CD$_3$CN, 293 K): δ 14.3 [-(C*H*$_3$)$_6$ of hmb], 31.6 [*C*(4-4')], 42.2 [*C*(3-3')], 89.9 [*C*$_6$ of hmb], 97.3 [*C*(1)], 115.0 [*C*(7-7')], 129.3 [*C*(6-6')], 132.6 [*C*(5-5')], 155.2 [*C*(8-8')], 188.0 [*C*(2-2')=O]. ESI-MS (+) CH$_3$CN (m/z [relative intensity, %]): 575 [100] [Ru(hmb)(L^{14})]$^+$.

[Ru(benz)(L^{14})Cl] (**24**). HL^{14} (62 mg, 0.2 mmol) and KOH (11 mg, 0.2 mmol) were dissolved in CH$_3$OH (5 mL). After 1 h stirring at room temperature, [Ru(benz)Cl$_2$]$_2$ (50 mg, 0.1 mmol) was added. The resulting solution was stirred at room temperature for 4 h, after which **24** formed and was filtered and dried. The orange precipitate (**Figure 68**, yield 95%) was characterized. It is completely soluble in in CH$_3$OH, CH$_3$CN, DMSO and CH$_3$Cl, it is partly soluble in H$_2$O and insoluble in hexane.
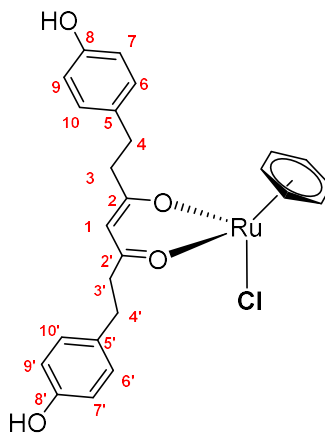

Figure 68 - *Structure of compound* **24**

Anal. Calcd. for $C_{25}H_{25}ClO_4Ru$: C, 57.09; H, 4.79. Found: C, 54.48; H, 4.74. mp: 206-207 °C. IR (cm^{-1}): 3338 mbr, 3176 mbr v(-OH); 3072 m, 3052 w, 3038 w, 3014 w, 2966 w, 2932 w, 2910 w, 2852 w v(aliphatic C-H); v(-C=O); v(Ru-Cl). ^{1}H-NMR (DMSO-d_6, 293 K): δ 2.33 (m, 4H, C(3-3')H)), 2.68 (4H, C(4-4')H), 5.14 (s, 1H, C(1)H), 5.59 (s, 6H, C_6H_6 of benz), 6.68 (d, 4H, C(7-7')H, $^3J_{trans}$ = 8 Hz), 7.00 (d, 4H, (C-6-6')H). ^{13}C{^{1}H}-NMR (DMSO-d_6, 293 K): δ 32.0 [C(4-4')], 42.3 [C(3-3')], 82.2 [C_6H_6 of benz], 100.7 [C(1)], 115.4 [C(7-7')], 129.6 [C(6-6')], 131.8 [C(5-5')], 155.9 [C(8-8')], 188.2 [C(2-2')=O]. ESI-MS (+) CH_3CN (m/z [relative intensity, %]): 491 [100] [Ru(benz)(L^{14})]$^+$.

3.2 RESULTS AND DISCUSSION

3.2.1 Synthesis and characterization of ligands

The tetrahydrocurcumin (**HL^{13}**) and tetrahydrobisdemethoxycurcumin (**HL^{14}**), were synthesized as reported in **Scheme 16**, starting from the commercially available curcumin and bisdemethoxycurcumin. The curcuminoid starting materials were dissolved in methanol and then, the mild reducing catalyst Pd/BaSO$_4$ was added to the chilled solution. The reaction mixture was stirred at room temperature for 10 hours under H$_2$ pressure (2 atm). Work up of the reaction mixture and purification by chromatography column gave **HL^{13}** and **HL^{14}** as white powders (77% and 60 % yield, respectively). In fact, the disappearance of the initial and characteristic yellow colour is the consequence of the loss of conjugation typical of the α,β-unsaturated system.
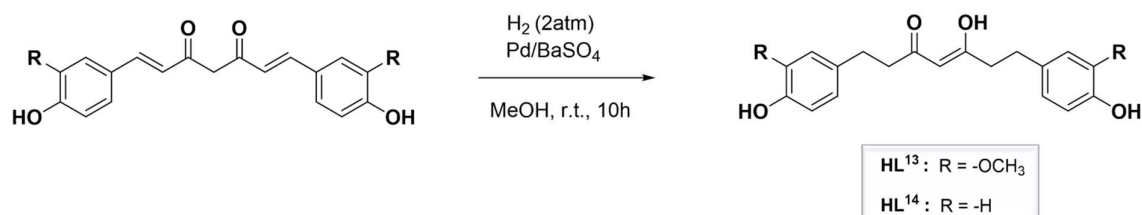
Scheme 16 - Synthetic procedure for the ligands HL^{13} and HL^{14}

The elemental analyses and ESI-MS spectrometry have confirmed the expected structures of the ligands **HL^{13}** and **HL^{14}**. The IR spectra of the two ligands possess aliphatic C-H absorption in the region of 3066-2841 cm^{-1} (as elucidated in **Figure 69**) and no longer show the typical v (C=C) vibration at around 1590-1530 cm^{-1}, characteristic of the α-β unsaturated chain.
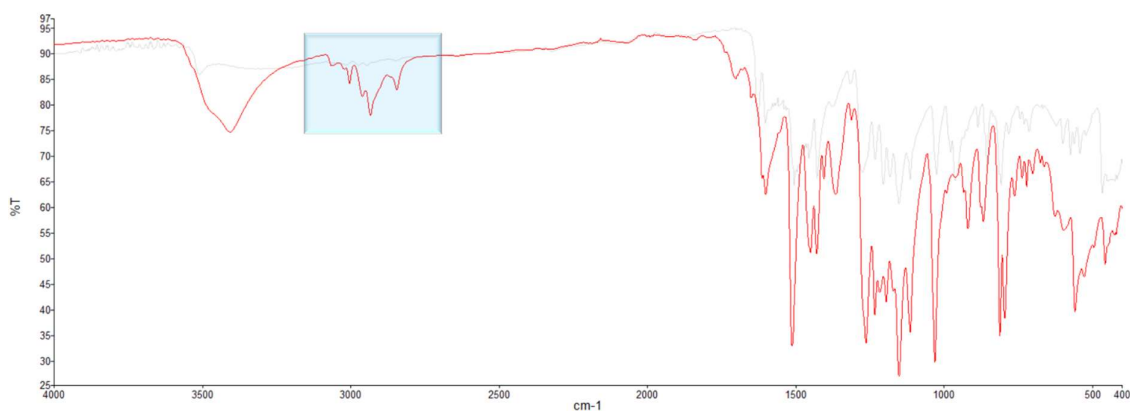
Figure 69 - *Comparison between the IR spectra of **HL**[13] ligand (red line) and the curcumin parent compound (grey line)*

In the ^{1}H-NMR spectrum is evident the loss of conjugation in the 7-carbon-linker by the disappearance of the signals belonging to the (3-3')-C*H* and (4-4')-C*H* protons from the olefinic region and the appearance in the aliphatic region of two triplets which integrate 4 protons each (**Figure 70a**).
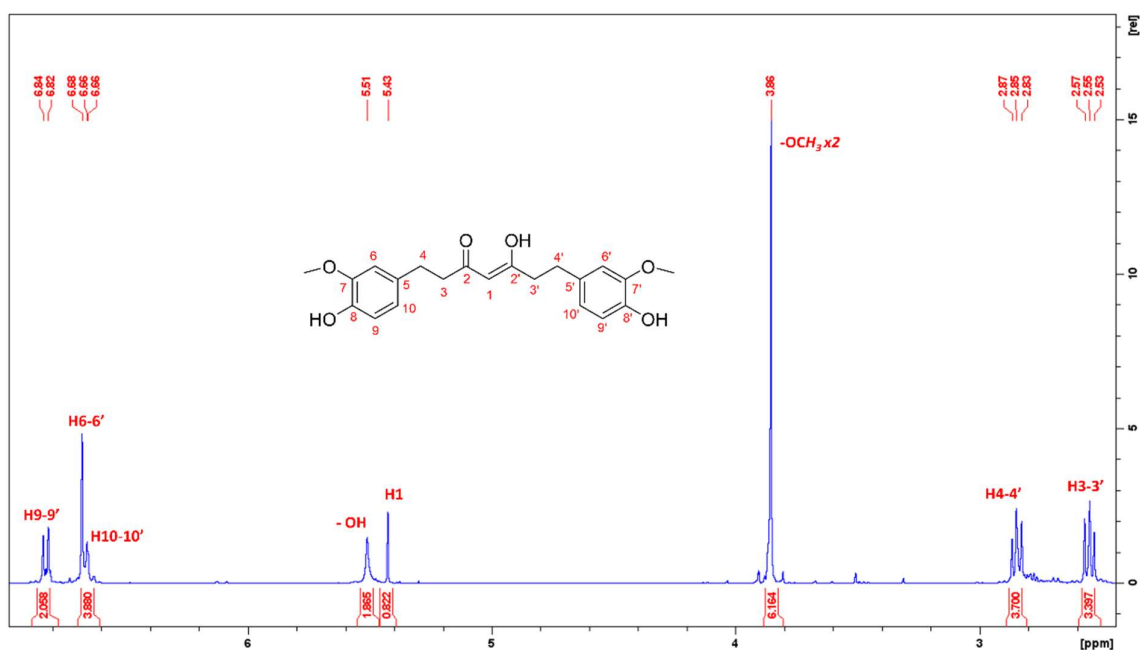

Figure 70a - *^{1}H-NMR spectrum of the ligand **HL**[13] recorded in CDCl₃*

Moreover, the ^{13}C-NMR spectrum underlines the presence of two more aliphatic carbon atoms (**Figure 70b**).
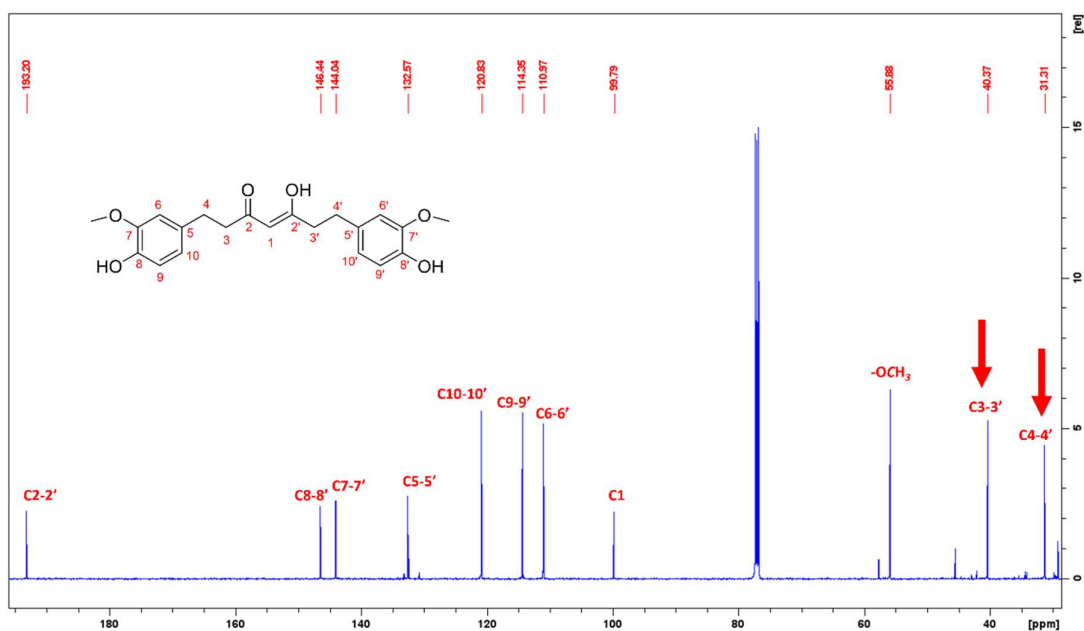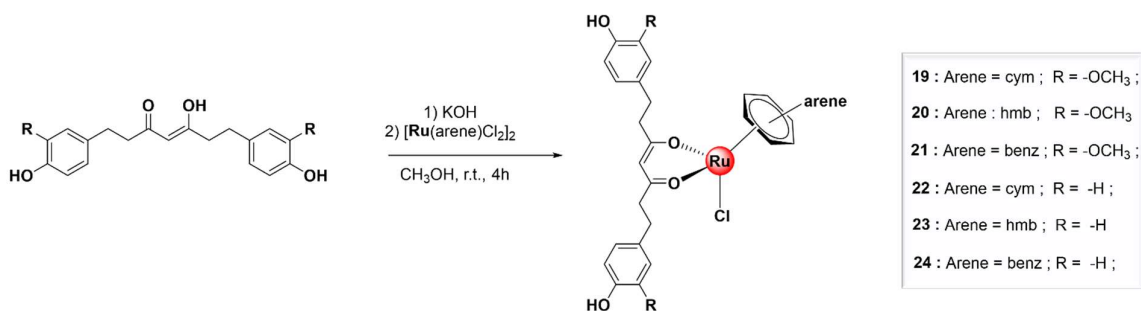
Figure 70b – *^{13}C-NMR spectrum of ligand HL^{13}*

3.2.2 Synthesis and characterization of the complexes

The complexes **19-24** were prepared from the reaction of the appropriate dimer, [Ru(arene)Cl$_2$]$_2$, [arene = *p*-cymene (cym), hexamethylbenzene (hmb) or benzene(benz)] with **HL^{13}** or **HL^{14}** and potassium hydroxide in methanol (**Scheme 17**).

Scheme 17 - *Synthetic procedure for the compounds 19-24*

Initially, the opportune ligand has been dissolved in the reaction medium together with the KOH, used as base, and stirred at room temperature for about 1 hour. Then, the metallic acceptor was added to the solution. After 4 hours the reaction was dried at reduced pressure and the salt KCl precipitated in CH$_2$Cl$_2$. The compounds **19-24** were isolated through precipitation using a mixture of solvents composed by CH$_2$Cl$_2$ and *n* – Hexane.

All the obtained complexes show a very high purity as confirmed by the narrow melting points and the elemental analyses. They are air-stable and soluble in acetone, acetonitrile, DMSO, chlorinated, alcoholic solvents and are slightly soluble in water. Electrospray ionization (ESI) mass spectra of **19**–**24** in positive ion mode, recorded in CH$_3$CN, show the

expected isotopic patterns and display peaks that correspond to [Ru(arene)(L^{13}/L^{14})]$^+$ arising from the dissociation of the chloride ligand. Their IR spectra contain the typical v(C=O) vibrations of the β-diketo moiety at lower wavenumbers than in the corresponding free ligands due to coordination through the carbonyl O-atoms to the metal. In the far-IR region can be assigned the v(Ru–Cl) stretch absorptions in the range of 230-295 cm^{-1}.

Through the ^{1}H-NMR spectroscopy is possible to demonstrate the occurred complexation thanks to the shifting of signals related to the protons closer to the coordination environment. As an example, the ^{1}H-NMR spectrum of compound **21** in **Figure 71**, shows a shift at higher fields for both the 1-C*H* signal, coming from the proton in *alpha* position, and the two protons belonging to the (3-3')-C*H*$_2$. Similarly, proton 6-C*H* of the aromatic moiety of the curcuminoid ligands is also affected by the coordination being more deshielded.
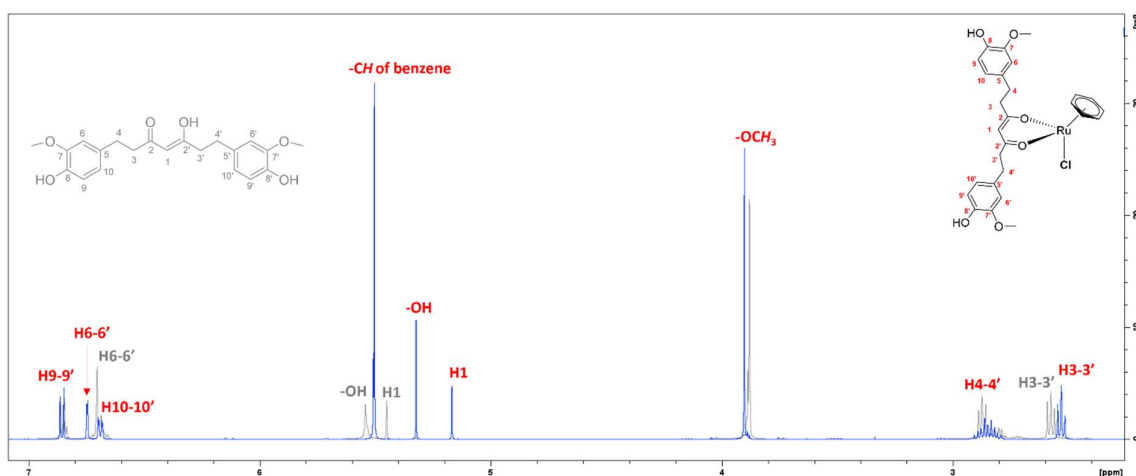

Figure 71 - *Comparison between the ^{1}H-NMR spectra recorded in CDCl$_3$ of compound **21** (blu line) and its relative ligand **HL^{13}** (grey line)*

Furthermore, the signal of the aliphatic protons, as for instance the (4-4')-C*H*$_2$ protons of compound **20**, are split into different pattern and this phenomena is more or less enhanced according to the bulk of the aromatic group, in fact, the most sterically hindered hexamethylbenzene ring gives the higher separation contribution for those protons (**Figure 72**) considering all the different [Ru(arene)(L^{13})(Cl)] analogues.

This, evaluating a sort of coupling through space established inside the structure of the complex which differentiate those protons despite the molecular symmetry, as it is shown in the {^{1}H−^{13}C}-HSQC spectrum in **Figure 73**.

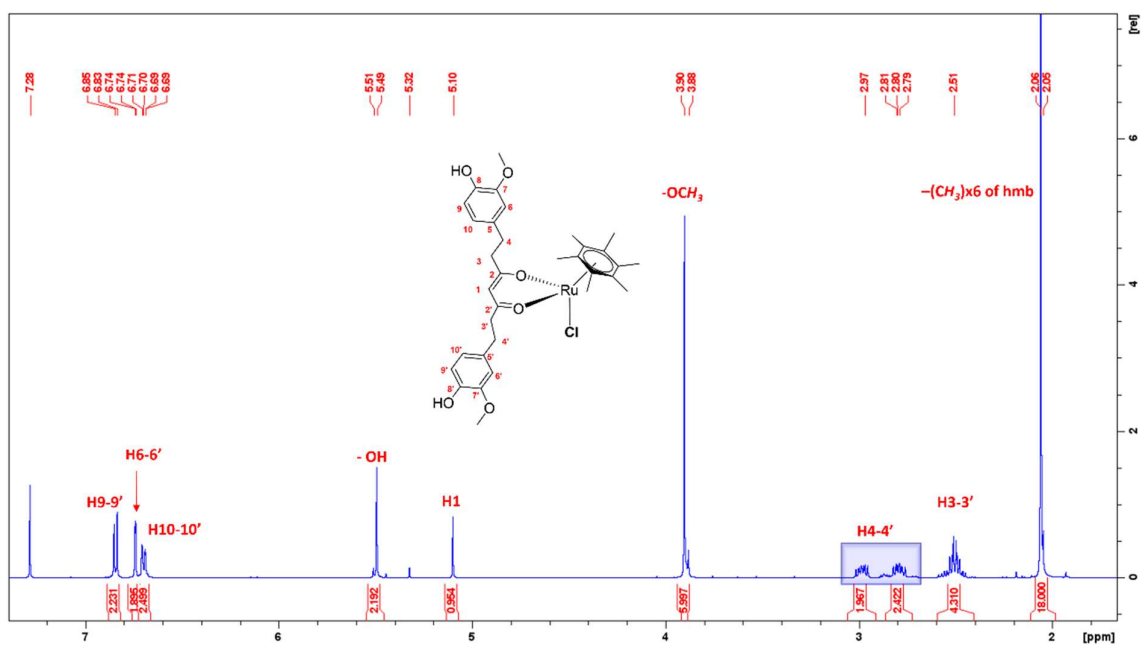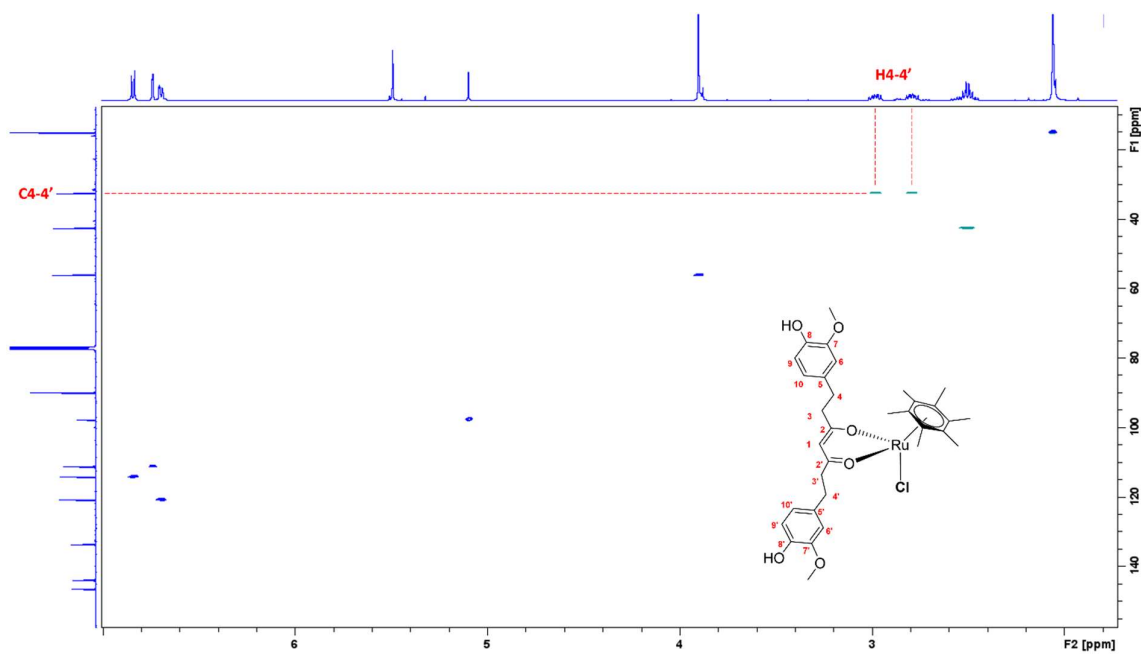**Figure 72 -** *¹H-NMR spectrum of compound **20** recorded in CDCl₃*

Figure 73 - *{ ¹H-¹³C}-HSQC NMR of **20** recorded in CDCl₃*

3.2.3 Stability studies

The stability of the complexes has been investigate through a series of ^{1}H-NMR spectra (conducted for **19** and **22**) that were recorded in DMSO-d^6 solution over time. The δ values of the characteristic peaks in all the spectra remained unchanged over 5 days, indicating that the complexes are stable (an example of compound **22** in **Figure 74a**). However, additional peaks appear in the spectrum which could be referred to secondary species (either aquo or DMSO species) formed by the hydrolysis of Ru-Cl bond. In fact, ^{1}H-NMR spectrum of compound **22** recorded in CD$_3$CN does not show during time any additional peaks and result perfectly unchanged (**Figure 74b**).
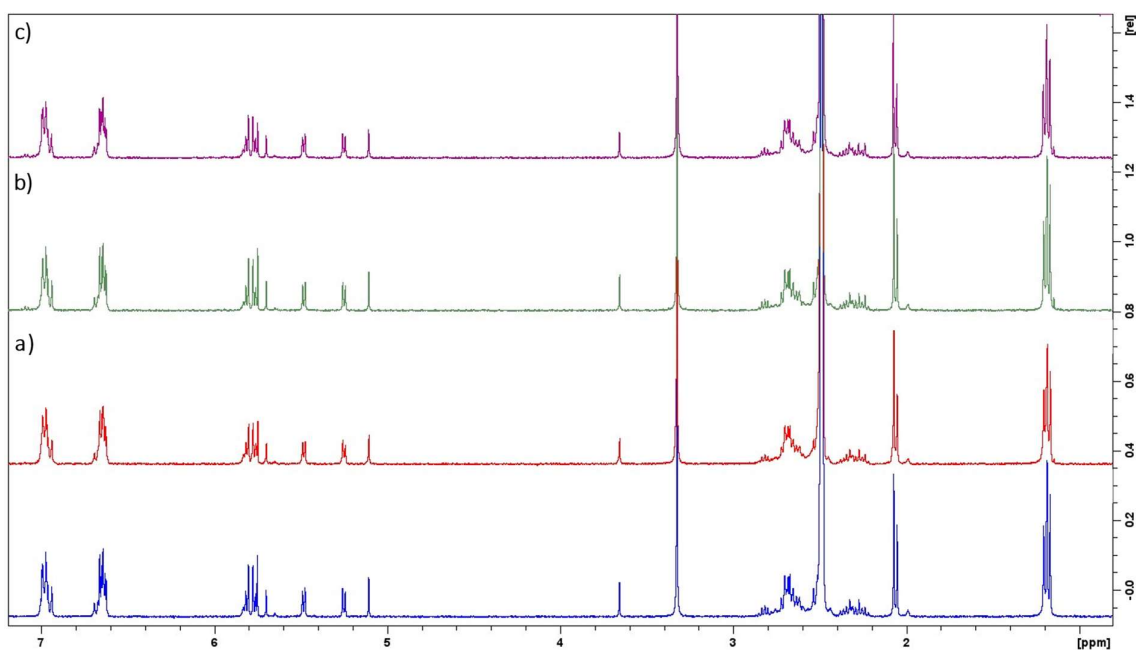

Figure 74a *-^{1}H-NMR stability studies of **22** after 24h (**a**), 48h (**b**) and 5 days (**c**) in DMSO-d^6 solution*
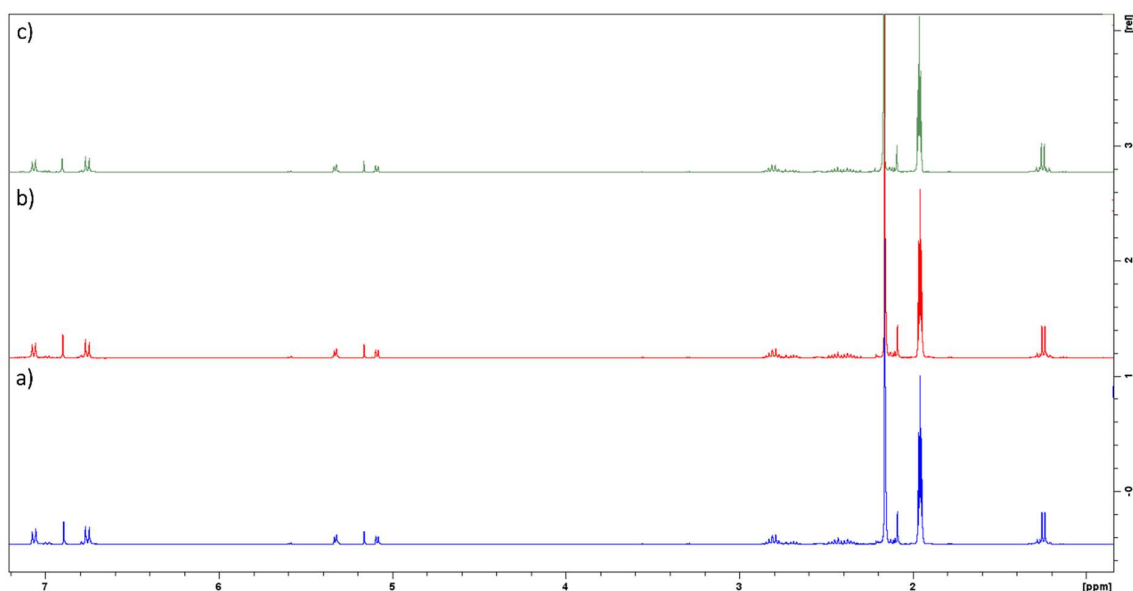
***Figure 74b** –¹H-NMR stability studies of **22** at t=0 (**a**), after 48h (**b**) and 5 days (**c**) in CD₃CN solution*

Additionally, the stability profile of complexes **19-24** and ligands **HL^{13}** and **HL^{14}** has been evaluated under physiologically relevant conditions in a phosphate-buffered solution (PBS, pH = 7.4). The solutions, with a concentration of about 10^{-6} M, were monitored over time using UV-Visible spectroscopy. The compounds were initially solubilized in DMSO and then diluted to 10% DMSO with PBS. The absorbance spectra were collected after 24, 48 and 72 h. At the end of our studies, we observed that the hydrogenated ligands **HL^{13}** and **HL^{14}** show greater stability than their parents unmodified curcuminoids, as expected from the literature. [156] [157] In fact, the absorbance profile of curcumin and bisdemethoxycurcumin (**Figure 75a**) gradually decrease during time indicating the instability of their structure under physiological conditions. On the other hand, the reduced ligands **HL^{13}** and **HL^{14}** maintain for longer time the absorbance profile being the **HL^{13}** perfectly unchanged within 72 hours and the **HL^{14}** stable for at least 48 hours (**Figure 75a**). Accordingly, all the novel organometallic compound show good stability on the same physiological solution even if the relative complexes **19-21** that contain the **L^{13}** moiety result generally more stable than their analogue with **L^{14}**, **22-24**, for which appear an overall trend of reduced absorption energy in the time (**Figure 75b**). Among all, compound **1** is the most stable for which, no changes in the absorption band have been observed. However, different behaviour in the absorption spectra has been observed according to the different aromatic substituent. In detail the worst stability profile has been found for complexes bearing a benzene as aromatic group. Except for compound **19**, all the complexes, show an hypochromism in the maximum absorption intensity at about 270 nm, accompanied by a 3-5 nm red shift in 72 h likely due to aquation phenomena derived from the replacement of chloride ligand with a solvent molecule. This behavior is not only typical

but also it represents a crucial step in the activation of ruthenium-arene anticancer compounds. [158]

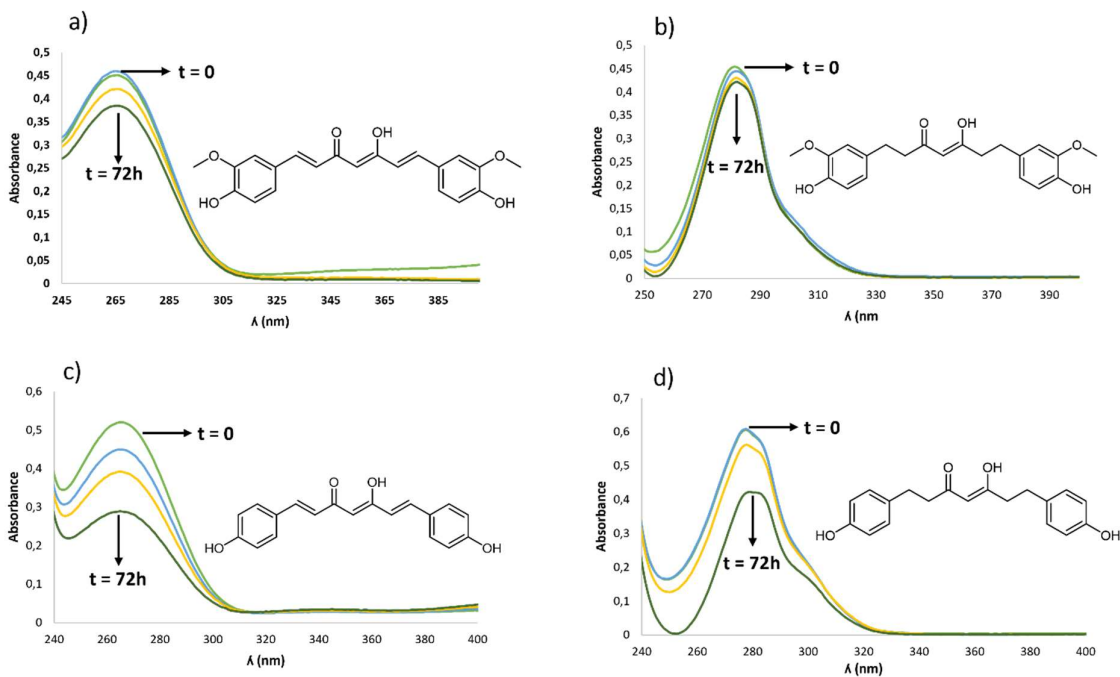**Figure 75a -** *Comparison of UV-visible spectra of ligands HL^{13} (b) and HL^{14} (d) and their parent curcuminoid Curcumin (a) and bisdemethoxycurcumin (c) collected within 72 hours in 10% DMSO-PBS solution*
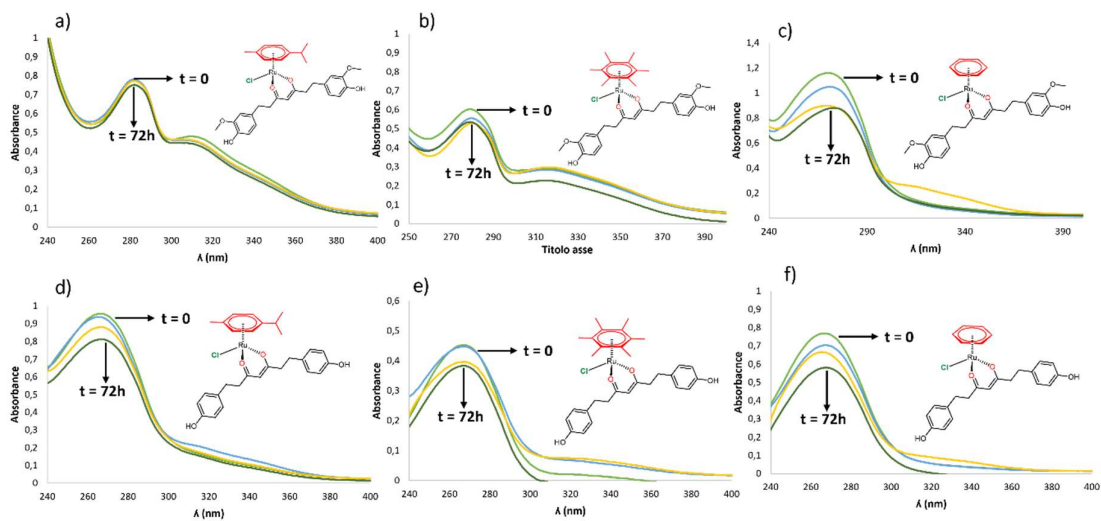

Figure 76b - *UV-visible spectra of compounds 19 (a), 20 (b), 21 (c), 22 (d), 23 (e) and 24 (f) collected within 72 hours in 10% DMSO-PBS solution*

3.2.4 Cytotoxicity studies

To assess the cytotoxicity of the compounds, the MTT assay was performed using human ovarian carcinoma cell line (A2780) and its cisplatin resistant form (A2780cisR), human breast adenocarcinoma cells (MCF-7) and its cisplatin resistant counterpart (MCF-7CR), as well as against non-tumorous human embryonic kidney cells (HEK293) and human breast (MCF-10A) cells over an incubation period of 72 h. The resulting IC_{50} values are presented **Table 4**.

Compound	A2780	A2780cisR	HEK293T	MCF-7	MCF7CR	MCF10A
HL[13]	57 ± 30	56 ± 25	82 ± 27	>100	>100	44 ± 13
HL[14]	56 ± 10	51 ± 10	>100	50 ± 9.2	>100	47 ± 16
19	47 ± 8	64 ± 18	72 ± 16	8.0 ± 3.9	19 ± 2	6.2 ± 1.7
20	26 ± 3	32 ± 3	32 ± 10	8.5 ± 1.6	19 ± 7	7.5 ± 1.6
21	74 ± 14	72 ± 13	>100	>100	>100	>100
22	77 ± 19	>100	>100	57 ± 2	29 ± 9	33,6 ± 7
23	72 ± 17	86 ± 17	70 ± 29	20 ± 7	37 ± 6	17 ± 7
24	64 ± 8	72 ± 8	88 ± 3	>100	>100	98 ± 9
cisplatin	1.1 ± 0.6	9.0 ± 3.5	3.0 ± 1.1	4.2 ± 2.3	49 ± 7	12 ± 4
RAPTA-C	>100	>100	>100	>100	>100	>100

Table 4 - IC_{50} values in μM of HL[13], HL[14], complexes 19-24, cisplatin and RAPTA-C on cisplatin sensitive and resistant human ovarian carcinoma (A2780 and A2780cisR), human embryonic kidney (HEK293T), cisplatin sensitive and resistant breast adenocarcinoma (MCF-7 and MCF-7CR), and epithelial normal breast cells (MCF-10A). Values are given as the mean obtained from 3 independent experiments ± standard deviation

The modified curcumin ligands, **HL[13]** and **HL[14]**, display a similar and moderate toxicity on the ovarian cancer cell lines A2780 and A2780cis with IC_{50} values around 50 μM. The bisdemethoxycurcumin derivative **HL[14]** has one of the best selectivity profiles as it appears to be inactive on the human embryonic cell line HEK293T (IC_{50} > 100 μM) while having one of the lowest IC_{50} values of 56 ± 10 μM on the A2780 cells. Among the studied complexes, **20** is the most potent on all tested cell lines, followed by **19** which has a notable selectivity on the HEK293T cell line with an IC_{50} of 72 ± 16 μM compared to 47 ± 8 μM on the A2780 cell line. Despite having a lower cytotoxicity on the ovarian cancer cell line, complexes **21** and **22** are inactive on the HEK293T cells (IC_{50} > 100 μM), conferring them with a higher selectivity than **23** and **26**. Conversely, with the exception of the benzene derivatives **21** and **24**, complexation of **HL[13]** and **HL[14]** to the Ru(II)-arene unit dramatically increases the cytotoxicity toward MCF-7 breast cancer cells, with **19** and **20** in particular displaying in the low micromolar range (8.0 ± 3.9 and 8.5 ± 1.6, respectively). Generally, the acquired resistance

to cisplatin partially reduced the cytotoxicity of the treatments, this evidence supporting the hypothesis that both cisplatin-like and non-cisplatin-like mechanisms of action may be at play. Nevertheless, the complexes showed no selectivity for cancer cells.

3.2.5 Binding with the DNA

DNA is a primary target for metal-based anticancer agents, the formation of drug-DNA adducts being an established apoptosis-triggering event. The DNA binding ability of **HL**[13] and **HL**[14] and Ru complexes thereof was kinetically characterized using a standard biosensor-based approach, and the binding modes were further explored both spectrophoto-fluorometrically and by molecular docking. Generally, the molecules showed low-to-moderate affinity for DNA, with equilibrium dissociation constants in the sub millimolar-to-micromolar range (**Table 5**).

Compound	k_{ass} ($M^{-1} s^{-1}$)	k_{diss} (s^{-1})	K_D (μM)
HL[13]	1250.20 ± 22.40	0.02 ± 0.005	15.99 ± 4.01
HL[14]	970.20 ± 16.00	0.07 ± 0.006	72.15 ± 6.29
19	2500.00 ± 55.90	0.04 ± 0.007	16.00 ± 2.82
20	620.20 ± 15.7	0.03 ± 0.01	48.37 ± 16.17
21	2250.70 ± 30.3	0.02 ± 0.01	8.88 ± 4.44
22	2920.90 ± 46.70	0.05 ± 0.009	17.11 ± 3.09
23	1090.70 ± 22.60	0.07 ± 0.005	64.17 ± 4.77
24	520.20 ± 15.30	0.08 ± 0.01	153.78 ± 19.74

Table 5 - *Kinetic and equilibrium parameters of HL[13] and HL[14] and arene-Ru complexes thereof binding to DNA*

The global analysis of the binding kinetics revealed that **HL**[13] has higher affinity for DNA compared to **HL**[14] both due to faster association phase (higher value of k_{ass}) and higher stability of the ligand-DNA complex (lower value of k_{diss}). With the only exception of complexes **19**, **22** and mostly **21**, the modification of the curcuminoid ligands negatively affected their binding affinity for DNA, as evident from the increase in the values of the equilibrium dissociation constant, K_D.

Additionally, competitive assays with two established site-specific DNA binders (namely DAPI and Methyl Green) and docking analyses confirmed the ability of all curcuminoids and derivatives thereof to selectively form a complex with DNA at the minor groove (**Figure 76**).
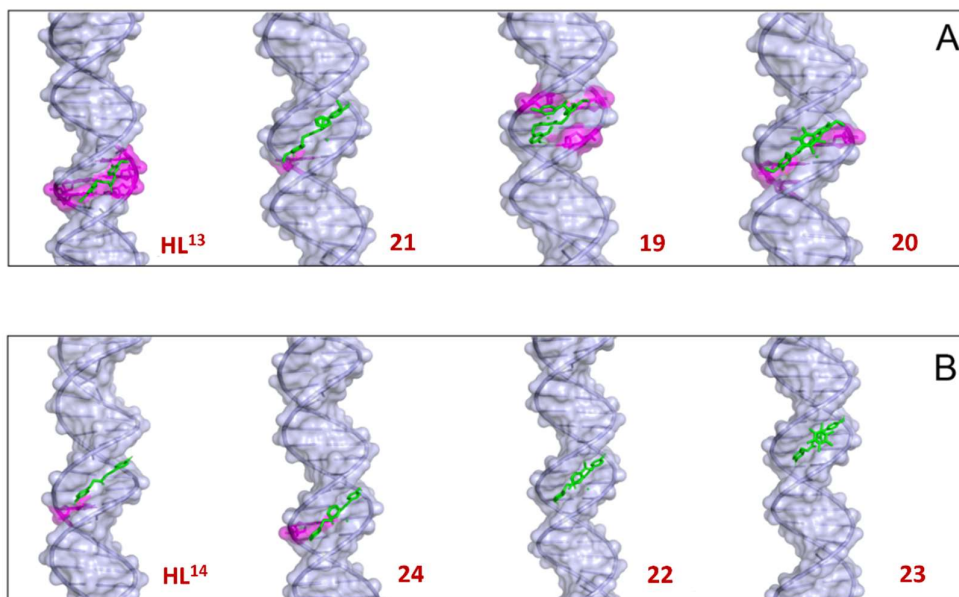
Figure 77 - *Visualization of best scoring complexes formed upon docking of the HL^13 series (panel A) and HL^14 (panel B) on dsDNA (represented as transparent grey surface); nucleotides involved in the formation of H-bonds are visualized as solid purple sticks*

3.2.6 Quantification of p62 levels

We also evaluated the effects of the most cytotoxic complex **19** against the MCF-7 cell line, on the expression levels of p62/SQSTM1, a multidomain protein hub which is involved in several pathways, among these, apoptosis and autophagy, the major cellular proteolytic systems. In particular, p62 can be degraded in autophagolysosomes, and its expression levels correlate inversely with the autophagic activity. As reported in **Figure 77**, we observed a significant decrease of p62/SQSTM1 levels in MCF7 cancer cells upon treatment with complex **19** and (to a lower, still significant extent) its parent **HL^13**, suggesting the activation of the autophagic flux.
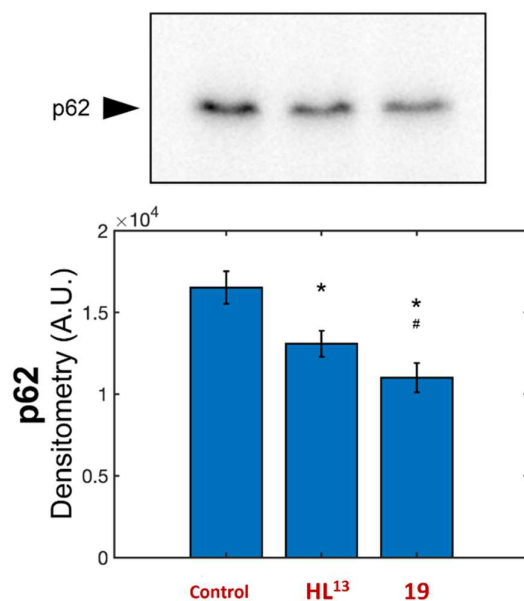
Figure 78 - *Autoradiographs and densitometric analyses of p62/SQSTM1 levels in MCF7 cells after treatment with 5 μM of complex **19** for 24 h (*p < 0.01 compared with the control; #p < 0.01 compared with **HL¹³**)*

3.2.7 X-ray crystallography

Complexes **20-22** have been crystallized and structurally characterized by X-ray studies. Their structures show the expected piano stool geometry around the Ru(II) center (**Figure 78**).

Figure 79 - *Molecular structure of **20** (**a**), of **21** where CH₂Cl₂ solvate is not shown (**b**) and of **22** (**c**)*

The Ru-Cl bond lengths are within the typical 2.40-2.43 Å range, and the Ru-arene centroid distances are close to 1.65 Å as usual in neutral complexes. The **HL**[13] and **HL**[14] ligands coordinate the ruthenium centre in a similar fashion, with Ru-O distances between 2.06 and 2.09 Å. Selected structural parameters are collected in **Table 6**.
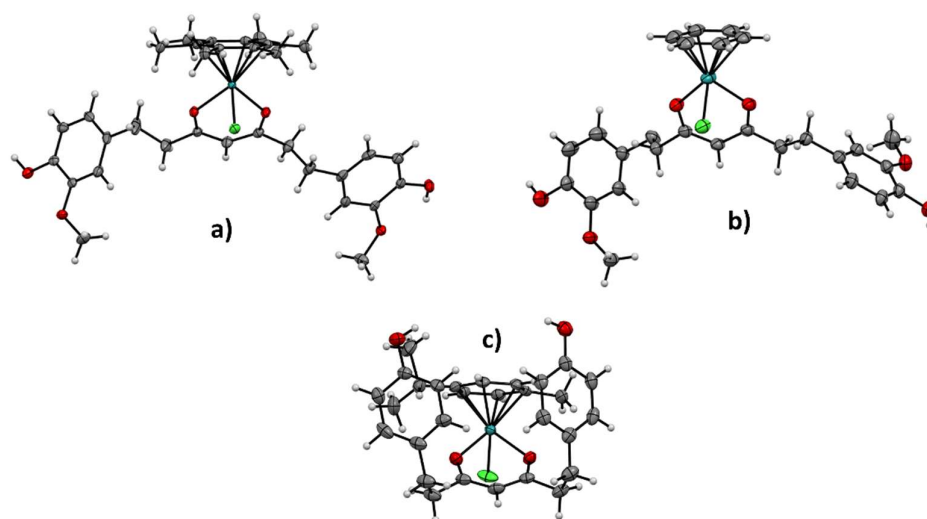
These values are similar to those found for related Ru complexes with curcumin and bisdemethoxycurcumin ligands in which this distance is close to 2.06 Å. The curcuminoid metallacycle is delocalized and the C-O distances in **20-22** are around 1.27-1.28 Å, which are longer than those calculated for the localized C=O bonds in the **HL**[13] and **HL**[14] precursors (1.24 Å, see **Scheme 18**).

From an inspection of the structures, the anomalous conformation of the **HL**[14] ligand in **22** attracts attention (see **Figures 78c**). Whereas the C(O)-CH$_2$-CH$_2$-C$_{ipso}$ torsion angles are close to 60º in **22** (closed conformation), the same angles for **20** and **21** are close to 168 and 177º, respectively (open conformation).

Compounds	**20**		**21**		**22**	
Bond distances (Å), angles and torsion angles(°)	**X-ray**	**DFT**	**X-ray**	**DFT**	**X-ray**	**DFT**
Ru-Cl	2.4308(5)	2.451	2.4254(7)	2.431	2.4033(7)	2.439
Ru-O	2.069(1)	2.094	2.065(2)	2.076	2.076(2)	2.086
	2.080(1)	2.096	2.068(2)		2.087(2)	2.089
Ru-centroid	1.646	1.739	1.644	1.745	1.646	1.738
C$\cdots$O	1.276(3)	1.277	1.275(3)	1.278	1.271(3)	1.273
	1.283(3)		1.277(3)		1.276(3)	1.274
O-Ru-O	89.24(6)	88.4	89.14(7)	89.0	87.86(8)	88.8
Cl-Ru-O	85.02(5)	85.8	84.21(6)	85.2	83.74(6)	85.5
	85.45(5)	86.0		85.3	84.39(6)	86.2
C(O)-CH$_2$-CH$_2$-C$_{ipso}$	168.2	178.3	176.0	177.3	56.7	63.1
	168.7	178.7	177.2	179.9	63.0	64.1

Table 6 - *Comparison of selected experimental and calculated structural parameters for complexes* ***20-22***

For this reason, the 3D crystal packing of **20-22** was analysed. In the crystal of **20**, two types of hydrogen bonds are observed. One is formed between the coordinated chloro ligand and the O-H bond of the curcuminoid ligand. The Ru-Cl…H-O distance of 2.298 Å falls into the region of intermediate hydrogen bonds (**Figure 79a**). The second are hydrogen bonds formed as a result of a double interaction between the -OH and -OMe substituents of **L**[13] (**Figure 79b**), with a Me-O…H-O distance of 2.307 Å. In addition to this hydrogen bonding

network, there are additional short contacts of the chloro ligand with two methyl groups of two adjacent molecules (**Figure 79c**), one from the -OMe group of **L¹³** and the other from a Me group of hexamethylbenzene (hmb).
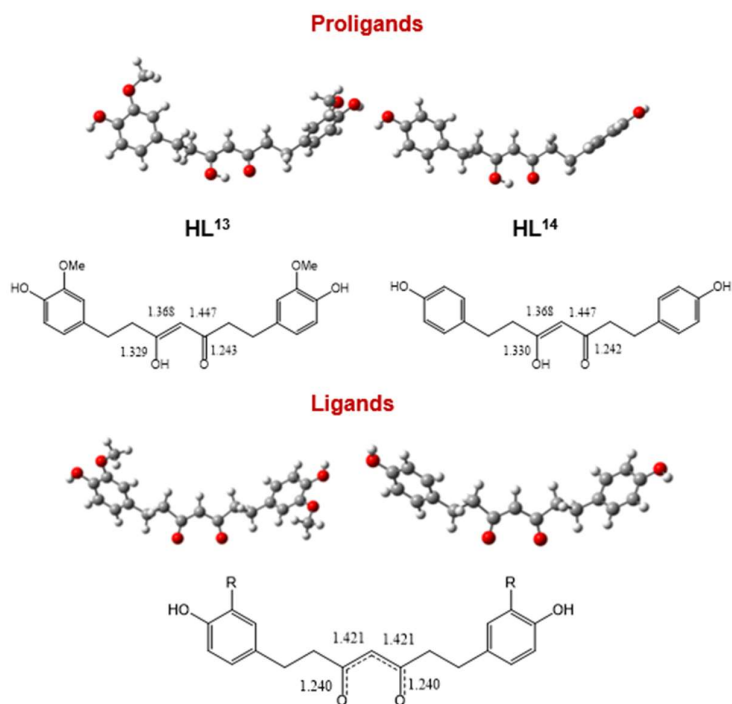
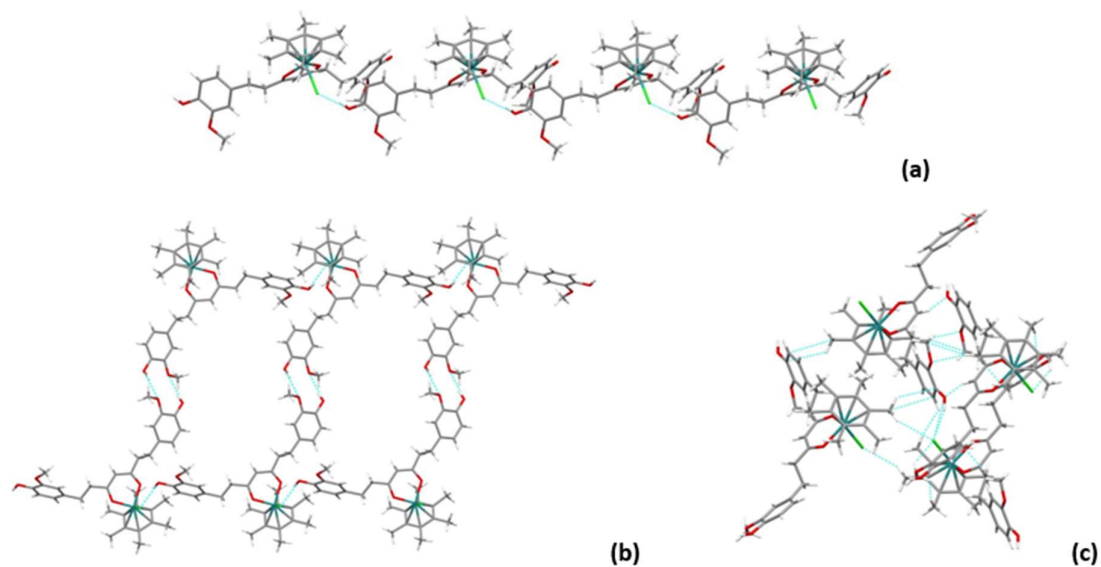**Scheme 18 -** *Optimized structures of proligands HL¹³, HL¹⁴ and their anions and selected bond distances*

Figure 80 - *Crystal packing of complex 20 showing Ru-Cl···H-O hydrogen bonds (a); Me-O···H-O hydrogen bonds (b); hydrogen bonds and short contacts with the chloro ligand (c)*

The crystal packing of **21** is built up by a hydrogen bonding network created by interactions between the -OH substituents of **L¹³** of two adjacent molecules (H-O…H-O distance of 2.043 Å, **Figure 80a**) and some other weak short contacts between the Ru-Cl moiety and adjacent C-H bonds (see unit cell in **Figure 80b**).
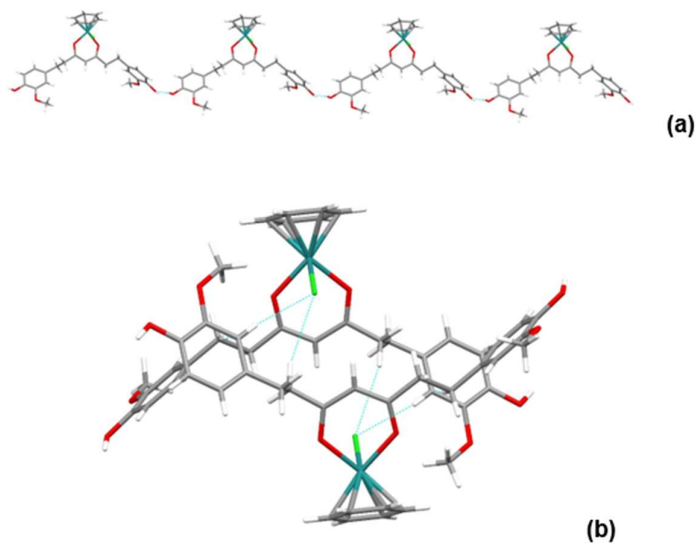

(a)

(b)

Figure 81 - Crystal packing of complex **21** showing O···H-O hydrogen bonds (**a**) and short contacts within the unit cell (**b**)

The asymmetric unit of **22** contains two molecules with a π-π stacking interaction between the *p*-cymene ligands characterized by a centroid-centroid distance of 3.945 Å (**Figure 81a**). The presence of two -OH functionalities in the **L¹⁴** ligand allows the formation of two possible intermolecular Ru-Cl···H-O hydrogen bonds. However, both -OH groups are involved in hydrogen bonding with the same chloro ligand. **Figure 81b** shows the orientation of the Ru-Cl···H-O hydrogen bonds and additional short contacts of the chloro ligand with C-H bonds of the *p*-cymene ligand. All these intermolecular interactions are viable only if a *closed* conformation is attained in the crystal.
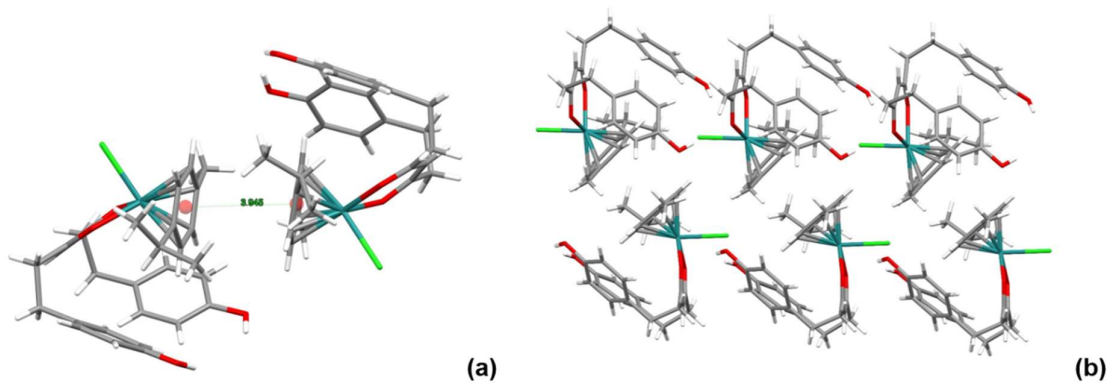

(a)

(b)

Figure 82 - Crystal packing of complex **22** showing π-π stacking in the asymmetric unit (**a**) and short contacts within the unit cell (**b**)

3.2.8 Theoretical studies

The proligands **HL¹³** and **HL¹⁴**, their anions and ruthenium complexes **19-24** were analyzed using density functional theory (DFT) to obtain information about their frontier molecular orbitals (MOs) of the precursors and ligands and about the electronic structure of the complexes. Geometry optimizations were performed with the actual compounds, without symmetry restrictions, and starting from the experimental X-ray coordinates for complexes **20-22**. Significant differences in the structural parameters of the proligands with respect to the previously reported curcumin and bisdemethoxycurcumin proligands are not observed, except for the presence of the C-C double bond. Analysis of the frontier MOs obtained for the **HL¹³** and **HL¹⁴** anions reveals that HOMO-9 and HOMO-10 are the *in-phase* and *out-of-phase* combinations, respectively, of the σ lone pairs of oxygen atoms (**Table 7**).
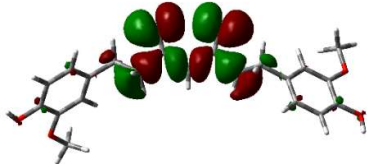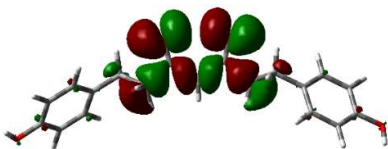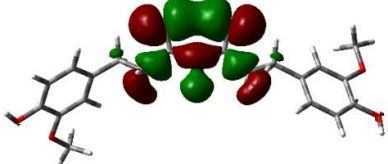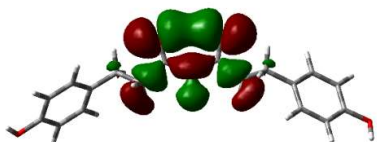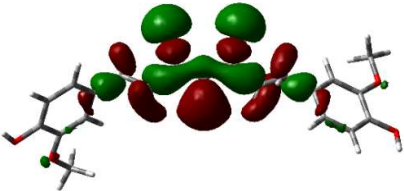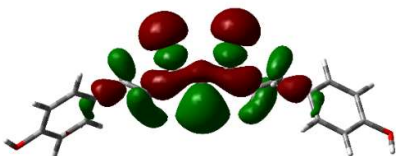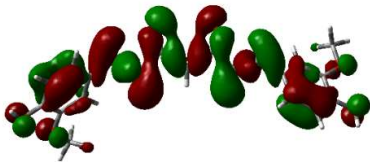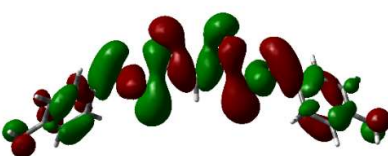
HL¹³	HL¹⁴
HOMO-1	
HOMO-2	
HOMO-9	
HOMO-10	

Table 7 - *Selected MOs of anions of HL¹³ and HL¹⁴*

These orbitals are primarily responsible for σ-coordination of the ligands to the ruthenium centre, although there are also minor contributions from HOMO-1 and HOMO-2. The topology of these MOs is essentially identical to that calculated for the anions of curcumin and bisdemethoxycurcumin (not shown). Even their energies are quite similar and,

consequently, no major differences between unsaturated and saturated curcuminoid ligands are expected when bonded to the Ru centre.

The optimized structures of the complexes are shown in **Figure 82**. As previously reported in DFT studies of related Ru systems, the selected combination of method and basis sets provides a satisfactory structural description of these complexes. A comparison of the structural parameters of **20-22** with those determined by X-ray diffraction is good (see **Table 6**). The exception is the bond distance from the Ru ion to the arene centroid, which is always slightly overestimated, as noted previously in similar Ru-arene complexes. The calculated IR spectra of **19-24** confirm the IR assignments. For instance, the symmetrical v(C-O) stretching calculated at around 1570 cm^{-1} and the v(Ru-Cl) stretching calculated at around 266 cm^{-1}.
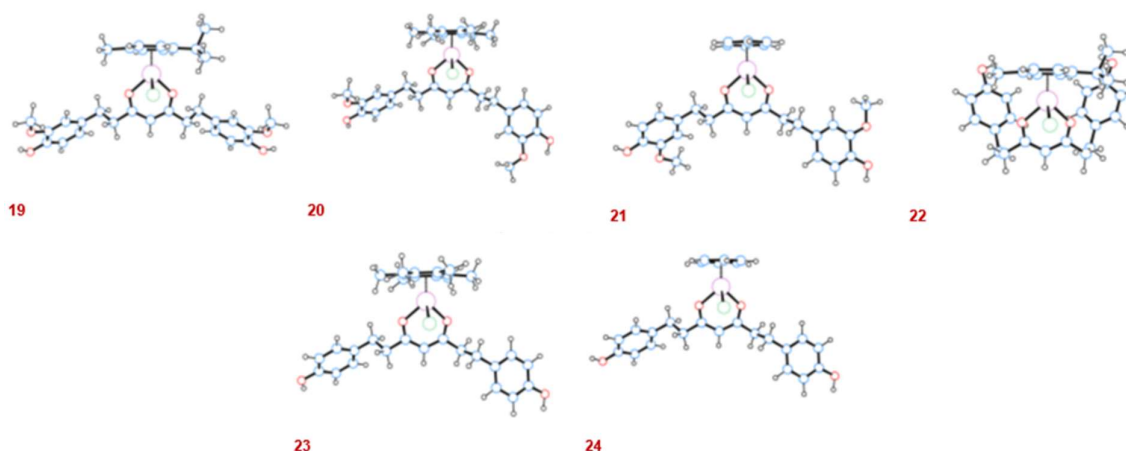
Figure 83 - *Optimized structures of 19-24*

As evident from **Figure 82**, the optimized structure of **22** with a *closed* conformation is different from the other structures and was obtained by an optimization starting from the crystallographic coordinates. To identify whether the *open* conformation of **22** is more stable, both the *closed* and *open* conformations of complexes **19-24** were calculated in gas phase without intermolecular interactions. The resulting optimized structures of the conformers are displayed in **Figure 83**. The open conformation is always the most stable with relative ΔG energy differences within the range of 1.3-11.9 kcal/mol (**Table 8**). The energy differences are higher for **L**[13] than for **L**[14] ligand and the lowest difference is found for the less sterically demanding benzene ligand. In any case, the closed conformation of **L**[14] found in the crystal structure of **22** is due to the presence of intermolecular interactions in the solid state. The hydrogen bonds and π-π stacking interactions counterbalance the energy difference between both conformations.
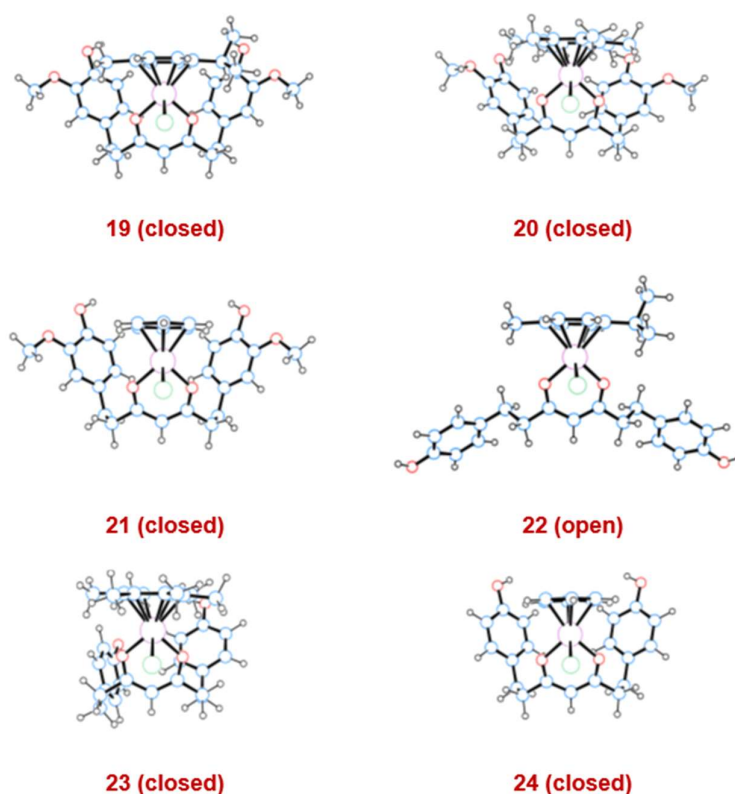
Figure 84 - *Optimized structures of conformers of complexes 19-24*

	19		20		21		22		23		24	
	closed	*open*	*closed*	*open*	*closed*	*open*	*closed*	*open*	*closed*	*open*	*closed*	*open*
ΔE	9.2	0	6.5	0	0.3	0	0.4	0	2.0	0	1.1	0
ΔG	11.3	0	8.4	0	3.2	0	3.7	0	4.1	0	1.9	0

Table 8 - *Relative energies (kcal/mol) of the open and closed conformations for 19-24*

With the aim of comparing the behaviour of L^{13} and L^{14} as ligands in **19-24** with their curcumin and bisdemethoxycurcumin analogues, complexes **19a-24a** were additionally calculated, at the same theoretical level. In these complexes, the L^{13} and L^{14} ligands were replaced by curcumin and bisdemethoxycurcumin, respectively (herein not showed). The presence of the C-C double bond in curcumin and bisdemethoxycurcumin ligands of complexes **19a-24a** excludes the possibility of ligand conformations. To compare the bonding capabilities of these ligands, the Mayer indexes of the Ru-O bonds were calculated for all derivatives **19-24a**. No significant differences were found between the two types of ligands with respect to the coordination to ruthenium. Only minor differences were encountered in the C-O bonds, where lower Mayer indexes were calculated for curcumin and bisdemethoxycurcumin than for L^{13} and L^{14}, in agreement with the slightly longer C-O distances (around 1.284 Å) in **19a-24a** with respect to those of **19-24**.

4.1 Aim of the work

In the introductory chapters has been reported that the structural modification of curcumin on the level of β -diketone group may improve both stability and biological activity of the final compound. According to this, the current section is based on the synthesis and biological evaluation of novel half-sandwich Ruthenium(II) complexes containing derivatives of the curcuminoids bearing a pyrazole group. The new Ru(II) and Os(II)-*p*-cymene complexes were completely characterized by NMR spectroscopy and ESI mass spectrometry, and the crystal structures of the Ru complexes containing both curcumin and bisdemethoxycurcumin pyrazole analogues were determined by X-ray diffraction analysis. Compared to the other derivatives, these curcuminoids have a completely different functional group where the nitrogen atoms replace the oxygen ones. This fact reflects the different coordination environment found for the related complexes having a -N,N chelation instead of the typical -O,O. The new complexes result soluble in water medium and highly stable under physiological condition.

4.1.1 Materials and methods

The dimer [(*p*-cymene)RuCl$_2$]$_2$ was purchased from Aldrich, the [(*p*-cymene)OsCl$_2$]$_2$ was synthesized using literature methods.[144] Curcumin and bisdemethoxycurcumin were purchased from TCI Europe and were used as received. All reactions for the syntheses of proligands and the corresponding complexes were carried out in the air. The samples for microanalyses were dried in vacuo to constant weight (35 °C, ca. 0.1 Torr). Elemental analyses (C, H, N) were performed in-house with a Fisons Instruments 1108 CHNS-O Elemental Analyser. IR spectra were recorded on a Perkin-Elmer Frontier FT-IR instrument. ^{1}H and ^{13}C NMR spectra were recorded on a 500 Bruker Ascend (500 MHz for ^{1}H, 125 MHz for ^{13}C) instrument operating at room temperature relative to TMS. Positive ion electrospray mass spectra were obtained on a Series 1100 MSI detector HP spectrometer, using acetonitrile as solvent for all complexes 1-5. Solutions (3 mg/mL) for electrospray ionization mass spectrometry (ESI-MS) were prepared using reagent-grade methanol. Masses and intensities were compared to those calculated using IsoPro Isotopic Abundance Simulator, version 2.1.28. Melting points were recorded on a STMP3 Stuart scientific instrument and on a capillary apparatus. Samples for microanalysis were dried in vacuo to constant weight

(20°C, ca. 0.1 Torr) and analysed on a Fisons Instruments 1108 CHNS-O elemental analyser. UV-stability studies have been conducted with a Varian Caryl spectrometer.

4.1.2 General procedure for synthesis of ligands

HL[15] **(4,4'-((1E,1'E)-(1-(pyridin-2-yl)-1H-pyrazole-3,5-diyl) bis(ethene-2,1-diyl)) bis(2-methoxyphenol)).** Compound **HL[15]** has been synthesized according to the literature procedures.[159,121] Curcumin (442 mg, 1.2 mmol) and 2-hydrazinopyridine (218 mg, 2 mmol) have been dissolved in *n*-butanol (10 mL) together with a solution of glacial acetic acid (9 mL). The reaction has been stirred at reflux for 8 hours then the solvent has been removed and the product isolated through a chromatographic separation in CH_2Cl_2 obtaining **HL[15]** (**Figure 84**), as orange powder, yield 55%. It is completely soluble in CH_3OH, CH_3CN, DMSO and CH_3Cl and insoluble in H_2O. m.p. 91-93 °C. IR (cm^{-1}): 3386 mbr v(C=N-H); 3059 w, 3009 w, 2960 w, 2935 w, 2837 w v(C-H); 1588 s, 1575 m, 1537 m, 1510 vs, 1469 s, 1444 s, 1428 s, 1366 m v(C=C, C-N). ^{1}H-NMR (DMSO-d_6, 293 K): δ 3.83 (s, 3H, -OC*H*$_3$), 3.86 (s, 3H, -OC*H*$_3$), 6.80 (t, 2H, C(9-9)*H*), 7.00 (d, 2H, C(10-10')*H*), 7.06 (d, 1H, C(3)*H*), 6.11 (d, 1H, C(6')*H*), 7.17 (s, 1H, C(1)*H*), 7.19 (d, 1H, C(4')*H*), 7.23 (s, 1H, C(4)*H*), 7.25 (s, 1H, C(6)*H*), 7.41 (t, 1H, C(13)*H*), 7.79 (d, 1H, C(3')*H*), 7.87 (d, 1H, C(15)*H*), 8.03 (t, 1H, C(14)*H*), 8.58 (d, 1H, C(12)*H*), 9.22 sbr, 9.29 sbr (2H, O-*H*). ^{13}C{^{1}H}-NMR (DMSO-d_6, 293 K): δ 56.1 [-OC*H*$_3$], 102.5 [*C*(1)], 110.3 [*C*(6)], 111.0 [*C*(6')], 115.1 [*C*(3')], 116.1, 116.3 [*C*(9-9')], 116.9 [*C*(15)], 117.5 [*C*(3)], 120.6, 120.9 [*C*(10-10')], 122.3 [*C*(13)], 128.7, 128.7 [*C*(5-5')], 132.3 [*C*(4)], 132.8 [*C*(4')], 139.7 [*C*(14)], 144,1 [*C*(2')], 147.5, 147.8 [*C*(8-8')], 148.3, 148.4 [*C*(7-7') and *C*(12)], 152.2 [*C*(2)] and 153.4 [*C*(11)].
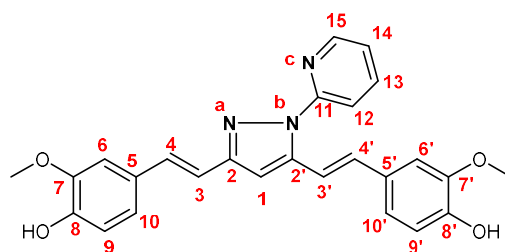
*Figure 85 - Structure of ligand **HL**[15]*

HL[16] **(4,4'-((1E,1'E)-(1-(pyridin-2-yl)-1H-pyrazole-3,5-diyl)bis(ethene-2,1-diyl))diphenol).** For this synthesis the bisdemethoxycurcumin (369 mg, 1.2 mmol) has been used as starting material following the same procedure for compound **HL[15]**. The reaction has been stirred at reflux for 8 hours then the solvent has been removed and the product isolated through a chromatographic separation using 100 mL of a solution of hexane: ethyl acetate, 70 : 30 and 100 mL of the same eluents in 60 : 40 ratio. The so obtained **HL[16]** (**Figure 85**), is an orange powder (67 % of yield). It is completely soluble in CH_3OH, CH_3CN, DMSO, $CHCl_3$ partly

soluble in CH_2Cl_2 and insoluble in H_2O. m.p. 137-138 °C. IR (cm^{-1}): 3202 sbr v(C=N-H); 1640 s, 1604 w, 1590 w, 1547 m, 1524 m, 1505 s, 1472 m, 1441 s, 1388 s, 1379 s v(C=C, C-N).
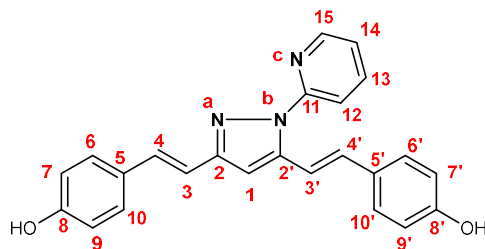
Figure 86 - *Structure of ligand HL[16]*

4.1.3 General procedure for synthesis of complexes

[Ru(*p*-cymene)(L[15])Cl]Cl (25). HL[15] (88 mg, 0.2 mmol) and the dimer [Ru(*p*-cymene)Cl$_2$]$_2$ (61 mg, 0.1 mmol) were dissolved in CH_3CN (5 mL). After 24 h stirring at room temperature the solvent has been partly removed at reduced pressure and the compound **25** (**Figure 86**) precipitated from the solution using Et_2O. The orange precipitate (86 mg, yield 58%) was characterized. It is completely soluble in all the polar solvents like alcohols, CH_3CN, DMSO and H_2O and insoluble in CH_3Cl, hexane and acetone.

Figure 87 - *Structure of compound 25*

Anal. Calcd. for $C_{36}H_{37}Cl_2N_3O_4Ru$: C, 57.83; H, 4.99; N 5.62. Found: C, 55.75; H, 4.99; N, 5.37. m.p. 157-159 °C. IR (cm^{-1}): 3059 mbr, 3007 mbr, 2960 mbr, 2931 mbr, 2843 w v(C=N-H and C-H); 1590 s, 1535 m, 1515 s, 1470 vs, 1455 sh, 1412 w, 1384 s, 1312 w, 1300 w 1278 vs v(C=C, C-N). ^{1}H-NMR (DMSO-d_6, 293 K): δ 0.97 (dd, 6H, CH(CH_3)$_2$ of *p*-cymene), 2.30 (s, 3H, CH_3 of *p*-cymene), 2.52 (m, 1H, CH(CH$_3$)$_2$ of *p*-cymene), 3.87 s, 3.93 s (6H, -OCH_3), 6.08 d, 6.10 d, 6.23 d, 6.31 d (4H, AA′BB′ system, CH$_3$-C$_6$H$_4$-CH(CH$_3$)$_2$ of *p*-cymene, ^3J = 6 Hz), 6.89 d, 6.97 d (2H, C(9-9')H), 7.04 d (1H, C(3')H), 7.17 (d, C(10)H), 7.26 (d, 1H, C(10')H), 7.30 (s, 1H, C(6')H), 7.37 (d, 1H, C(4)H), 7.40 (s, 1H, C(6)H), 7.47 (d, 1H, C(3)H), 7.61 (s, 1H, C(1)H), 7.63 (t, 1H, C(13)H), 7.69 (d, 1H, C(4')H), 8.00 (d, 1H, C(15)H), 8.28 (t, 1H, C(14)H), 9.38 (d, 1H, C(12)H), 9.64 s, 9.70 s (2H, -OH). ^{13}C{^{1}H}-NMR (DMSO-d_6, 293 K):

δ 19.2 [-CH_3 of *p*-cymene], 22.0, 22.4 [-CH(CH_3)$_2$ of *p*-cymene], 30.9 [-CH(CH$_3$)$_2$ of *p*-cymene], 56.2, 56.4 [-OCH_3 of **L**^{15}], 81.6, 83.3 [*C*(a-a')], 85.9, 87.5 [*C*(b-b')], 103. 7 [*C*i'], 106.4 [*C*i], 107.6 [*C*(1)], 110.8 [*C*(3)], 111.7, 111.8 [*C*(6-6')], 114.0 [*C*(3')], 114.1 [*C*(15)], 116.2 [*C*(9)], 116.5 [*C*(9')], 122.1 [*C*(10')], 122.8 [*C*(10)], 123.8 [*C*(13)], 127.2, 127.3 [*C*(5-5')], 139.4 [*C*(4)], 139.7 [*C*(4')], 142.8 [*C*(14)], 147.2 [*C*(2')], 148.5, 149.3 [*C*(7-7')], 148.6 [*C*(11)], 155.7 [*C*(12)], 157.4 [*C*2]. ESI-MS (+) CH$_3$CN (m/z [relative intensity, %]): 712 [100] [Ru(*p*-cymene)(L^{15})Cl]$^+$.

[Os(*p*-cymene)(L^{15})Cl]Cl (26). HL^{15} (88 mg, 0.2 mmol) and the dimer [Os(*p*-cymene)Cl$_2$]$_2$ (60 mg, 0.1 mmol) were dissolved in CH$_3$CN (5 mL). After 4 h stirring at room temperature the solvent has been partly removed at reduced pressure and the compound **26** (**Figure 87**) precipitated from the solution using Et$_2$O and subsequently washed with CH$_3$Cl. The dark yellow precipitate (76 mg, yield 45%) was characterized. It is completely soluble in all the polar solvents like alcohols, CH$_3$CN, DMSO and H$_2$O and insoluble in CH$_3$Cl, hexane and acetone.
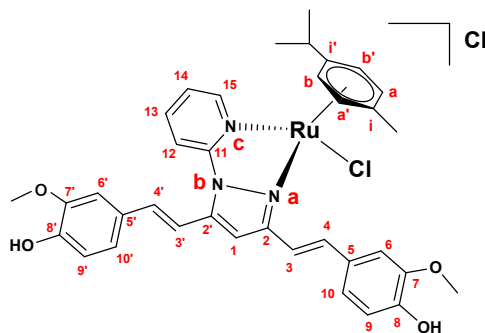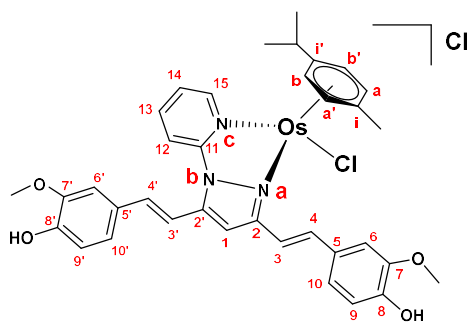

Figure 88 - *Structure of compound 26*

Anal. Calcd. for C$_{36}$H$_{37}$Cl$_2$N$_3$O$_4$Os: C, 51.67; H, 4.46; N 5.02. Found: C, 50.26; H, 4.45; N, 4.73. m.p. 125-127 °C. IR (cm^{-1}): 3059 wbr, 2964 w, 2934 w, 2879 wbr, 2829 wbr v(C=N-H and C-H); 1623 sh, 1589 s, 1575 sh, 1540 m, 1513 vs, 1471 vs, 1455 m, 1444 mbr, 1434 w, 1427 w, 1393 m, 1385 sh, 1370 m, 1277 vs v(C=C, C-N). ^{1}H-NMR (DMSO-d_6, 293 K): δ 0.91 (dd, 6H, CH(CH_3)$_2$ of *p*-cymene), 2.36 (s, 3H, CH_3 of *p*-cymene), 2.42 (m, 1H, CH(CH$_3$)$_2$ of *p*-cymene), 3.87 s, 3.93 s (6H, -OCH_3), 6.27 d, 6.31 d, 6.48 d, 6.50 d (4H, AA'BB′ system, CH$_3$-C$_6$H$_4$-CH(CH$_3$)$_2$ of *p*-cymene, ^{3}J = 6 Hz), 6.88-6.96 (m, 3H, C(9')H, C(10')H, C(3')H), 7.18-7.27 (m, 4H, C(9)H, C(10)H, C(3)H, C(6)H), 7.38-7.41 (m, 2H, C(4)H, C(6')H), 7.54 (s, 1H, C(1)H), 7.57 (t, 1H, C(13)H), 7.66 (d, 1H, C(4')H), 8.14 (d, 1H, C(15)H), 8.29 (t, 1H, C(14)H), 9.31 (d, 1H, C(12)H), 9.63 s, 9.68 s (2H, O-H). ^{13}C{^{1}H}-NMR (DMSO-d_6, 293 K): δ 19.0 [-CH_3 of *p*-cymene], 22.3, 22.8 [-CH(CH_3)$_2$ of *p*-cymene], 31.2 [-CH(CH$_3$)$_2$ of *p*-cymene], 56.2, 56.4 [-OCH_3 of **L**^{15}], 70.9, 73.5 [*C*(a-a')], 77.8, 79.2 [*C*(b-b')], 94.6 [*C*i], 100.3 [*C*i'], 107.2 [*C*(3)], 110.4 [*C*(1)], 111.8, 111.9 [*C*(6-6')], 113.6 [*C*(3')], 114.1, 116.1, 122.2, 23.0 [*C*(9-9') and *C*(10-10')], 116.5 [*C*(11)], 124.3 [*C*(13)], 127.2 [*C*(3')], 140.0 [*C*(4-4')], 143.1 [*C*(14)], 146.9

[*C*(2)], 148.9 [*C*(8-8')], 149.3 [*C*(7-7')], 155.8 [*C*(12)], 156.2 [*C*(2')]. ESI-MS (+) CH$_3$CN (m/z [relative intensity, %]): 802 [100] [Os(*p*-cymene)(L^{15})Cl]$^+$.

[Ru(*p*-cymene)(L^{16})Cl]Cl (27). **HL^{16}** (76 mg, 0.2 mmol) and the dimer [Ru(*p*-cymene)Cl$_2$]$_2$ (61 mg, 0.1 mmol) were dissolved in CH$_3$CN (5 mL). After 4 h stirring at room temperature the compound **27** (**Figure 88**) precipitated from the solution was filtered. The orange precipitate (118 mg, yield 86%) was characterized. It is completely soluble in all the polar solvents like alcohols, DMSO, partly soluble in H$_2$O and insoluble in CH$_3$Cl, CH$_3$CN, hexane and acetone.

Figure 89 - *Structure of compound* **27**

Anal. Calcd. for C$_{34}$H$_{33}$Cl$_2$N$_3$O$_2$Ru: C, 59.39; H, 4.84; N, 6.11. Found: C, 58.14; H, 4.75; N, 5.98. m.p. 235-237 °C. IR (cm^{-1}): 3121 wbr, 3088 wbr, 3064 wbr, 3018 w, 2985 w, 2962 w, 2924 w, 2877 w, 2803 w, 2726 w, 2671 w, 2589 w, 2504 w, 2444 w v(C=N-H and C-H); 1625 w, 1604 s, 1585 m, 1574 m, 1551 m, 1512 s, 1479 vs, 1447 m, 1397 m, 1387 sh, 1378 sh, 1355 m, 1324 m, 1313 sh, 1291 w, 1272 s, 1241 sh, 1226 vs, 1171 s v(C=C, C-N); 291 m v(Ru-Cl). ^{1}H-NMR (DMSO-*d*$_6$, 293 K): δ 0.96 (d, 6H, CH(C*H*$_3$)$_2$ of *p*-cymene), 2.29 (s, 3H, CH$_3$ of *p*-cymene), 6.06 d, 6.10 d, 6.20 d, 6.29 d (4H, AA'BB′ system, CH$_3$-C$_6$*H*$_4$-CH(CH$_3$)$_2$ of *p*-cymene, ^{3}J = 6 Hz), 6.92 (dd, 4H, C(6-6')*H* and C(10-10')*H*), 7.02 d (d, 1H, C(3)*H*), 7.62-7.64 (m, 6H, C(7-7')*H*, C(9-9')*H*, C(3)*H*, C(4)*H* and C(13)*H*), 7.68 (d, 1H, C(4)*H*), 7.99 (d, 1H, C(15)*H*), 8.27 (t, 1H, C(14)*H*), 9.35 (d, 1H, C(12)*H*), 10.05 (sbr, 2H, -O*H*). ^{13}C{^{1}H}-NMR (DMSO-*d*$_6$, 293 K): δ 19.1 [-CH$_3$ of *p*-cymene], 22.0, 22.4 [-CH(CH$_3$)$_2$ of *p*-cymene], 30.9 [-CH(CH$_3$)$_2$ of *p*-cymene], 81.5, 83.3 [*C*(b-b')], 86.0, 87.5 [*C*(a-a')], 103.7 [*C*i], 106.5 [*C*i'], 107.5, 123.8, 130.1 [*C*(13), *C*(4), *C*(3), *C*(7-7') and *C*(9-9')], 110.5 [*C*(5')], 113.7 [*C*(3)], 114.1 [*C*(15)], 116.3, 116.5 [*C*(6-6') and *C*(10-10')], 139.3 [*C*(4')], 142.8 [*C*(14)], 147.1 [*C*(2')], 148.6 [*C*(11)], 155.7 [*C*(12)], 157.4 [*C*(2)] 159.7 [*C*(8-8')]. ESI-MS (+) CH$_3$CN (m/z [relative intensity, %]): 652 [100] [Ru(*p*-cymene)(L^{16})]$^-$.

[Os(*p*-cymene)(L^{16})Cl]Cl (28). **HL^{16}** (76 mg, 0.2 mmol) and the dimer [Os(*p*-cymene)Cl$_2$]$_2$ (60 mg, 0.1 mmol) were dissolved in CH$_3$CN (5 mL). After 4 h stirring at room temperature the compound **28** (**Figure 89**) precipitated from the solution was filtered. The dark yellow precipitate (95 mg, yield 61%) was characterized. It is completely soluble in all the polar solvents like alcohols, DMSO, partly soluble in H$_2$O and insoluble in CH$_3$Cl, CH$_3$CN, hexane and acetone.
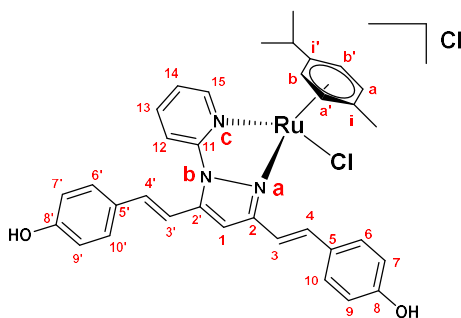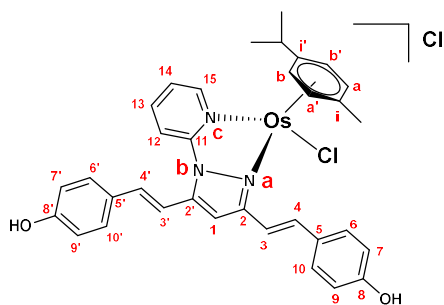
Figure 90 - *Structure of compound 28*

Anal. Calcd. for $C_{34}H_{33}Cl_2N_3O_2Os$: C, 52.57; H, 4.28; N, 5.41. Found: C, 52.96; H, 4.29; N, 5.22. m.p. 198-200 °C. IR (cm^{-1}): 3038 mbr, 3009 mbr, 2965 w, 2926 w, 2868 w, 2798 w, 2727 w, 2678 w, 2586 w, 2448 w v(C=N-H and C-H); 1631 w, 1603 vs, 1583 m, 1572 w, 1542 m, 1512 s, 1476 vs, 1445 s, 1397 m, 1372 m, 1321 w, 1274 vs v(C=C, C-N); 226 vs v(Os-Cl). ^{1}H-NMR (DMSO-d_6, 293 K): δ 0.91 (d, 6H, CH(CH_3)$_2$ of *p*-cymene), 2.36 (s, 3H, CH_3 of *p*-cymene), 2.41 (m, 1H, CH(CH$_3$)$_2$ of *p*-cymene), 6.27 d, 6.32 d, 6.45 d, 6.49 d (4H, AA′BB′ system, CH$_3$-C$_6$H$_4$-CH(CH$_3$)$_2$ of *p*-cymene, ^3J = 6 Hz), 6.92 (dd, 4H, C(6-6')H and C(10-10')H)7.45 (dd, 2H, C(3)H, C(4)H), 7.56 (t, 1H, C(13)H), 7.62-7.67 (m, 6H, C(7-7')H, C(9-9')H, C(4')H and C(3')H), 8.13 (d, 1H, C(15)H), 8.27 (t, 1H, C(14)H), 9.30 (d, 1H, C(12)H), 10.09 (sbr, 2H, O-H). ^{13}C{^{1}H}-NMR (DMSO-d_6, 293 K): δ 19.0 [-CH$_3$ of *p*-cymene], 22.3, 22.8 [-CH(CH$_3$)$_2$ of *p*-cymene], 31.2 [-CH(CH$_3$)$_2$ of *p*-cymene], 70.8, 73.4 [C(a-a')], 77.9, 79.2 [C(b-b')], 94.6 [Ci], 100.4 [Ci'], 107.1, 130.2, 139.7 [C(4'), C(3'), C(7-7') and C(9-9')], 110.0, 128.6 [C(3) and C(4)], 113.8 [C(15)], 116.3, 116.5 [C(6-6') and C(10-10')], 124.3 [C(13)], 130.1, 130.2 [C(5) and C(5')], 143.1 [C(14)], 146.9 [C(2)], 148.6 [C(11)], 155.7 [C(12)], 157.43 [C(2)], 1148.9 [C(11)], 155.8, 156.2 [C(12) and C(8-8')], 159.8 [C(2')]. ESI-MS (+) CH$_3$CN (m/z [relative intensity, %]): 742 [100] [Os(*p*-cymene)(L^{16})Cl]$^+$.

4.2 RESULTS AND DISCUSSION

4.2.1 Synthesis and characterization of ligands

The curcumin containing pyrazole (**HL^{15}**) and bisdemethoxycurcumin containing pyrazole (**HL^{16}**) ligands, were synthesized as reported in **Scheme 19** starting from the commercially available curcumin and bisdemethoxycurcumin. The relative curcuminoid was dissolved in *n*-butanol together with an excess of 2-hydrazinopyridine in the presence of glacial acetic acid to favor the condensation step. The relative products have been separated from the reaction mixture through chromatographic purification.
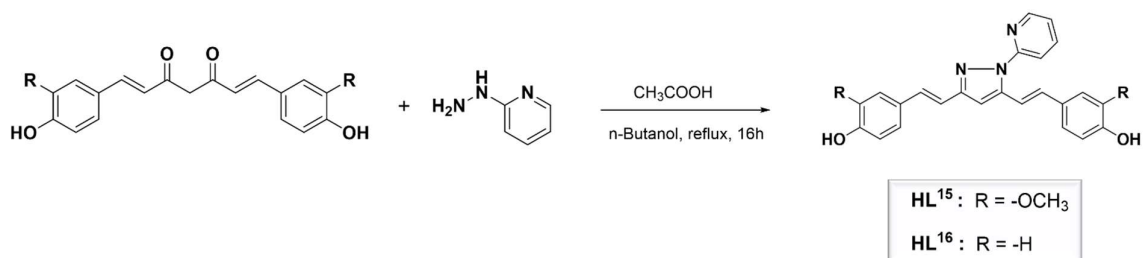
Scheme 19 - *Synthetic procedure for the ligands HL¹⁵ and HL¹⁶*

The elemental analyses and ESI-MS spectrometry have confirmed the expected structures of the ligands **HL¹⁵** and **HL¹⁶**. Additionally, the IR spectra shows the disappearance of the typical absorption band at 1627 cm⁻¹ (for curcumin) and 1640 cm⁻¹ (for bisdemethoxycurcumin) characteristic of C=O double bond (**Figure 90**).
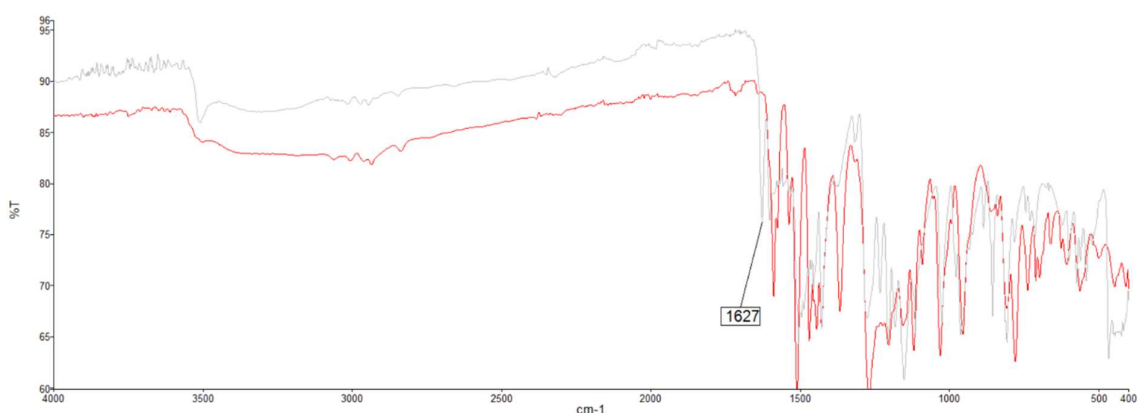
Figure 91 - *Comparison between the IR spectra of HL¹⁵ ligand (red line) and the curcumin parent compound (grey line)*

4.2.2 Synthesis and characterization of the complexes

The compounds **25-28** were obtained by dissolving the respective, previously reported, curcuminoid ligands in a CH₃CN solution under magnetic stirring and letting them to react with the metallic dimer [(p-cymene)MCl₂]₂ (where M = Ru or Os) at room temperature for 4 hours (**Scheme 20**). For these syntheses the use of a deprotonating base was not necessary since the absence of the keto-enolic form of curcuminoids. The complexes containing the bisdemethoxycurcumin derivatives **27** and **28** directly precipitated from the solution differently from their curcuminoid analogues which remain in solution.

Due to the fact that the curcuminoids used are neutral bidentate ligands, the final complexes **25-28** have an ionic configuration with a chloride specie acting as counterion in the outer coordination sphere. Furthermore, the ionic dissociation and, therefore, the presence of 1:1

electrolyte ratio in water solution has been confirmed for compound **25** through conductivity analysis.
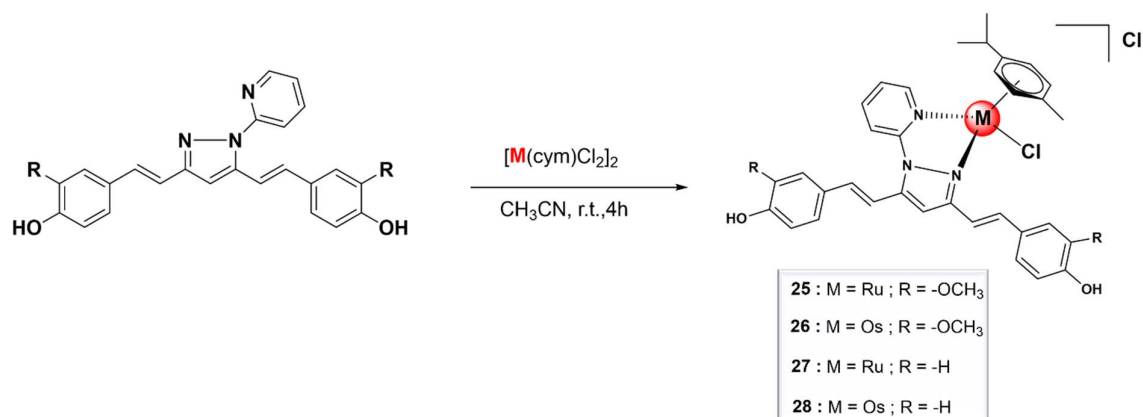
Scheme 20 - *Synthetic procedure for compounds 25-28*

All the obtained complexes show a very high purity as confirmed by the narrow melting points and the elemental analyses. They are air-stable and soluble in all the polar solvents, including water. The electrospray ionization (ESI) mass spectra of **25–28** in positive ion mode, recorded in CH_3CN, show the expected isotopic patterns and display peaks that correspond to $[M(p\text{-cymene})(L^{15}/L^{16})Cl]^+$ arising from the dissociation of the chloride present in the outer coordination sphere.

All the ^{1}H-NMR spectra have been recorded in DMSO-d_6 and the assignations of each peak have been done according to the bidimensional analysis. The occurred coordination can be justified by the presence in the spectra of both curcuminoid ligand and *p*-cymene signals. The same analogues of curcumin and bisdemethoxycurcumin between them, show the same similarity of the NMR spectra as always.

An interesting difference, with respect to the previous compounds synthesized, comes from the presence of multiple set of signals arising from the loss of symmetry inside the curcuminoid structure (an example in **Figure 91**).

In fact, the presence of the pyridine as substituent in the pyrazole ring generates a steric hindrance which affects the electronic environment of just one of the two portions of the curcuminoid's structure and, as a consequence, the protons in the molecule do not show magnetic equivalence anymore, as appears evident for phenolic and methoxy protons where there are two separated set of signals instead of one each: there are two singlets for the two O-*H* groups at about 9.7 and 9.6 ppm and two singlets for the two -OC*H*$_3$ groups around 3.9 and 3.8 ppm. In **Figure 92** is showed the complexity of the ^{1}H-NMR spectrum of the ligand **HL**^{15} (down) and how the coordination with a metal centre further split the protons' signals (up).
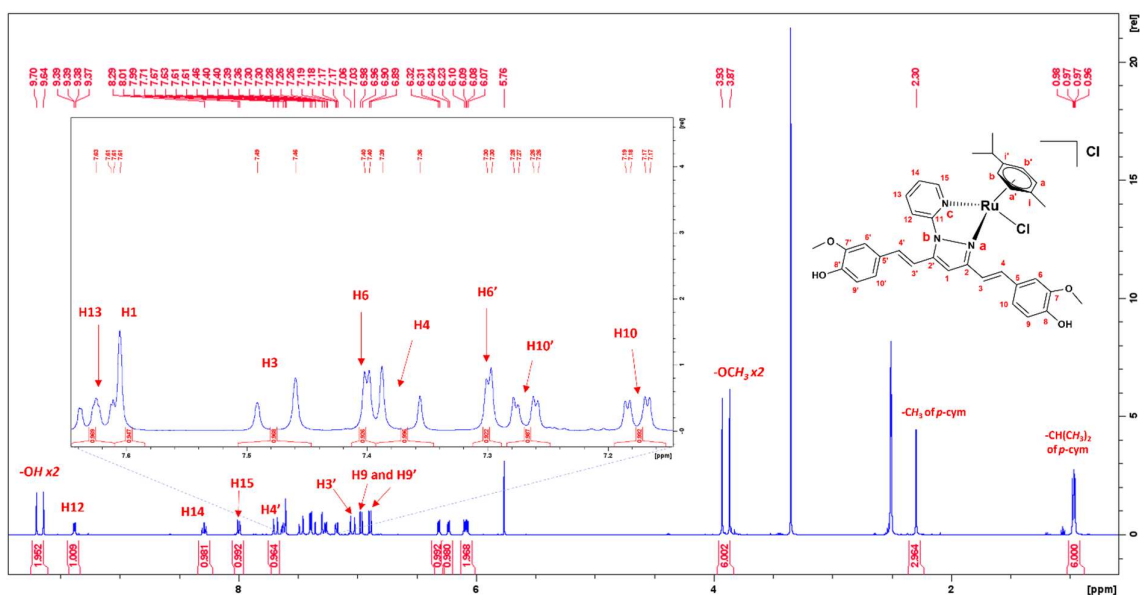
Figure 92 - *¹H-NMR of **25** recorded in DMSO-d⁶*
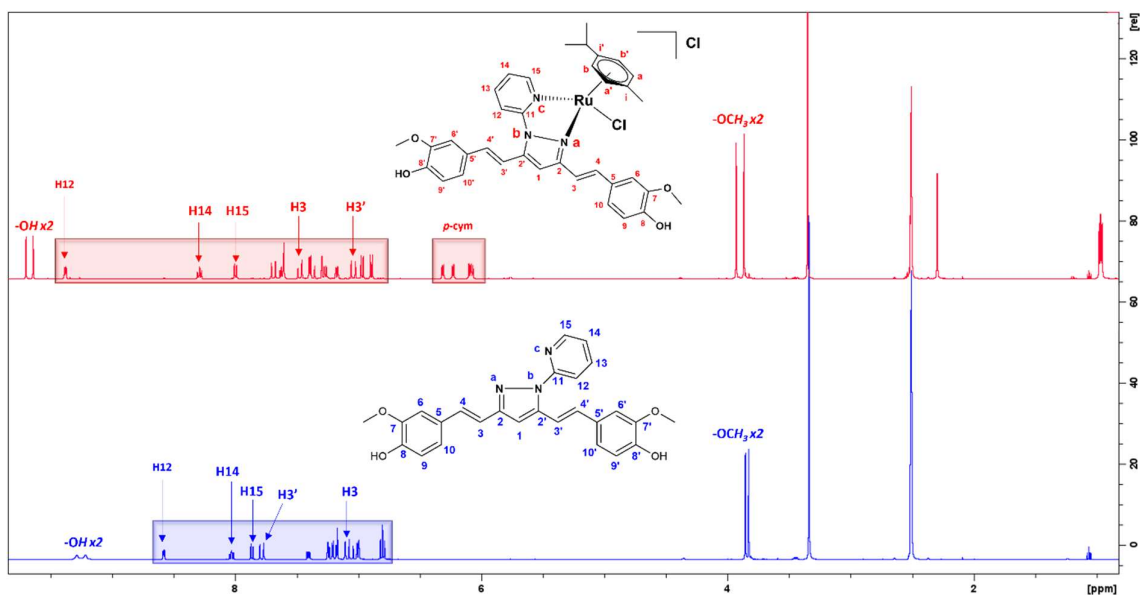
Figure 93 - *Comparison between the ¹H-NMR spectra recorded in DMSO-d⁶ of compound **25** (red line) and **HL¹⁵** (blue line)*

In particular, is possible to observe how deep is the shift of those signals which are very close to the coordination sphere, such as 12-C*H*, 14-C*H*, 15-C*H*, 3-C*H* and 3'-C*H*. Moreover, even the protons which are more far from the coordination with the metal centre, still suffer a shifting of ppm as occurs for -OH and -OC*H₃* protons.

A comparison between the ¹H-NMR spectra of Ru and Os with the bisdemethoxycurcumin analogue (**27** and **28** respectively), shows almost the same pattern but with different chemical shift due to the different electronic impact given by the two metal centres (**Figure 93**).
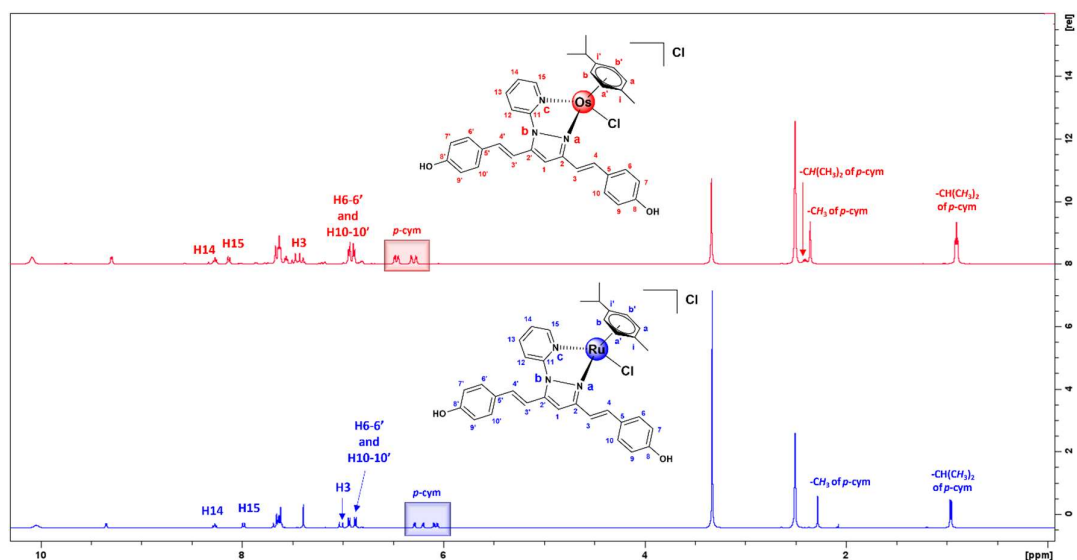
Figure 94 - *Comparison between the ¹H-NMR spectra recorded in DMSO-d⁶ of Ru analogue **27** (blue line) and Os analogue **28** (red line)*

Additionally, the {¹H-¹⁵N}-HMBC can be used to monitor the change in the nitrogen chemical shifts before and after the coordination (**Figure 94**).
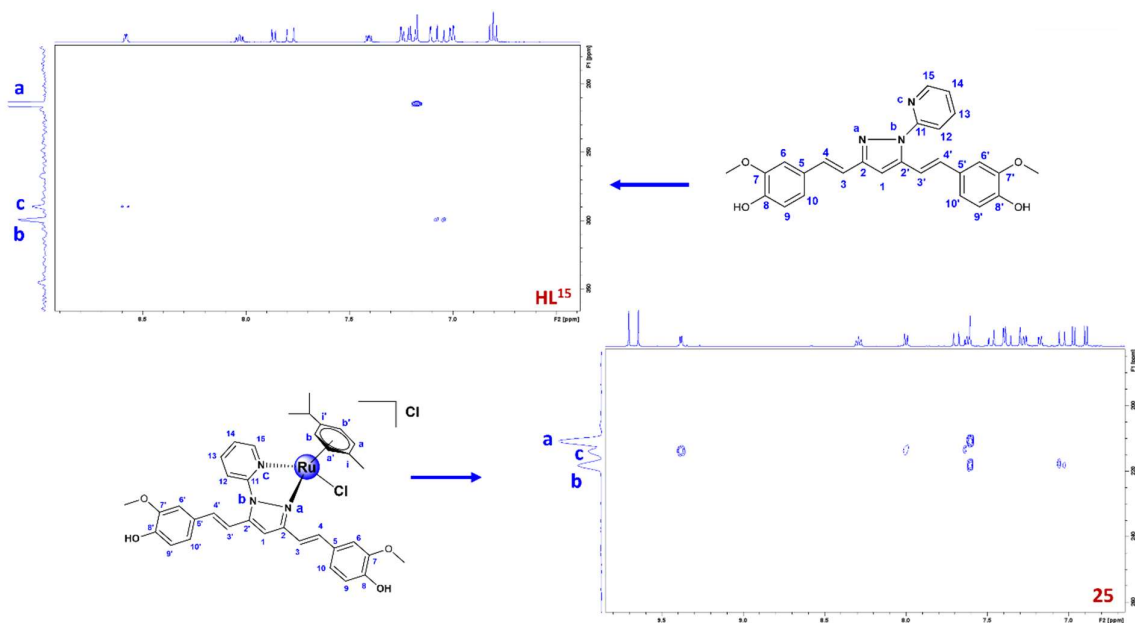
Figure 95 - *Comparison between the {¹H-¹⁵N}-HMBC spectra recorded in DMSO-d⁶ of **25** and **HL¹⁵***

Additionally, the final confirmation of the complexes' structure came from the preliminary crystallographic studies made for compounds **25** and **26** (**Figure 95**).
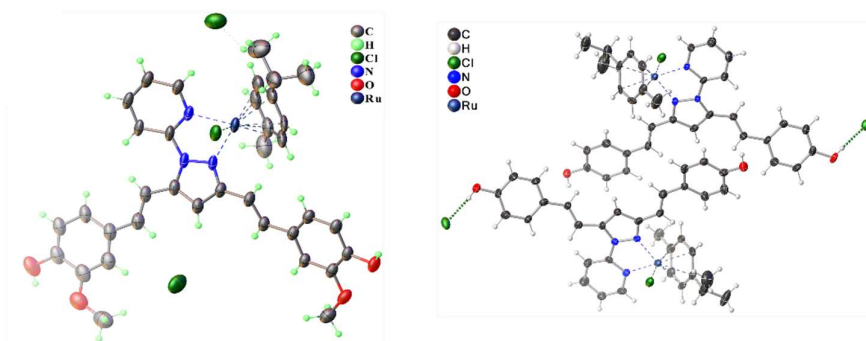
Figure 96 - *Molecular structures of* **25** *(left), and* **26** *(right)*

4.2.3 Stability studies

To investigate the stability of the complexes, the absorbance profile of **25** was evaluated under physiologically relevant conditions using a phosphate-buffered solution (PBS, pH = 7.4). The solution was monitored over time using UV-Visible spectroscopy. The complex was initially solubilized in DMSO and then diluted to 5% DMSO with PBS. It was found that the complex **25** possesses an unchanged absorbance profile within 72 hours (**Figure 96**) underling the greatest stability found with respect all the previous curcuminoids tested.
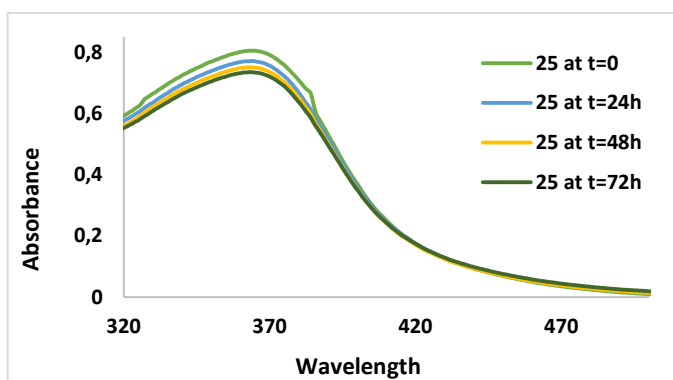
Figure 97 - *UV-visible stability studies of* **25** *under physiological condition*

Furthermore, a series of UV-visible spectra have been recorded also in the F-12 Nutrient Mixture (Ham's) Formulation, which is the solution where the cells grow. In the experiment we compared the absorbance profile within 24 hours of the ligand **HL**[16] and their related complexes of Ruthenium and Osmium analogues, **27** and **28** (**Figure 97**).
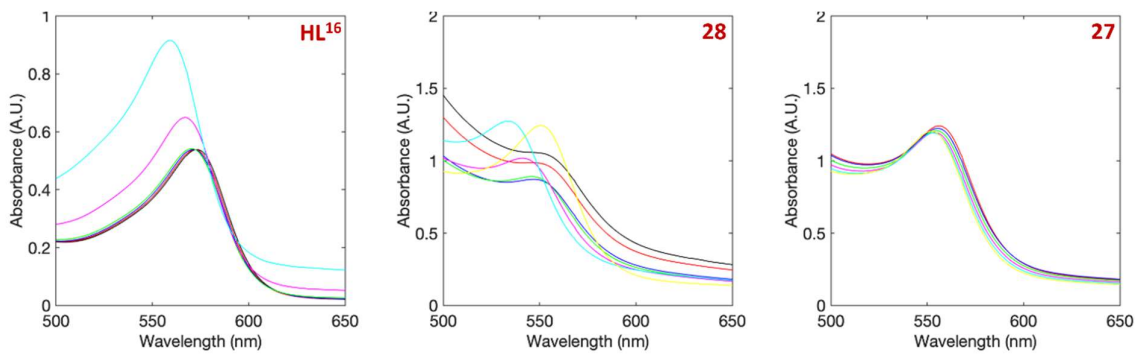
Figure 98 - *UV-visible stability studies in cellular growth medium of **HL**[16], **27** and **28***

From the graphs showed in figure appears evident the improving in stability for ligand **HL**[16] after the coordination and this phenomenon is much more accentuated for ruthenium analogue **27** being the change in the absorbance profile of osmium derivative **28** sharper.

Chapter 5: Conclusion and future perspectives

The overall aim of this doctoral thesis was focused on the synthesis of novel organometallic compounds having biological and antitumoral activity. For this purpose, were selected:

- the metals belonging to the group XVIII of the periodic table (Ru and Os), according to their well-known anticancer activity;
- modified curcuminoids (curcumin and bisdemethoxycurcumin) as ligands with enhanced bioavailability.

Firstly, as reported in **Chapter 2**, we synthesized new Ruthenium(II)-*p*-cymene compounds (**1**-**18**) containing modified curcuminoid ligands as diesterified products obtained by replacing the aromatic OH- groups present in the curcumin and bisdemethoxycurcumin, with different substituents having a cyclic, aliphatic, branched, aromatic or heteroaromatic moiety. We temporarily focused our studies on the Ruthenium(II)-*p*-cymene derivatives **1** and **2** with the palmitoyl residue having a very long hydrophobic chain. The same Osmium(II) analogues **3** and **4** have been synthesized and also their ionic RAPTA-like derivatives **5**-**8** were obtained through metathesis reactions. The cytotoxicity studies for compounds **1**-**8** were reported in a work published in 2022 by this research group.[160] The compounds possess potent antitumor activity towards the ovarian cancer cell line (A2780) and its cisplatin-resistant form (A2780cis) and also an excellent selectivity not being cytotoxic for non-cancerous human embryonic kidney cells (HEK293T). Furthermore, the cytotoxicity values of these compounds were compared with those of Ru(II) and Os(II) analogues with the previously reported unmodified curcuminoid ligands, resulting with a better activity. This study highlights interesting structure-activity relationships (SARs) showing that bisdemethoxycurcumin complexes are generally more active and selective than complexes containing curcumin, likely due to a more efficient internalization process, rather than to the direct binding to DNA. The healing power of turmeric has always been attributed to the main component, namely curcumin and perhaps the role of bisdemethoxycurcumin, the secondary component of turmeric, has so far been underestimated. A conclusion of this first part of the work could be the need for a better investigation on the role of compounds containing the bisdemethoxycurcumin derivative and, more importantly, toward this type of diesterified curcuminoid-like analogues. Additionally, biological tests for the remaining compounds **9**-**18** are still ongoing and once the cytotoxicity values have been obtained it will be possible to shed more light on which is the best contributions for the antitumoral activity of this class of compounds.

In the second part of this work, described in **Chapter 3**, are reported the first examples of Ruthenium(II)-arene complexes containing two curcuminoid metabolites, (i.e. tetrahydrocurcumin and tetrahydrobisdemethoxycurcumin) (**19**-**24**). The complexes were fully

characterized in solution and in the solid-state. The X-ray structures obtained confirm that the **HL¹³** and **HL¹⁴** ligands coordinate the ruthenium centre without significant differences between them and with respect to those found for related Ru complexes with unmodified curcumin and bisdemethoxycurcumin. However, an unprecedent *closed* conformation of the **L¹⁴** ligand was found in **22,** where both -OH groups are involved in intermolecular hydrogen bonding with the same chloro ligand. Both *closed* and *open* conformations were analysed in gas phase by DFT studies which showed that the *open* conformation is the most stable. Hence, the *closed* conformation of **L¹⁴** found in the crystal of **22** may be attributed to the presence of intermolecular interactions in the solid state. Despite of being associated with a concerted mechanism of cytotoxicity involving apoptosis and autophagy (as demonstrated by the ability of the complexes of interest to target DNA and to lower the levels of p62/SQSTM1, respectively), all compounds displayed only a modest anticancer property *in vitro* against ovarian and breast cancer cells. This research work is currently under revision in the *Inorganic Chemistry* jurnal.

In the last Chapter of this experimental part (**Chapter 4**) is developed a new series of Ru(II) and Os(II)- *p*-cymene derivatives with both curcumin and bisdemethoxycurcumin containing-pyrazole analogues. The complexes **25-28**, differently from the previous ones, show a -N,N coordination environment and appear in an ionic form since the absence of a negatively charged chelating ligand, as has been confirmed by crystallographic studies. The compounds possess a loss of symmetry in the curcuminoids' structure and, according to this, the protons suffer a different chemical surrounding. The new complexes are water soluble and, especially the Ruthenium complexes are very stable under physiological relevant conditions. The cytotoxicity evaluation for these compounds is still ongoing and are related to *in vitro* studies against human breast adenocarcinoma cells (MCF-7 and MCF-7CR) and nontumorigenic human breast (MCF-10A) cells, compared to the free ligands and cisplatin.

To conclude, at the end of our studies, we can state that the Ruthenium derivatives have always shown better cytotoxicity than the Osmium analogues and we confirmed that the hydrophobic contribution has a huge impact on the anticancer efficiency being the more polar complexes less active due to a less pronounced internalization process. Once again, the bisdemethoxycurcumin derivatives are generally more active than the curcumin ones. In fact, up to now, the best cytotoxicity was found for the neutral Ruthenium complex containing the bisdemethoxycurcumin bioconjugate with palmitoyl residues, but many concerns are related to the stability in physiological medium. On the other hand, the complexes containing the curcuminoids' metabolites improved the stability aspect but decreased the anticancer power. However, interesting evaluation were done in terms of understanding the role of the planarity in the unmodified parent curcuminoids, given by the presence of sp^2 hybridized carbon atoms. Moreover, the absence of the diketo group further increased the stability in water

medium of such complexes. In fact, the water-soluble curcuminoid-containing pyrazole complexes of ruthenium, is, among all studied ones, the most stable complex under physiological conditions.

6.1 METALS COMPLEXES IN CATALYSIS

The term "catalysis" was coined for the first time by Berzelius more than 150 years ago since he noticed changes in substances when they were in contact with small amounts of certain species called "ferments". Years later, in 1895, Ostwald (who won the first Nobel Prize for catalysis in 1909) gave the definition of this phenomenon that we use until today: "*A catalyst is a substance that changes the rate of a chemical reaction without itself appearing into the products*". In the very begin these substances were mainly related to oxides, acids or peroxides until the Thenard's discovery of the role that metals, such as manganese, silver, platinum and gold, had in the evolution of molecular oxygen in alkaline solutions. The role of metals in chemical reactions was reinforced by Humphry Davy who was working on a safety lamp for coal miners: he discovered that the introduction of a red-hot platinum wire into a mixture of air and coal gas caused the wire to become hotter and to glow. This phenomenon was used to develop the first technological application of heterogeneous catalysis.[161] Therefore, the impact of metals in catalysis is known since long times ago as well as the influence that their electronic configuration has on the reaction, for instance depending on the state in which the metal is present, if in gas phase, metallic form or crystal lattice structures.[162-163] Although the organocatalysis has resulted in large numbers of scientific documents having been contributed from both academic and industrial researchers over the last 10 years, the organic synthesis has historically been dominated by transition metal catalysis and additionally, the presence of transition metal complexes in organocatalyst-promoted transformations confirmed the ability of the metal centres in tuning the reactivity of the reaction. Efforts in this direction have led to the discovery of unprecedented reactivities, which are not accessible through the use of either of these two catalytic systems separately.[164] The reason of why the transition metals are considered the essential ingredient of the catalyst system can be summarized under four main headings which affect the catalytical processes: bonding ability; catholic choice of ligands (ligand effect); variability of the oxidation state and variability of the coordination number.

The transition metals considered are those elements having partially filled *d* shells able to accommodate external electrons from the formation of hybrid molecular orbitals in bonding with other atoms or molecules defined as ligands. The availability of these valence orbitals put the metals on the position to be able to form both sigma, σ, and pi, π, bonds which is one of the key factors in imparting catalytic properties to the transition metals and their complexes. In fact, different ligands affect the electronic configuration of the *d*-orbitals of the

metals in different ways. Additionally, a ligand can influence the behaviour of a catalyst by modifying the steric environment at the active site.[165] Therefore, the proper choice of tailor-made and fine-tuned ligands may change considerably the behaviour of the catalytic system.

6.1.1 Homogeneous vs heterogeneous catalysis

Homogeneous catalysis, by definition, refers to a catalytic system in which the substrates of the reaction and the catalyst components are brought together in the same phase, most often the liquid one. Since the World War II, the use of homogeneous catalysis has grown dramatically, and a pioneering process was the oxo reaction developed by Otto Roelen in Germany in the late 1930s where olefins were reacted under high pressure with carbon monoxide and hydrogen to yield lower aldehydes, ketones, and higher alcohols. During the years many other important chemical reactions (including the production of nylon and other polymeric intermediates) were developed in homogeneous conditions.[161] Nowadays many fundamental processes such as hydroformylation, carbonylation, oxidation, hydrogenation, metathesis, and hydrocyanation are homogeneously catalysed. Although the heterogeneous catalysis was the first historically applied method in a commercial scale, today, the role of the homogeneous catalysis has an important impact especially from an environmental point of view being considered a more sustainable process. It is more than coincidental that the majority of the contributions of the journal *Green Chemistry* deals with homogeneous catalysis ensuring high atom economies or E factors (mass of waste over the mass of final product). Furthermore, homogeneous conditions allow high diffusivity of the reactants and high heat-transfer, it has a well-defined active site and can be easily modified (by tuning the electronic and steric properties on the metal by varying donor atoms or by tuning the donating abilities of the ligands) gaining high reaction selectivity. Additionally, homogeneous catalysis does not suffer from the severe drawbacks of heterogeneous catalysis, such as high temperatures, pressure gap or the lack of deeper mechanistic understanding of the multiphase processes on surfaces. However, the challenge of homogeneous catalysis is based on solving the problem of separating the reactants, the catalyst, and the reaction products (which are all in the same phase).[166]

6.2 KNOEVENAGEL CONDENSATION REACTION

The olefin reaction is a quest that has required a lot of research throughout the last 125 years of history of chemistry. The formation of new C-C bonds is the key to produce a wide variety of advanced products, with great impact in every aspect of the human life, and the Knoevenagel condensation reaction is one of the most important methodologies for this

purpose.[167] This reaction represents a variant of the aldol condensation where there is a nucleophilic addition, of a compound with an active hydrogen atom, to a carbonyl group followed by a dehydration reaction and it represents the most common synthetic procedure to generate an electron deficient olefins.

Emil Knoevenagel is generally regarded as a pioneer in the field of the carbon–carbon bond formation with his discovery in 1894 of the reaction between formaldehyde and diethyl malonate. He demonstrated that a bis-adduct product was formed in the presence of diethylamine as a catalyst (**Figure 98a**).
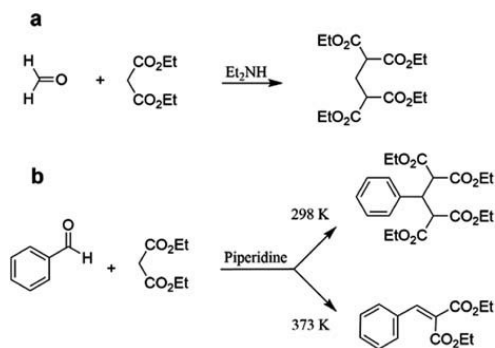

Figure 99 - *Original Knoevenagel condensation reaction: formaldehyde and diethyl malonate under alkaline conditions yielding the bis adduct (**a**); benzaldehyde with diethyl malonate producing the bis adduct at 298 K, and the unsaturated mono-compound at 373 K (**b**)*

Two years later, in 1896, Knoevenagel verified that with the addition of piperidine as a catalyst, a similar carbon–carbon bond formation reaction was possible using aromatic aldehyde compounds (**Figure 98b**). In fact, has been observed that the presence of basic sites within the catalytic structure can promote and accelerate the Knoevenagel condensation reactions and it is vital for reaction proceeding and, as a consequence, all the Knoevenagel reactions are performed with nitrogen-based catalysts which are able to deprotonate the alpha-carbon of one of the two starting material. All the four nitrogen-containing groups (specifically tertiary amines, secondary amines, primary amines, and ammonia) show different catalytical routes in the formation of the carbon–carbon bond. Although using different amines results overall in high conversions, these various amines react through diverse reaction mechanisms. A distinction can be explained by examining the intermediates in the various reaction-mechanisms of aromatic aldehydes: the tertiary amines do not generate intermediates but only deprotonates the reactants, and therefore, according to the scientists, it cannot be qualified as a Knoevenagel condensation but instead it is considered a "base-catalyzed aldol condensation", likewise Hann and Lapworth indicated. Just as Emil Knoevenagel already mentioned, the use of secondary amines yields catalytic intermediates like aminals for aldehydes or enamines for ketones. The primary amines produce Schiff-base intermediates.[168]
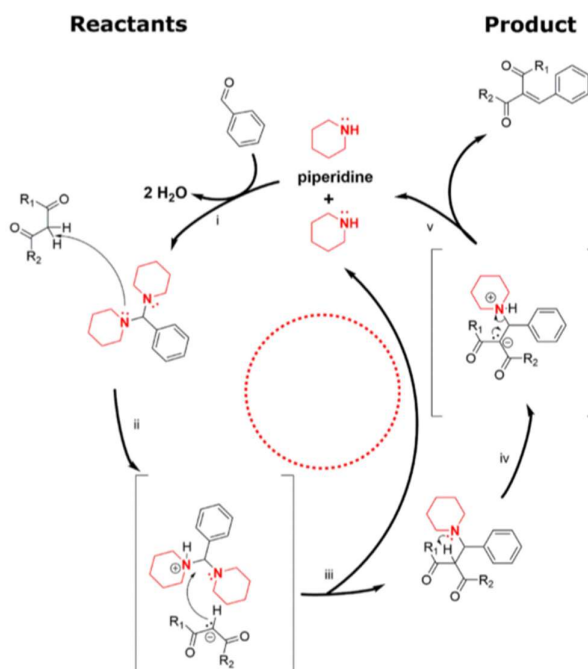
Scheme 21 - *Proposed mechanism of the reaction between benzaldehyde and β-keto compound forming the α,β-unsaturated diketo product catalyzed by the secondary amine (piperidine)*

In **Scheme 21** is showed a proposed mechanism of Knoevenagel condensation using secondary amine: first, in step (i), benzaldehyde undergoes a double nucleophilic attack initiated by piperidine and expelling water; in step (ii), one of the attached piperidines deprotonates the methylene compound producing a carbanion, which subsequently initiates a nucleophilic attack expelling the first piperidine in step (iii); step (iv) is an intramolecular proton shift, leading to step (v) where the removal of the second piperidine gives the final product.

The presented "classic" Knoevenagel reaction was followed by the Doebner-Verley modification, which focuses on the reaction with malonic acid and the same reaction was later extended with other modification including the introduction of different aromatic benzaldehyde compounds in a "Knoevenagel-like-way" providing many precursors and intermediate compounds for the pharmaceutical industry in a biobased manner. In fact, the products generated during this reaction are useful as important intermediates for cosmetics, perfumes and pharmaceuticals.[169,170] Furthermore, many of Knoevenagel adducts have significant biological properties such as antiviral, antitubercular, anti-Parkinson's, anti-diabetic, anti-oxidant, and anti-cancer activity. [168, 171–173] Therefore, the Knoevenagel reaction has a great impact in every aspect of the human life and, for this reason, the introduction of new methods, inexpensive reagents and environmentally friendly conditions has attracted the attention of many research groups which are dealing with the development of a *Green Chemistry's* approach for this field. Traditionally, the reaction was carried out in organic

solvents like DMF and DMSO (which are toxic, teratogenic and suspected carcinogens) and catalysed by weak bases, such as secondary or primary amines, pyridine or by suitable combinations of amines and carboxylic or Lewis acids under homogeneous conditions, giving considerable amounts of waste. Especially, the use of organic solvents is an important issue in *Green Chemistry*, since they are one of the major sources for volatile organic compound (VOC) emissions from the chemical industry and for this reason, the use of second generation green solvents such as water, ionic liquids, and supercritical fluids hold considerable additional promise for industrial sectors. The use of water as a solvent in organic synthesis is often surprisingly effective even for reactions which are traditionally carried out under anhydrous conditions. The Knoevenagel condensation, often carried out with water removal, could be surprisingly favoured in aqueous medium, even though the reaction involves a dehydration step. In fact, it is known that the Knoevenagel reaction is solvent dependent and that usually dipolar aprotic solvents since the 1,2-elimination step is inhibited by protic solvents.[174] Moreover, has been confirmed through ^{1}H-NMR studies in D_2O that there is an exchange between the deuterium and one methylene hydrogen (present in a malonitrile molecule) due to dissociation phenomena. According to this, it is possible to think of a mechanism involving the ionization of the reaction's nucleophile occurring in water.[175]

Over the years, many inorganic materials like complexes, clays,[176] zeolites[177] and metal oxides[178] have been used as catalysts for this reaction and in literature there are also many examples of Knoevenagel condensation reactions conducted in aqueous medium[179–181] and in most of the case, the reactions are performed in organic medium with high temperatures or quite long reaction times.[182–185]

According to all of this, the innovations in catalysis (i.e. the design and development of new superior catalysts) are constantly required in the manufacturing of chemicals.

6.3 SCHIFF-BASE METAL COMPLEXES

The imines (-C=N-) have been characterized for the first time in 1864 by Hugo Schiff and, in his honour, these groups of compounds, are known also as Schiff bases. These compounds are easily formed via the condensation of a primary amine and a carbonyl molecule. Interesting properties of this class of compounds arise when they possess more than one imine group such as hydroxyl groups (–OH), amines (–NH$_2$) or thiols (-SH) that may act as donor ligands in metal complexes having bi, tri, tetra or even higher coordination states being typically categorized as bidentate, tridentate, tetradentate, pentadentate, and hexadentate, as indicated in **Figure 99**.
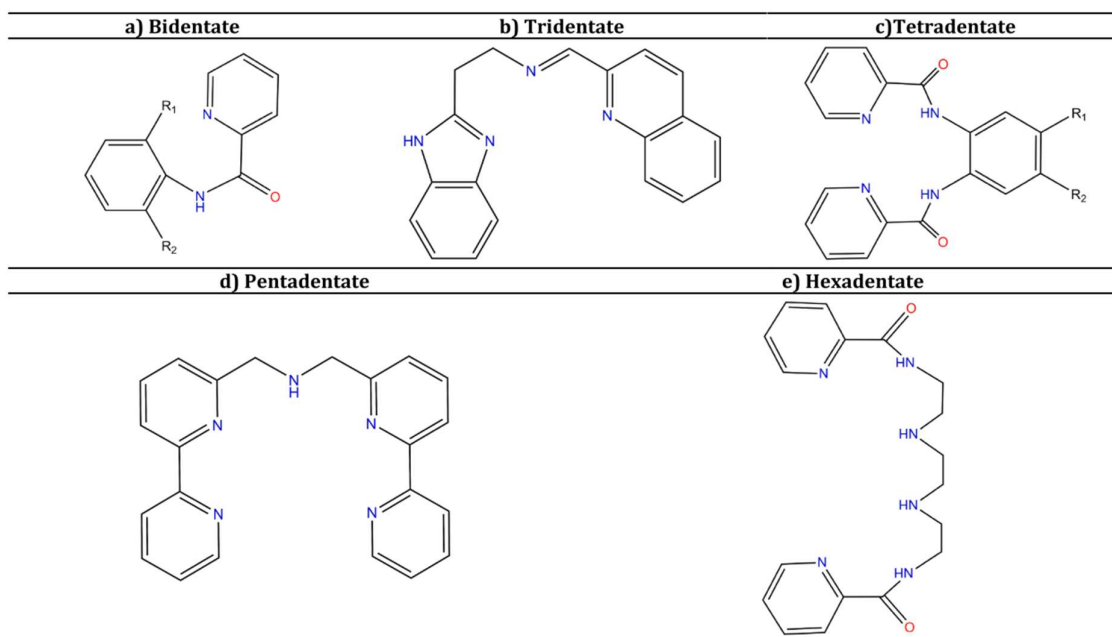
Figure 100 *- Examples of polydentate Schiff base ligands*

In fact, the majority of Schiff bases are attractive ligands since they construct complexation efficiently, with most transition metals owing to the possible tunability of the stereo-electronic structures of the final complexes varying their geometries and oxidization states.[186] These type of ligands are widely studied due to their σ donor ability towards metal cation and π acceptor properties. One of the most studied Schiff base ligands is a Salen ligand system, first reported in 1933 by Pfeiffer et al.,[187] obtained from the reaction between the salicylaldehyde and diamine derivatives. The Salen Schiff base compounds formed have a tridentate nature with 2 nitrogen and one hydroxyl groups as donor atoms. They have unique properties and versatile applications across various fields, including industry and biology but, most importantly, they possess exceptional catalytic activity for a wide range of compounds.[188] Additionally, derivatives of salicylaldehyde and phenylenediamine (salophen type), derivatives of carbonyl compounds with hydrazine/hydrazide (hydrazone type) and derivatives of carbonyl compound with thiosemicarbazide or semicarbazide (semicarbazone type) are other important examples of Schiff base organic ligands utilized in the formation of Schiff base metal complexes.[188]

More in detail, the complexes containing Schiff base ligands have been used as catalysts in various homogenous and heterogeneous reactions including polymerization, aldol condensation, Heck reaction, Henry reaction, Diels Alder reaction, Hydroformylation, Hydrosilylation, Allylic alkylation, cycloporpanation, epoxidation, oxidation and reduction reactions.[189] In fact the dimers [Cp*MCl$_2$]$_2$ (M = Ir, Ru, Rh) are often utilized as precursors to prepare a variety of novel half-sandwich complexes containing Schiff bases because of their several advantages, such as the easy preparation of starting metal precursors, high yields of

the target products, and the easy alteration of the properties of such half-sandwich complexes.[190]

The importance of these catalysts is growing, due to its high efficiency, good selectivity, mild reaction condition, reusability, and easy work-up conditions. The activity of such catalyst can be enhanced by changing the metal centre, ligand types, and ligand coordination sites. Scientific studies have noticeably confirmed that transition metal Schiff base complexes are flexible and competent catalyst for commercially important reactions and can catalyse a variety of reactions under mild experimental conditions, that is why, more research and development in the field of Schiff base metal complexes toward more eco-friendly practices would be extremely beneficial to industry and academia.

6.3.1 Hydrazone ligands

Hydrazone is a class of organic compounds belonging to Schiff base family, having the basic structure $R_1R_2C=N-NH_2$. The most general and oldest method for the synthesis of hydrazones is the reaction of an hydrazine with a carbonyl compounds.[191] The multitude of active sites is responsible for the wide physical and chemical properties of this class of compounds[192] and justify the versatile use in various fields ranging from catalytic activity[193] and medicinal chemistry[194] to supramolecular chemistry[195].

They are distinguished from other members of this class (imines, oximes, etc.) by the presence of the two interlinked nitrogen atoms that have different nature: one has an amine-like configuration while the other one has an imine structure with a C=N double bond (**Figure 100**).
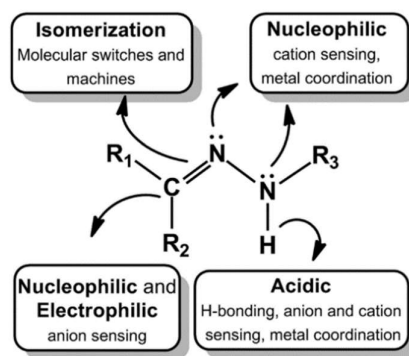

Figure 101 - *Structure and functional diversity of hydrazone functional group*

Both nitrogen atoms of the hydrazone group are nucleophilic, although the amino-type nitrogen is more reactive and additionally the acidic N-H proton can form intramolecular H-

bonding, being capable of anion sensing and even coordination with metals. The carbon atom of hydrazone group has both electrophilic and nucleophilic character and configurational isomerism of the C=N group is easily present in fact, in solution can exist in either the E or Z forms.[195]

Moreover, if another functional group is present, such as an heterocyclic pyrazolone ring, many tautomeric forms may be present in both solid and solution due to the additional acyl group (**Figure 101**).[196]
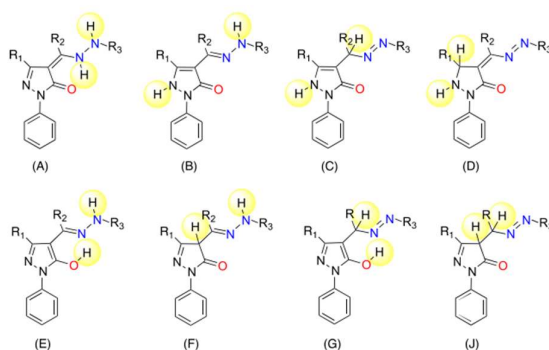
Figure 102 - *Tautomeric forms of pyrazolone-containing hydrazone derivatives*

Especially, a recent study made by this research group, confirmed the presence of a pyridine moiety in the hydrazine structure, even in the solid state, confers an unexpected zwitterionic form to the final ligand, as confirmed by its crystal structure (**Figure 102**).[40]
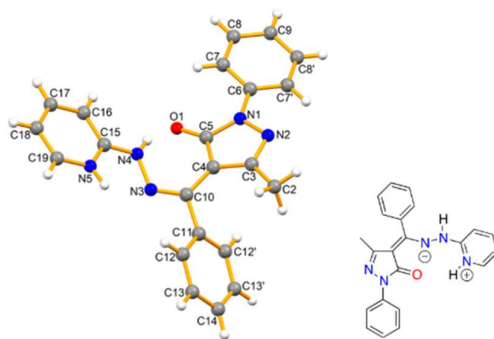
Figure 103 - *Zwitterionic form found for the pyridine derivatives of pyrazolone-containing hydrazone*

The presence of more donor atoms, together with the different ligand structures reflect different coordination environments found in the complexes which vary from metal to metal.[40] The tunability of these more sophisticated Schiff base ligands makes them a more important precursor able to achieve better and more efficient performances.

6.4 Ru(II), Rh(III) AND Ir(III) COMPLEXES

Half-sandwich complexes of platinum group metals (especially Ruthenium, Rhodium and Iridium) have an important position in organometallic chemistry due to their ability to form stable complexes with a variety of ligands.[197] Starting from the dimeric chloro bridged complexes of such metals like [{(arene)M(μ-Cl)Cl}₂] (where M= Ru and Arene= *p*-cymene; hexamethylbenzene; benzene) and [{Cp*M(μ-Cl)Cl}₂] (where Cp* = 1,2,3,4,5-pentamethyl-cyclopentadienyl and M= Rh or Ir) many complexes have been synthesized and studied for their catalytic activity in water oxidation[198], hydrogen activation[199], transfer hydrogenation[200] and aerobic alcohol oxidation[201]. In addition, their complexes are also found to be biologically active against cancer and bacteria.[202] More importantly, the reactivity of *p*-cymene-Ruthenium and Cp*-Rhodium/Iridium complexes bearing hydrazone derivatives have been quite often evaluated.[203]

Among all the transition metals, the attention has been mainly focused on ruthenium complexes since they were always used for variety of purposes including hydrogenation, oxidation, polymerization and carbon–carbon bond formation and most importantly, hydrogen-transfer.[204] Furthermore, its half-sandwich transition-metal complexes have been largely explored in organometallic and catalysis chemistry because of their good stability, diverse reactivity, and catalytic efficiency and recent reports show that the presence of Schiff base as ligands, for Ru(II) complexes, has effectiveness in many catalytic processes since it has been observed that the -NH moiety plays an important role in involving atom-transfer intermediate species.[205-206] Similarly, many Rh(I) and Rh(III) catalysts have showed promising results in favor of catalysing hydrogen transfer for hydrogenation and hydroformylation reactions.[189] Moreover, Ir(III) complexes showed important hydrogenation activity of carbonyl substrates.[207] Additionally, metal atoms like Rh(III) and Ir(III) are known for their oxidant ability[208-209] and their half-sandwich derivatives with Cp* rings have also shown great stability and remarkable catalytic activities for oxidation reactions. Other benefits are also present from the strong π-donor character of the Cp* unite which can stabilize the high oxidation states required by the reaction.[210] In addition, half-sandwich (Cp*)-Ir and (Cp*)-Rh metalacycles containing N, N'-Schiff base ligands are able to form unlocalized large organic π-conjugated bond and provide an electron rich environment, which can stabilize the necessary high-valent intermediates.[211-212]

As appear evident, the effect of ligand on the structure and reactivity of transition metal complexes plays an important role in catalysis. Furthermore, in the pyrazolone-containing hydrazone ligands the presence of one additional acyl group (C=O) confers to the final compounds more flexibility and versatility. Accordingly, such hydrazones act as good polydentate chelating agents that can form a variety of complexes. Unfortunately, only limited

reports are available for catalytic activity of hydrazone-Schiff base complexes and, as far as we know, no studies have been performed for their pyrazolone-containing Schiff base derivatives. Hence, synthesis of new with hydrazone Schiff base ligands and their related transition metal complexes is of great importance.

Chapter 7: Ru(II)-*p*-cymene complexes containing pyrazolone-based hydrazones ligands as suitable catalysts for tandem deacetalization–Knoevenagel condensation reactions

7.1 Aim of the work

In this chapter, the syntheses of new Ruthenium(II)-*p*-cymene derivatives containing several different pyrazolone-based hydrazones ligands are reported. All the compounds have been completely characterized and the crystallographic studies confirmed the pseudo-octahedral coordination geometry possessed by the complexes and, most importantly, how the presence of either a neutral or zwitterionic ligand affects their coordination environment. In fact the polydentate pyrazolone-based hydrazones ligands may have either κ-N,O or -N,N binding mode. The complexes have been evaluated form a catalytic point of view toward a one-pot tandem reaction having two steps: a deacetalization reaction followed by the Knoevenagel condensation. The formation of a carbon–carbon bond is the key to produce a wide variety of advanced products, with great impact in every aspect of the human life and, as has been underlined introductory chapters, the Knoevenagel condensation reaction is one of the most important methodologies for this purpose. Moreover, to have a process which allows to obtain, through a tandem reaction, such adducts starting from different precursors represents a fundamental achievement for the organic chemistry synthesis. For this purpose, the novel organometallic compounds may act as bifunctional catalyst having the synergistic effect of both the pyrazolone-based hydrazones ligands (acting as a Lewis base) and the metal centre (behaving as Lewis acid).

7.1.1 Materials and methods

The dimer [(*p*-cymene)RuCl$_2$]$_2$, 1-Fenil-3-metil-5-pirazolone and the hydrazines were purchased from Aldrich. All other materials were obtained from commercial sources and were used as received. IR spectra were recorded from 4000 to 200 cm^{-1} on a Perkin-Elmer Spectrum 100 FT-IR instrument. ^{1}H, ^{13}C-NMR, {^{1}H-^{1}H}-COSY NMR, {^{1}H-^{13}C}-HSQC and {^{1}H-^{13}C}-HMBC spectra were recorded with a 500 Bruker Ascend (500.1 MHz for ^{1}H, 100 MHz for ^{13}C). Referencing is relative to TMS (^{1}H). Positive and negative ion electrospray ionisation mass spectra (ESI-MS) were obtained on a Series 1100 MSI detector HP spectrometer using methanol as the mobile phase. Solutions (3 mg/mL) analysis were prepared using reagent-grade methanol. Masses and intensities were compared to those calculated using IsoPro Isotopic Abundance Simulator, version 2.1.28. Melting points were recorded on an STMP3

Stuart scientific instrument and a capillary apparatus. Samples for microanalysis were dried in vacuo to constant weight (20 °C, ca. 0.1 Torr) and analysed on a Fisons Instruments 1108 CHNS-O elemental analyzer.

7.1.2 Catalytic procedure for one-pot tandem deacetalization–Knoevenagel condensation reactions

1.0 mmol of benzaldehyde dimethyl acetal (152 µL), 2.0 mmol of malononitrile (132 mg) and 1 mol% of Ru-catalyst (6.9 mg of **29**, 6.9 mg of **30**, 7.4 mg of **31**, 7.2 mg of **32**, 5.7 mg of **33** and 6.4 mg of **34**) were placed in a 2 mL glass vessel. The glass vial was capped and heated at 75 °C for the required time. Afterwards the mixture was extracted with chloroform and the extracts were dried over anhydrous sodium sulphate. The crude product was obtained after evaporation of the solvent and the final product yield was determine by ^{1}H NMR in CDCl$_3$. This yield was calculated according to the previously reported method.[213]

7.1.3 General procedure for synthesis of ligands

HL^{17} [(E)-3-methyl-4-(1-(2-(4-nitrophenyl)hydrazineylidene)-2-phenylethyl)-1-phenyl-1H-pyrazol-5-ol]. The proligand **HL^{17}** was synthesized from (5-hydroxy-3-methyl- 1-phenyl-1H-pyrazol-4-yl)2phenylethanone (292 mg, 1 mmol) and 4-nitrophenylhydrazine (155 mg, 1.01 mmol) following the general procedure (80 °C, reaction time 4 h).[40] The product precipitated out of the hot solution as the reaction proceeded. After cooling, the product was filtered and dried to give a brown solid (332 mg, yield 78%) was identified as the pure compound **HL^{17}** (**Figure 103**). It is completely soluble in DMSO, DMF, acetone, CH$_3$CN, chlorinated solvents, and alcohols and insoluble in H$_2$O, n-hexane, and petroleum ether.
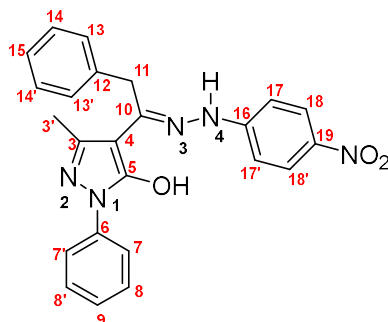
Figure 104 - *Structure of ligand HL^{17}*

Anal. Calcd. for C$_{24}$H$_{21}$N$_5$O$_3$: C, 67.44; H, 4.95; N, 16.38; Found: C, 67.14; H, 4.94; N, 16.23. mp: 219-220°C. IR (cm^{-1}): 3183 w ν(N-H); 3062w, 2986w, 2924w ν(unsaturated C-H); 1615m, 1592s, 1529m, 1504m, 1490s ν(C=O, C=C, C=N); 1451w, 1440w, 1425w, 1400w,

1376m, 1325s, 1309s, 1274s, 1216m, 1176m, 1125w, 1107m; 691m, 652w, 632w, 617w, 555w, 509w, 494w, 475w, 436w, 417w, 396w, 379w, 356w, 338w, 315w, 288w, 245w, 228w, 212w, 203w. ^{1}H-NMR (CDCl$_3$, 293 K): δ 2.43 (s, 3H, C(3')*H*), 4.14 (s, 2H, C(11)*H*), 6.52 (s, 1H, N-H), 6.65 (d, 2H, C(17-17')*H*), 7.17 (d, 2H, C(13-13')*H*), 7.23-7.30 (m, 4H), 7.46 (t, 2H, C(8-8')*H*), 8.00 (d, 2H, C(7-7')*H*), 8.07 (d, 2H, C(18-18')*H*), 12.42 (br, 1H, O-H).^{13}C{^{1}H}-NMR (CDCl$_3$, 293 K): δ 16.7 [*C*(3')], 33.7 [*C*(11)], 100.8 [*C*(17-17')], 111.9 [*C*(4)], 119.5 [*C*(7-7')], 125.1 [*C*(9)], 125.9 [*C*(18-18')], 127.6 [*C*(15)], 127.9 [*C*(13-13')], 128.9 [*C*(8-8')], 129.3 [*C*(14-14')], 134.2 [*C*(12)], 141.8 [*C*(6)], 147.0 [*C*(10)], 151.4 [*C*(19)], 165.3 [*C*(3)], 167.0 [*C*(5)]. ESI-MS(-) CH$_3$OH (m/z [relative intensity, %]): 426 [100] [L^{17}]$^-$.

HL^{18} [(E)-3-methyl-4-(1-(2-(3-nitrophenyl)hydrazineylidene)-2-phenylethyl)-1-phenyl-1H-pyrazol-5-ol]. The proligand **HL^{18}** was synthesized from (5-hydroxy-3-methyl- 1-phenyl-1H-pyrazol-4-yl)2phenylethanone (292 mg, 1 mmol) and 3-nitrophenylhydrazine (125 mg, 1.01 mmol) following the procedure of previous compound. The light yellow solid (218 mg, yield 51%) was identified as the pure compound **HL^{18}** (**Figure 104**). It is completely soluble in DMSO, DMF, acetone, chlorinated solvents; slightly soluble in CH$_3$CN and alcohols and insoluble in H$_2$O, n-hexane, and petroleum ether.

Figure 105 - Structure of ligand HL^{18}

Anal. Calcd. for C$_{24}$H$_{21}$N$_5$O$_3$: C, 67.44; H, 4.95; N, 16.38; Found: C, 67.17; H, 4.87; N, 16.31. mp: 221-222 °C. IR (cm^{-1}): 3193 w v(N-H); 3128w, 3093w, 3061w, 3061w, 3032w v(unsaturated C-H); 1615s, 1594m, 1577m, 1525vs, 1488s v(C=O, C=C, C=N); 1472m, 1455w, 1424w, 1380m, 1349s, 1319w, 1275w, 1248w, 1220w, 1174w, 1144w, 1089w, 1047w; 694m, 681w, 673w, 657w, 645w, 629w, 601w, 552w, 531w, 503w, 468w, 417w, 376w, 354w, 281w, 271w, 246w, 227w, 208w. ^{1}H-NMR (CDCl$_3$, 293 K): δ 2.45 (s, 3H, C(3')*H*), 4.21 (s, 2H, C(11)*H*), 6.12 (s, 1H, N-H), 6.98 (dd, 1H, C(17')*H*), 7.17 (d, 2H, C(13-13')*H*), 7.20-7.26 (m, 4H), 7.30 (d, 2H, C(14-14')*H*), 7.34 (t, 1H, C(18')*H*), 7.45 (t, 2H, C(8-8')*H*), 7.48 (t, 1H, C(19)*H*), 7.76 (dd, 1H, C(17)*H*), 8.02 (d, 2H, C(7-7')*H*), 12.48 (br, 1H, O-H).^{13}C{^{1}H}-NMR (CDCl$_3$, 293 K): δ 16.8 [*C*(3')], 33.7 [*C*(11)], 100.7 [*C*(4)], 107.9 [*C*(19)], 116.4 [*C*(17)], 118.5 [*C*(17')], 119.4 [*C*(7-7')], 124.9 [*C*(9)], 127.5 [*C*(5)], 128.0 [*C*(13-13')], 128.8 [*C*(8-8')], 129.3 [*C*(14-14')], 130.3 [*C*(18')], 134.4 [*C*(12)], 138.7 [*C*(6)], 146.7 [*C*(3)],

147.3 [C(16)], 149.1 [C(18)], 165.7 [C(5)], 167.3 [C(10)]. ESI-MS(-) CH₃OH (m/z [relative intensity, %]): 426 [100] [L¹⁸]⁻.

HL¹⁹ [(E)-4-(1-(2-(2,4-dinitrophenyl)hydrazineylidene)-2-phenylethyl)-3-methyl-1-phenyl-1H-pyrazol-5-ol]. The proligand **HL¹⁹** was synthesized from (5-hydroxy-3-methyl- 1-phenyl-1H-pyrazol-4-yl)2phenylethanone (292 mg, 1.1 mmol) and 2,4-dinitrophenylhydrazine (236 mg, 1.01 mmol) following the procedure of previous compound. The light yellow solid (425 mg, yield 89%) was identified as the pure compound **HL¹⁹** (**Figure 105**). It is completely soluble in DMSO, DMF, acetone, chlorinated solvents, CH₃CN and alcohols and insoluble in H_2O, n-hexane, and petroleum ether.
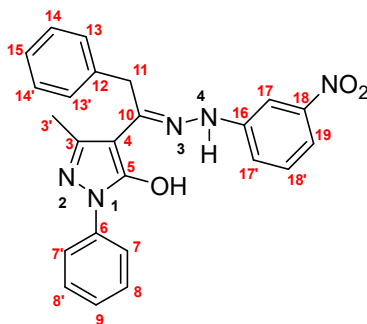

Figure 106 - Structure of ligand HL¹⁹

Anal. Calcd. for $C_{24}H_{20}N_6O_5$: C, 61.01; H, 4.27; N, 17.79; Found: C, 61.08; H, 4.33; N, 17.63. mp: 203-204 °C. IR (cm⁻¹): 3277 w v(N-H); 3113w, 3055w, 3027w, 2990w, 2955w v(unsaturated C-H); 1611vs, 1592vs, 1525m, 1495m, 1456w, 1420w, 1403w v(C=O, C=C, C=N); 1366 s, 1337vs, 1313s, 1269m, 1235w, 1208w, 1177w, 1142w, 1119w, 1063w; 691m, 649w, 634w, 595w, 565w, 508w, 484m, 435w, 416w, 398w, 355w, 331w, 301w, 280w, 253w, 221m, 204w. ¹H-NMR (CDCl₃, 293 K): δ 2.50 (s, 3H, C(3')H), 4.21 (s, 2H, C(11)H), 7.18 (d, 1H, C(17')H), 7.23 (d, 2H, C(13-13')H), 7.27-7.34 (m, 4H, C(13-13')H, C(14-14')H and C(15)H), 7.48 (t, 2H, C(8-8')H), 7.98 (d, 2H, C(7-7')H), 7.45 (t, 2H, C(8-8')H), 8.22 (t, 1H, C(18')H), 9.08 (s, 1H, C(18)H), 10.18 (sbr, 1H, N-H), 12.46 (br, 1H, O-H).¹³C{¹H}-NMR (CDCl₃, 293 K): δ 16.3 [C(3')], 34.4 [C(11)], 100.9 [C(4)], 114.3 [C(17')], 120.0 [C(7-7')], 123.4 [C(18)], 125.8 [C(9)], 127.9 [C(15)], 128.0 [C(13-13')], 129.0 [C(8-8')], 129.6 [C(14-14')], 130.3 [C(18')], 132.8 [C(6)], 138.1, 138.7 [C(17) and C(19)], 145.5 [C(5)], 146.8 [C(3)], 161.0 [C(16)], 162.5 [C(10)]. ESI-MS(-) CH₃OH (m/z [relative intensity, %]): 471 [100] [L¹⁹]⁻.

HL²⁰ [(E)-3-methyl-1-phenyl-4-(2-phenyl-1-(2-(4-(trifluoromethyl)-phenyl)-hydrazine-ylidene)-ethyl)-1H-pyrazol-5-ol]. The proligand **HL²⁰** was synthesized from (5-hydroxy-3-methyl- 1-phenyl-1H-pyrazol-4-yl)2phenylethanone (292 mg, 1 mmol) and 4-trifluoromethylphenylhydrazine (178 mg, 1.01 mmol) following the procedure of previous compound. The white solid (265 mg, yield 59%) was identified as the pure compound **HL²⁰** (**Figure 106**). It is completely soluble in DMSO, DMF, acetone, chlorinated solvents, CH₃CN and alcohols and insoluble in H_2O, n-hexane, and petroleum ether.
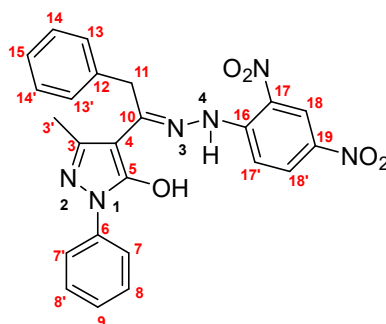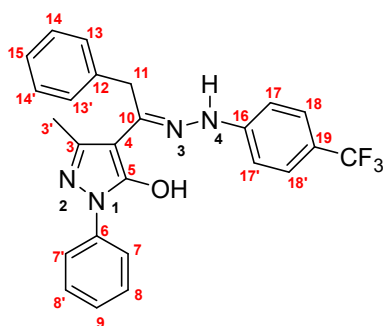
Figure 107 - *Structure of ligand HL²⁰*

Anal. Calcd. for $C_{25}H_{21}F_3N_4O$: C, 66.66; H, 4.70; N, 12.65; Found: C, 66.20; H, 4.60; N, 12.70. mp: 195-196 °C. IR (cm⁻¹): 3214w v(N−H), 3063w, 3130wbr, 2700wbr v(unsaturated C−H), 1619vs, 1590vs, 1534s, 1495s, 1488vs v(C=O, C=C, C=N), 1327vs, 1317vs, 1112vs, 1064s; 693vs, 652m, 637w, 662s, 616s, 599m, 582w, 536w, 518w, 508w, 499s, 479w, 432w, 405w, 392w, 362w, 349w, 330w, 304w, 293w, 265w, 248w, 225w. ¹H-NMR (CDCl₃, 293 K): δ 2.41 (s, 3H, C(3')*H*), 4.15 (s, 2H, C(11)*H*), 6.44 (s, 1H, N-H), 6.68 (d, 2H, C(17-17')*H*), 7.16 (d, 2H, C(13-13')*H*), 7.23 (t, 1H, C(9)*H*), 7.25-7.30 (m, 3H), 7.42 (d, 2H, C(18-18')*H*), 7.45 (t, 2H, C(8-8')*H*), 7.99 (d, 2H, C(7-7')*H*), 12.40 (br, 1H, O-H).¹³C{¹H}-NMR (CDCl₃, 293 K): δ 16.7 [*C*(3')], 33.5 [*C*(11)], 100.1 [*C*(4)], 112.7 [*C*(17-17')], 119.6 [*C*(7-7')], 123.2 [*C*(20)], 123.6 [*C*(19)], 125.0 [*C*(9)], 126.7 [*C*(18-18')], 127.4 [*C*(15)], 127.9 [*C*(13-13')], 128.9 [*C*(8-8')], 129.2 [*C*(4-4')], 134.4 [*C*(12)], 138.5 [*C*(6)], 147.2 [*C*(16)], 148.9 [*C*(3)], 165.5 [*C*(10)], 167.9 [*C*(5)]. ESI-MS (-) CH₃OH (m/z [relative intensity, %]): 449 [100] [L²⁰]⁻.

HL²¹ **[(E)-3-methyl-1-phenyl-4-(1-(2-(pyridin-2-yl)hydrazineylidene)ethyl)-1H-pyrazol-5-ol].** The proligand **HL²¹** was synthesized from (5-hydroxy-3-methyl- 1-phenyl-1H-pyrazol-4-yl)ethanone (216 mg, 1 mmol) and 2-hydrazinopyridine (110 mg, 1.01 mmol) following the procedure of previous compound. The light yellow solid (178 mg, yield 58%) was identified as the pure compound **HL²¹** (**Figure 107**). It is completely soluble in DMSO, DMF, acetone, chlorinated solvents, CH₃CN; slightly soluble in alcohols and insoluble in H₂O, n-hexane, and petroleum ether.

Figure 108 - *Structure of ligand HL²¹*

Anal. Calcd. for $C_{17}H_{17}N_5O$: C, 66.43; H, 5.58; N, 22.79; Found: C, 66.25; H, 5.40; N, 22.60. mp: 213-214°C. IR (cm⁻¹): 3152w v(N-H); 3075w, 2921w v(unsaturated C-H); 1615m, 1628m, 1591s, 1537m, 1503w, 1487m, 1462m, 1443m v(C=O, C=C, C=N); 1409w, 1373s, 1356s,

1309s, 1285m, 1253m, 1207m, 1172w, 1162w, 1151w, 1103w, 1051w, 1043m, 1024m, 994m; 687s, 651m, 630w, 602m, 548m, 511s, 469w, 407w, 392m, 377w, 357m, 284w, 254w, 247m, 229m, 212w, 202m. ^{1}H-NMR (DMSO-d_6, 293 K): δ 2.37 (s, 3H, C(11)H), 2.48 (s, 3H, C(3')H), 6.78 (d, 1H, C(13)H), 6.89 (t, 1H, C(15)H), 7.12 (t, 1H, C(9)H), 7.39 (t, 2H, C(8-8')H), 7.67 (t, 1H, C(14)H), 8.01 (d, 2H, C(7-7')H), 8.18 (d, 1H, C(16)H), 9.34 (br, 1H, O-H).^{13}C{^{1}H}-NMR (DMSO-d_6, 293 K): δ 14.9 [C(11)], 17.3 [C(3')], 97.5 [C(4)], 108.4 [C(13)], 116.8 [C(15)], 118.4 [C(7-7')], 124.1 [C(9)], 129.1 [C(8-8')], 138.6 [C(14)], 139.7 [C(6)], 147.7 [C(10)], 148.3 [C(16)], 157.5 [C(12)], 165.4 [C(5)]. ESI-MS(-) CH$_3$OH (m/z [relative intensity, %]): 306 [100] [L^{21}]$^-$.

HL^{22} [(E)-5-methyl-2-phenyl-4-(1-(2-(pyridin-2-yl)hydrazineylidene)heptyl)-2,4-dihydro-3H-pyrazol-3-one]. The proligand **HL^{22}** was synthesized from (5-hydroxy-3-methyl- 1-phenyl-1H-pyrazol-4-yl)hexanone (286 mg, 1 mmol) and 2-hydrazinopyridine (110 mg, 1.01 mmol). The methanolic solution has been stirred at reflux for 6 hours after that the reaction mixture has been dried at reduced pressure and purified through liquid chromatography with hexane:ethylacetate 70:30. The light yellow solid (256 mg, yield 68%) was identified as the pure compound **HL^{22}** (**Figure 108**). It is completely soluble in DMSO, DMF, acetone, chlorinated solvents and CH$_3$CN; slightly soluble in alcohols and insoluble in H$_2$O, n-hexane and petroleum ether.
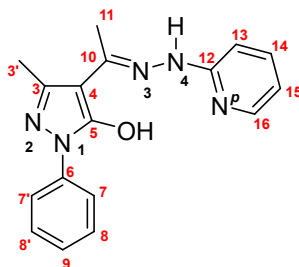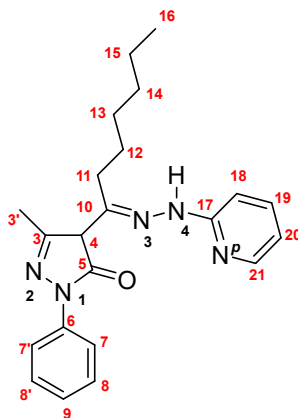

Figure 109 - *Structure of ligand HL^{22}*

Anal. Calcd. for C$_{22}$H$_{27}$N$_5$O: C, 70.00; H, 7.21; N, 18.55; Found: C, 69.87; H, 7.20; N, 18.32. mp: 131-132 °C. IR (cm^{-1}): 3174w ν(N-H); 3060w, 2955w, 2922w, 2852w ν(unsaturated and aliphatic C-H); 1738w, 1626s, 1593vs, 1580s, 1537s, 1499s, 1485m, 1462m, 1435s, 1402w, 1374vs ν(C=O, C=C, C=N); 1315m, 1290w, 1235w, 1207w, 1155w, 1096w, 1068w, 1047w, 1027m, 1007m, 997m; 690s, 651m, 626m, 599m, 550m, 520w, 509m, 471w, 459w, 409w, 395w, 383w, 356w, 301w, 253w, 225w. ^{1}H-NMR (CDCl$_3$, 293 K): δ 0.89 (m, 3H, H16), 1.30 (m, 4H, H15-14), 1.46 (m, 2H, H13), 1.67 (m, 2H, H12), 2.45 (s, 3H, H3'), 2.85 (t, 2H, H11), 6.75 (d, 1H, H18), 6.93 (t, 1H, H20), 7.17 (t, 1H, H9), 7.41 (t, 2H, H8-8'), 7.63 (t, 1H, H19), 8.01 (d, 2H, H7-7'), 8.24 (d, 1H, H21), 12.54 (br, 1H, N-H).^{13}C{^{1}H}-NMR (CDCl$_3$, 293 K): δ

13.9 [$C(16)$], 16.8 [$C(3')$], 22.4 [$C(15)$], 28.1 [$C(11)$], 29.0 [$C(12)$], 29.5 [$C(13)$], 31.3 [$C(14)$], 98.7 [$C(10)$], 107.0 [$C(18)$], 117.3 [$C(20)$], 119.4 [$C(7-7')$], 124.6 [$C(9)$], 128.7 [$C(8-8')$], 138.9 [$C(6)$], 139.1 [$C(19)$], 146.9 [$C(3)$], 147.7 [$C(21)$], 158.2 [$C(17)$], 165.6 [$C(5)$], 171.0 [$C(4)$]. ESI-MS (-) CH$_3$OH(m/z [relative intensity, %]): 376 [100] [L[22]]⁻.

7.1.4 General procedure for synthesis of complexes

[**Ru(*p*-cymene)(L[17])Cl] (29).** **HL[17]** (85 mg, 0.2 mmol) and KOH (11 mg, 0.2 mmol) were dissolved in CH$_3$OH (5 mL). After 1 h stirring at room temperature the dimer [Ru(*p*-cymene)(Cl)$_2$]$_2$ (61 mg, 0.1 mmol) was added, and the solution was stirred for 5 h at room temperature. The red precipitate has been filtered off and dried. The product (62 mg, yield 44%) was identified as the pure compound **29** (**Figure 109**). It is completely soluble in DMSO, acetone, chlorinated solvent, acetonitrile, and toluene; insoluble in H$_2$O and n-hexane.
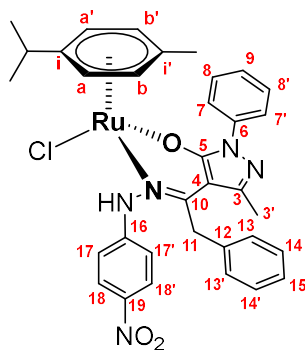

Figure 110 - *Structure of compound* ***29***

Anal. Calcd. for C$_{34}$H$_{34}$ClN$_5$ORu: C, 58.57; H, 4.92; N, 10.05; Found: C, 58.62; H, 4.88; N, 10.12. mp: 208-211 °C. IR (cm⁻¹): 3222m v(N-H); 3107w, 3038w, 3064w, 3028w v(unsaturated C-H); 1589s, 1567s, 1531m, 1518w, 1484vs, 1455 m, 1445m v(C=O, C=C, C=N); 1414w, 1400w, 1376m, 1351w, 1318m, 1304vs, 1275s, 1224w, 1180m, 1107s, 1051w, 1030m, 1004m; 426w v(Ru-O), 236m v(Ru-Cl). ¹H-NMR (CDCl$_3$, 248 K): δ 1.12d, 1.15d (6H, -CH(C*H*)$_3$), 2.07 (s, 3H, -C*H*$_3$ of *p*-cymene), 2.33 (s, 3H, C(3')*H*), 2.70 (m, 1H, C*H*(CH$_3$)$_2$ of *p*-cymene), 4.02 (dd, 2H, C(11)*H*), 4.87 d, 5.14 d, 5.51 d, 5.64 d (4H, AA′BB′ system, CH$_3$-C$_6$H$_4$-CH(CH$_3$)$_2$ of *p*-cymene, ³J = 6 Hz), 6.77dd, 7.04dd (2H, C(17-17')*H*), 7.06 (d, 2H, C(13-13')*H*), 7.16-7.28 (m, 4H, C(14-14')*H*, C(9)*H* and C(15)*H*), 7.44 (t, 2H, C(8-8')*H*), 8.00 (d, 2H, C(7-7')*H*), 8.25 dd, 8.41 dd (2H, C(18-18')*H*), 8.27 (s, 1H, N-H).¹³C{¹H}-NMR (CDCl$_3$, 293 K): δ 17.1 [$C(3')$], 18.1 [-C*H*$_3$ of *p*-cymene], 21.2, 22.7 [-CH(C*H*$_3$)$_2$ of *p*-cymene], 30.7 [C*H*(CH$_3$)$_2$ of *p*-cymene], 35.2 [$C(11)$], 78.6, 81.1, 81.7, 83.8 [Ca,Ca',Cb,Cb' of *p*-cymene], 95.2, 100.9 [Ci and Ci'], 103.6 [$C(4)$], 120.2 [$C(7-7')$], 125.1 [$C(14-14')$], 126.5,

126.8 [C(18-18') and C(17-17')], 125.5 [C(9)], 127.8 [C(13-13')], 128.6 [C(8-8')], 135.3 [C(12)], 138.9 [C(6')], 140.5 [C(16)], 147.5 [C(10)]. ESI-MS(+) CH_3OH (m/z [relative intensity, %]): 661 [85] [Ru(p-cymene)(L[17])][+].

[Ru(p-cymene)(L[18])Cl] (30). HL[18] (85 mg, 0.2 mmol) and KOH (11 mg, 0.2 mmol) were dissolved in CH_3OH (5 mL). After 1 h stirring at room temperature the dimer [Ru(p-cymene)(Cl)$_2$]$_2$ (62 mg, 0.1 mmol) was added and the solution was stirred for 5 h at room temperature. The red precipitate has been filtered off and dried. The red product (90 mg, yield 81%) was identified as the pure compound **30** (**Figure 110**). It is completely soluble in DMSO, acetone, chlorinated solvent, and acetonitrile; slightly soluble in toluene; insoluble in H_2O and n-hexane.
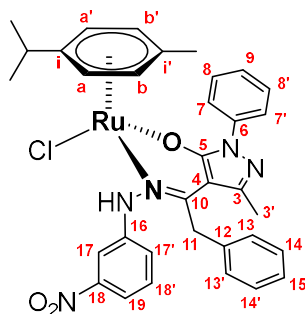

Figure 111 - *Structure of compound 30*

Anal. Calcd. for $C_{34}H_{34}ClN_5ORu$: C, 58.57; H, 4.92; N, 10.05; Found: C, 55.23; H, 4.75; N, 10.22. mp: 110-111 °C. IR (cm^{-1}): 3239w v(N-H); 3061w, 2961w, 2925w, 2870w v(unsaturated C-H); 1591m, 1569s, 1524vs, 1496m, 1479s, 1445m, v(C=O, C=C, C=N); 1374m, 1347s, 1252w, 1076w, 1054w, 1028w, 1009w, 510w v(Ru-O), 270w v(Ru-Cl). ^{1}H-NMR (CDCl$_3$, 293 K): δ 1.09 d, 1.17 d (6H, -CH(CH)$_3$), 2.04 (s, 3H, -CH_3 of p-cymene), 2.35 (s, 3H, C(3')H), 2.66 (m, 1H, CH(CH$_3$)$_2$ of p-cymene), 4.01-4.22 (m, 2H, C(11)H), 4.63, 5.11, 5.50 (4H, AA'BB' system, CH$_3$-C$_6$H$_4$-CH(CH$_3$)$_2$ of p-cymene), 7.08 (d, 2H, C(13-13')H), 7.06 (d, 2H, C(13-13')H), 7.15 (t, 1H, C(18')H), 7.19-7.26 (m, 4H, C(14-14')H, C(15)H and C(9)H), 7.43 (t, 2H, C(8-8')H), 7.50 (m, 1H, C(19)H), 7.69 (sbr, 1H,C(17)H), 7.81 (d, 2H, C(17')H), 8.00 (m, 2H, C(7-7')H).^{13}C{^{1}H}-NMR (CDCl$_3$, 293 K): δ 17.0 [C(3)], 21.2, 22.9 [-CH(CH$_3$)$_2$ of p-cymene], 30.7 [-CH$_3$ of p-cymene], 35.4 [C(11)], 80.3, 80.6, 81.3, 83.3 [Ca, Ca', Cb, Cb' of p-cymene], 96.1, 96.8 [Ci and Ci'], 101.1 [C(4)], 114.9 [C(17')], 116.2 [C(17)], 119.4 [C(7-7')], 126.6 [C(18')], 127.3 [C(15)], 127.9 [C(13-13')], 128.6 [C(8-8')], 128.9, 129.4 [C(14-14')], 130.1 [C(9)], 130.5 [C(19)], 135.6 [C(12)], 138.9 [C(6)], 147.5 [C(3)], 149.5 [C(18)], 162.0 [C(5)], 165.6 [C(10)]. ESI-MS(+) CH_3OH (m/z [relative intensity, %]): 661 [100] [Ru(p-cymene)(L[18])][+].

[Ru(p-cymene)(L[19])Cl] (31). HL[19] (94 mg, 0.2 mmol) and KOH (11 mg, 0.2 mmol) were dissolved in CH_3OH (5 mL). After 1 h stirring at room temperature the dimer [Ru(p-

cymene)(Cl)$_2$]$_2$ (62 mg, 0.1 mmol) was added, and the solution was stirred for 5 h at room temperature. The red precipitate has been filtered off and dried. The product (83 mg, yield 56%) was identified as the pure compound **31** (**Figure 111**). It is completely soluble in DMSO, acetone, chlorinated solvent, acetonitrile, and toluene; insoluble in H$_2$O and n-hexane.
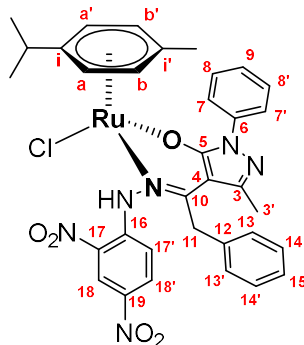

Figure 112 - *Structure of compound 31*

Anal. Calcd. for C$_{34}$H$_{33}$ClN$_6$O$_5$Ru: C, 55.02; H, 4.48; N, 11.32; Found: C, 55.56; H, 4.61; N, 11.04. mp: 143-144 °C. IR (cm^{-1}): 3068w v(N-H); 2959w, 2923w, 2868w v(unsaturated C-H); 1615m, 1588m, 1568s, 1520m, 1483s, 1455m, 1423m v(C=O, C=C, C=N); 1377m, 1331vs, 1308m, 1269m, 1227m, 1135m, 113m, 1061m, 1027m, 1007m; 466w v(Ru-O), 269w v(Ru-Cl). ^{1}H-NMR (CDCl$_3$, 293 K): δ 1.26 d, 1.28 d (6H, -CH(C*H*)$_3$), 2.03 (s, 3H, -C*H*$_3$ of *p*-cymene), 2.33 (s, 3H, C(3')*H*), 2.81 (m, 1H, C*H*(CH$_3$)$_2$ of *p*-cymene), 3.68d, 4.25d (2H, C(11)*H*), 4.18, 5.17, 5.31, 5.41 (4H, AA′BB′ system, CH$_3$-C$_6$H$_4$-CH(CH$_3$)$_2$ of *p*-cymene, ^{3}J = 6 Hz), 7.01 (d, 2H, C(7-7')*H*), 7.21 (t, 1H, C(9)*H*), 7.25-7.27 (m, 3H, C(8-8')*H* and C(15)*H*), 7.45 (t, 2H, C(14-14')*H*), 7.94 (d, 2H, C(13-13')*H*), 8.09 (d, 1H, C(18)*H*), 8.30 (d, 1H, C(17')*H*), 9.13 (d, 1H, C(18)*H*), 10.40 (s, 1H, N-H).^{13}C{^{1}H}-NMR (CDCl$_3$, 293 K): δ 17.4 [*C*(3')], 18.8 [-CH$_3$ of *p*-cymene], 21.3, 23.3 [-CH(*C*H$_3$)$_2$ of *p*-cymene], 30.9 [*C*H(CH$_3$)$_2$ of *p*-cymene], 36.0 [*C*(11)], 79.8, 82.3, 82.8, 86.3 [*C*a, *C*a', *C*b, *C*b' of *p*-cymene], 98.4, 101.5 [*C*i and *C*i'], 102.3 [*C*(4)], 118.0 [*C*(18')], 120.7 [*C*(13-13')], 123.3 [*C*(18)], 125.5 [*C*(9)], 127.5 [*C*(15)], 128.7 [*C*(14-14')], 129.5 [*C*(8-8')], 130.2 [*C*(17')], 134.8 [*C*(12)], 137.9, 138.7 [*C*(17) and *C*(19)], 145.7 [*C*(16)], 147.9 [*C*(3)], 162.0 [*C*(6)], 171.9 [*C*(10)]. ESI-MS(+) CH$_3$OH (m/z [relative intensity, %]): 707 [100] [Ru(*p*-cymene)(L^{19})]$^+$.

[Ru(*p*-cymene)(L^{20})Cl] (32). HL^{20} (90 mg, 0.2 mmol) and KOH (11 mg, 0.2 mmol) were dissolved in CH$_3$OH (5 mL). After 1 h stirring at room temperature the dimer [Ru(*p*-cymene)(Cl)$_2$]$_2$ (62 mg, 0.1 mmol) was added, and the solution was stirred for 5 h at room temperature. The red precipitate has been filtered off and dried. The product (50 mg, yield 70%) was identified as the pure compound **32** (**Figure 112**). It is completely soluble in DMSO, acetone, chlorinated solvent, acetonitrile, and toluene; insoluble in H$_2$O and n-hexane.
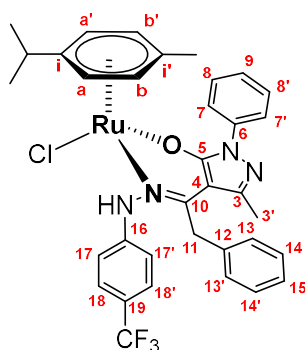
Figure 113 - *Structure of compound 32*

Anal. Calcd. for $C_{35}H_{34}ClF_3N_4ORu$: C, 58.37; H, 4.76; N, 7.78; Found: C, 58.30; H, 4.84; N, 7.74. mp: 222-224 °C. IR (cm^{-1}): 3264wbr ν(N-H); 3070w, 3025w, 2969w, 2926w, 2876w ν(unsaturated C-H); 1613m, 1592m, 1573vs, 1524m, 1495s, 1470s, 1445m ν(C=O, C=C, C=N); 1374m, 1315vs, 1265m, 1184m, 1154m, 1099vs, 1063s, 1029m, 1008m; 511w ν(Ru-O), 262w ν(Ru-Cl). ^{1}H-NMR (CDCl$_3$, 293 K): δ 1.11 d, 1.16 d (6H, -CH(C*H*)$_3$), 2.06 (s, 3H, -C*H*$_3$ of *p*-cymene), 2.32 (s, 3H, C(3')*H*), 2.68 (m, 1H, C*H*(CH$_3$)$_2$ of *p*-cymene), 3.97 d, 4.24 d (2H, C(11)*H*), 4.73, 5.11, 5.44, 5.53 (4H, AA'BB′ system, CH$_3$-C$_6$H$_4$-CH(CH$_3$)$_2$ of *p*-cymene), 7.01 (sbr, 1H, N-H), 7.08 (d, 2H, C(14-14')*H*), 7.15-7.26 (m, 4H, C(13-13')*H*, C(15)*H* and C(9)*H*), 7.42 (t, 2H, C(8-8')*H*), 7.64 (sbr, 4H, C(18-18')*H* and C(17-17')*H*), 8.04 (d, 2H, C(7-7')*H*).^{13}C{^{1}H}-NMR (CDCl$_3$, 293 K): δ 17.1 [*C*(3')], 18.5 [-CH$_3$ of *p*-cymene], 21.0, 22.8 [-CH(*C*H$_3$)$_2$ of *p*-cymene], 30.6 [-*C*H(CH$_3$)$_2$ of *p*-cymene], 35.2 [*C*(11)], 80.8, 83.1 [*C*(a-a') and *C*(b-b')], 100.8 [*C*(4)], 120.0 [*C*(7-7')], 124.8 [*C*(9)], 126.6 [*C*(15)], 127.5 [*C*(17-17') and *C*(18-18')], 127.8 [*C*(14-14')], 128.6 [*C*(18-18')], 128.9 [*C*(13-13')], 135.6 [*C*(12)], 139.1 [*C*(6)], 147.3 [*C*(3)], 149.2 [*C*(16)], 161.7 [*C*(19)]. ESI-MS (+) CH$_3$CN (m/z [relative intensity, %]): 685 [100] [Ru(*p*-cymene)(L^{20})]$^+$.

[Ru(*p*-cymene)(L²¹)Cl] (33). HL²¹ (61 mg, 0.2 mmol) and KOH (11 mg, 0.2 mmol) were dissolved in CH$_3$OH (5 mL). After 1 h stirring at room temperature the dimer [Ru(*p*-cymene)(Cl)$_2$]$_2$ (62 mg, 0.1 mmol) was added, and the solution was stirred for 5 h at room temperature. The dark-yellow precipitate has been filtered off and dried. The product (55 mg, yield 95%) was identified as the pure compound **33** (**Figure 113**). It is completely soluble in DMSO, acetone, chlorinated solvent, and acetonitrile; slightly soluble in toluene; insoluble in H$_2$O and n-hexane.
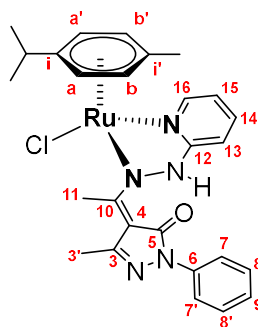
Figure 114 - *Structure of compound 33*

Anal. Calcd. for $C_{27}H_{30}ClN_5ORu$: C, 56.20; H, 5.24; N, 12.14; Found: C, 56.49; H, 5.19; N, 11.93. mp: 130-140 °C. IR (cm^{-1}): 3318w v(N-H); 3062w, 2961w, 2926w, 2827w v(unsaturated C-H); 1741w, 1597w, 1488vs, 1455w, 1417s, 1380m, 1360m v(C=O, C=C, C=N); 1282w, 1151w, 1079w, 1023w; 433w v(Ru-N), 320w v(Ru-Cl). ^{1}H-NMR (DMSO-d_6, 293 K): δ 1.05 d, 1.11 d (6H, -CH(CH)$_3$), 2.23 (s, 3H, -CH$_3$ of *p*-cymene), 2.27 (s, 3H, C(3')*H*), 2.88 (s, 2H, C(11)*H*), 5.65 , 5.81, 6.13 (4H, AA'BB′ system, CH$_3$-C$_6$H$_4$-CH(CH$_3$)$_2$ of *p*-cymene, ^{3}J = 6 Hz), 6.71 (d, 1H, C(13)*H*), 6.79 (t, 1H, C(15)*H*), 7.12 (t, 1H, C(9)*H*), 7.38 (t, 2H, C(8-8')*H*), 7.62 (t, 1H, C(14)*H*), 7.98 (d, 2H, C(7-7')*H*), 8.52 (d, 1H, C(16)*H*), . ^{13}C{^{1}H}-NMR (DMSO-d_6, 293 K): δ 14.4 [*C*(3')], 18.9 [-CH$_3$ of *p*-cymene], 22.1, 22.3 [-CH(CH$_3$)$_2$ of *p*-cymene], 28.5 [*C*(11)], 82.0, 83.9, 84.7, 87.0 [of *p*-cymene], 100.8 [*C*(4)], 102.2 [*C*i], 107.4 [*C*i'], 107.1 [*C*(13)], 115.5 [*C*(15)], 119.6 [*C*(7-7')], 121.7 [*C*(6)], 124.2 [*C*(9)], 126.6 [*C*(5)], 129.0 [*C*(8-8')], 139.5 [*C*(14)], 146.5 [*C*(3)], 152.1 [*C*(16)], 156.8 [*C*(12)], 157.9 [*C*(10)]. ESI-MS(+) CH$_3$OH (m/z [relative intensity, %]): 542 [100] [Ru(*p*-cymene)(L^{21})]$^+$.

[Ru(*p*-cymene)(L²²)Cl] (34). HL²² (75 mg, 0.2 mmol) and KOH (11 mg, 0.2 mmol) were dissolved in CH$_3$OH (5 mL). After 1 h stirring at room temperature the dimer [Ru(*p*-cymene)(Cl)$_2$]$_2$ (62 mg, 0.1 mmol) was added and the solution was stirred for 5 h at room temperature after that, the reaction mixture has been dried at reduced pressure and the product crystalized from a solution of CH$_2$Cl$_2$/Hexane. The dark-brown precipitate has been filtered off and dried. The product (37 mg, yield 57%) was identified as the pure compound **34** (**Figure 114**). It is completely soluble in DMSO, acetone and chlorinated solvent; slightly soluble in toluene and acetonitrile; insoluble in H$_2$O and n-hexane.
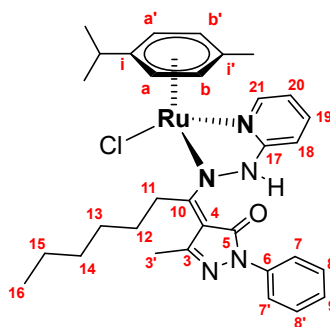
Figure 115 - *Structure of compound 34*

Anal. Calcd. for $C_{32}H_{40}ClN_5ORu$: C, 59.38; H, 6.23; N, 10.82; Found: C, 59.01; H, 6.13; N, 10.56. mp: 132-134 °C. IR (cm⁻¹): 3058w ν(N-H); 2957w, 2924w, 2855w ν(aliphatic and unsaturated C-H); 1594w, 1575w, 1487s, 1455m, 1417m ν(C=O, C=C, C=N); 1376m, 1332w, 1283w, 1243w, 1150w, 1112w, 1075m, 1023w, 1003m; 540w ν(Ru-N), 280w ν(Ru-Cl). ¹H-NMR (CDCl₃, 293 K): δ 0.95 (t, 3H, C(16)*H*), 1.18 d, 1.26 d (6H, -CH(C*H*)₃), 1.40 (m, 4H, C(15)*H* and C(14)*H*), 1.53 (m, 2H, C(13)*H*), 1.67 (m, 2H, C(12)*H*), 2.34 (s, 3H, C(3')*H*), 2.36 (s, 3H, -C*H₃* of *p*-cymene), 2.68 (m, 1H, C*H*(CH₃)₂ of *p*-cymene) , 3.29 (m, 2H, C(11)*H*), 5.26, 5.41, 5.61 (4H, AA'BB' system, CH₃-C₆*H₄*-CH(CH₃)₂ of *p*-cymene, ³J = 6 Hz), 6.59 (t, 1H, C(20)*H*), 6.69 (d, 1H, C(18)*H*), 7.14 (t, 1H, C(9)*H*), 7.40 (t, 3H, C(8-8')*H* and C(19)*H*), 8.03 (d, 2H, C(7-7')*H*), 8.15 (d, 1H, C(21)*H*), 15.31 (s, 1H, N-*H*). ¹³C{¹H}-NMR (CDCl₃, 293 K): δ 14.0 [*C*(16)], 14.1 [*C*(3')], 18.1 [-*C*H₃ of *p*-cymene], 22.0, 22.5 [-CH(*C*H₃)₂ of *p*-cymene], 22.7 [*C*(15)], 29.7 [*C*(13)], 31.0 [-*C*H(CH₃)₂ of *p*-cymene], 31.6 [*C*(12)], 31.8 [*C*(4)], 40.9 [*C*(11)], 82.0, 83.9, 84.7, 87.0 [of *p*-cymene], 102.0 [*C*i'], 103.9 [*C*i], 107.7 [*C*(18)], 114.7 [*C*(20)], 120.5 [*C*(7-7')], 124.3 [*C*(9)], 126.3 [*C*(3)], 128.6 [*C*(8-8')], 129.1 [*C*(4)], 138.2 [*C*(19)], 145.7 [*C*(10)], 150.0 [*C*(21)], 156.3 [*C*(17)], 165.2 [*C*(5)]. ESI-MS(+) CH₃CN (m/z [relative intensity, %]): 612 [95] [Ru(*p*-cymene)(L²²)]⁺.

7.2 RESULTS AND DISCUSSION

7.2.1 Synthesis and characterization of ligands

The reaction to obtain the ligands **HL¹⁷-HL²²** occurs in several steps. First, the acylpyrazolone precursors have been synthesised starting from the Edavarone molecule, 1-phenyl-3-methylpyrazol-5-one (**A**, **Scheme 22**)[214] which, through an acylation in C-4 position (in dioxane under basic conditions provided by calcium hydroxide) made by using an acyl chloride, have favoured the formation of the intermediates **B** (**Scheme 22**), which has been precipitated in high yield from the solution using HCl 2N. Subsequently, the pyrazolone-based hydrazone ligands **C** (in **Scheme 22**) have been obtained via a condensation reaction, by using an slight excess of hydrazine, catalysed by traces of glacial acetic acid in

methanolic solution. The ligands **HL¹⁷**-**HL²¹** precipitated from the solution and the respective powders have been collected through filtration and dried. Differently, the ligand **HL²²** remains in solution and was purified through liquid chromatography using as mobile phase a solution of hexane:ethylacetate 70:30.
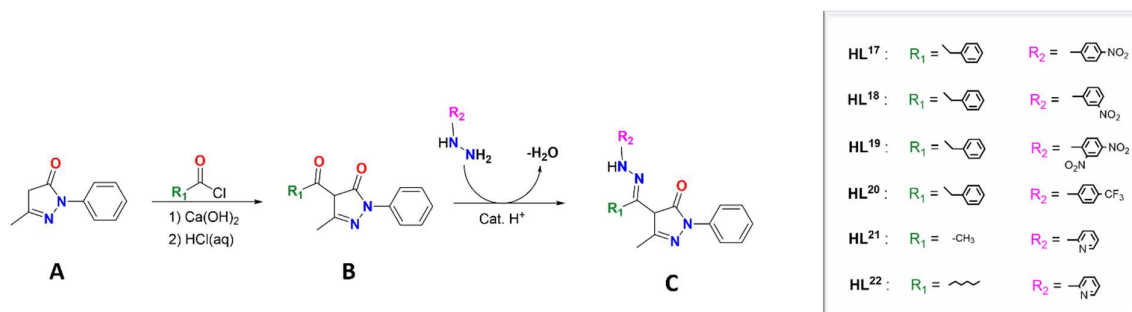
Scheme 22 - *Synthetic procedure for the ligands HL¹⁷-HL²²*

The ligands **HL¹⁷-HL²²** were therefore obtained in high yields. They are air-stable and soluble in most of the organic solvents. Furthermore, the ^{1}H NMR, ^{13}C NMR and Mass spectrometry confirmed the structures and purity expected. In fact, X-ray studies confirmed that the ligands have two different structural typologies according to the hydrazine moiety (R_2 residue), more precisely: the pyridine-containing ligands **HL²¹** and **HL²²** have been found in a zwitterionic form (ligand typology B, **Figure 115**), differently, the other ligands have been found in the expected imine/Schiff's base configuration (ligan typology A, **Figure 115**).
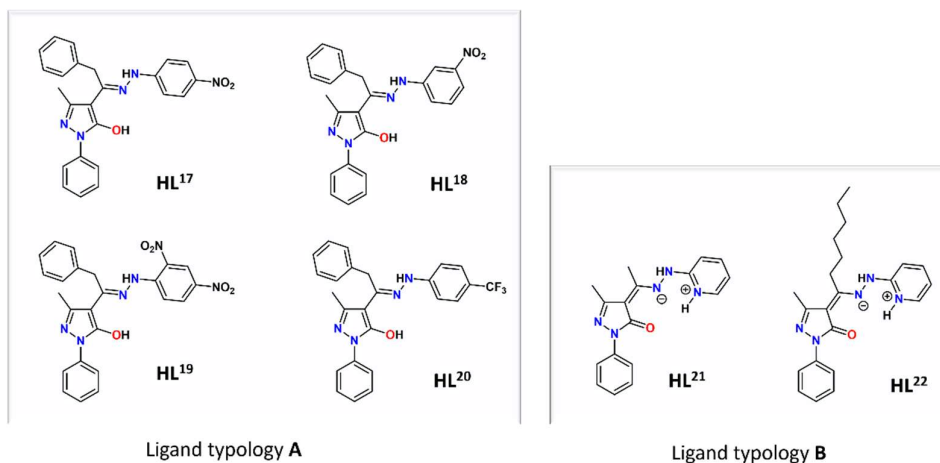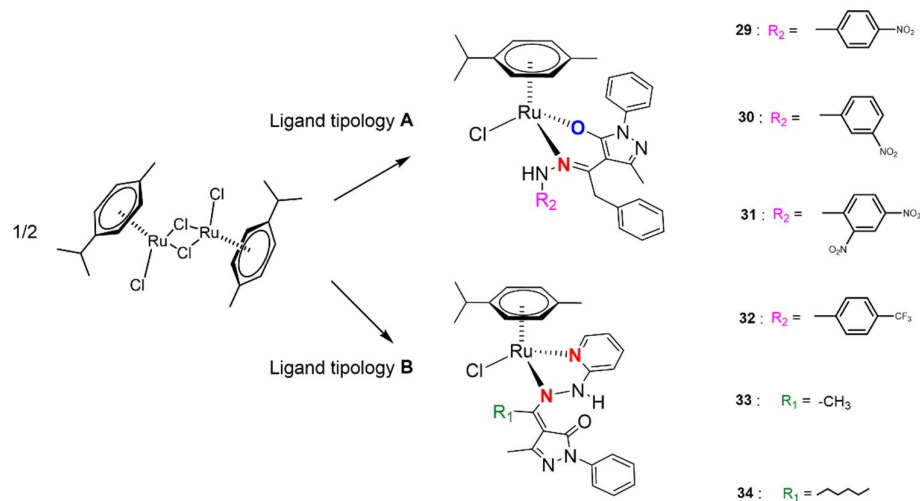

Ligand typology **A**   Ligand typology **B**

Figure 116 - *Different ligand typologies A and B*

7.2.2 Synthesis and characterization of the complexes

Complexes **29**-**34** were prepared from the reaction of the ligands **HL^{17}**-**HL^{22}**, in the presence of KOH as a deprotonating agent, with the Ruthenium dimer, [Ru(*p*-cymene)Cl$_2$]$_2$ in methanol solution for 5 hours (**Scheme 23**).

Scheme 23 - *Synthesis of compounds **29-34***

The novel ruthenium arene complexes, as confirmed by the X-ray studies, demonstrated the presence of two different ligand structures by reflecting different coordination environment around the metal centre. For compounds **29**-**32** the expected -N,O chelation occurs with the formation of six-membered ring, as it is possible to see in **Figure 116** from the final crystal structures of compounds **31** and **32**. On the other hand, the pyridine-containing ligands (in complexes **33** and **34**) prefer to coordinate through the N donor atom of the pyridine ring (labelled as N^p in **Figure 116**) instead of the oxygen present in the pyrazolone ring (O1), affording a five-membered ring with the metal centre (again in **Figure 116**).

The complexes are air-stable and soluble in alcohols, acetone, acetonitrile, chlorinated solvents, DMF and DMSO. The IR spectra of all complexes show the typical v(C=O) band at lower wavenumbers than the corresponding band in the free ligands as a consequence of coordination through the carbonyl arms to the metal. On the other hand, the complexes **33** and **34** show strong changes in the region of C=C/C=N stretching which confirm the coordination through N- donor atoms. In the far-IR region, strong absorptions at about 270 cm^{-1} have been assigned to v(Ru–Cl) stretches. The electrospray ionisation (ESI) mass spectra in positive ion mode, recorded in CH$_3$CN, show the typical isotopic patterns expected for Ru and display peaks that correspond to the species [Ru(*p*-cymene)L^n]$^+$ (where n = 17-22) arising from the dissociation of the chloride anion.
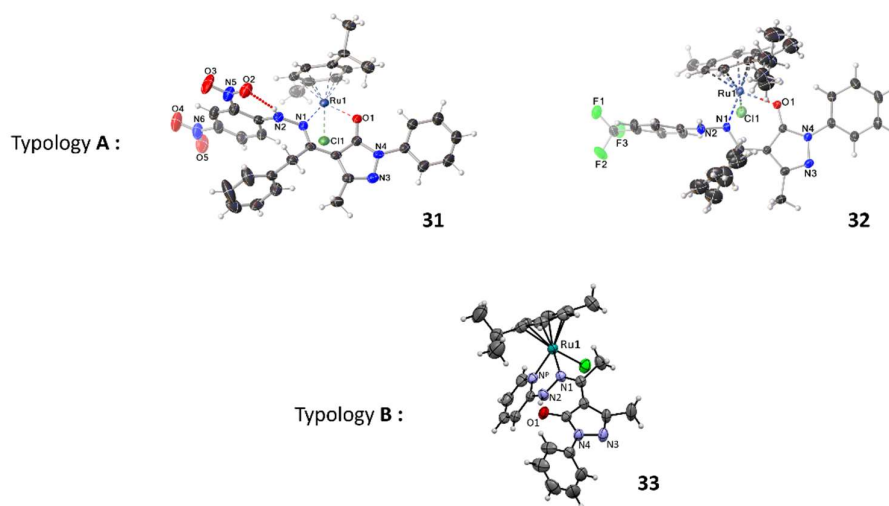
Typology A :

31

32

Typology B :

33

Figure 117 - *Crystal structures of Ru compounds **31** and **32** (with a κ-N,O coordination environment, typology **A**) and **33** (with a κ-N,N coordination environment, typology **B**)*

All the ^{1}H-NMR spectra have been recorded in CDCl$_3$ solution except for the compound **33** for which DMSO-d^6 has been used. In the spectra all the set of signals related to the ligands' protons, which are far from the coordination environment, are just a little bit shifted compared to the signals of the free ligands. In the case of compound **29**, at 298 K a broad set of resonances is observed, and by cooling a splitting into more sets has been detected, probably due to the presence of different interconvertible species in solution. At 248 K the exchange peaks between protons of the conformers are clearly distinguishable (**Figure 117**).
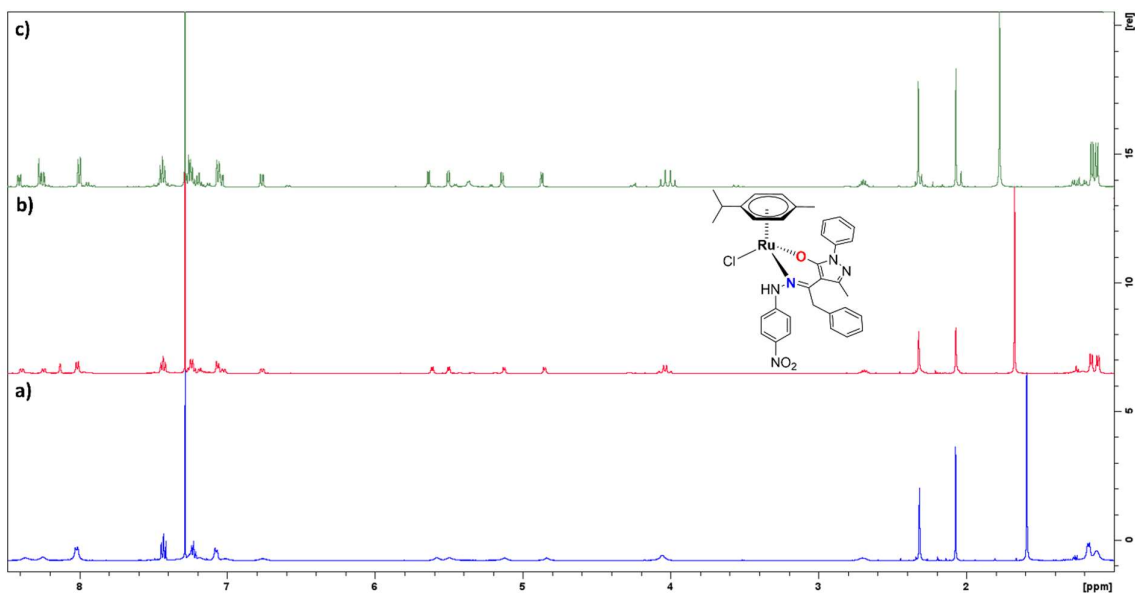

Figure 118 - *^{1}H-NMR spectra in CDCl$_3$ of compound **29** recorded at 298 K (**a**), 273 K (**b**) and 248 K (**c**)*

An interesting feature of the ^{1}H-NMR spectra is related to the *p*-cymene system, where a doublet for each of the four *p*-cymene ring protons is observed. One of the four proton

resonances is strongly shifted to higher fields, below 4.9 ppm, whereas the other three doublets are in the expected range of 5.10−5.60 ppm. The lowest ppm value has been found for the dinitro-substituted complex **31** for which the Hb' signal falls at 4.10 (**Figure 118**). On the other hand, in the ^{1}H-NMR spectra of compounds κ-N,N coordinated, **33** and **34**, the signals related to the p-cymene system are found at lower fields.

Additionally, the occurred metalation of the ligands can be seen by the split into two doublets of the 11-CH$_2$ protons belonging to the benzyl group for compounds **29-32** which, after the coordination, become diasterotopic as it is showed always in **Figure 118**.
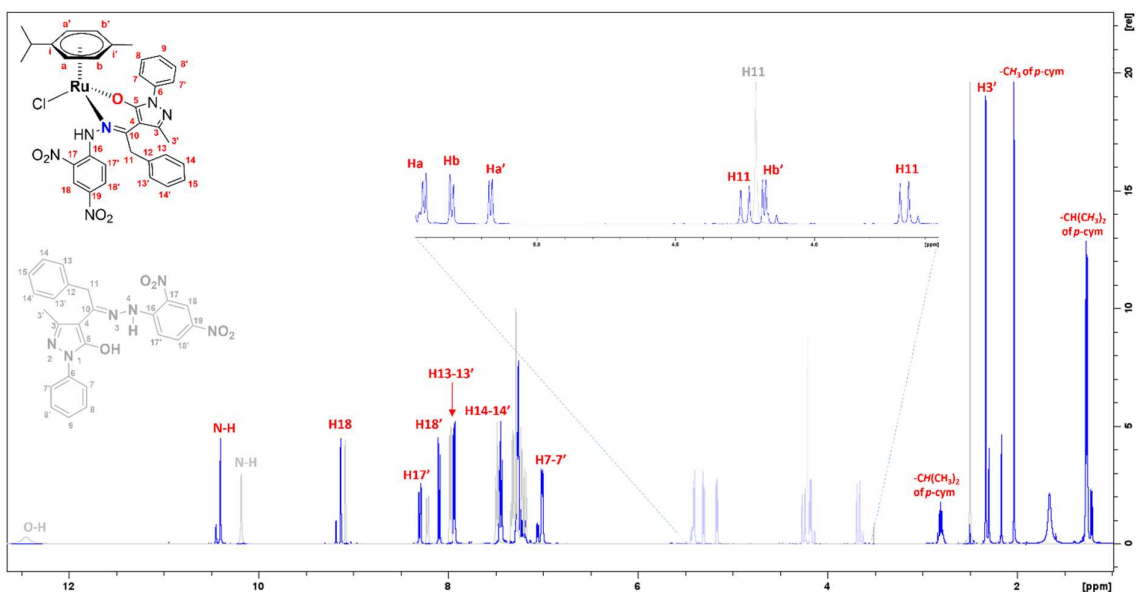
Figure 119 - *Comparison between the ^{1}H-NMR spectra in CDCl$_3$ of complex 31 (blue line) and the parent ligand HL^{19} (grey line)*

However, the most shifted and representative signals of the occurred complexation are the disappearance of the hydroxyl proton (for the N,O- coordinating ligands) and the strong shift at about 15 ppm relative to the endocycle N-H bond in the N,N- coordination environment (**Figure 119**).
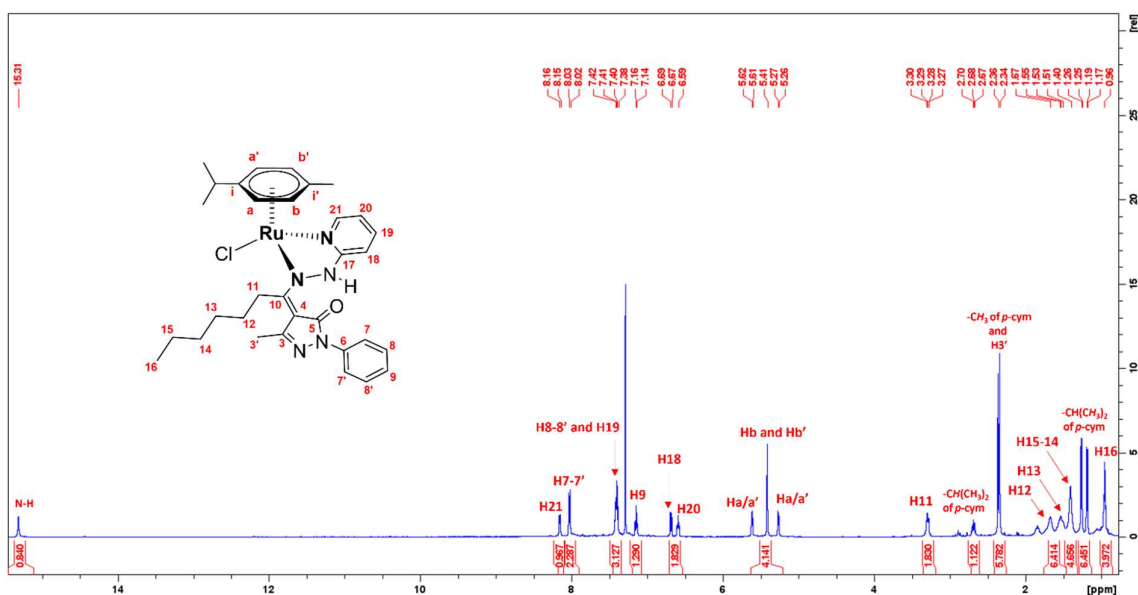
Figure 120 -*¹H-NMR spectrum in CDCl₃ of compound 34*

7.2.3 Catalytic studies

The synthesized complexes have been evaluated from a catalytic point of view in order to develop a one-pot tandem reaction where the first step is a deacetalization followed by the Knoevenagel condensation (**Scheme 24**).
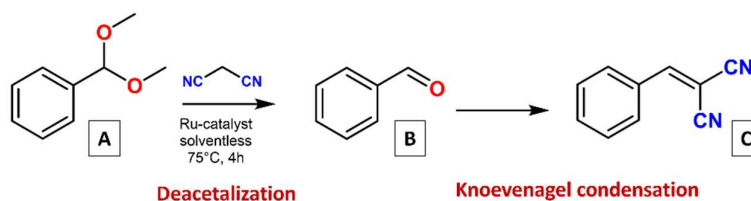
Scheme 24 - *Tandem deacetalization-Knoevenagel condensation reaction catalyzed by Ru-compounds*

Benzaldehyde dimethyl acetal and malononitrile have been selected as test compounds. The acetal (**A**, in **Scheme 24**) was used as staring material which, in the presence of the Ru-catalysts, produces *in situ* the aldehyde (**B**) needed for the Knoevenagel condensation, occurring in the presence of one malonitrile molecule, to obtain the benzylidene malononitrile (**C**) as reaction product.

Upon performing these tandem reactions in solvent-free conditions at 75 °C for 4h in the presence of complexes **29-34**, used as homogeneous catalysts, we found that compound **33** led to a higher product yield (92%) as compared to the others (entry 5, **Table 9**). With **29, 30, 31, 32,** and **34**, yields of 77 %, 64%, 68%, 70 % and 65% were obtained, respectively (entries 1-4 and 6, **Table 9**). Hence, the catalytic efficacy toward the tandem

deacetalization−Knoevenagel condensation reactions follows the order **33** > **29** > **32** > **31** > **34** > **30**. A blank test (without using any catalyst) was also performed, and no final product was produced under the optimised reaction conditions, and only a slight amount of the intermediate benzaldehyde was obtained (entry 7, **Table 9**). A relatively low yield of benzylidene malononitrile (9%) was detected utilising just the [Ru(p-cymene)(Cl)$_2$]$_2$ precursor dimer (entry 8, **Table 9**).

Entry	Catalyst	Unreacted A (%)[a]	Yield of B (%)[a]	Yield of C (%)[a]
1	29	16	7	77
2	30	28	9	64
3	31	24	9	68
4	32	19	11	70
5	33	5	3	92
6	34	29	7	65
7	Blank	92	8	0
8	[Ru(p-cymene)(Cl)$_2$]$_2$	10	81	9

[a]Calculated by ^{1}H NMR analysis. A = benzaldehyde dimethyl acetal (reactant); B = benzaldehyde (intermediate product); C = benzylidene malononitrile (final product).
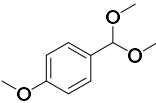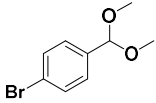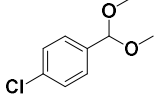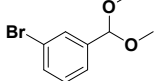
Table 9 - *Catalytic results of the one-pot deacetalization−Knoevenagel condensation reactions between benzaldehyde dimethyl acetal and malononitrile with Ru-catalysts (1%mol) at 75°C for 4h in solvent-free conditions*

According to this, we have selected catalyst **33** to optimise the reaction conditions by changing the temperature (25-100°C), catalyst amount (0.5-3 mol %), solvents and reaction time (up to 5 h) and the achieved results are shown in **Table 10.**

To optimize the reaction temperature, we have performed the tandem reaction in four different temperatures. At room temperature (25˚C) no benzylidene malononitrile was formed and only a low quantity of intermediate benzaldehyde was obtained (entry 9, **Table 10**). However, increasing the reaction temperature to 50˚C and 75˚C significantly increases the formation of benzylidene malononitrile up to 54% and 92%, respectively (entries 10, **Table 10** and 5**, Table 9**). A further raise in the reaction temperature (100 ˚C) leads to a slight decrease of the final product yield (entry 11, **Table 10**). In order to obtain a suitable catalyst load, we varied it from 0.5 mol% to 3 mol% (with respect to the amount of benzaldehyde dimethyl acetal) employing the aforementioned experimental conditions. By using the lowest amount of catalyst **33** (0.5 mol%) the final product yield was reduced substantially to 66% (entry 12, **Table 10**), although by increasing the amount to 1 mol% caused a marked yield enhancement to 92% (entry 5, **Table 9**). However, a further rise in the catalyst amount (3 mol%) did not improve the yield (entry 13, **Table 10**), demonstrating that 1 mol% of catalyst

load of **33** is suitable for this reaction. The solvent can play a major role in catalytic reactions, but avoiding the use of any added solvent (solvent-free conditions) is significantly important in the context of green chemistry.[215] The solvent-free reactions have advantages, such as absence of waste solvents, easy work up and possible shorter reaction time. Accordingly, we have performed the tandem reactions in solvent-free conditions as well as using various solvents (DMF, CH₃CN, MeOH and THF). The reactions under solvent-free conditions produce the highest yield of 92% (entry 5, **Table 9**). By using DMF, CH₃CN or MeOH, only 46%, 18% or 24% yield of benzylidene malononitrile is obtained, respectively (entries 14-16, **Table 10**).

Different Temperatures[b]				
Entry	*T (℃)*	**Unreacted A (%)[a]**	**Yield of B (%)[a]**	**Yield of C (%)[a]**
9	25	85	15	0
10	50	44	2	54
11	100	7	2	91

Different Catalyst amounts[c]				
Entry	*%mol* of catalyst	**Unreacted A (%)[a]**	**Yield of B (%)[a]**	**Yield of C (%)[a]**
12	0.5	27	8	66
13	3	6	4	91

Different Solvents[d]				
Entry	*Solvent*	**Unreacted A (%)[a]**	**Yield of B (%)[a]**	**Yield of C (%)[a]**
14	DMF	47	8	46
15	CH₃CN	76	7	18
16	MeOH	68	9	24
17	THF	13	3	85

Time dependence[e]				
Entry	*Time*	**Unreacted A (%)[a]**	**Yield of B (%)[a]**	**Yield of C (%)[a]**
18	1	15	4	82
19	2	11	2	87
20	3	7	2	91
21	4	5	3	92
22	5	4	2	94

Different Substrates				
Entry	Substrate	Unreacted A (%)*a*	Yield of B (%)*a*	Yield of C (%)*a*
23*f*		0	2	98
24*g*		0	0	>99
25*h*		2	2	96
26*i*		48	0	52

Reaction conditions: [b]1 %mol of **33** after 4h in solvent-free conditions; [c] after 4h in solvent-free conditions at 75°C; [d]1 %mol of **33** after 4h at 75°C; [e]1 %mol of **33** in solvent-free conditions at 75°C; [f]4-Methoxybenzaldehyde dimethyl acetal as substrate; [g]4-Bromobenzaldehyde dimethyl acetal as substrate; [h]4-Chlorobenzaldehyde dimethyl acetal as substrate; [i]3-Bromobenzaldehyde diethyl acetal as substrate.

Table 10 - *Optimization reactions of the one-pot deacetalization−Knoevenagel performed with catalyst **33***

However, the use of THF leads to the 2nd highest yield of benzylidene malononitrile (85%, entry 17, **Table 10**). Thus, solvent-free conditions turn out to be the best choice for these tandem reactions. To determine a suitable reaction time, the reaction was scrutinised until 5 h at regular intervals. The yield *vs.* time plot for the Ru-catalyst **33** is presented in **Figure 120** (up). Upon increasing the reaction time from 0.5h to 5h the yield of benzylidene malononitrile (**C**) increased continuously and the amount of benzaldehyde dimethyl acetal (**A**) decreased constantly. However, after ca. 3-4 h reaction time, only a low yield variation occurred. Moreover, the yield of the intermediate benzaldehyde (**B**) increases with time until 0.5h reaching a maximum after which it started to decrease.

Furthermore, the activity of the catalyst **33** have been also tested in the reactions of a variety of substituted benzaldehyde dimethyl and diethyl acetals. The *para*-substituted methoxy (−OMe) and bromo (−Br) dimethyl acetals give the highest yields of 98-99%, whereas the 4-chlorobenzaldehyde dimethyl acetal produced a slightly lower yield of 96%. However, for 3-bromo benzaldehyde diethyl acetal, just 52% of the final product yield was achieved under the optimised reaction conditions (**Figure 120**, down).
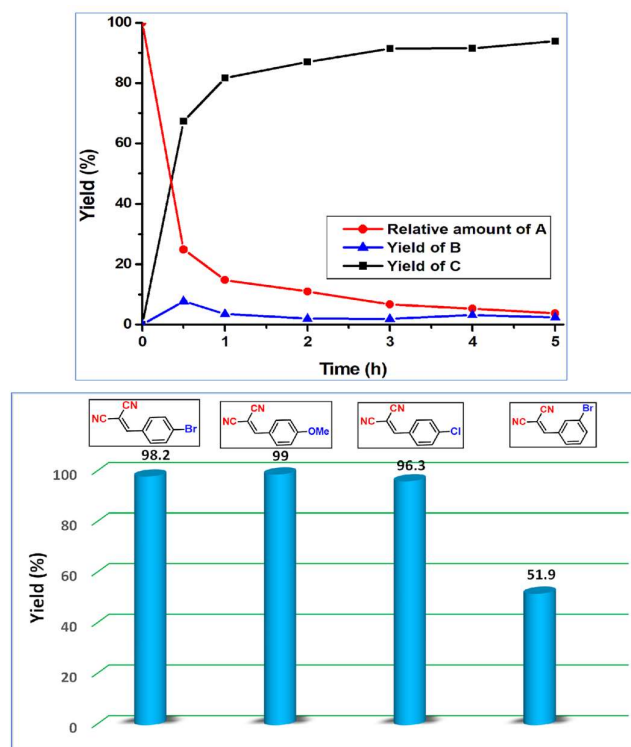
Figure 121 -(up) Yield vs. time plot for the one-pot tandem deacetalization-Knoevenagel condensation reactions catalysed by compound **33** [black line: yield of benzylidene malononitrile (**C**); blue line: yield of intermediate benzaldehyde (**B**); red line: yield of unreacted benzaldehyde dimethyl acetal (**A**)]. (down) Yield for one-pot tandem deacetalization-Knoevenagel condensation reactions for different substituted acetals catalysed by compound **33**

Chapter 8: Tandem oxidation-Knoevenagel condensation reactions promoted by novel organometallic Ir(III) and Rh(III) complexes containing Shiff base ligands

8.1 Aim of the work

According to what reported up to now, there is a great demand for developing even greener, more efficient and more sustainable multifunctional catalytic systems able to promote the formation of new carbon–carbon bonds. Moreover, the oxidation of alcohols to carbonyl compounds also represent a relevant reaction in synthetic organic chemistry and in the chemical industry.[216-217] Various catalytic methods have been developed for such a process using green oxidants, such as O_2 or peroxides [H_2O_2 or tert-butylhydroperoxide (t-TBHP)], to overcome the formation of harmful waste.[218] Furthermore, the use of solvent-free conditions together with green oxidants and efficient catalysts could represent an ecofriendly way to carry out this type of reactions.

Thus, in this section is reported the syntheses of new Rhodium(III) and Iridium(III) half sandwich complexes bearing a pentamethylcyclopentadienyl ring (Cp*) and pyrazolone-based hydrazones as bidentate κ-N,N chelating ligands. The great stability from thermal stress and oxidating environments of such complexes gave the possibility to test them as catalyst for tandem reaction which includes Knoevenagel condensation together with an oxidation step.

8.1.1 Materials and methods

All the materials referred to the synthesis of the ligands, proligands and metal chlorides were obtained from commercial sources and were used as received. IR spectra were recorded from 4000 to 400 cm^{-1} on a PerkinElmer Spectrum 100 FT-IR instrument. ^{1}H and ^{13}C-NMR, {^{1}H–^{1}H}-COSY NMR, {^{1}H–^{13}C}-HSQC and {^{1}H–^{13}C}- HMBC spectra were recorded on a 500 Bruker Ascend (500.1 MHz for ^{1}H, 100 MHz for ^{13}C). Referencing is relative to TMS (^{1}H). Positive and negative ion electrospray ionization mass spectra (ESI-MS) were obtained on a Series 1100 MSI detector HP spectrometer using methanol as the mobile phase. Solutions (3 mg mL^{-1}) analysis were prepared using reagent-grade methanol. Masses and intensities were compared to those calculated using IsoPro Isotopic Abundance Simulator, version 2.1.28. Melting points were recorded on an STMP3 Stuart scientific instrument and a capillary apparatus. Samples for microanalysis were dried in vacuo to constant weight (20 °C, ca. 0.1 Torr) and analysed on a Fisons Instruments 1108 CHNS-O elemetal analyzer.

8.1.2 Catalytic procedure for the oxidation reactions

1.25 mmol of both primary alcohol (benzyl alcohol, 130 μL) and secondary alcohol (1-phenylethanol, 151 μL), together with TBHP (2.5 mmol, 241 μL) and 1 mol% of catalyst (3.7 mg of **35**, 3.7 mg of **36**, 4.0 mg of **37**, 3.3 mg of **38**, 3.2 mg of **39**, 3.1 mg of **40**) were placed in a 2 mL glass vessel. The reaction has been heated at 100°C for 4h in the case of secondary alcohol and 24h for the primary one. Afterwards the mixtures were extracted with chloroform and dried over anhydrous sodium sulphate. The crude products were obtained after evaporation of the solvent and the yields determined by ^{1}H NMR in CDCl$_3$. The yields were calculated by the use of mesitylene as internal standard.

8.1.3 Catalytic procedure for the Knoevenagel condensation reactions

1.25 mmol of benzaldehyde (146 μL), 2.5 mmol of malonitrile (165 mg) and 1 mol% of catalyst (3.7 mg of **35**, 3.7 mg of **36**, 4.0 mg of **37**, 3.3 mg of **38**, 3.2 mg of **39**, 3.1 mg of **40**) were placed in a 2 mL glass vessel. In the cases where the reactions were performed in water, 1 mL of solvent has been added.

The reaction has been heated at 80°C for 5h in solventless condition. Afterwards the mixtures were directly analysed by ^{1}H NMR spectroscopy. On the other hand, the reactions performed in water were heated for 7 minutes and, after that, extracted with chloroform and dried over anhydrous sodium sulphate. The crude products were obtained after evaporation of the solvent and the yields determined by in CDCl$_3$. The yields were calculated by the use of mesitylene as internal standard.

8.1.4 Catalytic procedure for tandem Oxidation−Knoevenagel condensation reactions

1.25 mmol of benzyl alcohol (130 μL), 2.5 mmol of TBHP (241 μL) and 1 mol% of **35** (3.7 mg) were placed in a 2 ml glass vessel. The glass vial was capped and heated at 100 °C for 24 hours. Afterwards 2.5 mmol of malonitrile (165 mg) was added to the mixture and let to react for one more hour. After that the mixture was extracted with chloroform and dried over anhydrous sodium sulphate. The crude product was obtained after evaporation of the solvent and the final product yield was determine by ^{1}H NMR in CDCl$_3$. This yield was calculated according to the previously reported method.[213]

8.1.5 General procedure for synthesis of the dimers

[Ir(Cp*)Cl₂]Cl₂. The reactant $IrCl_3(H_2O)_n$ was added in the methanolic solution with an excess of 1,2,3,4,5-pentamethylcyclopentadiene. After 5 hours of magnetic stirring at reflux the reaction mixture has been cooled down and filtered. The yellow precipitate formed was filtered off and washed with Et_2O.

[Rh(Cp*)Cl₂]Cl₂. The dimer has been synthesized with a microwave assisted method. The reactants $RhCl_3(H_2O)_n$ (500 mg, 1.92 mmol) and 1,2,3,4,5-pentamethylcyclopentadiene (0.45 mL, 2.85 mmol) have been added in the methanolic solution (10 mL) and stirred for 3 minutes at 140 °C. The red precipitate formed (60% of yield) was filtered off and washed with cold CH_3OH.

8.1.6 General procedure for synthesis of ligands

According to the previous procedures,[40,219] the ligands **HL²³** and **HL²⁴** (**Figure 121**) have been synthesized starting from a mixture of the appropriate acylpyrazolone proligand (1.0 eq.) and 2-hydrazinopyridine (1.1 eq.) in methanol (10 mL), containing 5 drops of glacial acetic acid, was heated at reflux for 5 hours and the reaction was monitored by TLC (CH_3Cl/ MeOH 96:4 v/v). A precipitate slowly formed from the hot solution, and after completion, the reaction mixture was placed at 4 °C overnight. The obtained precipitate was filtered, redissolved in ethanol (10 mL) and recrystallized from slow evaporation of the solution, to give all the light yellow solids which were collected by filtration and dried.
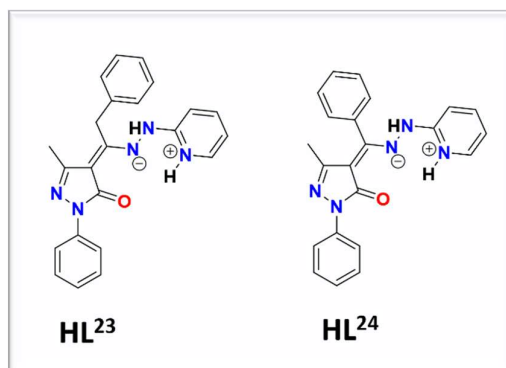

Figure 122 - *Structure of ligands **HL²³** and **HL²⁴***

The synthesis of **HL²¹** ligand is reported in the previous section.

8.1.7 General procedure for synthesis of complexes

[Ir(Cp*)(L²³)Cl] (35). The ligand **HL²³** (77 mg, 0.2 mmol) and the KOH (11 mg, 0.2 mmol) were dissolved in CH_3OH (15 mL). After one hour the $[Ir(Cp^*)Cl_2]_2$ dimer (80 mg, 01 mmol) has been added to the reaction mixture. After 5 hours the solution has been dried and the product has been crystalized by CH_2Cl_2/Hexane solvent mixture. The compound **35** (**Figure 122**) has been collected as a yellow powder, yield 73%. It is completely soluble in CH_3CN, DMSO, EtOH and CH_3Cl, partly soluble in acetone and CH_3OH and insoluble in H_2O, Et_2O and Hexane.
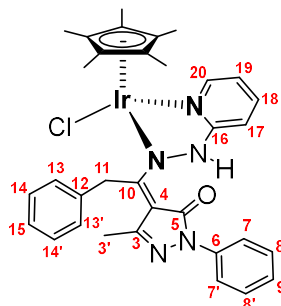

Figure 123 - *Structure of compound 35*

Anal. Calcd. for $C_{33}H_{35}ClIrN_5O$: C, 53.18, H, 4.73, N, 9.40. Found: C, 54.72; H, 5.14 ,N, 8.95. m.p. 183-185 °C. IR (cm^{-1}): 3420 wbr v(N-H); 3062w, 3030w, 2957w, 2920w, 2858w v(unsaturated C-H); 1617m, 1596m (C=O), 1491vs, 1458m, 1451m, 1420m, 1413mbr v(C=C, C=N); 1379m, 1364sh, 1303w, 1285w, 1255sh, 1186w, 1154w, 1125w, 1083s, 1027s. ^{1}H-NMR $(CDCl_3$, 293 K): δ 1.51 (s, 15H, $-(CH_3)$x5 of Cp*), 2.07 (s, 3H, C(3')*H*), 4.72 (dd, 2H, C(11)*H*), 6.59 (t, 1H, C(18)*H*), 6.84 (d, 1H, C(20)*H*), 7.13 (t, 1H, C(15)*H*), 7.15-7.18 (m, 3H, C(7-7')*H* and C(9)*H*), 7.26 (t, 2H, C(8-8')*H*), 7.39 (t, 2H, C(14-14')*H*), 7.46 (t, 1H, C(19)*H*), 7.89 (d, 1H, C(17)*H*), 8.07 (d, 2H, C(13-13')*H*), 15.68 (N-H). $^{13}C\{^1H\}$-NMR $(CDCl_3$, 293 K): δ 8.9 [$-(CH_3)$x5 of Cp*], 16.7 [*C*(3')], 46.1 [*C*(11)], 87.6 [-iC_5 of Cp*], 100.0 [*C*(4)], 107.1 [*C*(20)], 114.6 [*C*(18)], 119.3 [*C*(5)], 120.0 [*C*(13-13')], 123.9 [*C*(15)], 126.1 [*C*(9)], 128.1 [*C*(7-7')], 128.5 [*C*(8-8') and *C*(14-14')], 138.1 [*C*(19)], 139.4 [*C*(12)], 140.0 [*C*(6)], 146.3 [*C*(17)], 157.4 [*C*(6)], 162.4 [*C*(10)]. ESI-MS (+) CH_3CN (m/z [relative intensity, %]): 710 [100] $[Ir(Cp^*)(L^{23})]^+$.

[Ir(Cp*)(L²⁴)Cl] (36). The ligand **HL²⁴** (74 mg, 0.2 mmol) and the KOH (11 mg, 0.2 mmol) were dissolved in CH_3OH (5 mL). After one hour the $[Ir(Cp^*)Cl_2]_2$ dimer (80 mg, 01 mmol) has been added to the reaction mixture. After 5 hours the suspension formed was filtered off and the product **36** (**Figure 123**) has been dried obtaining a yellow powder, yield 70%. It is completely soluble in DMSO and CH_3Cl, partly soluble in acetone, CH_3CN and CH_3OH and insoluble in H_2O, Et_2O, EtOH and Hexane.
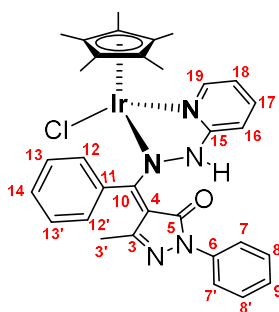
Figure 124 - *Structure of compound 36*

Anal. Calcd. for $C_{32}H_{33}ClIrN_5O$: C, 52.56, H, 4.55, N, 9.58. Found: C, 50.35; H, 4.44 ,N, 9.13. m.p. 326-328 °C. IR (cm^{-1}): 3064w, 3048w, 3030w, 3010w, 2987w, 2964w, 2917w v(unsaturated C-H); 1614mbr, 1596m v(-C=O); 1505 m, 1495m, 1478vs, 1417 mbr, 1384sh, 1371m, 1359m (C=C, C=N); 1310w, 1285m, 1274sh, 1238w, 1180w, 1156m, 1130m, 1080s, 1073s, 1026s, 1012m. ^{1}H-NMR (CDCl$_3$, 293 K): δ 1.25 (s, 18H, C(3')*H* and -(C*H$_3$*)x5 of Cp*), 6.71 (t, 1H, C(17)*H*), 6.94 (d, 1H, C(19)*H*), 7.16 (t, 1H, C(14)*H*), 7.41-7.53 (m, 8H, C(7-7')*H*, C(3-13')*H*, C(8-8')*H*, C(18)*H* and C(9)*H*), 7.96 (d, 1H, C(16)*H*), 8.10 (d, 2H, C(12-12')*H*), 15.08 (N-H). ^{13}C{^{1}H}-NMR (CDCl$_3$, 293 K): δ 8.4 [-(C*H$_3$*)x5 of Cp*], 16.7 [*C*(3')], 87.6 [-i*C$_5$* of Cp*], 102.7 [*C*(4)], 118.2 [*C*(19)], 115.7 [*C*(17)], 120.1 [*C*(12-12')], 124.0 [*C*(14)], 128.5 [*C*(9)], 128.1 [*C*(7-7')], 128.5 [*C*(8-8') and *C*(7-7')], 129.9 [*C*(9)], 133.7 [*C*(13-13')], 138.0 [*C*(18)], 138.9 [*C*(11)], 146.3 [*C*(16)], 148.5 [*C*(10)], 158.0 [*C*(15)], 162.2 [*C*(6)], 163.0 [*C*(5)]. ESI-MS (+) CH$_3$CN (m/z [relative intensity, %]): 696 [100] [Ir(Cp*)(L^{24})]$^+$.

[Ir(Cp*)(L^{21})Cl] (37). The ligand **HL^{21}** (61 mg, 0.2 mmol) and the KOH (11 mg, 0.2 mmol) were dissolved in CH$_3$OH (5 mL). After one hour the [Ir(Cp*)Cl$_2$]$_2$ dimer (80 mg, 01 mmol) has been added to the reaction mixture. After 5 hours the solution has been dried and the product has been crystalized by CH$_2$Cl$_2$/Hexane solvent mixture. The compound **37** (**Figure 124**) has been collected as a yellow powder, yield 56%. It is completely soluble in CH$_3$CN, DMSO and CH$_3$Cl, partly soluble in CH$_3$OH and insoluble in H$_2$O and Hexane.

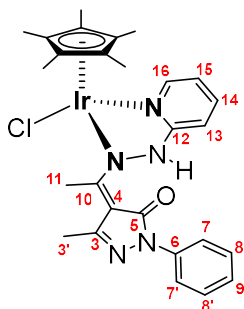**Figure 125 -** *Structure of compound 37*

Anal. Calcd. for $C_{27}H_{31}ClIrN_5O$: C, 48.46, H, 4.67, N,10.46. Found: C, 50.42; H, 5.05 ,N, 11.02. m.p. 178-180 °C. IR (cm^{-1}): 2959w, 2920w, 2870w, 2853w v(unsaturated C-H); 1616m, 1594 mbr v(-C=O); 1536w, 1494vs, 1488vs, 1453m, 1418 sbr, 1378 mbr, 1359m v(C=C, C=N); 1325w, 1308w, 1281w, 1150w, 1079s, 1055w, 1024s. ^{1}H-NMR (CDCl$_3$, 293 K): δ 1.63

(s, 15H, -(CH₃)x5 of Cp*), 2.44 (s, 3H, C(3'0)H), 2.93 (s, 3H, C(11)H), 6.61 (t, 1H, C(14)H), 6.79 (d, 1H, C(16)H), 7.18 (t, 1H, C(9)H), 7.42 (m, 2H, C(8-8')H), 7.46 (t, 1H, C(15)H), 7.86 (d, 1H, C(13)H), 8.01 (d, 2H, C(7-7')H), 15.58 (N-H). ^{13}C{^{1}H}-NMR (CDCl₃, 293 K): δ 9.0 [-(CH₃)x5 of Cp*], 22.6 [C(3')], 28.2 [C(11)], 87.4 [-iC₅ of Cp*)], 100.6 [C(4)], 107.1 [C(16)], 115.1 [C(14)], 120.7 [C(7-7')], 124.7 [C(9)], 128.6 [C(8-8')], 138.2 [C(15)], 139 [C(6)], 146.6 [C(13)], 147.15 [C(3)], 157.3 [C(12)], 159.4 [C(10)], 161.2 [C(5)]. ESI-MS (+) CH₃CN (m/z [relative intensity, %]): 634 [50] [Ir(Cp*)(L²¹)]⁺.

[Rh(Cp*)(L²³)Cl] (38). The ligand **HL²³** (77 mg, 0.2 mmol) and the KOH (11 mg, 0.2 mmol) were dissolved in CH₃OH (5 mL). After one hour the [Rh(Cp*)Cl₂]₂ dimer (62 mg, 01 mmol) has been added to the reaction mixture. After 5 hours the solution has been dried and the product has been crystalized by CH₂Cl₂/Hexane solvent mixture. The compound **38** (**Figure 125**) has been collected as a red powder, yield 62%. It is completely soluble in DMSO, CH₃OH, CH₃CN and CH₃Cl, partly soluble in acetone and insoluble in H₂O and Hexane.
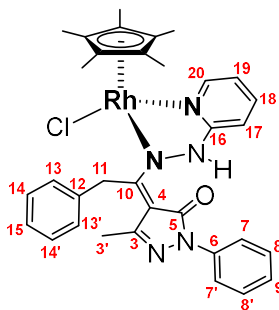

Figure 126 - *Structure of compound **38***

Anal. Calcd. for C₃₃H₃₅ClRhN₅O: C, 60.42, H, 5.38, N, 10.68. Found: C, 57.67, H, 5.27,N, 9.33. m.p. 198-200 °C. IR (cm⁻¹): 3061w, 3028w, 2985w, 2958w, 2919w, 2871w, 2855w ν(unsaturated C-H); 1614m, 1599m ν(-C=O); 1532w, 1494sh, 1486vs, 1453m, 1416s, 1376m, 1359m ν(C=C, C=N); 1308w, 1284m, 1268sh, 1223w, 1186w, 1154w, 1140w, 1122w 1080s, 1021s 1007s. ^{1}H-NMR (CDCl₃, 293 K): δ 1.53 (s, 15H, -(CH₃)x5 of Cp*), 2.08 (s, 3H, C(3')H), 4.67 (dd, 2H, C(11)H), 6.70 (t, 1H, C(18)H), 6.78 (d, 1H, C(20)H), 7.13-7.19(m, 2H, C(9)H) and C(15)H), 7.22 (d, 2H, C(8-8')H), 7.26 (d, 2H, C(7-7')H), 7.39 (t, 2H, C(14-14')H), 7.48 (t, 1H, C(19)H), 7.90 (d, 1H, C(17)H), 8.06 (d, 2H, C(13-13')H), 15.18 (-NH). ^{13}C{^{1}H}-NMR (CDCl₃, 293 K): δ 9.1 [-(CH₃)x5 of Cp*], 16.4 [C(3')], 45.4 [C(11)], 95.6 [-iC₅ of Cp*], 100.6 [C(4)], 107.5 [C(20)], 115.3 [C(18)], 120.1 [C(13-13')], 124.1 [C(9)], 126.2 [C(15)], 128.1, 128.5, 128.6 [C(8-8'), C(14-14') and C(7-7')], 138.5, 138.9, 139.6 [C(12), C(6) and C(19)], 146.1 [C(5)], 147.2 [C(17)], 156.3 [C(16)], 162.5 [C(10)]. ESI-MS (+) CH₃CN (m/z [relative intensity, %]): 620 [100] [Rh(Cp*)(L²³)]⁺.

[Rh(Cp*)(L²⁴)Cl] (39). The ligand **HL²⁴** (74 mg, 0.2 mmol) and the KOH (11 mg, 0.2 mmol) were dissolved in CH₃OH (5 mL). After one hour the [Rh(Cp*)Cl₂]₂ dimer (62 mg, 01 mmol) has been added to the reaction mixture. After 5 hours the suspension formed was filtered off

and the product **39** (**Figure 126**) has been dried obtaining a red powder, yield 72%. It is completely soluble in DMSO and CH_3Cl, partly soluble in acetone, CH_3CN, CH_3OH and insoluble in H_2O and Hexane.
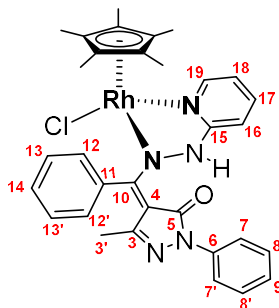

Figure 127** - Structure of compound **39

Anal. Calcd. for $C_{32}H_{33}ClRhN_5O$: C, 59.87, H, 5.18, N, 10.91. Found: C, 59.74; H, 5.15,N, 10.80. m.p. 320-322 °C. IR (cm^{-1}): 3064w, 3029w, 2986w, 2959w, 2915w, 2848w v(unsaturated C-H); 1607sh, 1596m v(-C=O); 1505m, 1495m, 1475vs, 1462sh, 1456m, 1435m, 1417mbr, 1385w, 1368w, 1356m, 1344sh v(C=C, C=N); 1328w, 1310w, 1283m, 1268sh, 1237w, 1180w 1156m, 1128m, 1109wbr, 1080sh, 1072sbr, 1021s, 1010s. ^{1}H-NMR ($CDCl_3$, 293 K): δ 1.27 (s, 15H, -(CH_3)x5 of Cp*), 1.30 (s, 3H, C(3')H), 6.78 (t, 1H, C(17)H), 6.85 (d, 1H, C(19)H), 7.15 (t, 1H, C(14)H), 7.40-7.51 (m, 8H, C(13-13')H, C(7-7')H, C(8-8')H, C(9)H and C(18)H), 7.98 (d, 1H, C(16)H), 8.10 (d, 2H, C(12-12')H), 14.75 (N-H). ^{13}C{^{1}H}-NMR ($CDCl_3$, 293 K): δ 8.6 [-(CH_3)x5 of Cp*], 14.9 [C(3')], 95.5 [-iC_5 of Cp*], 102.9 [C(4)], 108.7 [C(19)], 116.2 [C(17)], 120.1 [C(12-12')], 124.0 [C(14)], 127.9, 128.6, 128.8, 130.1, 133.2, 138.3 [C(13-13'), C(7-7'), C(8-8'), C(9) and C(18)], 138.6 [C(11)], 147.4 [C(16)], 148.1 [C(10)], 157.0 [C(15)], 162.4 [C(6)], 163.1 [C(5)]. ESI-MS (+) CH_3CN (m/z [relative intensity, %]): 607 [100] [Rh(Cp*)(L^{24})]$^+$.

[Rh(Cp*)(L^{21})Cl] (40). The ligand **HL^{21}** (61 mg, 0.2 mmol) and the KOH (11 mg, 0.2 mmol) were dissolved in CH_3OH (5 mL). After one hour the [Rh(Cp*)Cl$_2$]$_2$ dimer (62 mg, 01 mmol) has been added to the reaction mixture. After 5 hours the solution has been dried and the product has been crystalized by CH_2Cl_2/Hexane solvent mixture. The compound **40** (**Figure 127**) has been collected as a red powder, yield 38%. It is completely soluble in CH_3CN, CH_3OH, DMSO and CH_3Cl and insoluble in H_2O and Hexane.
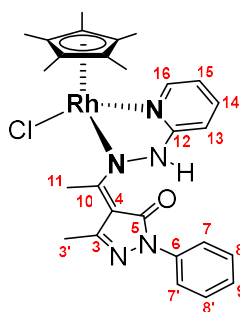
Figure 128 - *Structure of compound 40*

Anal. Calcd. for $C_{27}H_{31}ClRhN_5O$: C, 55.92, H, 5.39, N, 12.08. Found: C, 55.21; H, 5.62,N, 11.36. m.p. 198-199 °C. IR (cm^{-1}): 3062w, 2960w, 2924w, 2910w, 2871w, 2859w v(unsaturated C-H); 1613sh, 1598m v(-C=O); 1573w, 1536m, 1509sh, 1486vs, 1455m, 1420s, 1375m, 1357m v(C=C, C=N); 1305w, 1283m, 1152w, 1118w, 1079s, 1055w, 1019s. ^{1}H-NMR (CDCl$_3$, 293 K): δ 1.65 (s, 15H, -(CH_3)x5 of Cp*), 2.42 (s, 3H, C(3')H), 2.82 (s, 3H, C(11)H), 6.68-6.73 (m, 2H, C(14)H and C(16)H), 7.17 (t, 1H, C(9)H), 7.41 (d, 2H, C(8-8')H), 7.46 (t, 1H, C(15)H), 7.87 (d, 1H, C(13)H), 8.01 (d, 2H, C(7-7')H), 15.34 (N-H). ^{13}C{^{1}H}-NMR (CDCl$_3$, 293 K): δ 9.1 [-(CH_3)x5 of Cp], 15.5 [C(3')], 27.7 [C(11)], 95.4 [-iC_5 of Cp*], 101.3 [C(4)], 107.4 [C(14)], 115.5 [C(16)], 119.1 [C(6)], 120.6 [C(7-7')], 124.4 [C(9)], 128.6 [C(8-8')], 138.4 [C(15)], 146.8 [C(3)], 147.5 [C(13)], 156.7 [C(12)], 159.5 [C(10)], 161.5 [C(5)]. ESI-MS (+) CH$_3$CN (m/z [relative intensity, %]): 544 [100] [Rh(Cp*)(L^{21})]$^+$.

8.2 RESULTS AND DISCUSSION

8.2.1 Synthesis and characterization of the complexes

Coherently to the previous chapter, the hydrazone containing-pyridine ligands used are present in a zwitterionic form and act as Schiff base ligands for the Ir(III) and Rh(III) metal center in the synthesis of the related complexes in the presence of KOH as a deprotonating agent in methanol solution stirred at room temperature for 5 hours (**Scheme 25**). The more active anionic ligands' species (obtained by deprotonation) interact with Cp*-M(III) acceptor affording novel half-sandwich complexes **35-40**.
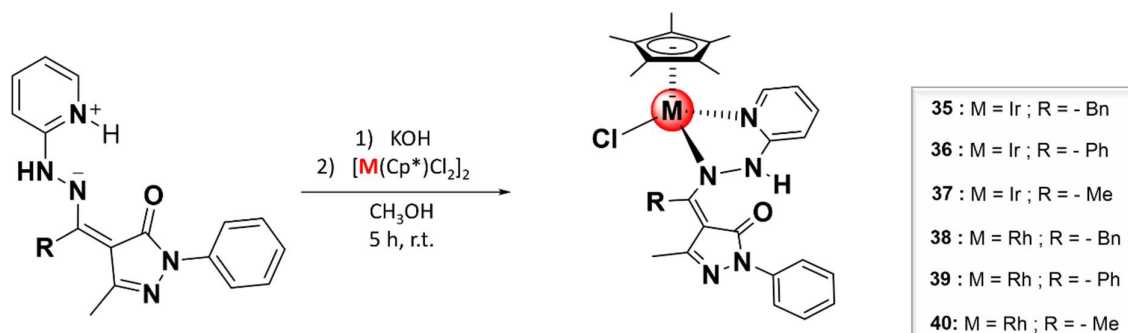
Scheme 25 - *Synthetic procedure for compounds 35-40*

Similarly for Ruthenium(II) complexes, also the Ir(III) and Rh(III) coordination occurs through an -N1,N3 binding, thus, once again, the chelating zwitterionic ligands form a five-membered ring with the metal centres through the coordination of the nitrogen atom present in the pyridine ring (labelled as N1 in **Figure 128**) instead of the oxygen of pyrazolone (O1). The X-ray studies showed below confirm this statement.
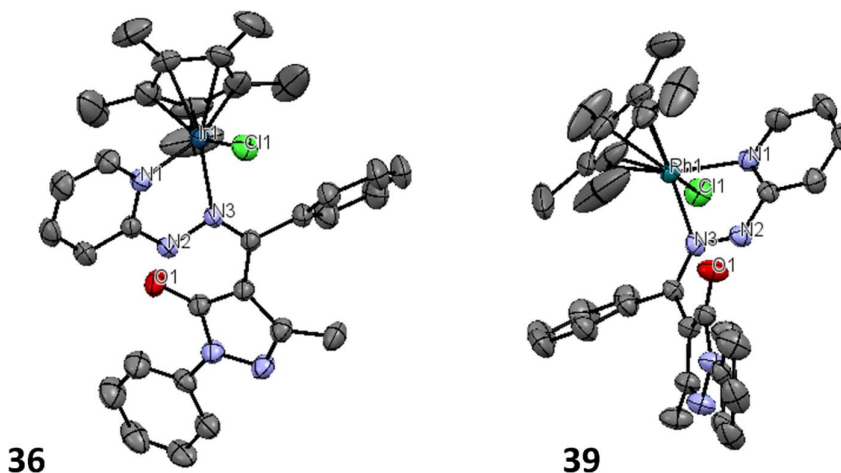

Figure 129 - *Crystal structures of compounds 36 and 39, of Ir(III) and Rh(III) respectively, with HL²⁴ ligand*

The complexes are air-stable and generally soluble in chlorinated solvents and DMSO. The IR spectra of the complexes show the typical ν(C=O) band at lower wavenumbers than the corresponding band in the free ligands as a consequence of coordination through the carbonyl arms to the metal. Strong changes are also observed in the region of C=C/C=N stretching which confirm the coordination through N- donor atoms. The electrospray ionization (ESI) mass spectra in positive ion mode, recorded in CH_3CN, show the typical isotopic patterns expected for both Ir and Rh and display peaks that correspond to the species $[M(Cp^*)L^n]^+$ (where n= 23, 24 and 21 and M= Ir or Rh) arising from the dissociation of the chloride. ^1H and ^{13}C chemical shifts were assigned based on the one-bond and long-range $^1H-^{13}C$ couplings, seen in the $\{^1H-^1H\}$-COSY, $\{^1H-^{13}C\}/\{^1H-^{15}N\}$-HSQC, and $\{^1H-^{13}C\}/\{^1H-^{15}N\}$-HMBC.

All the ^1H-NMR spectra have been recorded in $CDCl_3$ solution. In the spectra all the set of signals related to the ligands' protons, which are far from the coordination environment, are just a little bit shifted compared to the signals of the free ligands. Additionally, same ligands coordinated to the different metal centres present the same ^1H-NMR patterns except for the signals coming from the protons which are closer to the coordination site. An example of this is showed in **Figure 129** where in the ^1H-NMR appears evident the different electronic environment felt by 11-CH_2 protons and the 18-CH and 20-CH signals (belonging to the

pyridine ring) according to the different metal centre in compounds **35** and **38** (which are Ir and Rh complexes bearing **HL^{23}** ligand).
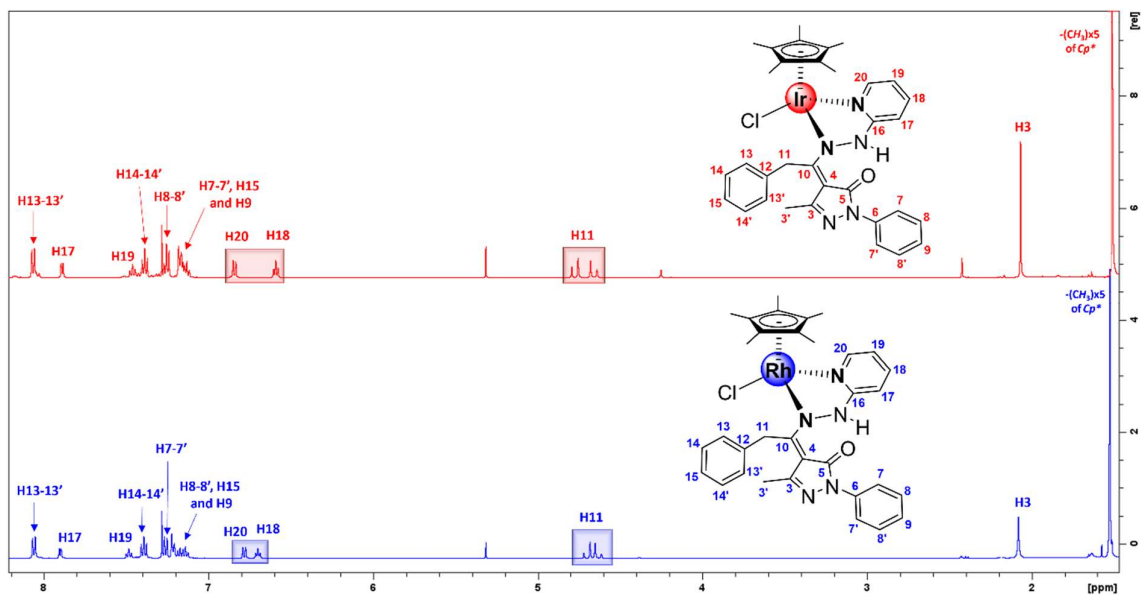
Figure 130 - *Comparison between ^{1}H-NMR spectra recorded in CDCl$_3$ of compounds containing the Iridium, 35 (red line), and Rhodium, 38 (blue line), analogues of **HL^{23}** ligand*

Also in this case is present a strong shift at about 15 ppm of the relative endocyclic N-H bond in the -N,N coordination environment (not showed in the zoomed **Figure 129** but elucidated in **Figure 130**).

Figure 131 - *^{1}H-NMR spectrum of compound 37 recorded in CDCl$_3$*

8.2.2 Catalytic studies

The complexes have been tested as homogeneous catalysts for tandem oxidation-Knoevenagel condensation reaction, under mild conditions, where each step has been studied and optimized separately.

8.2.2.1 Oxidation of alcohols

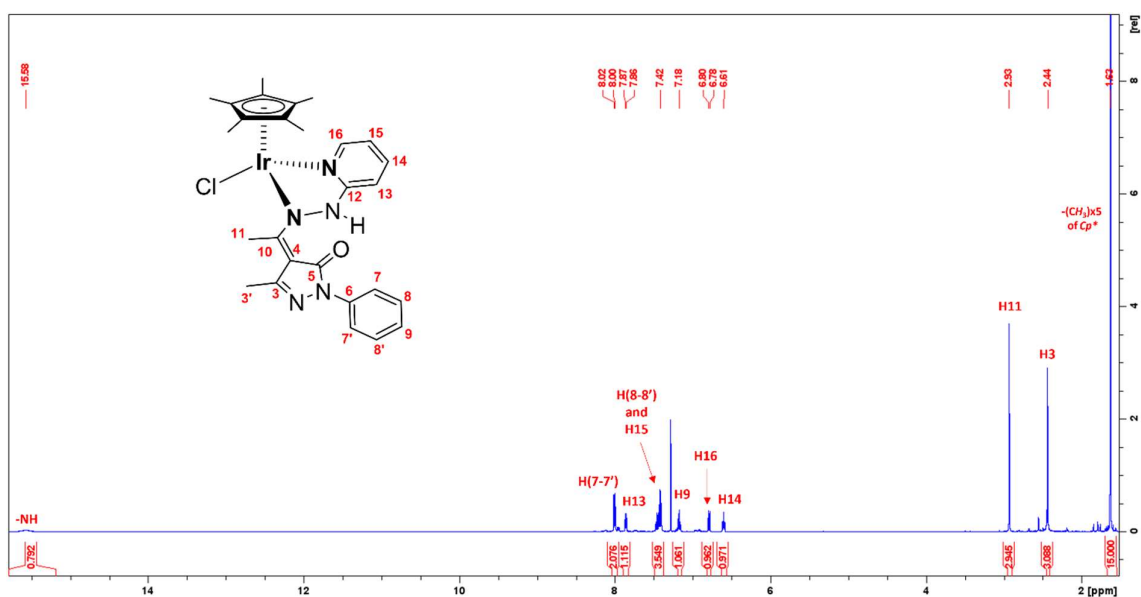First, the oxidation reaction toward both primary and secondary alcohols has been investigated (**Scheme 26**) and benzyl alcohol and 1-phenylethanol (1.25 mmol) have been selected as test compounds for this purpose. The reactants were placed in a capped glass vessel together with the catalysts **35-40** (1 mol%) without the addition of any solvent and the reaction has been investigated for the required reaction time (4 hours for the secondary alcohol and 24 hours for primary one) at 100°C and in the presence of the *tert*-butyl hydroperoxide (TBHP, 2.5 mmol). The product was extracted using a CH_3Cl/H_2O solution and analysed by ^{1}H-NMR spectroscopy. The results are elucidated in **Table 11**.
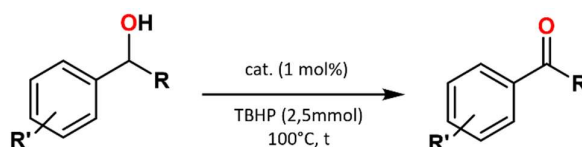
Scheme 26 - *Oxidation reaction catalysed by Ir(III) and Rh(III) complexes 35-40*

The best results have been obtained for the oxidation of secondary alcohols with the Iridium compounds **35** and **36** which give 96% and 97% of conversion (entries 1 and 4 in **Table 11**). The other complexes **37**, **38**, **39** and **40** led to 86%, 46%, 25% and 28% of yields respectively. Nonetheless, although low, the yields given by the Rhodium compounds, **38-40**, for the oxidation of benzyl alcohol are greater than those of 1-phenylethanol showing an apparent of selectivity for the oxidation of primary alcohols.

Entry	Catalyst	Substrate	time	Yield[a]
1		(1-phenylethanol)	4	96
2	35	(benzyl alcohol)	24	49
3		(4-nitrobenzyl alcohol)	24	60

Entry	Catalyst	Substrate	Time (h)	Yield (%)[a]
4	36	1-phenylethanol	4	97
5		benzyl alcohol	24	45
6	37	1-phenylethanol	4	86
7		benzyl alcohol	24	46
8	38	1-phenylethanol	4	46
9		benzyl alcohol	24	36
10	39	1-phenylethanol	4	25
11		benzyl alcohol	24	39
12	40	1-phenylethanol	4	28
13		benzyl alcohol	24	47
14	Blank	1-phenylethanol	4	46
15	$[Ir(Cp^*)Cl_2]_2$	1-phenylethanol	4	77

[a]Calculated by ^1H NMR analysis

Table 11 - *Reaction yields according to the different catalyst (1mol%) performed with 1.25 mmol of substrate and 2.5 mmol of TBHP at 100°C*

Hence, the catalytic efficacy toward the oxidation of secondary alcohol follows the order **36** ≃ **35** > **37** > **38** > **40** > **39**. However, the presence of an electron withdrawing group in the aromatic moiety, like for *p*-nitrobenzylalcohol, slightly increases the reaction yield for primary

alcohols (entry 3, **Table 11**) probably due to the enhancement for the nucleophilic attack. As showed in **Figure 131** (right side) the oxidation of the primary alcohol, by the Iridium compound **35**, has higher reaction times and gives less yields even within 24 hours (mainly due to side products of overoxidation that are formed during the reaction that have been monitored through GC-MS analysis) compared to that of the secondary alcohol that affords almost 100% of conversion in 4 hours (**Figure 131**, left side).
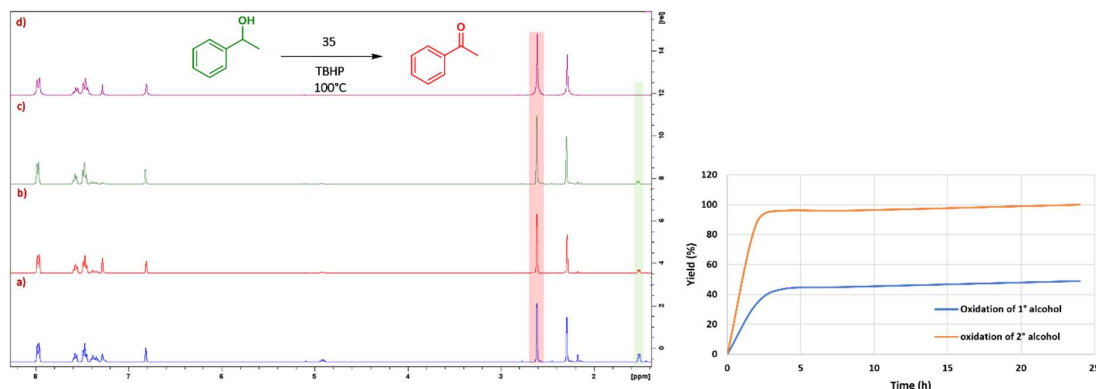

Figure 132 -(left side) Kinetic studies of complex **35** toward the oxidation reaction of 1-phenylethanol monitored by ^1H-NMR in CDCl$_3$ after 1 (**a**),2 (**b**),3 (**c**) and 4 hours (**d**). (right side) Comparison of the oxidant activity of **35** toward 1° and 2° alcohols

Thus, we have selected catalyst **36** to optimize the reaction conditions by changing the temperature (50-120°C), catalyst amount (0.5-3 mol %) and the nature and amount of the co-catalyst, the results are collected in **Table 12**. At the end of these studies, we can conclude that our catalyst maintain its activity even at lower concentrations (0.5 mol%) and, on the contrary, higher catalytic amount (3 mol%) deactivates the reaction proceeding (entries 16 and 17). Additionally, either a decrease or an increase of the temperature brings a reduction of the final yield (entries 21 and 22). Furthermore, the nature and the amount of oxidant agent strongly affects the reaction proceeding: both the use of H_2O_2 and the decreasing in the TBHP percentage drastically decreases the reaction yield (entries 18 and 20). On the contrary, by increasing the amount of THBP the yield reaches almost 100% of conversion.

The oxidation can conceivably occur upon hydrogen abstraction by t-BuOO· and t-BuO· radicals, formed by oxidation or reduction of t-BuOOH by the M(III) metal centre. Furthermore, the ligand appears to play a significant role in the catalytic oxidation of the alcohol, possibly by assisting proton transfer steps, by improving the catalytic activity of its complexes relative to the starting M(III) dimeric salt (entry 15, **Table 11**).

Entry	Oxidant agent	T (°C)	t (h)	Catalyst (mol%)	Yield
Catalyst amount					
16	TBHP (5mmol)	100	4	0.5	91
17	TBHP (5mmol)	100	4	3	87
Oxidant agent					
18	TBHP (2mmol)	100	4	1	37
19	TBHP (10mmol)	100	4	1	>99
20	H_2O_2 (5mmol)	100	4	1	9
Temperature					
21	TBHP (5mmol)	50	4	1	33
22	TBHP (5mmol)	120	4	1	49

Table 12 - *Optimization for the oxidation of secondary alcohol conducted by **36** in 4 hours*

8.2.2.2 Knoevenagel condensation reaction of carbonyl compounds

For the second part of our studies, the focus has been maintained just on the iridium complexes since they result more active with respect to their rhodium derivatives for the oxidation reactions and, according to this, more capable for the planned tandem reaction. Thus, the catalytic behaviour of the synthesized compounds was tested for the Knoevenagel condensation reaction of various aldehydes with a malononitrile molecule in order to give the unsaturated product (**Scheme 27**).
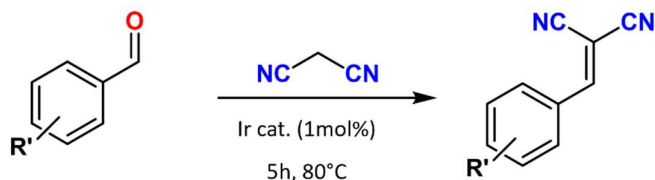
Scheme 27 - *Knoevenagel condensation reaction catalysed by Ir(III) catalysts **35-37***

In a typical reaction, a mixture of benzaldehyde (1.25 mmol), malononitrile (2.5 mmol) and the catalyst (1 mol%) was placed in a capped glass vessel in solventless condition. The mixture was left under magnetic stirring at 80 °C for 5 hours and the final yields, showed in **Table 13**, were calculated by ^{1}H-NMR. The catalytic activity follows the order **37** > **36** > **35**. In **Figure 132** is showed the progressive increase in the product concentration followed by ^{1}H-NMR analysis.
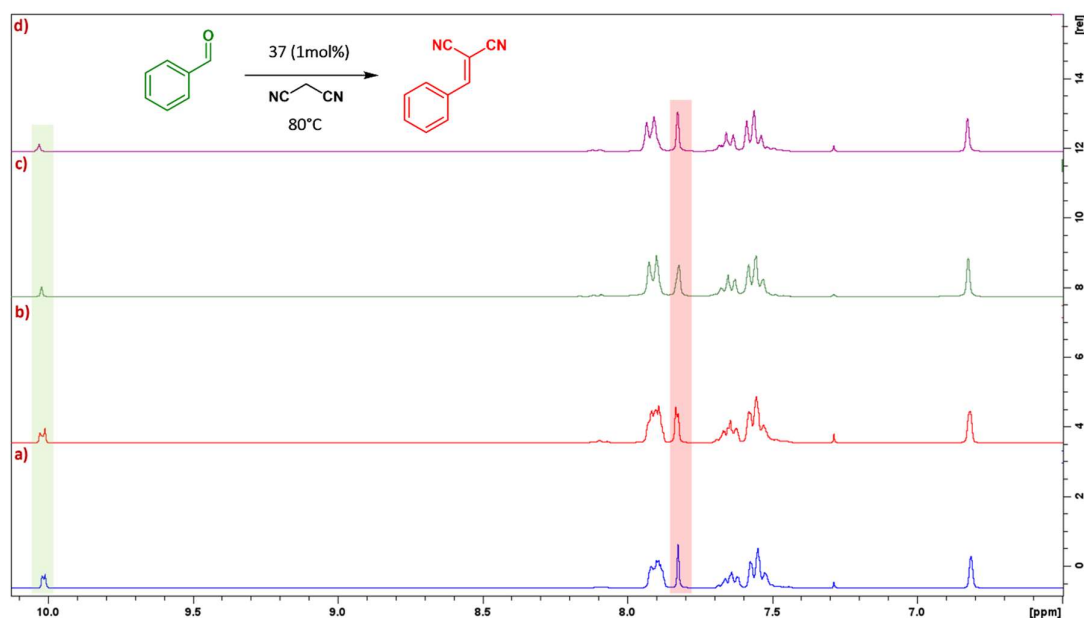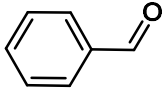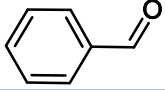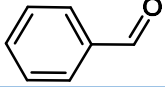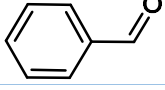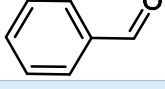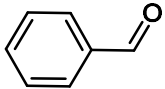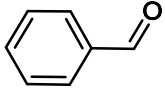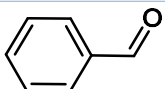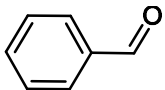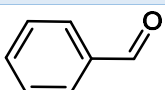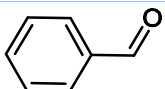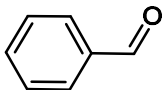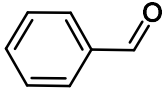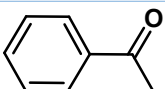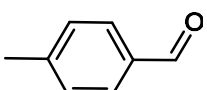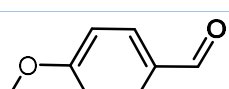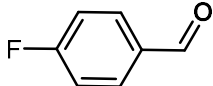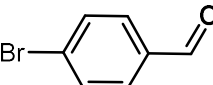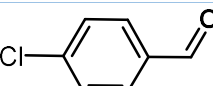
Figure 133 - *Kinetic studies of complex **37** toward the Knoevenagel condensation reaction of benzaldehyde monitored by ^{1}H-NMR in CDCl$_3$ after 1 (**a**),2 (**b**),3 (**c**) and 4 hours (**d**). The yields are calculated by the addition of mesitylene as internal standard (0.3 mmol)*

From the results is evident that the catalyst plays a pivotal role and, more importantly, the ligand strongly affects the reaction since the yield drastically decreases using the metallic dimer (entry 27, **Table 13**). Performing the condensation reaction in the presence of 3 mol% of catalyst **35**, a conversion of >99% of benzaldehyde into 2-benzylidenemalononitrile was achieved under the above mentioned conditions (entry 31, **Table 13**), on the contrary, smaller amount of catalyst (0.5 mol%) gives to lower yields (entry 30, **Table 13**). However, rising the temperature from 80 to 100°C, slightly increases the final yield but linearly decreases at room temperature (entries 29 and 28, respectively). We have also studied the catalytic activities of different substituted aromatic aldehydes with malononitrile in the presence of catalyst **37** (entries 37-41). The highest yields were obtained for 4-bromobenzaldehyde (>99) and 4-chlorobenzaldehyde (99%), while aldehyde such as 4-methoxybenzaldehyde, produced lower yield (79%). Moreover, the reaction does not proceed if, instead of an aldehyde, we use a ketone, such as the acetophenone, as starting material (entry 36). To decide the most appropriate solvent, some experiments were carried out with catalyst **35** in different medium like CH$_3$CN, THF, and H$_2$O (entries 32-35) and surprisingly, the reaction performed in water gave the best results with a yield higher than 99% confirming that the contribution given by the polarity of the solvent for this reaction is not fundamental and the key could be the proton-transfer step which is allowed by protic species.

Entry	Substrate	Solvent	Temp (°C)	Time (h)	Catalyst	Yield
23		solventless	80	5	35	80
24		solventless	80	5	36	82
25		solventless	80	5	37	89
26		solventless	80	5	Blank	39
27		solventless	80	5	$[Ir(Cp*)Cl_2]_2$	18
Different temperature						
28		solventless	r.t.	5	35	49
29		solventless	100	5	35	95
Catalyst amount[a]						
30		solventless	80	5	0.5%mol	70
31		solventless	80	5	3%mol	>99
Different solvents						
32		MeCN	80	3	35	26
33		THF	80	3	35	70
34		solventless	80	3	35	74
35		H_2O	80	3	35	>99
Different Substrates						
36		solventless	80	5	35	0
37		solventless	80	5	37	92
38		solventless	80	5	37	79

39	F–⟨benzaldehyde⟩	solventless	80	5	37	**92**
40	Br–⟨benzaldehyde⟩	solventless	80	5	37	**>99**
41	Cl–⟨benzaldehyde⟩	solventless	80	5	37	**99**

[a]Reaction performed using catalyst **35**

Table 13 - *Reaction yields for the Knoevenagel condensation catalyzed by **35-37***

This encouraged further studies towards the catalysis of the Knoevenagel condensation reaction and the results showed that the reaction conducted in water is much faster reaching very high yields in just few minutes. In **Figure 133a** is possible to see the kinetic studies performed for both Ir and Rh catalysts and to appreciate the comparison of the activities in both water and solventless conditions.
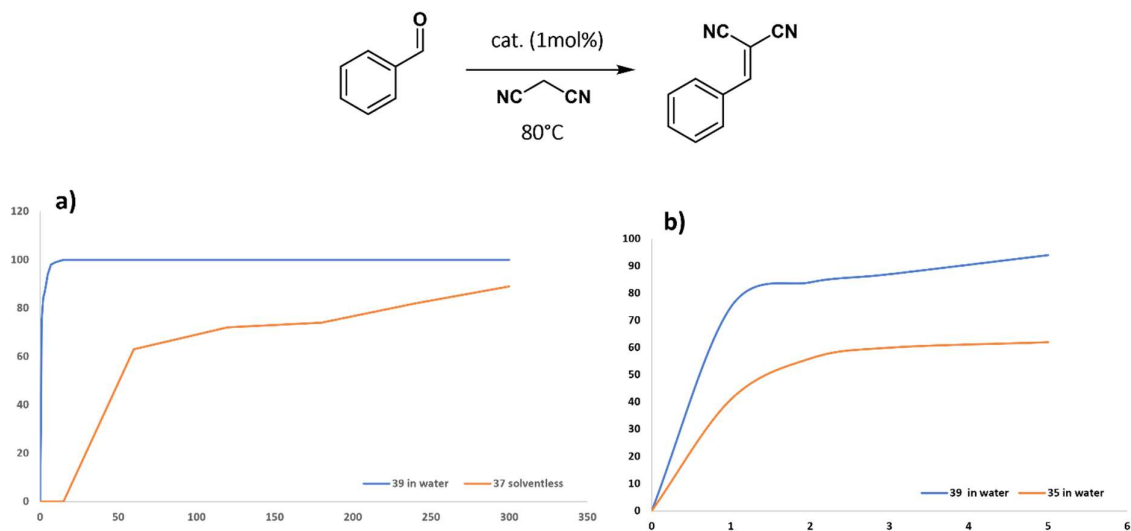
Figure 134 - *Comparison of the catalytic activity of Rh and Ir compounds (**39** and **37** respectively) for Knoevenagel condensation reaction in water and solventless condition (**a**) and for both Rh and Ir type of catalyst (**39** and **35** respectively) in water (**b**)*

The reactions were performed in the same conditions but adding 1mL of water and generally the Rhodium compounds showed better activity with respect to the Iridium ones (**Table 14** and **Figure 133b**) with almost a 100% of conversion as calculated using ^{1}H-NMR spectroscopy using an internal standard (**Figure 134**).
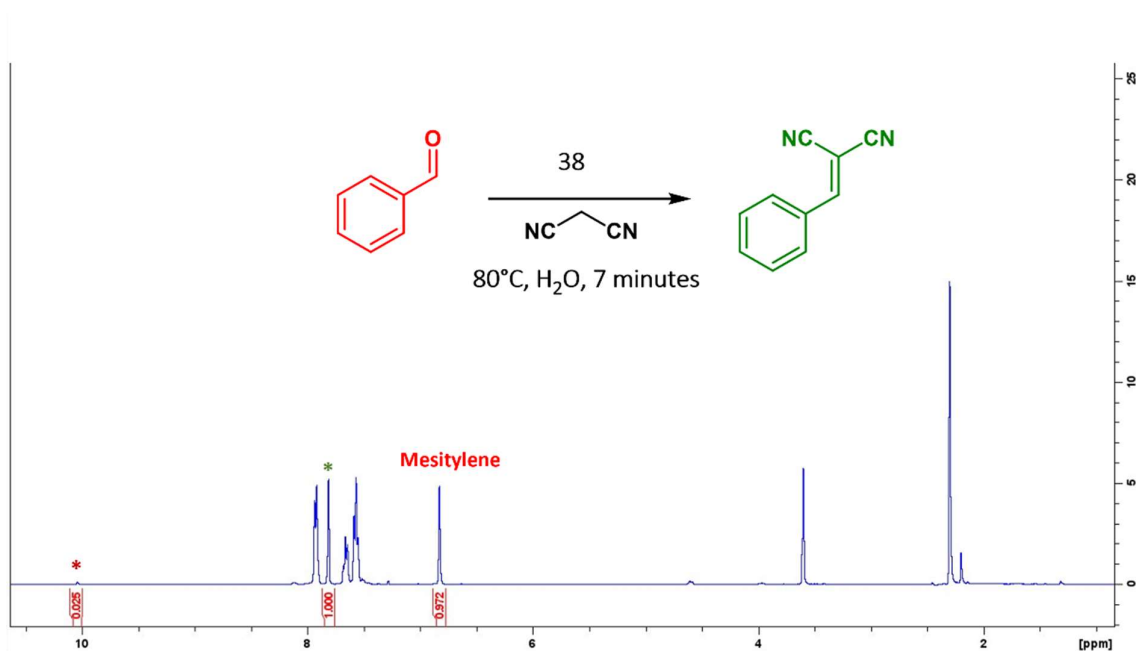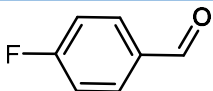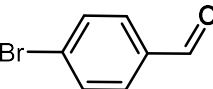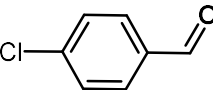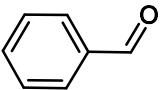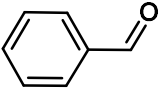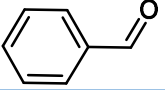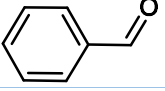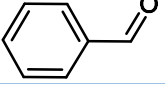
Figure 135 - *^{1}H-NMR spectrum in CDCl$_3$ of Knoevenagel condensation reaction catalyzed by* **38***. The product yield is calculated by the addition of mesitylene as internal standard (0.3mmol).*

Entry	Substrate	Solvent	Temp (°C)	Time (min)	Catalyst	Yield[a]
42		H$_2$O	80	7	35 (1mol%)	**73**
43		H$_2$O	80	7	36 (1%mol)	**75**
44		H$_2$O	80	7	37 (1%mol)	**75**
45		H$_2$O	80	7	38 (1%mol)	**>99**
46		H$_2$O	80	7	39 (1%mol)	**73**
47		H$_2$O	80	7	40 (1%mol)	**83**
48		H$_2$O	80	7	Blank	**56**
Different substrates						
49		H$_2$O	80	7	39 (1%mol)	**>99**
50		H$_2$O	80	7	39 (1%mol)	**77**

51	4-fluorobenzaldehyde structure	H$_2$O	80	7	39 (1%mol)	>99
52	4-bromobenzaldehyde structure	H$_2$O	80	7	39 (1%mol)	>99
53	4-chlorobenzaldehyde structure	H$_2$O	80	7	39 (1%mol)	89
Temperature						
54	benzaldehyde structure	H$_2$O	r.t.	7	39 (1%mol)	43
Catalyst amount						
55	benzaldehyde structure	H$_2$O	80	7	39 (0.5%mol)	86
56	benzaldehyde structure	H$_2$O	80	7	39 (2%mol)	90
Different solvents						
57	benzaldehyde structure	MeCN	80	7	39 (1%mol)	10
58	benzaldehyde structure	THF	80	7	39 (1%mol)	14

aThe yields were calculated using ^{1}H-NMR by the addition of mesitylene as internal standard (0.3 mmol)

Table 14 *- Reaction yields for the Knoevenagel condensation reaction catalyzed by **35-39** in H$_2$O*

The catalytic power of Rhodium catalysts follows the order **38 > 40 > 39**. The reaction has been optimized for catalyst **39** for which we observed that by increasing (2 mol%) or decreasing (0.5 mol%) the catalytic amount, under the above mentioned conditions, the reaction yields worsens slightly (**Table 14**, entries 55 and 56). However, performing the reaction at room temperature generates a decrease in the final yield (entry 54). We have also studied the catalytic activities of different substituted aromatic aldehydes with malononitrile in the presence of catalyst **39** (entries 49-53) obtaining very good yields for every substrate where, in most of the case the conversion was almost 100%.

Additionally, reaction in polar solvents like MeCN and THF, have been performed in the same reaction times (7 minutes) and the yield reported in entries 57 and 58 confirm the fundamental role possessed by the water in such reaction.

8.2.2.3 Tandem peroxidative oxidation– Knoevenagel condensation reaction

Moreover, we have also performed a tandem peroxidative oxidation–Knoevenagel condensation reactions (**Scheme 28**) using compound **35** as catalyst for which, the oxidation of primary alcohols was the most efficient.
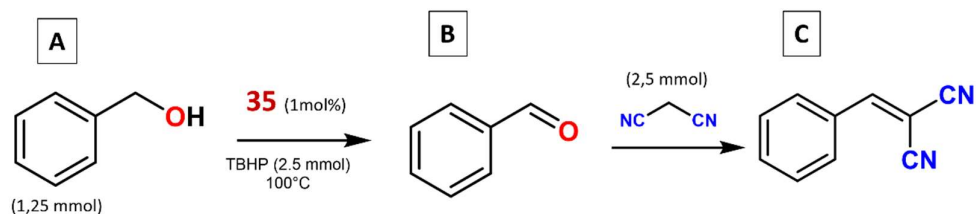
Scheme 28 - *Tandem oxidation-knoevenagel condensation reaction performed with compound **35***

The tandem reaction has been conducted under the optimum reaction conditions mentioned above.

Firstly, in the reaction vessel has been put the catalyst, the benzyl alcohol and the TBHP then, after 8 hours, even the malonitrile has been added. By adopting this method, a maximum conversion of 57% from benzyl alcohol to 2-benzylidenemalononitrile was achieved upon using 1mol% of catalyst **35** after 24 hours. In this tandem reaction the yield of the intermediate benzaldehyde (**B**) slowly increases during time according to the decrease of the starting material (benzyl alcohol, **A**), while the final product smoothly increases (**C**). The kinetic studies, showed in **Figure 135**, performed within 24 hours may confirm this trend.
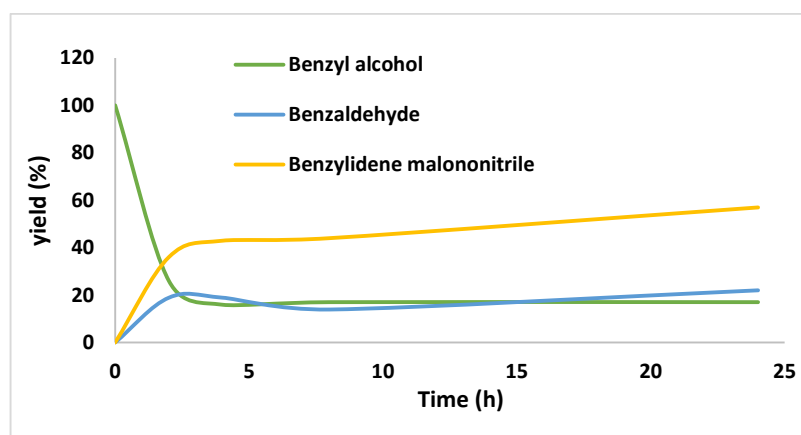
Figure 136 - *Kinetic studies upon oxidation-Knoevenagel condensation reaction performed with catalyst **35***

Chapter 9: Conclusion and future perspectives

To conclude, in this part of the research work is report the synthesis of novel Ruthenium(II)-*p*-cymene, Rh(III)-Cp* and Ir(III)-Cp* derivatives containing several different pyrazolone-based hydrazones ligands. The complete characterization of the ligands allowed us to classify them, according to the nature of hydrazine moiety, in two distinct categories: N,O- and N,N- coordinating agent. Their related Ru(II) complexes (**29-34**) reflect the different coordination environment imposed by the ligands and the structures have been confirmed by crystallographic studies. On the other hand, only the N-N- coordinating ligand (typology B) were able to coordinate the Rh(III) and Ir(III) metal centres.

The synthesised complexes have two potential catalytic sites: the metal centre (acting as a Lewis acid) and the nitrogen atoms present in the ligand structure (acting as Lewis bases). This makes them potential bifunctional catalysts suitable for tandem reactions.

Recently, various MOFs/CPs have been explored for the tandem deacetalization−Knoevenagel condensation reactions, but the use of Ru(III)-based catalysts has not yet been reported. Thus, in the work explained in **Chapter 7** we have prepared suitable Ru catalysts (**29-34**) containing Lewis acidic (Ru centre) and basic functional groups (hydrazone groups) and tested their catalytic activity towards tandem reactions of various acetals with malononitrile under mild conditions. The synthesised compounds act as good homogeneous catalysts, in solvent-free conditions, towards such reactions. Catalyst **33** leads to the highest product yield (94% at 75 °C after 5 h of reaction time) and the catalytic efficacy of the complexes follows the order **33** > **29** > **32** > **31** > **33** > **30**. The highest catalytic activity of **33** can possibly result from its less bulky structure (higher accessibility of active sites) in comparison with the others.

The use of homogenous catalysts for the tandem deacetalization-Knoevenagel condensation reactions is still rare and, moreover, to our knowledge, no Ru catalysts have yet been reported. Hence, we have performed a comparison of the catalytic activity of our homogeneous Ru-catalyst **33** with other reported heterogenous catalysts. For example, the 1D $[Zn(L1)(H_2O)_4]_n \cdot nH_2O$ (L1 = 1,1′-(ethane-1,2-diyl)bis(6-oxo-1,6-dihydropyridine-3-carboxylic acid) coordination polymer displayed an overall product yield of 91% after 4 h reaction time at 80 °C for the deacetalization-Knoevenagel condensation reactions.[220] The Cd(II) framework $[Cd_3(SIPA)_2(ABPY)_3(DMF)_2]_n \cdot (BPDB) \cdot (DMF)_2$ (SIPA: 5-sulfoisopthalate; ABPY: 4,4′-azopyridine; BPDB: 1,4-bis(4-pyridyl)-2,3-diaza-1,3-butadiene) led to an overall yield of 95% after 5 h reaction time at 80 °C.[221] Thus, our catalyst **33** leads to a similar final product yield at a lower reaction temperature (94% after 5 h at 75 °C). Moreover, the use of the 3D Sm(III) MOF $[(CH_3)_2NH_2]_2[Sm_6(OH)_8(BDC-NH_2)_6(H_2O)_6] \cdot x(solvent)$ (BDC-NH2: 2-amino terephthalate) and a Cu(II) MOF (Cu-HNUST-8) led to an yield of 76% and 99% at 50

°C after 24 h and 48 h of reaction time, respectively, which are much longer times than ours.[222-223] In terms of catalyst load, 3 mol% of Al-MOF [MIL-101(Al)-NH$_2$] leads to a yield of 94% after 3 h of reaction time at 90 °C, which concern higher reaction temperature and catalyst amount compared to ours.[224] Based on the above comparisons, the catalyst **33** displays a comparable or higher catalytic activity for the tandem deacetalization-Knoevenagel condensation reactions with respect to other reported catalysts.

On the other hand, the great stability for thermal stress and oxidating environments of Rh(III) and Ir(III) gave the possibility to test them as catalyst for tandem reaction which includes Knoevenagel condensation and where the first step is an oxidation of alcohols. Therefore, the catalytic activity, in homogeneous conditions, of compounds **35-40** was tested for a solvent-free peroxidative oxidation of alcohols and the Knoevenagel condensation reaction, as elucidated in *Chapter 9*. The tested complexes result more active toward the oxidation of secondary alcohols with respect to the primary ones, maybe due to the radical pathway followed by the reaction. Concerning the Knoevenagel condensation reaction, we achieved very good yields in relatively few reactions time and we also evaluated the importance of the ligand in this step, probably being involved is some atom-transfer process. Moreover, the study proves that peroxidative oxidation-Knoevenagel condensation cascade reactions can be performed using **35** as the catalyst showing a moderate activity.

The rhodium complexes **38-40** result very active toward the Knoevenagel condensation reaction performed in homogeneous condition and in water medium. Using those catalyst is possible to achieve very high yields of conversion (>99%, 73% and 83% for **38**, **39** and **40** respectively) in surprisingly low reaction times (7 minutes). In state of this**,** Rhodium(III) complexes bearing Schiff base ligands could be considered as interesting candidates for the developing of a green approach for the Knoevenagel condensation reaction and, according to this, it would be interesting further study this new compounds in order to improve the efficiency of the catalytic process.

The catalytic process for the Knoevenagel condensation reaction is assumed to follow a similar mechanism to that reported earlier,[225–227] where both the carbonyl group of the aldehyde and a cyano group of malononitrile interact with the Lewis acidic metal centre, with a resulting increase of the electrophilicity of the C=O group and of the acidity of the methylene moiety, respectively. The basic sites (hydrazine-N or pyridyl-N) abstract a proton from the methylene group, generating a nucleophilic species which attacks the carbonyl to form a C–C bond and further dehydration leads to 2-benzylidenemalononitrile. Nonetheless, the first part of catalytic process, where the role of the central metal is involved, is still unknown and an example of the hypothesized pathway is illustrated in **Scheme 29**. However, to shed more light on the matter, further future studies are focused on DFT

calculations which may confirm the previous hypothesis, together with the role of the metallic coordination (N,N- or N,O- type) and the steric hindrance of the substituents.
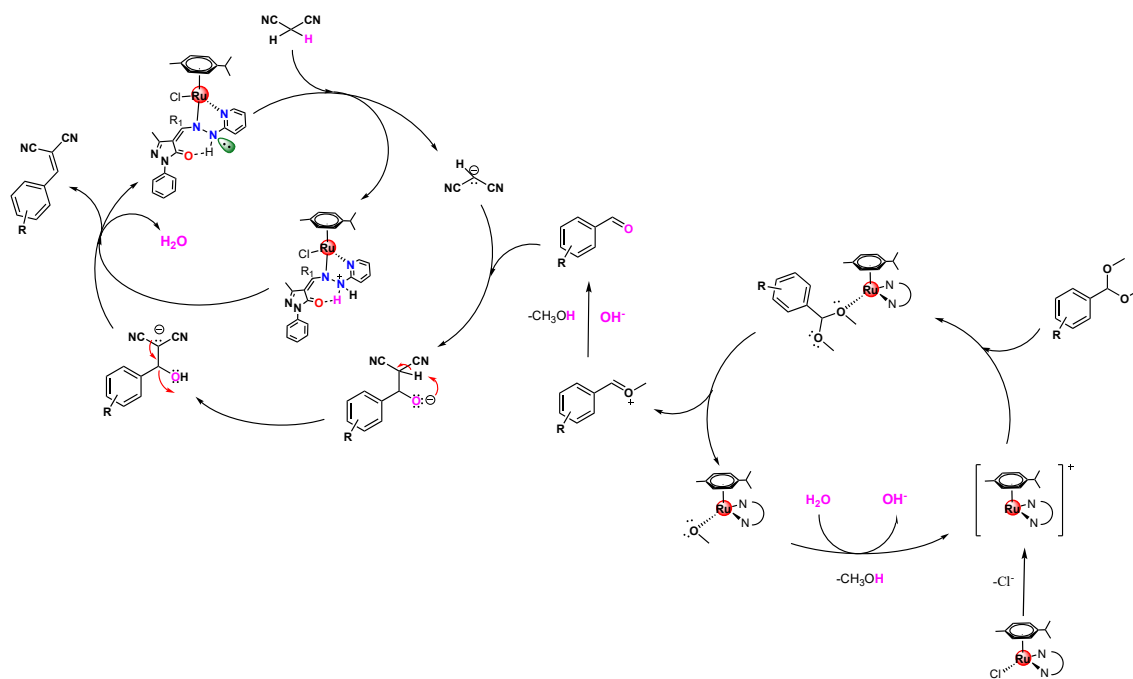
Scheme 29 - *Hypothesized tandem deacetalization-Knoevenagel condensation reaction catalysed by Ru-catalysts (typology B)*

REFERENCES

(1)   Khomskii, D. Transition Metal Compounds.

(2)   Winter, A.; Newkome, G. R.; Schubert, U. S. Catalytic Applications of Terpyridines and Their Transition Metal Complexes. *ChemCatChem* **2011**, *3* (9), 1384–1406.

(3)   Steinlandt, P. S.; Zhang, L.; Meggers, E. Metal Stereogenicity in Asymmetric Transition Metal Catalysis. *Chem. Rev.* **2022**, *123*, 4764–4794.

(4)   Abu-Dief, A. M.; Mohamed, I. M. A. A Review on Versatile Applications of Transition Metal Complexes Incorporating Schiff Bases. *Beni-Suef Univ. J. Basic Appl. Sci.* **2015**, *4* (2), 119–133.

(5)   Gasser, G.; Metzler-Nolte, N. The Potential of Organometallic Complexes in Medicinal Chemistry. *Curr. Opin. Chem. Biol.* **2012**, *16* (1–2), 84–91.

(6)   Yang, W.; Peng, Z.; Wang, G. An Overview: Metal-Based Inhibitors of Urease. *J. Enzyme Inhib. Med. Chem.* **2023**, *38* (1), 361–375.

(7)   Schwietert, C. W.; McCue, J. P. *Coordination Compounds in Medicinal Chemistry*; 1999; Vol. 184.

(8)   Keppler, B. K. Metal Complexes in Cancer Chemotherapy. **1993**.

(9)   Farrell, N. *Uses of Inorganic Chemistry in Medicine*; 1999.

(10)   Collier, W. A.; Krauss, F. Zur Experimentellen Therapie Der Tumoren - III. Mitteilung Die Wirksamkeit Verschiedener Schwermetallverbindungen Auf Den Experimentellen Mäusekrebs. *Z. Krebsforsch.* **1931**, *34* (1), 526–530.

(11)   Kauffman, G. B.; Pentimalli, R.; Doldi, S.; Hall, M. D. Michele Peyrone (1813-1883), Discoverer of Cisplatin. *Platin. Met. Rev.* **2010**, *54* (4), 250–256.

(12)   Rosenberg, B.; Van Camp, L.; Krigas, T. Inhibition of Cell Division in Escherichia Coli by Electrolysis Products from a Platinum Electrode. *Nature* **1965**, *205* (4972), 698–699.

(13)   Rosenberg, B. Cisplatin: Its History and Possible Mechanism of Action. *Cisplatin* **1980**, 9–20.

(14)   Jamieson, E. R.; Lippard, S. J. Structure, Recognition, and Processing of Cisplatin−DNA Adducts. *Chem. Rev* **1999**, *99*, 2467−2498.

(15)   Chapman, E. G.; DeRose, V. J. Enzymatic Processing of Platinated RNAs. *J. Am.*

Chem. Soc. **2010**, *132* (6), 1946–1952.

(16)   Wheate, N. J.; Walker, S.; Craig, G. E.; Oun, R. The Status of Platinum Anticancer Drugs in the Clinic and in Clinical Trials. *Dalt. Trans.* **2010**, *39* (35), 8113–8127.

(17)   Lokich, J. What Is the "Best" Platinum: Cisplatin, Carboplatin, or Oxaliplatin? *Cancer Invest.* **2001**, *19* (7), 756–760.

(18)   Franz, K. J.; Metzler-Nolte, N. Introduction: Metals in Medicine. *Chem. Rev.* **2019**, *119* (2), 727–729.

(19)   P.J.Sadler, Z. G. Metals in Medicine. *Angew. Chemie Int. Ed.* **1999**, *38*, 1512–1531.

(20)   Noffke, A. L.; Habtemariam, A.; Pizarro, A. M.; Sadler, P. J. Designing Organometallic Compounds for Catalysis and Therapy. *Chem. Commun* **2012**, *48*, 5219–5246.

(21)   Jaouen G. and Dyson P.J. *Medicinal Organometallic Chemistry*; 2010.

(22)   Jaouen, G. Bioorganometallics: Biomolecules, Labeling, Medicine. *Bioorganometallics Biomol. Labeling, Med.* **2006**, 1–444.

(23)   Hartinger, C. G.; Dyson, P. J. Bioorganometallic Chemistry-from Teaching Paradigms to Medicinal Applications. *Chem. Soc. Rev.* **2009**, *38* (391–401).

(24)   Eichhorn, G. L. *Inorganic Biochemistry*; 1975.

(25)   Martell, A. E.; Washington, D. C. Inorganic Chemistry in Biology and Medicine. *Am. Chem. Soc.* **1980**.

(26)   Bertini, I.; Messori, L.; Viezzoli, M. S. Coordination Compounds and Life Processes. *Coord. Chem. Rev.* **1992**, *120*, 163–192.

(27)   Whittam, R. *Transport and Diffusion in Red Blood Cells*; 1964.

(28)   M. A. Jakupec, M. Galanski, V. B. Arion, C. G. H. and B. K. K. Antitumour Metal Compounds: More than Theme and Variations. *Dalt. Trans.* **2008**, 183–194.

(29)   Hillard, E. A.; Pigeon, P.; Vessì, A.; Amatore, C.; Jaouen, G. The Influence of Phenolic Hydroxy Substitution on the Electron Transfer and Anti-Cancer Properties of Compounds Based on the 2-Ferrocenyl-1-Phenyl-but-1-Ene Motif. *Dalt. Trans.* **2007**, 5073–5081.

(30)   Hillard, E.; Vessières, A.; Thouin, L.; Jaouen, G.; Amatore, C. Ferrocene-Mediated Proton-Coupled Electron Transfer in a Series of Ferrocifen-Type Breast-Cancer Drug Candidates. *Angew. Chemie* **2006**, *118* (2), 291–296.

(31)   Köpf-Maier, P. Antitumor Activity of Titanocene Dichloride in Xenografted Human

Renal-Cell Carcinoma. *Anticancer Res.* **1999**, *19* (1A), 493–504.

(32) Jakupec, M. A.; Galanski, M.; Keppler, B. K. Tumour-Inhibiting Platinum Complexes--State of the Art and Future Perspectives. *Rev. Physiol. Biochem. Pharmacol.* **2003**, *146*, 1–54.

(33) Claffey, J.; Hogan, M.; Müller-Bunz, H.; Pampillón, C.; Tacke, M. Oxali-Titanocene Y: A Potent Anticancer Drug. *ChemMedChem* **2008**, *3* (5), 729–731.

(34) Nguyen, A.; Vessières, A.; Hillard, E. A.; Top, S.; Pigeon, P.; Jaouen, G. Ferrocifens and Ferrocifenols as New Potential Weapons against Breast Cancer. *Chimia (Aarau).* **2007**, *61* (11), 716.

(35) Pigeon, P.; Top, S.; Vessières, A.; Huché, M.; Hillard, E. A.; Salomon, E.; Jaouen, G. Selective Estrogen Receptor Modulators in the Ruthenocene Series. Synthesis and Biological Behavior. *J. Med. Chem.* **2005**, *48* (8), 2814–2821.

(36) Pettinari, R.; Marchetti, F.; Corrado,]; Nicola, D.; Pettinari, C. Half-Sandwich Metal Complexes with-Diketone-Like Ligands and Their Anticancer Activity. *Eur. J. Inorg. Chem* **2018**, 3521–3536.

(37) Pettinari, R.; Marchetti, F.; Pettinari, C.; Petrini, A.; Scopelliti, R.; Clavel, C. M.; Dyson, P. J. Synthesis, Structure, and Antiproliferative Activity of Ruthenium(II) Arene Complexes with N,O-Chelating Pyrazolone-Based β-Ketoamine Ligands. *Inorg. Chem.* **2014**, *53* (24), 13105–13111.

(38) Palmucci, J.; Marchetti, F.; Pettinari, R.; Pettinari, C.; Scopelliti, R.; Riedel, T.; Therrien, B.; Galindo, A.; Dyson, P. J. Synthesis, Structure, and Anticancer Activity of Arene-Ruthenium(II) Complexes with Acylpyrazolones Bearing Aliphatic Groups in the Acyl Moiety. *Inorg. Chem.* **2016**, *55* (22), 11770–11781.

(39) Pettinari, R.; Pettinari, C.; Marchetti, F.; Clavel, C. M.; Scopelliti, R.; Dyson, P. J. Cytotoxicity of Ruthenium-Arene Complexes Containing β-Ketoamine Ligands. *Organometallics* **2013**, *32* (1), 309–316.

(40) Pettinari, R.; Marchetti, F.; Di Nicola, C.; Pettinari, C.; Galindo, A.; Petrelli, R.; Cappellacci, L.; Cuccioloni, M.; Bonfili, L.; Eleuteri, A. M.; Guedes Da Silva, M. F. C.; Pombeiro, A. J. L. Ligand Design for N, O- or N, N-Pyrazolone-Based Hydrazones Ruthenium(II)-Arene Complexes and Investigation of Their Anticancer Activity. *Inorg. Chem.* **2018**, *57* (22), 14123–14133.

(41) Caruso, F.; Monti, E.; Matthews, J.; Rossi, M.; Gariboldi, M. B.; Pettinari, C.; Pettinari, R.; Marchetti, F. Synthesis, Characterization, and Antitumor Activity of Water-Soluble

(Arene)Ruthenium(II) Derivatives of 1,3-Dimethyl-4-Acylpyrazolon-5- Ato Ligands. First Example of Ru(Arene)(Ligand) Antitumor Species Involving Simultaneous Ru−N7(Guanine) Bonding and Li. *Inorg. Chem* **2014**, *53*, 3668–3677.

(42) Pettinari, R.; Pettinari, C.; Marchetti, F.; Skelton, B. W.; White, A. H.; Bonfili, L.; Cuccioloni, M.; Mozzicafreddo, M.; Cecarini, V.; Angeletti, M.; Nabissi, M.; Eleuteri, A. M. Arene-Ruthenium(II) Acylpyrazolonato Complexes: Apoptosis-Promoting Effects on Human Cancer Cells. *J. Med. Chem.* **2014**, *57* (11), 4532–4542.

(43) Pettinari, R.; Marchetti, F.; Petrini, A.; Pettinari, C.; Lupidi, G.; Smoleński, P.; Scopelliti, R.; Riedel, T.; Dyson, P. J. From Sunscreen to Anticancer Agent: Ruthenium(II) Arene Avobenzone Complexes Display Potent Anticancer Activity. *Organometallics* **2016**, *35* (21), 3734–3742.

(44) Pettinari, R.; Petrini, A.; Marchetti, F.; Pettinari, C.; Riedel, T.; Therrien, B.; Dyson, P. J. Arene–Ruthenium(II) Complexes with Bioactive Ortho-Hydroxydibenzoylmethane Ligands: Synthesis, Structure, and Cytotoxicity. *Eur. J. Inorg. Chem.* **2017**, *2017* (12), 1800–1806.

(45) Winkhaus, G.; Singer, H. Ruthen(II)-Komplexe Mit Zweizähnigem Cycloheptatrien Und Benzol. *J. Organomet. Chem.* **1967**, *7* (3), 487–491.

(46) Zelonka, R. A.; Baird, M. C. Benzene Complexes of Ruthenium(II). *Can. J. Chem.* **2011**, *50* (18), 3063–3072.

(47) Martin Bennett, B. A.; Smith, A. K.; Winkhaus, G.; Singer, H.; Organoinetallic Chem, J.; Abel, E. W.; Bennett, R. A.; Wilkinson, G.; Chem Soc, J.; Zelonka, R. A.; Baird, M. C.; Organometallic Chern, J.; Bennett, A.; Robertson, G. B.; Zelonlra, R. A.; Chem, C. J. Arene Ruthenium(Ii) Complexes Formed by Dehydrogenation of Cyclo-Hexadienes with Ruthenium(Iii) Trichloride. *Organornetallic Chem* **1969**, *43*, 383.

(48) Singh, A. K.; Pandey, D. S.; Xu, Q.; Braunstein, P. Recent Advances in Supramolecular and Biological Aspects of Arene Ruthenium(II) Complexes. *Coord. Chem. Rev.* **2014**, *270–271* (1), 31–56.

(49) Süss-Fink, G. Arene Ruthenium Complexes as Anticancer Agents. *Dalt. Trans.* **2010**, *39* (7), 1673–1688.

(50) Smith, G. S.; Therrien, B. Targeted and Multifunctional Arene Ruthenium Chemotherapeutics. *Dalt. Trans.* **2011**, *40* (41), 10793–10800.

(51) Clarke, M. J. Ruthenium Metallopharmaceuticals. *Coord. Chem. Rev.* **2002**, *232* (1–2), 69–93.

(52) Durig, J. R.; Danneman, J.; Behnke, W. D.; Mercer, E. E. The Induction of Filamentous Growth in Escherichia Coli by Ruthenium and Palladium Complexes. *Chem. Biol. Interact.* **1976**, *13* (3–4), 287–294.

(53) Keppler, B. K.; Rupp, W. Antitumor Activity of Imidazolium-Bisimidazole-Tetrachlororuthenate (III). A Representative of a New Class of Inorganic Antitumor Agents. *J. Cancer Res. Clin. Oncol.* **1986**, *111* (2), 166–168.

(54) Alessio, E.; Balducci, G.; Calligaris, M.; Costa, G.; Attia, W. M.; Mestroni, G. Synthesis, Molecular Structure, and Chemical Behavior of Hydrogen Trans-Bis(Dimethyl Sulfoxide)Tetrachlororuthenate(III) and Mer-Trichlorotris(Dimethyl Sulfoxide)Ruthenium(III): The First Fully Characterized Chloride-Dimethyl Sulfoxide-Ruthenium (III) Com. *Inorg. Chem* **1991**, *30*, 609–618.

(55) Alessio, E.; Messori, L. Anticancer Drug Candidates Face-to-Face: A Case Story in Medicinal Inorganic Chemistry. *Molecules* **2019**, *24*, 1–20.

(56) Hartinger, C. G.; Jakupec, M. A.; Zorbas-Seifried, S.; Groessl, M.; Egger, A.; Berger, W.; Zorbas, H.; Dyson, P. J.; Keppler, B. K. KP1019, a New Redox-Active Anticancer Agent - Preclinical Development and Results of a Clinical Phase I Study in Tumor Patients. *Chem. Biodivers.* **2008**, *5* (10), 2140–2155.

(57) Kapitza, S.; Pongratz, M.; Jakupec, M. A.; Heffeter, P.; Berger, W.; Lackinger, L.; Keppler, B. K.; Marian, B. Heterocyclic Complexes of Ruthenium(III) Induce Apoptosis in Colorectal Carcinoma Cells. *J. Cancer Res. Clin. Oncol.* **2005**, *131* (2), 101–110.

(58) Mestroni, G.; Alessio, E.; Calligaris, M.; Attia, W. M.; Quadrifoglio, F.; Cauci, S.; Sava, G.; Zorzet, S.; Pacor, S.; Monti-Bragadin, C.; Tamaro, M.; Dolzani, L. Chemical, Biological and Antitumor Properties of Ruthenium(II) Complexes with Dimethylsulfoxide. *Prog. Clin. Biochem. Med.* **1989**, 71–87.

(59) Dougan, S. J.; Sadler, P. J. The Design of Organometallic Ruthenium Arene Anticancer Agents. *Chimia (Aarau).* **2007**, *61* (11), 704–715.

(60) Habtemariam, A.; Melchart, M.; Fernández, R.; Parsons, S.; Oswald, I. D. H.; Parkin, A.; Fabbiani, F. P. A.; Davidson, J. E.; Dawson, A.; Aird, R. E.; Jodrell, D. I.; Sadler, P. J. Structure-Activity Relationships for Cytotoxic Ruthenium(II) Arene Complexes Containing N,N-, N,O-, and O,O-Chelating Ligands. *J. Med. Chem.* **2006**, *49* (23), 6858–6868.

(61) Zhang, C. X.; Lippard, S. J. New Metal Complexes as Potential Therapeutics. *Curr. Opin. Chem. Biol.* **2003**, *7* (4), 481–489.

(62)   Aird, R. E.; Cummings, J.; Ritchie, A. A.; Muir, M.; Jodrell, D. I.; Morris, R. E.; Chen, H.; Sadler, P. J. In Vitro and in Vivo Activity and Cross Resistance Profiles of Novel Ruthenium (II) Organometallic Arene Complexes in Human Ovarian Cancer. *Br. J. Cancer* **2002**, *86* (10), 1652–1657.

(63)   Murray, B. S.; Babak, M. V; Hartinger, C. G.; Dyson, P. J. The Development of RAPTA Compounds for the Treatment of Tumors. *Coord. Chem. Rev.* **2016**, *306*, 86–114.

(64)   Article, E.; Weiss, A.; Berndsen, R. H.; Dubois, M.; Cristina, M. In Vivo Anti-Tumor Activity of the Organometallic Ruthenium(II)-Arene Complex [Ru(H6-p-Cymene)-Cl2(Pta)] (RAPTA-C) in Human Ovarian and Colorectal Carcinomas. *Chem. Sci.* **2014**, *1019*, 4742–4748.

(65)   Nowak-Sliwinska, P.; Van Beijnum, J. R.; Casini, A.; Nazarov, A. A.; Wagnières, G.; Van Den Bergh, H.; Dyson, P. J.; Griffioen, A. W. Organometallic Ruthenium(II) Arene Compounds with Antiangiogenic Activity. *J. Med. Chem.* **2011**, *54* (11), 3895–3902.

(66)   Scolaro, C.; Bergamo, A.; Brescacin, L.; Delfino, R.; Cocchietto, M.; Laurenczy, G.; Geldbach, T. J.; Sava, G.; Dyson, P. J. In Vitro and in Vivo Evaluation of Ruthenium(II)-Arene PTA Complexes. *J. Med. Chem.* **2005**, *48* (12), 4161–4171.

(67)   Hanif, M.; Babak, M. V.; Hartinger, C. G. Development of Anticancer Agents: Wizardry with Osmium. *Drug Discov. Today* **2014**, *19* (10), 1640–1648.

(68)   Li, R.; Dalton, /; Zhang, P.; Huang, H. Future Potential of Osmium Complexes as Anticancer Drug Candidates, Photosensitizers and Organelle-Targeted Probes. *Dalt. Trans.* **2018**, *47*, 14841.

(69)   Meier-Menches, S. M.; Gerner, C.; Berger, W.; Hartinger, C. G.; Keppler, B. K. Structure-Activity Relationships for Ruthenium and Osmium Anticancer Agents-towards Clinical Development. *Chem. Soc. Rev* **2018**, *47*, 909.

(70)   Cebrián-Losantos, B.; Krokhin, A. A.; Stepanenko, I. N.; Eichinger, R.; Jakupec, M. A.; Arion, V. B.; Keppler, B. K. Osmium NAMI-a Analogues: Synthesis, Structural and Spectroscopic Characterization, and Antiproliferative Properties. *Inorg. Chem.* **2007**, *46* (12), 5023–5033.

(71)   Egger, A.; Cebrián-Losantos, B.; Stepanenko, I. N.; Krokhin, A. A.; Eichinger, R.; Jakupec, M. A.; Arion, V. B.; Keppler, B. K. Hydrolysis and Cytotoxic Properties of Osmium(II)/(III)-DMSO-Azole Complexes. Short Communication. *Chem. Biodivers.* **2008**, *5* (8), 1588–1593.

(72)   Büchel, G. E.; Stepanenko, I. N.; Hejl, M.; Jakupec, M. A.; Keppler, B. K.; Arion, V. B.

En Route to Osmium Analogues of KP1019: Synthesis, Structure, Spectroscopic Properties and Antiproliferative Activity of Trans-[OsIVCl4(Hazole)2]. *Inorg. Chem.* **2011**, *50* (16), 7690.

(73)   Fu, Y.; Habtemariam, A.; Pizarro, A. M.; Van Rijt, S. H.; Healey, D. J.; Cooper, P. A.; Shnyder, S. D.; Clarkson, G. J.; Sadler, P. J. Organometallic Osmium Arene Complexes with Potent Cancer Cell Cytotoxicity. *J. Med. Chem.* **2010**, *53* (22), 8192–8196.

(74)   Mendoza-Ferri, M. G.; Hartinger, C. G.; Nazarov, A. A.; Eichinger, R. E.; Jakupec, M. A.; Severin, K.; Keppler, B. K. Influence of the Arene Ligand, the Number and Type of Metal Centers, and the Leaving Group on the in Vitro Antitumor Activity of Polynuclear Organometallic Compounds. *Organometallics* **2009**, *28* (21), 6260–6265.

(75)   Dorcier, A.; Han Ang, W.; Bolaño, S.; Gonsalvi, L.; Juillerat-Jeannerat, L.; Laurenczy, G.; Peruzzini, M.; Phillips, A. D.; Zanobini, F.; Dyson, P. J. In Vitro Evaluation of Rhodium and Osmium RAPTA Analogues: The Case for Organometallic Anticancer Drugs Not Based on Ruthenium. *Organometallics* **2006**, 4090–4096.

(76)   Akram, M.; Mohiuddin, E.; Asif, M. Curcuma Longa and Curcumin: A Review Article. *Rom J Biol Plant Biol* **2010**, *55*, 65–70.

(77)   Indira Priyadarsini, K. The Chemistry of Curcumin: From Extraction to Therapeutic Agent. *Molecules* **2014**, *19*, 20091–20112.

(78)   Naie, K. P. P. N. *The Agronomy and Economy of Turmeric and Ginger: The Invaluable Medicinal Spice Crops*; 2013.

(79)   Oppenheimer, A. Tumeric (Curcumin) in Biliary Diseases. *Lancet* **1937**, *229* (5924), 619–621.

(80)   Esatbeyoglu, T.; Huebbe, P.; Ernst, I. M. A.; Chin, D.; Wagner, A. E.; Rimbach, G. Curcumin—From Molecule to Biological Function. *Angew. Chemie Int. Ed.* **2012**, *51* (22), 5308–5332.

(81)   Lampe, V. Synthese von Curcumin. *Berichte der Dtsch. Chem. Gesellschaft* **1918**, *51* (2), 1347–1355.

(82)   Hewlings, S. J.; Kalman, D. S. Curcumin: A Review of Its Effects on Human Health. *Foods* **2017**, *6* (10), 92.

(83)   Bharat B. Aggarwal, A. K. and A. C. B. Anticancer Potential of Curcumin: Preclinical and Clinical Studies. *Anticancer Res.* **2003**, *23*, 363–398.

(84)   Tomeh, M. A.; Hadianamrei, R.; Zhao, X. A Review of Curcumin and Its Derivatives as Anticancer Agents. *Int. J. Mol. Sci.* **2019**, *20* (5), 1033.

(85)   Natalia G. Vallianou, Angelos Evangelopoulos, N. S. and C. K. Curcumin's Mechanisms of Action: The Role of STAT3 and NF-κB. *Anticancer Res.* **2015**, *35*, 645–652.

(86)   Pi, Z.; Wang, J.; Jiang, B.; Cheng, G.; Zhou, S. A Curcumin-Based TPA Four-Branched Copper(II) Complex Probe for in Vivo Early Tumor Detection. *Mater. Sci. Eng. C* **2015**, *46*, 565–571.

(87)   Si, G. F.; Zhou, Y.; Wang, J. F.; Xu, G. Y.; Zhou, S. S. Preparation, Two-Photon Absorption, and Bioimaging Application of a Curcumin-Based Copper(II) Complex. *Russ. J. Coord. Chem. Khimiya* **2021**, *47* (1), 66–74.

(88)   Anand, P.; Kunnumakkara, A. B.; Newman, R. A.; Aggarwal, B. B. Bioavailability of Curcumin: Problems and Promises. *Mol. Pharm.* **2007**, 807–818.

(89)   Sharma, O. P. Antioxidant Activity of Curcumin and Related Compounds. *Biochem. Pharmacol.* **1976**, *25* (15), 1811–1812.

(90)   KSandur, S.; KPandey, M.; Sung, B.; Seok Ahn, K.; Murakami, A.; Sethi, G.; Limtrakul, P.; Badmaev, V.; BAggarwal Ã, B. Curcumin, Demethoxycurcumin, Bisdemethoxycurcumin, Tetrahydrocurcumin and Turmerones Differentially Regulate Anti-Inflammatory and Anti-Proliferative Responses through a ROS-Independent Mechanism. *Carcinogenesis* **2007**, *28* (8), 1765–1773.

(91)   Buhrmann, C.; Yazdi, M.; Bashiri Dezfouli, A.; Samani Sahraneshin, F.; Ebrahimi, S. M.; Hamidollah Ghaffari, S.; Yaghmaie, M.; Barin, A.; Shakibaei, M.; Shayan, P. Significant Decrease in the Viability and Tumor Stem Cell Marker Expression in Tumor Cell Lines Treated with Curcumin. *J. Herb. Med.* **2020**, *22*, 100339.

(92)   Maheshwari, R. K.; Singh, A. K.; Gaddipati, J.; Srimal, R. C. Multiple Biological Activities of Curcumin: A Short Review. *Life Sci.* **2006**, *78* (18), 2081–2087.

(93)   Nelson, K. M.; Dahlin, J. L.; Bisson, J.; Graham, J.; Pauli, G. F.; Walters, M. A. The Essential Medicinal Chemistry of Curcumin. *J. Med. Chem.* **2017**, *60* (5), 1620–1637.

(94)   Aggarwal, B. B.; Bhatt, I. D.; Ichikawa, H.; Ahn, K. S.; Sethi, G.; Sandur, S. K.; Natarajan, C.; Seeram, N.; Shishodia, S. *Curcumin-Biological and Medicinal Properties*; 2006.

(95)   Abd El-Hack, M. E.; El-Saadony, M. T.; Swelum, A. A.; Arif, M.; Abo Ghanima, M. M.; Shukry, M.; Noreldin, A.; Taha, A. E.; El-Tarabily, K. A. Curcumin, the Active

Substance of Turmeric: Its Effects on Health and Ways to Improve Its Bioavailability. *J. Sci. Food Agric.* **2021**, *101* (14), 5747–5762.

(96) Celik, H.; Aydin, T.; Solak, K.; Khalid, S.; Farooqi, A. A. Curcumin on the "Flying Carpets" to Modulate Different Signal Transduction Cascades in Cancers: Next-Generation Approach to Bridge Translational Gaps. *J. Cell. Biochem.* **2018**, *119* (6), 4293–4303.

(97) Terlikowska, K. M.; Witkowska, A. M.; Zujko, M. E.; Dobrzycka, B.; Terlikowski, S. J. Potential Application of Curcumin and Its Analogues in the Treatment Strategy of Patients with Primary Epithelial Ovarian Cancer. *Int. J. Mol. Sci* **2014**, *15*, 21703–21722.

(98) Chakraborti, S.; Dhar, G.; Dwivedi, V.; Das, A.; Poddar, A.; Chakraborti, G.; Basu, G.; Chakrabarti, P.; Surolia, A.; Bhattacharyya, B. Stable and Potent Analogues Derived from the Modification of the Dicarbonyl Moiety of Curcumin. *Biochemistry* **2013**, *52* (42), 7449–7460.

(99) Chang, M.; Wu, M.; Li, H. Antitumor Activities of Novel Glycyrrhetinic Acid-Modified Curcumin-Loaded Cationic Liposomes in Vitro and in H22 Tumor-Bearing Mice. *Drug Deliv.* **2018**, *25* (1), 1984–1995.

(100) Ohtsu, H.; Xiao, Z.; Ishida, J.; Nagai, M.; Wang, H. K.; Itokawa, H.; Su, C. Y.; Shih, C.; Chiang, T.; Chang, E.; Lee, Y. F.; Tsai, M. Y.; Chang, C.; Lee, K. H. Antitumor Agents. 217. Curcumin Analogues as Novel Androgen Receptor Antagonists with Potential as Anti-Prostate Cancer Agents. *J. Med. Chem.* **2002**, *45* (23), 5037–5042.

(101) Ferrari, E.; Lazzari, S.; Marverti, G.; Pignedoli, F.; Spagnolo, F.; Saladini, M. Synthesis, Cytotoxic and Combined CDDP Activity of New Stable Curcumin Derivatives. *Bioorg. Med. Chem.* **2009**, *17* (8), 3043–3052.

(102) Ireson, C. R.; Jones, D. J. L.; Orr, S.; Coughtrie, M. W. H.; Boocock, D. J.; Williams, M. L.; Farmer, P. B.; Steward, W. P.; Gescher, A. J. Metabolism of the Cancer Chemopreventive Agent Curcumin in Human and Rat Intestine. *Cancer Epidemiol. Biomarkers Prev.* **2002**, *11* (1), 105–111.

(103) Garcea, G.; Jones, D. J. L.; Singh, R.; Dennison, A. R.; Farmer, P. B.; Sharma, R. A.; Steward, W. P.; Gescher, A. J.; Berry, D. P. Detection of Curcumin and Its Metabolites in Hepatic Tissue and Portal Blood of Patients Following Oral Administration. *Br. J. Cancer* **2004**, *90* (5), 1011.

(104) Wang, K.; Qiu, F. Curcuminoid Metabolism and Its Contribution to the Pharmacological Effects. *Curr. Drug Metab.* **2013**, *14* (7), 791–806.

(105) Holder, G. M.; Plummer, J. L.; Ryan, A. J. The Metabolism and Excretion of Curcumin (1,7-Bis-(4-Hydroxy-3-Methoxyphenyl)-1,6-Heptadiene-3,5-Dione) in the Rat. *Xenobiotica* **1978**, *8* (12), 761–768.

(106) Wu, J. C.; Tsai, M. L.; Lai, C. S.; Wang, Y. J.; Ho, C. T.; Pan, M. H. Chemopreventative Effects of Tetrahydrocurcumin on Human Diseases. *Food Funct.* **2014**, *5* (1), 12–17.

(107) Aggarwal, B. B.; Deb, L.; Prasad, S. Curcumin Differs from Tetrahydrocurcumin for Molecular Targets, Signaling Pathways and Cellular Responses. *Molecules* **2015**, *20* (1), 185–205.

(108) Pandey, A.; Chaturvedi, M.; Mishra, S.; Kumar, P.; Somvanshi, P.; Chaturvedi, R. Reductive Metabolites of Curcumin and Their Therapeutic Effects. *HLY* **2020**, *6*.

(109) Anand, P.; Thomas, S. G.; Kunnumakkara, A. B.; Sundaram, C.; Harikumar, K. B.; Sung, B.; Tharakan, S. T.; Misra, K.; Priyadarsini, I. K.; Rajasekharan, K. N.; Aggarwal, B. B. Biological Activities of Curcumin and Its Analogues (Congeners) Made by Man and Mother Nature. *Biochem. Pharmacol.* **2008**, *76* (11), 1590–1611.

(110) Pfeiffer, E.; Hoehle, S. I.; Walch, S. G.; Riess, A.; Sólyom, A. M.; Metzler, M. Curcuminoids Form Reactive Glucuronides in Vitro. *J. Agric. Food Chem.* **2007**, *55* (2), 538–544.

(111) Lin, J. K.; Pan, M. H.; Lin-Shiau, S. Y. Recent Studies on the Biofunctions and Biotransformations of Curcumin. *BioFactors* **2000**, *13* (1–4), 153–158.

(112) Qi, Z.; Wu, M.; Fu, Y.; Huang, T.; Wang, T.; Sun, Y.; Feng, Z.; Li, C. Palmitic Acid Curcumin Ester Facilitates Protection of Neuroblastoma against Oligomeric Aβ40 Insult. *Cell. Physiol. Biochem.* **2017**, *44* (2), 618–633.

(113) Patra, M.; Johnstone, T. C.; Suntharalingam, K.; Lippard, S. J. A Potent Glucose–Platinum Conjugate Exploits Glucose Transporters and Preferentially Accumulates in Cancer Cells. *Angew. Chemie* **2016**, *128* (7), 2596–2600.

(114) Mikata, Y.; Shinohara, Y.; Yoneda, K.; Nakamura, Y.; Brudzin˜skabrudzin˜ska, I.; Tanase, T.; Kitayama, T.; Takagi, R.; Okamoto, T.; Kinoshita, I.; Doe, M.; Orvig, C.; Yano, S. Unprecedented Sugar-Dependent In Vivo Antitumor Activity of Carbohydrate-Pendant Cis-Diamminedichloroplatinum(II) Complexes. *Bioorg. Med. Chem. Lett.* **2001**, *11*.

(115) Bairwa, K.; Grover, J.; Kania, M.; Jachak, S. M. Recent Developments in Chemistry and Biology of Curcumin Analogues. *R. Soc. Chem.* **2014**, *4*, 13946–13978.

(116) Wang, R.; Zhang, X.; Chen, C.; Chen, G.; Zhong, Q.; Zhang, Q.; Zheng, S.; Wang, G.; Chen, Q.-H. Synthesis and Evaluation of 1,7-Diheteroarylhepta-1,4,6-Trien-3-Ones as Curcumin-Based Anticancer Agents. *Eur. J. Med. Chem.* **2016**, *110*, 164–180.

(117) Anand, P.; Thomas, S. G.; Kunnumakkara, A. B.; Sundaram, C.; Harikumar, K. B.; Sung, B.; Tharakan, S. T.; Misra, K.; Priyadarsini, I. K.; Rajasekharan, K. N.; Aggarwal, B. B. Biological Activities of Curcumin and Its Analogues (Congeners) Made by Man and Mother Nature. *Biochem. Pharmacol.* **2008**, *76* (11), 1590–1611.

(118) Wang, R.; Chen, C.; Zhang, X.; Zhang, C.; Zhong, Q.; Chen, G.; Zhang, Q.; Zheng, S.; Wang, G.; Chen, Q. H. Structure-Activity Relationship and Pharmacokinetic Studies of 1,5-Diheteroarylpenta-1,4-Dien-3-Ones: A Class of Promising Curcumin-Based Anticancer Agents. *J. Med. Chem.* **2015**, *58* (11), 4713–4726.

(119) Ali, I.; Haque, A.; Saleem, K.; Hsieh, M. F. Curcumin-I Knoevenagel's Condensates and Their Schiff's Bases as Anticancer Agents: Synthesis, Pharmacological and Simulation Studies. *Bioorganic Med. Chem.* **2013**, *21* (13), 3808–3820.

(120) Kumar, B.; Yadav, A.; Hideg, K.; Kuppusamy, P.; Teknos, T. N.; Kumar, P. A Novel Curcumin Analog (H-4073) Enhances the Therapeutic Efficacy of Cisplatin Treatment in Head and Neck Cancer. *PLoS One* **2014**, *9* (3), 93208.

(121) Jordan, B. C.; Kumar, B.; Thilagavathi, R.; Yadhav, A.; Kumar, P.; Selvam, C. Synthesis, Evaluation of Cytotoxic Properties of Promising Curcumin Analogues and Investigation of Possible Molecular Mechanisms. *Chem. Biol. Drug Des.* **2018**, *91* (1), 332–337.

(122) Simoni, D.; Rizzi, M.; Rondanin, R.; Baruchello, R.; Marchetti, P.; Invidiata, F. P.; Labbozzetta, M.; Poma, P.; Carina, V.; Notarbartolo, M.; Alaimo, A.; D'Alessandro, N. Antitumor Effects of Curcumin and Structurally β-Diketone Modified Analogs on Multidrug Resistant Cancer Cells. *Bioorganic Med. Chem. Lett.* **2008**, *18* (2), 845–849.

(123) Lozada-García, M. C.; Enríquez, R. G.; Ramírez-Apán, T. O.; Nieto-Camacho, A.; Palacios-Espinosa, J. F.; Custodio-Galván, Z.; Soria-Arteche, O.; Pérez-Villanueva, J. Synthesis of Curcuminoids and Evaluation of Their Cytotoxic and Antioxidant Properties. *Molecules* **2017**, *22* (4), 1–12.

(124) Gangwar, R. K.; Tomar, G. B.; Dhumale, V. A.; Zinjarde, S.; Sharma, R. B.; Datar, S. Curcumin Conjugated Silica Nanoparticles for Improving Bioavailability and Its Anticancer Applications. **2013**.

(125) Wanninger, S.; Lorenz, V.; Subhan, A.; Edelmann, F. T. Metal Complexes of Curcumin – Synthetic Strategies, Structures and Medicinal Applications. *Chem. Soc. Rev.* **2015**,

44 (15), 4986–5002.

(126) Steel, T. R.; Walsh, F.; Wieczorek-Błauż, A.; Hanif, M.; Hartinger, C. G. Monodentately-Coordinated Bioactive Moieties in Multimodal Half-Sandwich Organoruthenium Anticancer Agents. *Coord. Chem. Rev.* **2021**, *439*, 213890.

(127) Valentini, A.; Conforti, F.; Crispini, A.; De Martino, A.; Condello, R.; Stellitano, C.; Rotilio, G.; Ghedini, M.; Federici, G.; Bernardini, S.; Pucci, D. Synthesis, Oxidant Properties, and Antitumoral Effects of a Heteroleptic Palladium(II) Complex of Curcumin on Human Prostate Cancer Cells. *J. Med. Chem.* **2009**, *52* (2), 484–491.

(128) Pucci, D.; Bloise, R.; Bellusci, A.; Bernardini, S.; Ghedini, M.; Pirillo, S.; Valentini, A.; Crispini, A. Curcumin and Cyclopalladated Complexes: A Recipe for Bifunctional Biomaterials. *J. Inorg. Biochem.* **2007**, *101* (7), 1013–1022.

(129) Song, Y. M.; Xu, J. P.; Ding, L.; Hou, Q.; Liu, J. W.; Zhu, Z. L. Syntheses, Characterization and Biological Activities of Rare Earth Metal Complexes with Curcumin and 1,10-Phenanthroline-5,6-Dione. *J. Inorg. Biochem.* **2009**, *103* (3), 396–400.

(130) Caruso, F.; Rossi, M.; Benson, A.; Opazo, C.; Freedman, D.; Monti, E.; Gariboldi, M. B.; Shaulky, J.; Marchetti, F.; Pettinari, R.; Pettinari, C. Ruthenium-Arene Complexes of Curcumin: X-Ray and Density Functional Theory Structure, Synthesis, and Spectroscopic Characterization, in Vitro Antitumor Activity, and DNA Docking Studies of (p-Cymene)Ru(Curcuminato)Chloro. *J. Med. Chem.* **2012**, *55* (3), 1072–1081.

(131) Garufi, A.; Garufi, A.; Baldari, S.; Baldari, S.; Pettinari, R.; Gilardini Montani, M. S.; D'orazi, V.; Pistritto, G.; Crispini, A.; Giorno, E.; Toietta, G.; Marchetti, F.; Cirone, M.; D'orazi, G. A Ruthenium(II)-Curcumin Compound Modulates NRF2 Expression Balancing the Cancer Cell Death/Survival Outcome According to P53 Status. *J. Exp. Clin. Cancer Res.* **2020**, *39* (1), 1–15.

(132) Cuccioloni, M.; Cecarini, V.; Bonfili, L.; Pettinari, R.; Tombesi, A.; Pagliaricci, N.; Petetta, L.; Angeletti, M.; Eleuteri, A. M. Enhancing the Amyloid-b-Anti-Aggregation Properties of Curcumin via Arene-Ruthenium(II)Derivatization. *Int. J. Mol. Sci.* **2022**, *23* (15), 8710.

(133) Bonfili, L.; Pettinari, R.; Cuccioloni, M.; Cecarini, V.; Mozzicafreddo, M.; Angeletti, M.; Lupidi, G.; Marchetti, F.; Pettinari, C.; Eleuteri, A. M. Arene–RuII Complexes of Curcumin Exert Antitumor Activity via Proteasome Inhibition and Apoptosis Induction. *ChemMedChem* **2012**, *7* (11), 2010–2020.

(134) Milacic, V.; Banerjee, S.; Landis-Piwowar, K. R.; Sarkar, F. H.; Majumdar, A. P. N.;

Dou, Q. P. Curcumin Inhibits the Proteasome Activity in Human Colon Cancer Cells In Vitro and In Vivo. *Cancer Res.* **2008**, *68* (18), 7283–7292.

(135) Caruso, F.; Pettinari, R.; Rossi, M.; Monti, E.; Gariboldi, M. B.; Marchetti, F.; Pettinari, C.; Caruso, A.; Ramani, M. V.; Subbaraju, G. V. The in Vitro Antitumor Activity of Arene-Ruthenium(II) Curcuminoid Complexes Improves When Decreasing Curcumin Polarity. *J. Inorg. Biochem.* **2016**, *162*, 44–51.

(136) Pettinari, R.; Marchetti, F.; Condello, F.; Pettinari, C.; Lupidi, G.; Scopelliti, R.; Mukhopadhyay, S.; Riedel, T.; Dyson, P. J. Ruthenium(II)-Arene RAPTA Type Complexes Containing Curcumin and Bisdemethoxycurcumin Display Potent and Selective Anticancer Activity. *Organometallics* **2014**, *33* (14), 3709–3715.

(137) Pettinari, R.; Condello, F.; Marchetti, F.; Pettinari, C.; Smoleński, P.; Riedel, T.; Scopelliti, R.; Dyson, P. J. Dicationic Ruthenium(II)–Arene–Curcumin Complexes Containing Methylated 1,3,5-Triaza-7-Phosphaadamantane: Synthesis, Structure, and Cytotoxicity. *Eur. J. Inorg. Chem.* **2017**, *2017* (22), 2905–2910.

(138) Pettinari, R.; Marchetti, F.; Tombesi, A.; Duan, F.; Zhou, L.; Messori, L.; Giacomelli, C.; Marchetti, L.; Trincavelli, M. L.; Marzo, T.; La Mendola, D.; Balducci, G.; Alessio, E. Ruthenium(II) 1,4,7-Trithiacyclononane Complexes of Curcumin and Bisdemethoxycurcumin: Synthesis, Characterization, and Biological Activity. *J. Inorg. Biochem.* **2021**, *218*, 111387.

(139) Giraldi, T.; Sava, G.; Mestroni, G.; Zassinovich, G.; Stolfa, D. Antitumour Action of Rhodium (I) and Iridium (I) Complexes. *Chem. Biol. Interact.* **1978**, *22* (2–3), 231–238.

(140) Sava, G.; Zorzet, S.; Perissin, L.; Mestroni, G.; Zassinovich, G.; Bontempi, A. Coordination Metal Complexes of Rh(I), Ir(I) and Ru(II): Recent Advances on Antimetastatic Activity on Solid Mouse Tumors. *Inorganica Chim. Acta* **1987**, *137* (1–2), 69–71.

(141) Barry, N. P. E.; Edafe, F.; Dyson, P. J.; Therrien, B. Anticancer Activity of Osmium Metalla-Rectangles. *Dalt. Trans.* **2010**, *39* (11), 2816–2820.

(142) Pettinari, R.; Marchetti, F.; Pettinari, C.; Condello, F.; Petrini, A.; Scopelliti, R.; Riedel, T.; Dyson, P. J. Organometallic Rhodium(Iii) and Iridium(Iii) Cyclopentadienyl Complexes with Curcumin and Bisdemethoxycurcumin Co-Ligands. *Dalt. Trans.* **2015**, *44* (47), 20523–20531.

(143) Pettinari, R.; Marchetti, F.; Di Nicola, C.; Pettinari, C.; Cuccioloni, M.; Bonfili, L.; Eleuteri, A. M.; Therrien, B.; Batchelor, L. K.; Dyson, P. J. Novel Osmium(Ii)–Cymene Complexes Containing Curcumin and Bisdemethoxycurcumin Ligands. *Inorg. Chem.*

Front. **2019**, *6* (9), 2448–2457.

(144) Werner, H.; Zenkert, K. Aromaten(Phosphan)Metall-Komplexe: XIII. Osmium(II)- Und Osmium(O)-Komplexe Mit p-Cymen Als Aromatischem Liganden. *J. Organomet. Chem.* **1988**, *345* (1–2), 151–166.

(145) Epps, D. E.; Raub, T. J.; Caiolfa, V.; Chiari, A.; Zamai, M. Determination of the Affinity of Drugs toward Serum Albumin by Measurement of the Quenching of the Intrinsic Tryptophan Fluorescence of the Protein. *J. Pharm. Pharmacol.* **2010**, *51* (1), 41–48.

(146) Cuccioloni, M.; Bonfili, L.; Cecarini, V.; Nabissi, M.; Pettinari, R.; Marchetti, F.; Petrelli, R.; Cappellacci, L.; Angeletti, M.; Eleuteri, A. M. Exploring the Molecular Mechanisms Underlying the in Vitro Anticancer Effects of Multitarget-Directed Hydrazone Ruthenium(II)–Arene Complexes. *ChemMedChem* **2020**, *15* (1), 105–113.

(147) Garrett M.Morris, Ruth Huey, William Lindstrom, Michel F. Sanner, Richard K. Belew, David S. Goodsell, A. J. O. AutoDock4 and AutoDockTools4: Automated Dockingwith Selective Receptor Flexibility. *J. Comput. Chem.* **2009**, *30*, 2785–2791.

(148) Sugio, S.; Kashima, A.; Mochizuki, S.; Noda, M.; Kobayashi, K. Crystal Structure of Human Serum Albumin at 2.5 Å Resolution. *Protein Eng. Des. Sel.* **1999**, *12* (6), 439–446.

(149) Mikhailov, A. A.; Komarov, V. Y.; Sukhikh, A. S.; Pishchur, D. P.; Schaniel, D.; Kostin, G. A. The Impact of Counterion on the Metastable State Properties of Nitrosyl Ruthenium Complexes. *New J. Chem.* **2020**, *44* (41), 18014–18024.

(150) CrysAlisPro Software System; Rigaku Oxford Diffraction; **2021**.

(151) Sheldrick, G. M. SHELXT - Integrated Space-Group and Crystal-Structure Determination. *Acta Crystallogr. Sect. A* **2015**, *71* (1), 3–8.

(152) Dolomanov, O. V; Bourhis, L. J.; Gildea, R. J.; Howard, J. A. K.; Puschmann, H. Olex2: A Complete Structure Solution, Refinement and Analysis Program. *J. Appl. Crystallogr.* **2009**, *42* (2), 339–341.

(153) Hanwell, M. D.; Curtis, D. E.; Lonie, D. C.; Vandermeerschd, T.; Zurek, E.; Hutchison, G. R. Avogadro: An Advanced Semantic Chemical Editor, Visualization, and Analysis Platform. *J. Cheminform.* **2012**, *4* (8), 1–17.

(154) Spence, P.; Fielden, J.; Waller, Z. A. E. Beyond Solvent Exclusion: I-Motif Detecting Capability and an Alternative DNA Light-Switching Mechanism in a Ruthenium(II) Polypyridyl Complex. *J. Am. Chem. Soc* **2020**, *11*, 42.

(155) Schneider, C. A.; Rasband, W. S.; Eliceiri, K. W. NIH Image to ImageJ: 25 Years of Image Analysis. *Nat. Methods 2012 97* **2012**, *9* (7), 671–675.

(156) Kharat, M.; Du, Z.; Zhang, G.; McClements, D. J. Physical and Chemical Stability of Curcumin in Aqueous Solutions and Emulsions: Impact of PH, Temperature, and Molecular Environment. *J. Agric. Food Chem.* **2017**, *65* (8), 1525–1532.

(157) Wang, Y. J.; Pan, M. H.; Cheng, A. L.; Lin, L. I.; Ho, Y. S.; Hsieh, C. Y.; Lin, J. K. Stability of Curcumin in Buffer Solutions and Characterization of Its Degradation Products. *J. Pharm. Biomed. Anal.* **1997**, *15* (12), 1867–1876.

(158) Scolaro, C.; Hartinger, C. G.; Allardyce, C. S.; Keppler, B. K.; Dyson, P. J. Hydrolysis Study of the Bifunctional Antitumour Compound RAPTA-C, [Ru(g 6-p-Cymene)Cl 2 (Pta)]. *J. Inorg. Biochem.* **2008**, *102*, 1743–1748.

(159) Selvam, C.; Jachak, S. M.; Thilagavathi, R.; Chakraborti, A. K. Design, Synthesis, Biological Evaluation and Molecular Docking of Curcumin Analogues as Antioxidant, Cyclooxygenase Inhibitory and Anti-Inflammatory Agents. *Bioorg. Med. Chem. Lett.* **2005**, *15* (7), 1793–1797.

(160) Pagliaricci, N.; Pettinari, R.; Marchetti, F.; Pettinari, C.; Cappellacci, L.; Tombesi, A.; Cuccioloni, M.; Hadiji, M.; Dyson, P. J. Potent and Selective Anticancer Activity of Half- Sandwich Ruthenium and Osmium Complexes with Modified Curcuminoid Ligands. **2022**, *51*, 13311.

(161) Smith, J. K. *History of Catalysis*; John Wiley & Sons, Ltd, 2002.

(162) Trmnell, B. M. W. Specificity in Catalysis by Metals. *Q. Rev. Chem. Soc.* **1954**, *8* (4), 404–421.

(163) Medford, A. J.; Vojvodic, A.; Hummelshøj, J. S.; Voss, J.; Abild-Pedersen, F.; Studt, F.; Bligaard, T.; Nilsson, A.; Nørskov, J. K. From the Sabatier Principle to a Predictive Theory of Transition-Metal Heterogeneous Catalysis. *J. Catal.* **2015**, *328*, 36–42.

(164) Zhong, C.; Shi, X. When Organocatalysis Meets Transition-Metal Catalysis. *European J. Org. Chem.* **2010**, *2010* (16), 2999–3025.

(165) Masters, C. *Homogeneous Transition-Metal Catalysis: A Gentle Art*; 2012.

(166) Cornils, B.; Herrmann, W. A. Concepts in Homogeneous Catalysis: The Industrial View. *J. Catal.* **2003**, *216* (1–2), 23–31.

(167) Berichte, D.; Berichte, D. 730 2 -. *Chem. Ber.* **1898**, *31*, 730–731.

(168) van Beurden, K.; de Koning, S.; Molendijk, D.; van Schijndel, J. The Knoevenagel

Reaction: A Review of the Unfinished Treasure Map to Forming Carbon–Carbon Bonds. *Green Chem. Lett. Rev.* **2020**, *13* (4), 85–100.

(169) Bigi, F.; Chesini, L.; Maggi, R.; Sartori, G. Montmorillonite KSF as an Inorganic, Water Stable, and Reusable Catalyst for the Knoevenagel Synthesis of Coumarin-3-Carboxylic Acids. *J. Org. Chem.* **1999**, *64* (3), 1033–1035.

(170) Yadav, J. S.; Basi,]; Reddy, V. S.; Basak, A. K.; Visali, B.; Akkirala,]; Narsaiah, V.; Nagaiah, K. Phosphane-Catalyzed Knoevenagel Condensation: A Facile Synthesis of α-Cyanoacrylates and α-Cyanoacrylonitriles. *Eur. J. Org. Chem.* **2004**, 546–551.

(171) Kumar, S.; Mukesh, K.; Harjai, K.; Singh, V. Synthesis of Coumarin Based Knoevenagel-Ugi Adducts by a Sequential One Pot Five-Component Reaction and Their Biological Evaluation as Anti-Bacterial Agents. *Tetrahedron Lett.* **2018**, *60*, 8–12.

(172) Tichotová, L.; Matoušová, E.; Špulák, M.; Kuneš, J.; Votruba, I.; Buchta, V.; Pour, M. Synthesis and Biological Activity of Desmethoxy Analogues of Coruscanone A. *Bioorganic Med. Chem.* **2011**, *21*, 6062–6066.

(173) de Abrantes, P. G.; de Abrantes, P. G.; dos Santos Silva, D. A.; Magalhães, R. R.; da Silva, P. B. N.; Militão, G. C. G.; de Menezes, R. P. B.; Scotti, L.; Scotti, M. T.; Vale, J. A. Synthesis of 2-Amino-4H-Chromenes Catalyst-Free via Sequential Knoevenagel-Michael Reaction and Evaluation of Biological Activity in Tumor Cells. *Med. Chem. Res.* **2023**, 2234–2244.

(174) Trost, B. M.; Fleming, I. *Comprehensive Organic Synthesis : Selectivity, Strategy, and Efficiency in Modern Organic Chemistry*; 1991.

(175) Bigi, F.; Conforti, M. L.; Maggi, R.; Piccinno, A.; Sartori, G. Clean Synthesis in Water: Uncatalysed Preparation of Ylidenemalononitriles. *Green Chem.* **2000**, *2* (3), 101–103.

(176) Balogh, M. (Maria); Laszlo, P. *Organic Chemistry Using Clays*; Springer-Verlag, 1993.

(177) Sen, S. E.; Smith, S. M.; Sullivan, K. A. Tetrahedron Report Number 508 Organic Transformations Using Zeolites and Zeotype Materials. *Tetrahedron* **1999**, *55*, 12657–12698.

(178) Kabalkd, G. W.; Pagni', R. M. Organic Reactions on Alumina. *CB Pergamon Terrakdron* **1991**, *53* (24), 7999–8065.

(179) Saha, E.; Jungi, H.; Dabas, S.; Mathew, A.; Kuniyil, R.; Subramanian, S.; Mitra, J. Amine-Rich Nickel(II)-Xerogel as a Highly Active Bifunctional Metallo-Organo Catalyst for Aqueous Knoevenagel Condensation and Solvent-Free CO 2 Cycloaddition. *Inorg. Chem.* **2023**, *62* (37), 14959–14970.

(180) de Abrantes, P. G.; de Abrantes, P. G.; Ferreira, J. M. G. de O.; Vale, J. A. NaCl as an Eco-Friendly and Efficient Promoter for Knoevenagel Condensation at Room Temperature. *Synth. Commun.* **2023**, *53* (2), 135–145.

(181) Xiao, W.; Wang, Z.; Yang, J.; Qiu, M.; Peng, Y.; Xiong, X.; Lu, Y.; Chen, T.; Xu, Z. Colloidal Polystyrene-Supported Cooperative Imidazolidinone/Thiourea Catalysts for Efficient Aldol Reaction and Substrate-Selective Knoevenagel Condensation in Water. *New J. Chem.* **2023**, 16785–16788.

(182) Jiang, Y.; Li, C.; Tang, S.; Tao, S.; Yuan, M.; Li, R.; Chen, H.; Fu, H.; Zheng, X. Practical Synthesis of (Z)-α,β-Unsaturated Nitriles via a One-Pot Sequential Hydroformylation/Knoevenagel Reaction. *J. Org. Chem.* **2021**, *86* (21), 15413–15422.

(183) Omar, S.; Dutta, B.; Natour, S.; Abu-Reziq, R. Rhodium-Complexed Hyperbranched Poly(Ethyleneimine) and Polyamidoamine and Their Non-Covalent Immobilization on Magnetic Nanoparticles. *J. Organomet. Chem.* **2016**, *818*, 48–57.

(184) Breit, B.; Zahn, S. K. Domino Hydroformylation/Knoevenagel/ Hydrogenation Reactions. *Angew. Chem. Int. Ed* **2001**, *40* (10).

(185) Li, F.; Zou, X.; Wang, N. Direct Coupling of Arylacetonitriles and Primary Alcohols to α-Alkylated Arylacetamides with Complete Atom Economy Catalyzed by a Rhodium Complex-Triphenylphosphine- Potassium Hydroxide System. *Adv. Synth. Catal.* **2015**, *357* (7), 1405–1415.

(186) Vigato, P. A.; Tamburini, S. The Challenge of Cyclic and Acyclic Schiff Bases and Related Derivatives. *Coord. Chem. Rev.* **2004**, *248* (17–20), 1717–2128.

(187) Pfeiffer, P.; Breith, E.; Lübbe, E.; Tsumaki, T. Tricyclische Orthokondensierte Nebenvalenzringe. *Justus Liebigs Ann. Chem.* **1933**, *503* (1), 84–130.

(188) Boulechfar, C.; Ferkous, H.; Delimi, A.; Djedouani, A.; Kahlouche, A.; Boublia, A.; Darwish, A. S.; Lemaoui, T.; Verma, R.; Benguerba, Y. Schiff Bases and Their Metal Complexes: A Review on the History, Synthesis, and Applications. *Inorg. Chem. Commun.* **2023**, *150*, 110451.

(189) Juyal, V. K.; Pathak, A.; Panwar, M.; Thakuri, S. C.; Prakash, O.; Agrwal, A.; Nand, V. Schiff Base Metal Complexes as a Versatile Catalyst: A Review. *J. Organomet. Chem.* **2023**, *999*, 122825.

(190) Li, R. J.; Ling, C.; Lv, W. R.; Deng, W.; Yao, Z. J. Cyclometalated Half-Sandwich Iridium(III) Complexes: Synthesis, Structure, and Diverse Catalytic Activity in Imine Synthesis Using Air as the Oxidant. *Inorg. Chem.* **2021**, *60* (7), 5153–5162.

(191) Brehme, R.; Enders, D.; Fernandez, R.; Lassaletta, J. M. Aldehyde N,N-Dialkylhydrazones as Neutral Acyl Anion Equivalents: Umpolung of the Imine Reactivity. *European J. Org. Chem.* **2007**, *2007* (34), 5629–5660.

(192) Belskaya, N. P.; Dehaen, W.; Bakulev, V. A. Synthesis and Properties of Hydrazones Bearing Amide, Thioamide and Amidine Functions. *Arkivoc* **2010**, *2010* (1), 275–332.

(193) Kobayashi, S.; Mori, Y.; Fossey, J. S.; Salter, M. M. Catalytic Enantioselective Formation of C-C Bonds by Addition to Imines and Hydrazones: A Ten-Year Update. *Chem. Rev.* **2011**, *111* (4), 2626–2704.

(194) Vicini, P.; Incerti, M.; La Colla, P.; Loddo, R. Anti-HIV Evaluation of Benzo[d]Isothiazole Hydrazones. *Eur. J. Med. Chem.* **2009**, *44* (4), 1801–1807.

(195) Su, X.; Aprahamian, I. Hydrazone-Based Switches, Metallo-Assemblies and Sensors. *Chem. Soc. Rev.* **2014**, *43* (6), 1963–1981.

(196) Marchetti, F.; Pettinari, C.; Di Nicola, C.; Tombesi, A.; Pettinari, R. Coordination Chemistry of Pyrazolone-Based Ligands and Applications of Their Metal Complexes. *Coord. Chem. Rev.* **2019**, *401*, 213069.

(197) Manikandan, R.; Viswanathamurthi, P.; Muthukumar, M. Ruthenium(II) Hydrazone Schiff Base Complexes: Synthesis, Spectral Study and Catalytic Applications. *Spectrochim. Acta Part A Mol. Biomol. Spectrosc.* **2011**, *83* (1), 297–303.

(198) Blakemore, J. D.; Schley, N. D.; Balcells, D.; Hull, J. F.; Olack, G. W.; Incarvito, C. D.; Eisenstein, O.; Brudvig, G. W.; Crabtree, R. H. Half-Sandwich Iridium Complexes for Homogeneous Water-Oxidation Catalysis. *J. Am. Chem. Soc.* **2010**, *132* (45), 16017–16029.

(199) Carmona, D.; Lamata, M. P.; Viguri, F.; Dobrinovich, I.; Lahoz, F. J.; Oro, L. A. On the Sense of the Enantioselection in Hydrogen Transfer Reactions from 2-Propanol to Ketones. *Adv. Synth. Catal.* **2002**, *344* (5), 499–502.

(200) Prakash, O.; Sharma, K. N.; Joshi, H.; Gupta, P. L.; Singh, A. K. Half-Sandwich Rhodium/Iridium(III) Complexes Designed with Cp* and 1,2-Bis(Phenylchalcogenomethyl)Benzene as Catalysts for Transfer Hydrogenation in Glycerol. *Organometallics* **2014**, *33* (10), 2535–2543.

(201) Ikariya, T.; Kuwata, S.; Kayaki, Y. Aerobic Oxidation with Bifunctional Molecular Catalysts. *Pure Appl. Chem.* **2010**, *82* (7), 1471–1483.

(202) Zhang, P.; Sadler, P. J. Advances in the Design of Organometallic Anticancer Complexes. *J. Organomet. Chem.* **2017**, *839*, 5–14.

(203) Dkhar, L.; Kaminsky, W.; Poluri, K. M.; Kollipara, M. R. Versatile Coordination Modes of Benzothiazole Hydrazone Derivatives towards Ru(II), Rh(III) and Ir(III) Complexes and Their Reactivity Studies with Azides and Activated Alkynes. *J. Organomet. Chem.* **2019**, *891*, 54–63.

(204) Drozdzak, R.; Allaert, B.; Ledoux, N.; Dragutan, I.; Dragutan, V.; Verpoort, F. Ruthenium Complexes Bearing Bidentate Schiff Base Ligands as Efficient Catalysts for Organic and Polymer Syntheses. *Coord. Chem. Rev.* **2005**, *249* (24), 3055–3074.

(205) Rath, R. K.; Nethaji, M.; Chakravarty, A. R. Transfer Hydrogenation of Acetophenone Promoted by (Arene)Ruthenium(II) Reduced Schiff Base Complexes: An X-Ray Structure of [(N6-p-Cymene)RuCl (OC6H4-2-CH2 NHC6H4-p-Me)]. *Polyhedron* **2001**, *20* (21), 2735–2739.

(206) Opstal, T.; Couchez, K.; Verpoort, F. Easily Accessible Ring Opening Metathesis and Atom Transfer Radical Polymerization Catalysts Based on Arene, Norbornadiene and Cyclooctadiene Ruthenium Complexes Bearing Schiff Base Ligands. *Adv. Synth. Catal.* **2003**, *345* (3), 393–401.

(207) Lv, W. R.; Li, R. J.; Liu, Z. J.; Jin, Y.; Yao, Z. J. Synthesis, Structure, and Catalytic Hydrogenation Activity of [NO]-Chelate Half-Sandwich Iridium Complexes with Schiff Base Ligands. *Inorg. Chem.* **2021**, *60* (11), 8181–8188.

(208) Tandon, P. K.; Gayatri; Sahgal, S.; Srivastava, M.; Singh, S. B. Catalysis by Ir(III), Rh(III) and Pd(II) Metal Ions in the Oxidation of Organic Compounds with H2O2. *Appl. Organomet. Chem.* **2007**, *21* (3), 135–138.

(209) Prakash, O.; Singh, P.; Mukherjee, G.; Singh, A. K. Efficient Catalysis of Transfer Hydrogenation of Ketones and Oxidation of Alcohols with Newly Designed Half-Sandwich Rhodium(III) and Iridium(III) Complexes of Half-Pincer Chalcogenated Pyridines. *Organometallics* **2012**, *31* (8), 3379–3388.

(210) Hull, J. F.; Balcells, D.; Blakemore, J. D.; Incarvito, C. D.; Eisenstein, O.; Brudvig, G. W.; Crabtree, R. H. Highly Active and Robust Cp* Iridium Complexes for Catalytic Water Oxidation. *J. Am. Chem. Soc.* **2009**, *131* (25), 8730–8731.

(211) Yu, W.-B.; He, Q.-Y.; Shi, H.-T.; Jia, J.-Y.; Wei, X. Azo-Conjugated Half-Sandwich Rh/Ru Complexes for Homogeneous Water-Oxidation Catalysis. *Daln. Trans.* **2014**, *43*, 6561.

(212) Tabata, M.; Mawatari, Y. Polymer Reviews Emerging π-Conjugated Stretched and Contracted Helices and Their Mutual Conversions of Substituted Polyacetylenes Prepared Using an Organo-Rhodium Catalyst Emerging p-Conjugated Stretched and

Contracted Helices and Their Mutual Conversions. *Polym. Rev.* **2016**, 65–88.

(213) Karmakar, A.; Paul, A.; Rúbio, G. M. D. M.; Soliman, M. M. A.; Guedes da Silva, M. F. C.; Pombeiro, A. J. L. Highly Efficient Bifunctional Amide Functionalized Zn and Cd Metal Organic Frameworks for One-Pot Cascade Deacetalization–Knoevenagel Reactions. *Front. Chem.* **2019**, *7*, 1–10.

(214) Marchetti, F.; Pettinari, C.; Pettinari, R. Acylpyrazolone Ligands: Synthesis, Structures, Metal Coordination Chemistry and Applications. *Coord. Chem. Rev.* **2005**, *249* (24), 2909–2945.

(215) Karmakar, A.; Paul, A.; Santos, P. M. R.; Santos, I. R. M.; Guedes da Silva, M. F. C.; Pombeiro, A. J. L. Design and Construction of Polyaromatic Group Containing Cd(Ii)-Based Coordination Polymers for Solvent-Free Strecker-Type Cyanation of Acetals. *New J. Chem.* **2022**, *46* (21), 10201–10212.

(216) Kopylovich, M. N.; Ribeiro, A. P. C.; Alegria, E. C. B. A.; Martins, N. M. R.; Martins, L. M. D. R. S.; Pombeiro, A. J. L. Catalytic Oxidation of Alcohols: Recent Advances. *Adv. Organomet. Chem.* **2015**, *63*, 91–174.

(217) Albonetti, S.; Mazzoni, R.; Cavani, F. *Homogeneous, Heterogeneous and Nanocatalysis*; 2014.

(218) Sutradhar, M.; Martins, L. M. D. R. S.; Guedes da Silva, M. F. C.; Pombeiro, A. J. L. Oxidovanadium Complexes with Tridentate Aroylhydrazone as Catalyst Precursors for Solvent-Free Microwave-Assisted Oxidation of Alcohols. *Appl. Catal. A Gen.* **2015**, *493*, 50–57.

(219) Marchetti, F.; Tombesi, A.; Nicola, D.; Pettinari, R.; Verdicchio, F.; Crispini, A.; Scarpelli, F.; Baldassarri, C.; Marangoni, E.; Hofer, A.; Galindo, A.; Petrelli, R. Zinc(II) Complex with Pyrazolone-Based Hydrazones Is Strongly Effective against Trypanosoma Brucei Which Causes African Sleeping Sickness. *Inorg. Chem* **2022**, *2022*, 13561–13575.

(220) Paul, A.; Karmakar, A.; F, M.; Guedes, C.; Pombeiro, A. J. L. 1D Zn (II) Coordination Polymers as Effective Heterogeneous. *Catalysts* **2021**, *11*, 90.

(221) Mistry, S.; Sarkar, A.; Natarajan, S. New Bifunctional Metal-Organic Frameworks and Their Utilization in One-Pot Tandem Catalytic Reactions. *Cryst. Growth Des.* **2019**, *19* (2), 747–755.

(222) Zhang, Y.; Wang, Y.; Liu, L.; Wei, N.; Gao, M. L.; Zhao, D.; Han, Z. B. Robust Bifunctional Lanthanide Cluster Based Metal-Organic Frameworks (MOFs) for

Tandem Deacetalization-Knoevenagel Reaction. *Inorg. Chem.* **2018**, *57* (4), 2193–2198.

(223) Zheng, B.; Luo, X.; Wang, Z.; Zhang, S.; Yun, R.; Huang, L.; Zeng, W.; Liu, W. An Unprecedented Water Stable Acylamide-Functionalized Metal-Organic Framework for Highly Efficient CH4/CO2 Gas Storage/Separation and Acid-Base Cooperative Catalytic Activity. *Inorg. Chem. Front.* **2018**, *5* (9), 2355–2363.

(224) Toyao, T.; Fujiwaki, M.; Horiuchi, Y.; Matsuoka, M. Application of an Amino-Functionalised Metal-Organic Framework: An Approach to a One-Pot Acid-Base Reaction. *RSC Adv.* **2013**, *3* (44), 21582–21587.

(225) Karmakar, A.; Paul, A.; Mahmudov, K. T.; Fá, M.; Guedes Da Silva, C.; Pombeiro, A. J. L. PH Dependent Synthesis of Zn(II) and Cd(II) Coordination Polymers with Dicarboxyl-Functionalized Arylhydrazone of Barbituric Acid: Photoluminescence Properties and Catalysts for Knoevenagel Condensation. *New J. Chem* **2016**, *40*, 1535.

(226) Karmakar, A.; Rúbio, G. M. D. M.; Guedes da Silva, M. F. C.; Pombeiro, A. J. L. Synthesis of Metallomacrocycle and Coordination Polymers with Pyridine-Based Amidocarboxylate Ligands and Their Catalytic Activities towards the Henry and Knoevenagel Reactions. *ChemistryOpen* **2018**, *7* (11), 865–877.

(227) Karmakar, A.; D M Ru, G. M.; Fa, M.; Guedes da Silva, tima C.; Hazra, S.; L Pombeiro, A. J. Solvent-Dependent Structural Variation of Zinc(II) Coordination Polymers and Their Catalytic Activity in the Knoevenagel Condensation Reaction. **2015**, *15* (9), 4185–4197.